

# Vibration Analysis of Thickness-Tapered Laminated Composite Square Plates Based on Ritz Method

Babak Arab

A thesis  
in  
the Department  
of  
Mechanical, Industrial and Aerospace Engineering (MIAE)

Presented in Partial Fulfillment of the Requirements  
For the Degree of  
Master of Applied Science (Mechanical Engineering) at  
Concordia University  
Montreal, Quebec, Canada

July 2019

©Babak Arab 2019

**CONCORDIA UNIVERSITY**  
**School of Graduate Studies**

This is to certify that the thesis prepared

By: Babak Arab

Entitled: Vibration Analysis of Thickness-Tapered Laminated Composite Square Plates Based on Ritz Method

and submitted in partial fulfillment of the requirements for the degree of

Master of Applied Science (Mechanical Engineering)

complies with the regulations of the University and meets the accepted standards with respect to originality and quality.

Signed by the final Examining Committee:

Dr. B. W. Gordon Chair

Dr. Behrooz Yousefzadeh Examiner

Dr. M. Omair Ahmad Examiner

Dr. R. Ganesan Supervisor

Approved by

Chair of Department or Graduate Program Director

Dean of Faculty

Date

July 19, 2019

## **ABSTRACT**

### **Vibration Analysis of Thickness-Tapered Laminated Composite Square Plates Based on Ritz Method**

Babak Arab

Thickness-tapered laminated composite plates provide stiffness- and mass-tailoring design capabilities such that they are widely used in aerospace applications including space structures. In the present work, the free and forced vibration response of symmetric linearly-thickness-tapered laminated composite square plates are considered with a variety of taper configurations and boundary conditions. Since exact and closed-form solutions for the natural frequencies and mode shapes of the plates could not be obtained from the corresponding complex partial differential equations in space and time coordinates, the Ritz method in conjunction with the Classical Laminated Plate Theory (CLPT) and then the First-order Shear Deformation Theory (FSDT) is used to obtain the system's mass and stiffness matrices for out-of-plane bending vibration. The natural frequencies and mode shapes are determined. Afterward, the forced vibration response to harmonic loadings of the plates are determined by using the assumed modes method using the mass and stiffness matrices along with the corresponding natural frequencies and mode shapes obtained from the free vibration analysis. Several distributed line loads are considered for the forced vibration analysis of the plates with and without damping. Then, the demonstration of solution accuracy is performed by comparing the results obtained in free and forced vibration analysis, with the solutions available in literature and the solution based on the Finite Element Method using ANSYS®. Moreover, hybrid (uniform thick – taper – uniform thin) laminated composite plates are studied for the effects of taper length and taper angle on the amplitudes of the maximum deflections of these plates.

## **ACKNOWLEDGEMENT**

Foremost, I would like to express my sincere gratitude to my dear parents Mrs. Shahnaz Karagahi and Mr. Abdolreza Arab for all their love, encouragement and support.

I would also wish to offer my special thanks of gratitude to my supervisor, Professor Rajamohan Ganesan, who has supported me throughout the research with his enthusiasm and immense knowledge.

I gratefully acknowledge the financial support provided by my supervisor and Concordia University, for my Master thesis.

I am thankful to all my friends at graduate research office EV 13.167 at Concordia University.

Thanks for all the encouragement.



## Table of Contents

---

ABSTRACT .....	iii
ACKNOWLEDGEMENT .....	iv
List of Figure .....	viii
List of Tables .....	xiii
Nomenclature .....	xiv
 <b>Chapter 1 : Introduction .....</b>	<b>1</b>
1.1 Vibration analysis .....	1
1.2 Free vibration .....	1
1.3 Forced vibration .....	2
1.4 Ritz Method .....	2
1.5 Composite materials.....	3
1.6 Tapered laminates .....	4
1.7 Literature survey .....	5
1.7.1 Free vibration .....	5
1.7.2 Forced vibration .....	7
1.8 Objectives of the thesis .....	8
1.9 Layout of the thesis .....	9
 <b>Chapter 2 : Free vibration analysis of tapered composite plates .....</b>	<b>11</b>
2.1 Introduction.....	11
2.2 Taper configurations .....	12
2.3 Stress and strain transformations .....	13
2.4 CLPT and FSDT .....	20

2.5 Strain and kinetic energies .....	26
2.5.1 Derivations .....	26
2.5.2 Matrices $[Z_\epsilon]$ and $[Z_u]$ .....	30
2.6 Stiffness and mass matrices .....	31
2.7 Rayleigh-Ritz formulation .....	34
2.8 Boundary conditions .....	37
2.9 Software limitation.....	41
2.10 Validation.....	42
2.10.1 Uniform composite plate.....	42
2.10.2 Solution using Finite Element Method (FEM) .....	43
2.10.3 Layer reduction test.....	45
2.11 Number of terms of the shape function and the accuracy of the calculation.....	52
2.12 Numerical results and discussion.....	55
2.13 Conclusion .....	64
 <b>Chapter 3 : Forced vibration analysis of tapered composite plates .....</b>	<b>66</b>
3.1 Introduction.....	66
3.2 Forced vibration response based on CLPT .....	66
3.2.1 Undamped forced vibration .....	67
3.2.2 Forced vibration with viscous damping.....	70
3.3 Loading types.....	72
3.4 Validation.....	75
3.4.1 Isotropic plate.....	75
3.4.2 Composite plate .....	76
3.4.3 Layer reduction test.....	81
3.5 Maximum deflection and excitation frequency .....	89
3.6 Numerical results .....	94
3.7 Conclusion .....	107

<b>Chapter 4 : Tapered composite plates with hybrid configuration .....</b>	<b>109</b>
4.1 Introduction.....	109
4.2 Hybrid configurations .....	110
4.3 Free vibration analysis of the hybrid plates .....	111
4.4 Forced vibration analysis of the hybrid plates .....	115
4.5 Conclusion .....	119
<b>Chapter 5 : Conclusion.....</b>	<b>120</b>
5.1 Contribution .....	120
5.2 Conclusion .....	121
5.3 Recommendations for future works.....	123
<b>References .....</b>	<b>125</b>
<b>Appendix A.....</b>	<b>130</b>
<b>Appendix B .....</b>	<b>139</b>

## List of Figures

---

<b>Figure 2.1</b> Taper configurations and the global coordinate system .....	12
<b>Figure 2.2</b> Rotation of a coordinate system about an axis .....	14
<b>Figure 2.3</b> Global and local coordinate systems .....	15
<b>Figure 2.4</b> Identical laminates considered for layer reduction test (no ply drop-off) .....	46
<b>Figure 2.5</b> Step 1: 2 plies dropped-off .....	46
<b>Figure 2.6</b> Step 2: 4 plies dropped-off .....	46
<b>Figure 2.7</b> Step 3: 6 plies dropped-off .....	46
<b>Figure 2.8</b> Step 4: 8 plies dropped-off .....	47
<b>Figure 2.9</b> Step 5: 10 plies dropped-off.....	47
<b>Figure 2.10</b> Step 6: 12 plies dropped-off .....	47
<b>Figure 2.11</b> Step 7: 14 plies dropped-off .....	47
<b>Figure 2.12</b> Step 8: 16 plies dropped-off .....	47
<b>Figure 2.13</b> Step 9: 18 plies dropped-off .....	48
<b>Figure 2.14</b> Step 10: 20 plies dropped-off .....	48
<b>Figure 2.15</b> Step 11: 22 plies dropped-off .....	48
<b>Figure 2.16</b> Step 12: 24 plies dropped-off .....	48
<b>Figure 2.17</b> The variation of fundamental frequencies of the thick, thin and tapered laminates with increase of dropped layers (CLPT and FSDT) .....	51
<b>Figure 2.18</b> Influence of I and J values on natural frequency calculation (configuration B, SSSS) .....	53
<b>Figure 2.19</b> Influence of I and J values on natural frequency calculation (configuration B, CCCC) .....	53
<b>Figure 2.20</b> Influence of I and J values on natural frequency calculation (configuration B, CCFF) .....	54
<b>Figure 2.21</b> Frequency ratio ${}_F \omega_{11} / {}^c \omega_{11}$ for different lengths of the taper configuration A .....	59

<b>Figure 2.22</b> Frequency ratio $^F \omega_{11} / ^c \omega_{11}$ for different lengths of the taper configuration D.....	60
<b>Figure 2.23</b> CLPT-based and FSDT-based fundamental frequencies for different boundary conditions and lengths (configuration A) .....	61
<b>Figure 2.24</b> CLPT-based and FSDT-based fundamental frequencies for different boundary conditions and lengths (configuration D) .....	62
<b>Figure 2.25</b> Two uniform laminates of same thickness and with difference in internal structure	63
<b>Figure 3.1</b> Line load type 1 .....	73
<b>Figure 3.2</b> Line load type 2 .....	74
<b>Figure 3.3</b> Line load type 3 .....	74
<b>Figure 3.4</b> Line load type 4 .....	74
<b>Figure 3.5</b> Deflection at the center of the laminate over time due to transverse sinusoidal excitation .....	80
<b>Figure 3.6</b> Layer reduction test in forced vibration analysis (no ply drop-off).....	82
<b>Figure 3.7</b> Layer reduction test in forced vibration analysis (step 1: 2 plies dropped-off).....	83
<b>Figure 3.8</b> Layer reduction test in forced vibration analysis (step 2: 4 plies dropped-off).....	83
<b>Figure 3.9</b> Layer reduction test in forced vibration analysis (step 3: 6 plies dropped-off).....	84
<b>Figure 3.10</b> Layer reduction test in forced vibration analysis (step 4: 8 plies dropped-off).....	84
<b>Figure 3.11</b> Layer reduction test in forced vibration analysis (step 5: 10 plies dropped-off).....	85
<b>Figure 3.12</b> Layer reduction test in forced vibration analysis (step 6: 12 plies dropped-off).....	85
<b>Figure 3.13</b> Layer reduction test in forced vibration analysis (step 7: 14 plies dropped-off).....	86
<b>Figure 3.14</b> Layer reduction test in forced vibration analysis (step 8: 16 plies dropped-off).....	86
<b>Figure 3.15</b> Layer reduction test in forced vibration analysis (step 9: 18 plies dropped-off).....	87
<b>Figure 3.16</b> Layer reduction test in forced vibration analysis (step 10: 20 plies dropped-off)....	87
<b>Figure 3.17</b> Layer reduction test in forced vibration analysis (step 11: 22 plies dropped-off)....	88
<b>Figure 3.18</b> Layer reduction test in forced vibration analysis (step 12: 24 plies dropped-off)....	88
<b>Figure 3.19</b> Effect of excitation frequency on maximum deflection (configuration A, SSSS) ...	90

<b>Figure 3.20</b>	Effect of excitation frequency on maximum deflection (configuration B, SSSS)....	90
<b>Figure 3.21</b>	Effect of excitation frequency on maximum deflection (configuration C, SSSS)....	90
<b>Figure 3.22</b>	Effect of excitation frequency on maximum deflection (configuration D, SSSS) ...	91
<b>Figure 3.23</b>	Effect of excitation frequency on maximum deflection (configuration A, CCCC)..	91
<b>Figure 3.24</b>	Effect of excitation frequency on maximum deflection (configuration B, CCCC)..	91
<b>Figure 3.25</b>	Effect of excitation frequency on maximum deflection (configuration C, CCCC)..	92
<b>Figure 3.26</b>	Effect of excitation frequency on maximum deflection (configuration D, CCCC)..	92
<b>Figure 3.27</b>	Effect of excitation frequency on maximum deflection (configuration A, CCFF) ..	92
<b>Figure 3.28</b>	Effect of excitation frequency on maximum deflection (configuration B, CCFF)...	93
<b>Figure 3.29</b>	Effect of excitation frequency on maximum deflection (configuration C, CCFF)...	93
<b>Figure 3.30</b>	Effect of excitation frequency on maximum deflection (configuration D, CCFF) ..	93
<b>Figure 3.31</b>	Configuration A, SSSS, loading type 1 .....	99
<b>Figure 3.32</b>	Configuration B, SSSS, loading type 1 .....	99
<b>Figure 3.33</b>	Configuration C, SSSS, loading type 1 .....	99
<b>Figure 3.34</b>	Configuration D, SSSS, loading type 1 .....	99
<b>Figure 3.35</b>	Configuration A, CCCC, loading type 1 .....	99
<b>Figure 3.36</b>	Configuration B, CCCC, loading type 1 .....	99
<b>Figure 3.37</b>	Configuration C, CCCC, loading type 1 .....	100
<b>Figure 3.38</b>	Configuration D, CCCC, loading type 1 .....	100
<b>Figure 3.39</b>	Configuration A, CCFF, loading type 1 .....	100
<b>Figure 3.40</b>	Configuration B, CCFF, loading type 1 .....	100
<b>Figure 3.41</b>	Configuration C, CCFF, loading type 1 .....	100
<b>Figure 3.42</b>	Configuration D, CCFF, loading type 1 .....	100
<b>Figure 3.43</b>	Configuration A, SSSS, loading type 2 .....	101
<b>Figure 3.44</b>	Configuration B, SSSS, loading type 2 .....	101
<b>Figure 3.45</b>	Configuration C, SSSS, loading type 2 .....	101

<b>Figure 3.46</b> Configuration D, SSSS, loading type 2 .....	101
<b>Figure 3.47</b> Configuration A, CCCC, loading type 2 .....	101
<b>Figure 3.48</b> Configuration B, CCCC, loading type 2.....	101
<b>Figure 3.49</b> Configuration C, CCCC, loading type 2.....	102
<b>Figure 3.50</b> Configuration D, CCCC, loading type 2 .....	102
<b>Figure 3.51</b> Configuration A, CCFF, loading type 2 .....	102
<b>Figure 3.52</b> Configuration B, CCFF, loading type 2 .....	102
<b>Figure 3.53</b> Configuration C, CCFF, loading type 2 .....	102
<b>Figure 3.54</b> Configuration D, CCFF, loading type 2 .....	102
<b>Figure 3.55</b> Configuration A, SSSS, loading type 3 .....	103
<b>Figure 3.56</b> Configuration B, SSSS, loading type 3 .....	103
<b>Figure 3.57</b> Configuration C, SSSS, loading type 3 .....	103
<b>Figure 3.58</b> Configuration D, SSSS, loading type 3 .....	103
<b>Figure 3.59</b> Configuration A, CCCC, loading type 3 .....	103
<b>Figure 3.60</b> Configuration B, CCCC, loading type 3.....	103
<b>Figure 3.61</b> Configuration C, CCCC, loading type 3.....	104
<b>Figure 3.62</b> Configuration D, CCCC, loading type 3 .....	104
<b>Figure 3.63</b> Configuration A, CCFF, loading type 3 .....	104
<b>Figure 3.64</b> Configuration B, CCFF, loading type 3 .....	104
<b>Figure 3.65</b> Configuration C, CCFF, loading type 3 .....	104
<b>Figure 3.66</b> Configuration D, CCFF, loading type 3 .....	104
<b>Figure 3.67</b> Configuration A, SSSS, loading type 4 .....	105
<b>Figure 3.68</b> Configuration B, SSSS, loading type 4 .....	105
<b>Figure 3.69</b> Configuration C, SSSS, loading type 4 .....	105
<b>Figure 3.70</b> Configuration D, SSSS, loading type 4 .....	105
<b>Figure 3.71</b> Configuration A, CCCC, loading type 4 .....	105

<b>Figure 3.72</b> Configuration B, CCCC, loading type 4.....	105
<b>Figure 3.73</b> Configuration C, CCCC, loading type 4.....	106
<b>Figure 3.74</b> Configuration D, CCCC, loading type 4 .....	106
<b>Figure 3.75</b> Configuration A, CCFF, loading type 4 .....	106
<b>Figure 3.76</b> Configuration B, CCFF, loading type 4 .....	106
<b>Figure 3.77</b> Configuration C, CCFF, loading type 4 .....	106
<b>Figure 3.78</b> Configuration D, CCFF, loading type 4 .....	106
<b>Figure 4.1</b> Hybrid (uniform-tapered-uniform) Configurations .....	110
<b>Figure 4.2</b> Fundamental frequency (rad/s) variation with increase in taper angle $\varphi$ (configuration $A^h$ ).....	113
<b>Figure 4.3</b> Fundamental frequency (rad/s) variation with increase in taper angle $\varphi$ (configuration $B^h$ ).....	114
<b>Figure 4.4</b> Fundamental frequency (rad/s) variation with increase in taper angle $\varphi$ (configuration $C^h$ ).....	114
<b>Figure 4.5</b> Fundamental frequency (rad/s) variation with increase in taper angle $\varphi$ (configuration $D^h$ ).....	114
<b>Figure 4.6</b> Maximum deflection at the center for different taper angles (configuration $A^h$ ).....	117
<b>Figure 4.7</b> Maximum deflection at the center for different taper angles (configuration $B^h$ ).....	117
<b>Figure 4.8</b> Maximum deflection at the center for different taper angles (configuration $C^h$ ).....	117
<b>Figure 4.9</b> Maximum deflection at the center for different taper angles (configuration $D^h$ ).....	118



## List of Tables

---

<b>Table 2.1</b> Direction cosines for rotation about axis $R$ .....	13
<b>Table 2.2</b> Direction cosines corresponding to taper angle $\varphi$ .....	17
<b>Table 2.3</b> Mechanical properties of NCT-301 Graphite-Epoxy ply and resin [26] .....	20
<b>Table 2.4</b> Boundary conditions for the plates .....	38
<b>Table 2.5</b> Appropriate series for SSSS.....	39
<b>Table 2.6</b> Appropriate series for CCCC .....	39
<b>Table 2.7</b> Appropriate series for CCFF .....	40
<b>Table 2.8</b> Comparison between Finite Element Method and Ritz Method Solutions.....	44
<b>Table 2.9</b> Fundamental frequency values for the laminates from layer reduction test .....	49
<b>Table 2.10</b> Difference between the fundamental frequencies obtained based on CLPT and FSDT .....	50
<b>Table 2.11</b> Fundamental frequency ( $rad/s$ ) values of tapered composite plates for different lengths and taper angles for configurations A and B.....	56
<b>Table 2.12</b> Fundamental frequency ( $rad/s$ ) values of tapered composite plates for different lengths and taper angles for configurations C and D.....	57
<b>Table 2.13</b> Fundamental frequency ( $rad/s$ ) values of tapered composite plates for different lengths and taper angles.....	58
<b>Table 3.1</b> Four types of loading .....	73
<b>Table 3.2</b> Comparison between assumed modes method, Galerkin method and Exact solutions	76
<b>Table 3.3</b> Maximum deflection (mm) at the center for all taper configurations and BCs .....	95
<b>Table 3.4</b> Maximum deflection (mm) at the center for all taper configurations and BCs .....	96
<b>Table 3.5</b> Maximum deflection (mm) at the center for all taper configurations and BCs .....	97
<b>Table 4.1</b> Lengths (cm) of laminate parts corresponding to different taper angles .....	112
<b>Table 4.2</b> Fundamental frequency (rads) of the hybrid plates.....	112
<b>Table 4.3</b> Maximum deflection (mm) at the center of the laminates due to transverse excitation .....	116

## Nomenclature

---

$[C]$	Stiffness matrix
$C_{ij}$	Element $ij$ of the stiffness matrix
$[S]$	Compliance matrix
$S_{ij}$	Element $ij$ of the Compliance matrix
$[Q]^{[k]}$	Reduced stiffness matrix of the $k$ th layer
$Q_{ij}^{[k]}$	Element $ij$ of the reduced stiffness matrix of the $k$ th layer
$\alpha$	An arbitrary angle
$R$	An arbitrary axis along which rotation occurs by an arbitrary angle $\alpha$
$^-R$	The previous axis to the $R$
$^+R$	The next axis to the $R$
$R'$	Axis $R$ after rotation along itself
$^-R'$	The previous axis to the $R'$
$^+R'$	The next axis to the $R'$
$l_1$	Direction cosines between $^-R'$ and $^-R$
$l_2$	Direction cosines between $^-R'$ and $R$
$l_3$	Direction cosines between $^-R'$ and $^+R$
$m_1$	Direction cosines between $R'$ and $^-R$
$m_2$	Direction cosines between $R'$ and $R$
$m_3$	Direction cosines between $R'$ and $^+R$
$n_1$	Direction cosines between $^+R'$ and $^-R$
$n_2$	Direction cosines between $^+R'$ and $R$
$n_3$	Direction cosines between $^+R'$ and $^+R$

$\varphi$	Taper Angle
$\theta$	Orientation of the plies
$xyz$	Global coordinate system
$x''y''z''$	Local Coordinate system
$\varepsilon_{ij}$	Normal strain, $i = j$
$\gamma_{ij}$	Shear strain, $i \neq j$
$\sigma_{ij}$	Normal stress, $i = j$
$\tau_{ij}$	Shear stress, $i \neq j$
$[\varepsilon]$	Strain vector
$[\sigma]$	Stress vector
$[\varepsilon]_{new}$	Strain vector in the rotated coordinate system
$[\sigma]_{new}$	Stress vector in the rotated coordinate system
$[\varepsilon]_{old}$	Strain vector in the original coordinate system
$[\sigma]_{old}$	Stress vector in the original coordinate system
$[T_{\sigma\alpha}]$	Stress transformation matrix due to angle $\alpha$
$[T_{\varepsilon\alpha}]$	Strain transformation matrix due to angle $\alpha$
$[ \quad ]^T$	Transpose of the matrix
$E_1$	Modulus of elasticity in fiber direction
$E_2$	Modulus of elasticity in transverse direction
$E$	Modulus of elasticity of resin
$\nu_{ij}$	Poisson ratio of a ply
$\nu$	Poisson ratio of resin
$G_{23}$	Out-of-Plane shear modulus

$G_{12}$	In-Plane shear modulus
$G$	Shear modulus of resin
$\rho_p$	Density of a ply
$\rho_r$	Density of resin
$u$	Displacement in $x$ direction
$v$	Displacement in $y$ direction
$L$	Length of the laminate
$h$	Thickness of the laminate
$w$	Displacement in $z$ direction
$u_o$	Mid-plane displacement in $x$ direction
$v_o$	Mid-plane displacement in $y$ direction
$w_o$	Mid-plane displacement in $z$ direction
$^c[u]$	Displacement vector based on CLPT
$_F[u]$	Displacement vector based on FSDT
$^c[\varepsilon]$	Strain vector based on CLPT
$_F[\varepsilon]$	Strain vector based on FSDT
$\varphi_x$	Rotation of transverse normal on mid-plane about $x$ axis
$\varphi_y$	Rotation of transverse normal on mid-plane about $y$ axis
$^cU$	Strain energy based on CLPT
$_F U$	Strain energy based on FSDT
$^cT$	Kinetic energy based on CLPT
$_F T$	Kinetic energy based on FSDT
$[K]$	Stiffness matrix of the plate

$[\sigma]$	Mass matrix of the plate
$\omega_{ij}$	The $ij$ th natural frequency of the plate
$\Omega$	Excitation frequency
$A_{ij}^{w_o}$	The $ij$ th parameter with which $w_o$ is expressed in series
$A_{ij}^{\varphi_x}$	The $ij$ th parameter with which $\varphi_x$ is expressed in series
$A_{ij}^{\varphi_y}$	The $ij$ th parameter with which $\varphi_y$ is expressed in series
$R_{ij}^{(1)}$	The $ij$ th element of extensional stiffness matrix
$R_{ij}^{(2)}$	The $ij$ th element of bending-extension coupling matrix
$R_{ij}^{(3)}$	The $ij$ th element of bending stiffness matrix
$k_o$	Total number of the layer within the laminate
$z_{(u_k)}$	$z$ - coordinate of the upper surface for the $k$ th layer
$z_{(l_k)}$	$z$ - coordinate of the lower surface for the $k$ th layer
$W$	Virtual work of non-conservative forces
$f$	Transverse excitation applied to the laminate
$p_o$	Excitation magnitude
$\Omega$	Excitation frequency
$w_o^F$	Transverse deflection function in forced vibration analysis
$D$	Flexural rigidity
$a$	Length of the plate
$b$	Width of the plate
$P_{ij}$	Parameters of the series with which the transverse loading is expressed
$e_{ij}$	Constant parameter of an ODE solution
$e'_{ij}$	Constant parameter of an ODE solution

# **Chapter 1 :**

## **Introduction**

### **1.1 Vibration analysis**

Vibration is a mechanical phenomenon in which oscillatory motions of bodies with associated forces occur about equilibrium points. In general, vibrations are undesired as they are responsible for wasting energy, creating noise and poor performance of mechanical, structural and mechatronic systems. Unfortunately, they are capable of creating devastating effects on the efficiency and/or operating lifetime of the machine components and structures. Vibration may cause fatigue, the most common failure mechanism in mechanical structures, and in some cases lead to catastrophic failure. Therefore, developing efficient methods for eliminating this phenomenon has always been a major research interest.

### **1.2 Free vibration**

Free vibration analysis is a well-known topic and a key component in the analysis of forced vibrations. In addition, another reason behind the importance of the free vibration analysis is to avoid resonance. Free vibration is a phenomenon in which a mechanical system is set in motion by initial displacement and/or velocity in the absence of any external forces. In this kind of oscillations, the total energy, and consequently, the amplitude of vibration stays the same if there is no damping. In practice, amplitude eventually decays away to zero due to the dissipation of energy (damping effect).

The term free vibration, also known as natural vibration, is always associated with natural frequency, the frequency with which a free vibrating system oscillates. A system may have several natural frequencies while the system is allowed to vibrate solely with one natural frequency at a time. The lowest natural frequency of an oscillatory system is called fundamental frequency which is usually the most important one in the analysis. For any natural frequency, there exists a normal mode or mode shape, a pattern of motion in which all parts of the system move with the same frequency.

### **1.3 Forced vibration**

In contrast to free vibration which, once started, is left alone, forced vibration occurs when a system is continuously driven by external stimulus. This external excitation can be a periodic and steady-state, a transient or a random input. In general, two types of forced vibration, deterministic and non-deterministic referred to as random, are defined. A deterministic vibration is the one that can be characterized precisely, whereas a random vibration is merely analyzed statistically. An example of deterministic vibration is that due to an applied load varying sinusoidally called harmonic loading. Harmonic excitation is often encountered in engineering systems. It is also commonly produced by the unbalance in rotating machinery. A phenomenon called resonance occurs in a system when the frequency of dynamic periodic load and the frequency of free vibration of the system coincide. Specifically, resonance occurs when the frequency of the applied force coincides with one of the natural frequencies of the driven system. In this coincidence, periodic excitation optimally transfers the energy to the system so that the amplitude with which the system vibrates, increases gradually until the system is damaged. Obvious examples of forced vibration include the vibration of the floor of a factory due to the running heavy machineries or the vibration of a building during an earthquake.

### **1.4 Ritz Method**

Differential equations originating from Newton's law and governing a vibrating system are the key components in solving a vibration problem. However, depending on the problem, solving the governing differential equations of a mechanical system can be a complicated task or in some cases, the exact analytical solution for the equations is not available. Due to the taper configuration of the laminated composite plates, the coefficients of the governing partial differential equations are expected to be functions of  $x$  (the direction of the taper) such that solving the differential equations is quite complicated if not impossible. Therefore, numerical methods of analysis provide the alternative methods for finding the solutions. The Ritz method referred to as classical variational method, one of the most powerful of existing techniques for the approximate analytical and numerical solution of functional equations, offers the alternative method to overcome the problem and typically has been used in the literature.

Lord Rayleigh was an English Physicist, published his renowned book “Theory of Sound” in 1877. He explained the calculation method to determine the fundamental natural frequency of a continuous system such as strings, bars, beams, membranes and plates in his book. The principle of Rayleigh’s method is based on assuming the mode shape and equating the maximum potential and kinetic energies in a cycle of motion, Ref. [1].

In 1908, Walter Ritz used the principle of multiple admissible displacement functions to determine the frequencies and mode shapes of any structural member. He demonstrated his method by determining the natural frequency of a completely free square plate. Consequently, Rayleigh used the same principle in his book and another publication. After a while, many researchers used this method, some calling it the ‘Ritz method’ and others, the ‘Rayleigh-Ritz’ method, Ref. [1].

The Ritz method has gained popularity in the last few decades to accurately determine the natural frequencies and mode shapes of vibration of continuous systems, especially if the exact solution is not available. This method became more applicable after the discovery of digital computer. The success of this method in a boundary value problem or in an eigenvalue problem depends on accurately assuming the solution in the form of series of approximate displacement functions which must satisfy the geometric boundary conditions, Ref. [1].

In the present study, the Ritz method is used to solve the eigenvalue problem of a tapered composite plate in natural vibration investigation.

## **1.5 Composite materials**

A composite material consists of an assemblage of two or more materials of different natures and allows us to obtain a material of which the set of performance characteristics such as high strength and high modulus to weight ratios, corrosion resistance, thermal properties, fatigue life and wear resistance and increased tolerance to damage is greater than that of the components taken separately, Refs. [2] and [3]. Fiber-reinforced composites (FRC) are lightweight materials and provide sufficient strength for carrying loadings. Therefore, in spite of high cost, they are used in aerospace components such as wings and fuselages. Weight reduction by use of tapered composite laminates in helicopter blades that rotate with high angular velocity (tip velocity of 200



m/s), results in less fuel consumption, and consequently, in longer operational range for the helicopter.

Carbon fiber is one of the most important high-performance fibers for military and aerospace applications. High-strength carbon fiber came out of the development laboratories in Japan, England, and the United States in the late 1960s. The initial fibers were very expensive (more than 400 to 500 dollars per pound) which limited their applications to high-value military aerospace and space systems. The results of early military composite development programs can be seen today in systems fielded by each of the military services. For example, more than 350 parts of the F-22 Raptor, accounting for 25 percent of the structural weight, are carbon-epoxy composites. But in the early 1970s, continuous processes were developed and the cost declined steadily over the next decade. The Air Force Materials Laboratory took the lead in U.S. government-sponsored material development and hardware demonstration. By the late 1970s, composite materials were used in the production of primary structures for military aircraft and missiles. These applications were followed by selective use in commercial aircraft. For 20 years, between 1969 and 1989, the carbon fiber industry had phenomenal technological success and double-digit annual growth in aerospace and defense industries, with additional use in sports equipment and some limited use in automotive and industrial applications. This growth attracted many large international companies into the industry. The vision was that continued growth in military and commercial aircraft use would be followed by a very large industrial market by the year 2000, Ref. [3].

## **1.6 Tapered laminates**

Due to outstanding mechanical properties, composite materials are widely used in industry and they come in various shapes and structures depending on the requirements. The tapered composite plates are popular in the aerospace industry and are used in manufacturing the structures such as rotor blades of helicopters or aircraft wings. Thickness reduction in tapered composites can be implemented by the termination of plies at different locations providing the tapered plate with customized-stiffness property which is an absent capability in uniform laminates. The initial application of tapered laminated composites dates back to mid-1980s when commercial and

military sectors demanded, elastically-customizable components with higher weight to stiffness ratio, Refs. [4], [5] and [6].

## **1.7 Literature survey**

In this section, a comprehensive literature survey is presented on the important studies carried out on the free and forced vibration response of uniform and thickness-tapered laminated composite plates, in some cases beams, and the application of the Ritz method in tapered composite plates. Before composite material is revealed, homogeneous materials were the main subjects for researchers to focus on, and engineers to build complex structures. When composites were introduced, due to unique mechanical properties, a lot of studies were completed on the material. The works that have been done on composite materials are mainly confined to uniform plates and there has been a limited amount of literature on the vibration analysis of thickness-tapered laminated composite plates, in spite of their applicability.

### **1.7.1 Free vibration**

There are lots of work done on natural vibration of uniform rectangular composite beams and plates using different approaches. In addition, some studies have been conducted on tapered composite beams and plates. This sub-section is dedicated to a review of these works.

By using stochastic Rayleigh-Ritz approach, Venini and Mariani, Ref. [7], studied the free vibrations of uncertain composite plates. Ganesan and Zabiholla, Ref. [8] analyzed the natural vibration response and buckling of uniform-width and thickness-tapered composite beams made of NCT-301 Graphite-Epoxy laminas using both conventional and advanced finite element methods based on CLPT and FSDT. Berthelot, Ref. [2], has found the exact solutions for the free vibrations of uniform laminated composite plates. Reddy, Ref. [9], Berthelot, Ref. [2], and Jones, Ref. [10], have found the exact solutions for the free vibrations of uniform laminated composite beams. Whitney, Ref. [11], analyzed the effect of boundary conditions on vibrations of uniform unsymmetrically laminated rectangular plates. Using Ritz method, Leissa and Baharlu, Ref. [12], developed a method for analysis of free vibration and buckling of uniform laminated composite plates with arbitrary boundary conditions. Natural frequencies and buckling stresses of uniform cross-ply laminated composite plates were investigated by Matsunaga, Ref. [13], considering the

effects of thickness change, shear deformation and rotary inertia. Wu and Chen, Ref. [14], by a higher-order theory of plate deformation, determined the natural frequencies and buckling loads of uniform laminated composite plates. Ganesan and Nabi, Ref. [15], based on FSDT, developed a general finite element formulation to study the natural vibration of laminated composite beams.

Bert and , Ref. [16], presented an analysis on varying-thickness thin rectangular plate with two opposite edges simply supported and general boundary conditions between the other two edges. The boundary conditions at these two edges may be quite general. For isotropic or especially orthotropic laminated plates, the derived solution method is capable of yielding highly accurate results with very small computational effort.

Malekzadeh, Ref. [17], has carried out large amplitude free vibration analysis of tapered Mindlin rectangular plates made of isotropic materials and with elastically restrained against rotation edges using differential quadrature method (DQM), and took advantage of direct iterative method to solve the nonlinear eigenvalue system of equations. The paper presents a parametric study on linearly and bi-linearly varying thickness plates.

An improved Fourier series method has been presented by Zhang *et al*, Ref. [18], for the free vibration analysis of the moderately thick uniform laminated composite rectangular plate with non-uniform boundary conditions. Under the framework, the displacement and rotation functions are generally sought, regardless of boundary conditions, in spectral form, as a double Fourier cosine series and three supplementary functions. All the series expansion coefficients are treated as the generalized coordinates and determined using the Ritz method. The authors claim that the method is capable to be applied universally to a wide spectrum of plate vibration problems involving different boundary conditions, varying material, and geometric properties while no modification is required for the basic functions.

Houmat, Ref. [19], studied the free vibration of variable stiffness laminated composite rectangular plates on the basis of three-dimensional elasticity theory combined with the  $p$ -version of the finite element method. Results are obtained for frequencies, modal displacements, and modal stresses of symmetric and anti-symmetric laminates with various boundary conditions. The frequencies predicted by the equivalent single-layer classical plate theory and first-order shear deformation theory show deviation from three-dimensional solutions.

### 1.7.2 Forced vibration

There are a lot of works done on free vibrations of plates and beams made of isotropic material or composite. However, studies on forced vibration of uniform beams and plates, particularly tapered ones, are remarkably less in numbers and many of them are confined to Finite Element Analysis.

Babu *et al*, Ref. [20], have investigated the free and forced transverse vibration characteristics of a tapered laminated thick composite plate due to harmonic excitation using finite element method based on First-order Shear Deformation Theory for three types of taper configurations considering rotary inertia effect. The study has been validated by experimental measurements and available literature. Eftakher, Ref. [21], investigated free and forced vibration of uniform-width thickness-tapered laminated composite beams using Ritz method by both conventional and advanced finite element formulations.

Reddy, Ref. [9], derived an analytical solution for uniform composite plates subjected to transverse loadings with all simply supported edges based on Classical Laminated Plate Theory. In the method, transverse excitation is expanded in Fourier series.

Kumar Gupta *et al*, Ref. [22], presented analysis of forced vibrations of non-homogeneous rectangular plate with linearly-varying thickness subjected to a uniformly distributed harmonic lateral load based on Classical Laminated Plate Theory. The non-homogeneity of the plate material is assumed to occur due to the linearly-changing density.

Babu *et al*, Ref. [23], also investigated the dynamic properties of three different configurations of the thickness tapered laminated composite plate with different boundary conditions using Finite Element Method based on Classical Laminated Plate Theory (CLPT) and studied dynamic response of free and forced vibration due to harmonic loading. Results obtained from computations have been compared with that of literature and experimental measurements in order to validate the study. The experimental measurements have been performed for CFFF and CFCF plates. The paper shows that dynamic properties of a composite plate could be tailored by dropping the plies.

Darabi and Ganesan, Ref. [24], investigated the dynamic instability of internally-thickness-tapered laminated composite plates subjected to harmonic in-plane loading based on non-linear vibration analysis. They considered the non-linear von Karman strains associated with large deflections and curvatures and examined the non-linear dynamic stability characteristics of symmetric cross-ply laminates with different taper configurations. In the paper, a comprehensive parametric study has been carried out to examine and compare the effects of the taper angles, magnitudes of both tensile and compressive in-plane loads and aspect ratios of the tapered plate including length-to-width and length-to-average-thickness ratios on the instability regions and the parametric resonance particularly the steady-state vibrations amplitude.

Seraj and Ganesan, Ref. [25], has conducted the dynamic instability analysis of doubly-tapered cantilever composite beams rotating with periodic rotational velocity for out-of-plane bending (flap), in-plane bending (lag) and axial vibrations. A comprehensive parametric study has been carried out to investigate the effects of taper configurations and various system parameters including mean rotational velocity, hub radius, double-tapering angles and stacking sequences, on the dynamic instability characteristics of the composite beam.

## **1.8 Objectives of the thesis**

The dynamic response of thickness-tapered laminated composite plates is concerned within the present thesis. The main objectives of the present study are the following:

1. To investigate the free vibration response of thickness-tapered laminated composite square plates using the Ritz method, based on Classical Laminated Plate Theory (CLPT) and First-order Shear Deformation Theory (FSDT) and to study the effects of taper angle, taper configuration and boundary conditions on the fundamental frequencies of the laminates.
2. To investigate the forced vibration response of undamped and damped thickness-tapered laminated composite square plates using assumed modes method and modal analysis approach and to study the effects of taper angle, taper configuration and boundary conditions on the transverse deflection amplitude of the plate.

3. To study the free and forced vibration response of laminated composite hybrid square plates using the formulations developed for the thickness-tapered laminated composite square plates.

## **1.9 Layout of the thesis**

The present chapter provides a brief introduction and literature survey on free and forced vibrations of thickness-tapered laminated composite plates.

In chapter 2, free vibration of thickness-tapered laminated composite plates using Ritz method based on Classical Laminated Plate Theory (CLPT) and First-order Shear Deformation Theory (FSDT) is analyzed. For demonstration, the obtained results are compared with that of available literature and the exact solution for the uniform laminate. Then, the layer reduction test is conducted to compare the fundamental frequency of the thickness-tapered laminated composite plates with the corresponding uniform thick and thin ones. A parametric study on laminate length, taper angle and laminate configurations for different boundary conditions is done and the obtained data based on CLPT and FSDT are displayed in the tables and compared by the graphs.

In chapter 3, forced vibration of thickness-tapered laminated composite plates is investigated based on assumed modes method and Multi Degree of Freedom System (MDOF) model using the natural frequencies, mode shapes, and mass and stiffness matrices determined in chapter 2. Then, the numerical results are validated using available literature as well as using the exact closed-form solution for the uniform laminate with all edges simply supported. The layer reduction test similar to that performed in chapter 2, is conducted on the transverse deflection of the tapered plates. The deflections of the thickness-tapered laminated composite plates due to applied line loads are plotted by the corresponding graphs for different taper configurations and boundary conditions.

In chapter 4, the free vibration analysis is carried out on the laminated composite hybrid square plates and based on that, the forced vibration response of the hybrid laminates due to transverse excitation is investigated and the obtained results are analyzed and discussed.

Chapter 5 provides an overall conclusion of the present work and some recommendations for the future works.

## **Chapter 2 :**

### **Free vibration analysis of tapered composite plates**

#### **2.1 Introduction**

Due to outstanding mechanical properties, composite laminates are increasingly used in industry and they come in various shapes and structures depending on the requirements. Tapered composite plates are popular in aerospace industry, i.e. in the structures such as rotor blades of helicopters or aircraft wings, wherein the thickness is gradually decreased towards the tip, tapered composite plates are used. Thickness reduction in tapered composites can be implemented by termination of plies at different locations providing the tapered plate with customized stiffness property which is an absent capability in uniform laminates.

Classical Laminated Plate theory known as CLPT based on ‘Kirchhoff Hypothesis’ is commonly used to model plate behavior. The ratio of the in-plane elastic modulus to the transverse shear modulus is large for composite plates and CLPT neglecting the transverse shear deformation is adequate for the analysis of the thin plates. However, for investigation of thick and moderately-thick plates, CLPT is unable to output a satisfying result, therefore, more advanced theories such as First-order Shear Deformation Theory (FSDT) developed by Reissner (1945) and Mindlin (1951) can be used to perform the analysis. Since this theory considers the transverse shear stresses, it is capable to produce more accurate results in comparison with CLPT.

In this chapter, free vibration analysis of tapered laminated composite plates with different configurations and boundary conditions is considered, based on CLPT and FSDT. Since exact closed-form solution cannot be obtained from the complex partial differential equation, the Ritz method is used to obtain the system’s mass and stiffness matrices and then natural frequencies, for out-of-plane bending vibration. Based on the theories, the stress and strain distributions determined in terms of fiber and taper angles are used to calculate kinetic and strain energies. Afterward, the natural frequencies and corresponding mode shapes are obtained by solving the eigenvalue problem obtained using the Ritz method. Then, the obtained result is compared with that available in literature and with Finite Element Analysis (ANSYS®) solution. A “layer reduction test” is also



carried out for concrete validation and to observe the fundamental frequency change with the increase in taper angle.

## 2.2 Taper configurations

In this section, four tapered composite laminated plate configurations are described on which analysis is carried out throughout the thesis. Similar taper configurations are commonly used in industry and have been studied in literature [3], [23], [34]. To provide a visual perception, these configurations are shown in Figure 2.1.

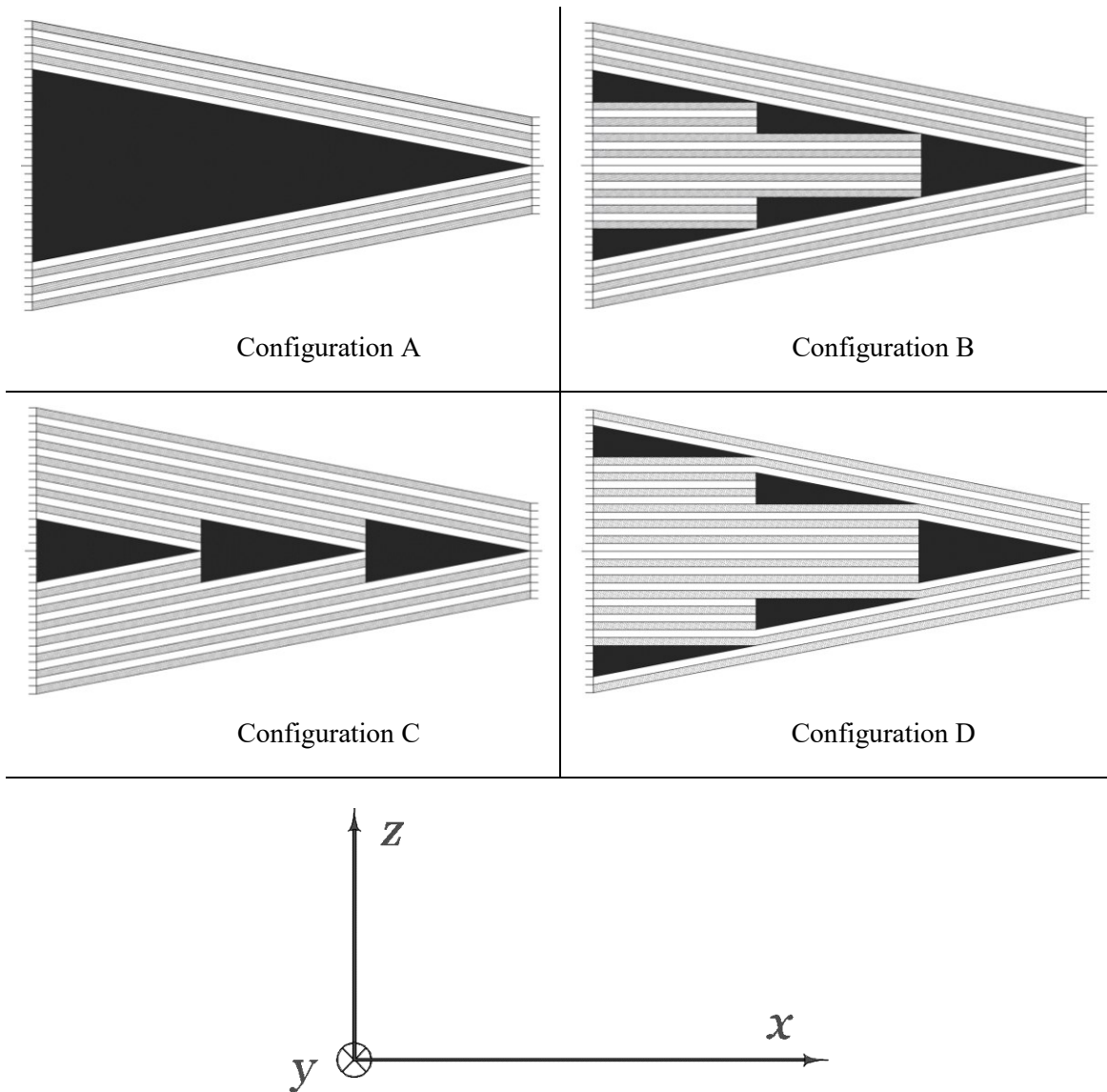


**Figure 2.1** Taper configurations and the global coordinate system

The tapered laminated square plates are considered with laminate configuration of  $(0/90)_{9s}$  and  $(0/90)_{3s}$  at the left and right ends, respectively, and to be made of resin and unidirectional NCT-301 Graphite-Epoxy material with ply thickness of  $125 \times 10^{-6}$  m. The lengths of the laminates are dependent on the taper angle. For each taper configuration, the study is carried out for different taper angles and boundary conditions that are introduced and explained in further sections.

### 2.3 Stress and strain transformations

Transformation of coordinate systems is a common problem in mechanics of materials. Here, the formulation for transformation of coordinate systems and the derivation corresponding to strains and stresses are performed according to Refs. [2] and [5] as a requirement for the vibration analysis.

The  $\bar{R} R^+ R$  coordinate system is considered according to the right-hand rule. If the axis about which rotation occurs by an arbitrary angle  $\gamma$  is called  $R$ , then, the direction cosines for the new (rotated) coordinate system  $\bar{R}' R'^+ R'$  with respect to the coordinate system  $\bar{R} R^+ R$ , are:

	$\bar{R}$	$R$	$^+R$
$\bar{R}'$	$\cos(\bar{R}, \bar{R}') = \cos(\gamma)$	$\cos(R, \bar{R}') = 0$	$\cos(^+R, \bar{R}') = -\sin(\gamma)$
$R'$	$\cos(\bar{R}, R') = 0$	$\cos(R, R') = 1$	$\cos(^+R, R') = 0$
$^+R'$	$\cos(\bar{R}, ^+R') = \sin(\gamma)$	$\cos(R, ^+R') = 0$	$\cos(^+R, ^+R') = \cos(\gamma)$

**Table 2.1** Direction cosines for rotation about axis  $R$

The Figure 2.2 shows the rotation of coordinate system  $\bar{R} R^+ R$  about axis  $R$  by an arbitrary angle  $\gamma$  and the new (rotated) coordinate system  $\bar{R}' R'^+ R'$ .

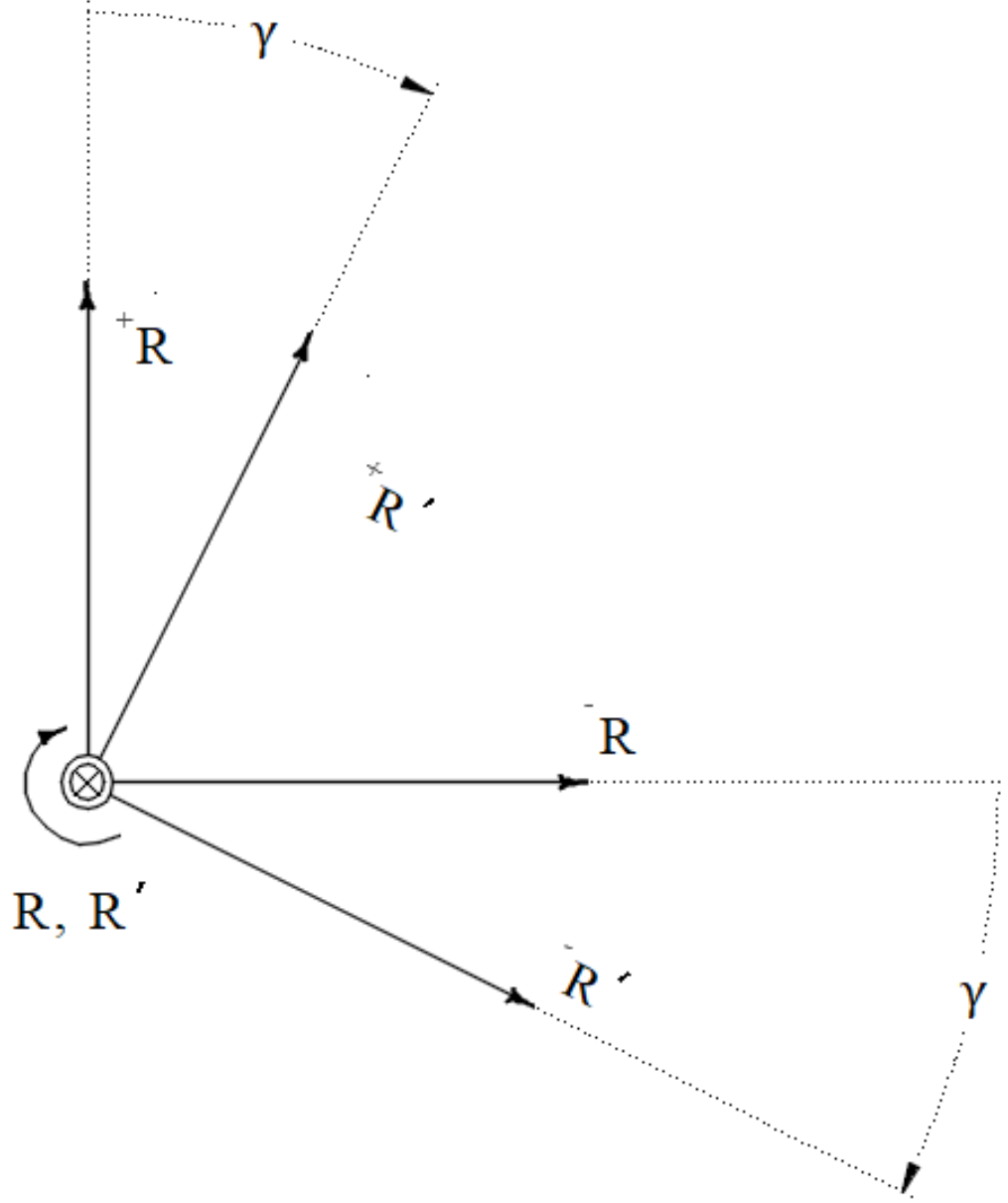


**Figure 2.2** Rotation of a coordinate system about an axis

Consider an arbitrary layer  $k$  from the tapered configurations shown by Figure 2.1. The local coordinate system  $x''y''z''$  is assumed on the layer  $k$ , with  $x''$  axis directed along the fiber orientation and  $z''$  perpendicular to the surface of the layer as shown in Figure 2.3. By taper angle  $\varphi$ , the global coordinate system  $xyz$  is rotated counterclockwise about the  $y$  axis to establish the coordinate system  $x'y'z'$ , and in turn,  $x'y'z'$  is rotated by fiber orientation angle  $\theta_k$

counterclockwise, about the  $z'$  axis, to correspond to local coordinate system  $x''y''z''$ . Figure 2.3 illustrates the coordinate systems  $xyz$ ,  $x'y'z'$  and  $x''y''z''$ .

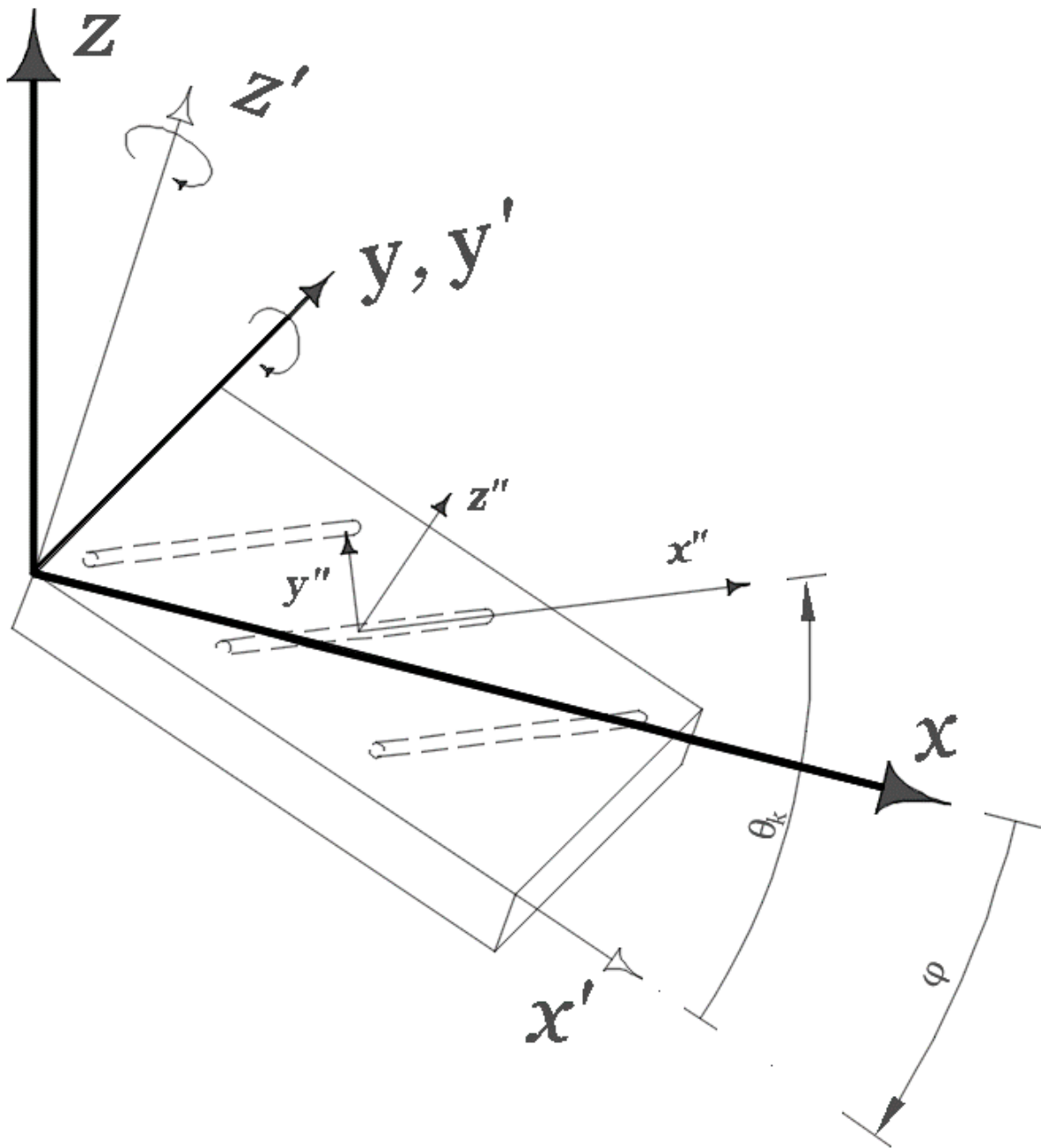


**Figure 2.3** Global and local coordinate systems

Transformation of stresses from the  $xyz$  coordinate system to the  $x'y'z'$  coordinate system is performed using transformation matrix  $[T_{\sigma\phi}]$ . In addition to  $[T_{\sigma\phi}]$ , this explanation corresponds

to strain transformation matrix  $[T_{\varepsilon\varphi}]$  in the same way. In equations (2.1) and (2.2), the stresses and strains in the  $xyz$  and  $x'y'z'$  coordinate systems are connected using transformation matrices  $[T_{\sigma\varphi}]$  and  $[T_{\varepsilon\varphi}]$ .

$$\begin{Bmatrix} \sigma_{x'x'} \\ \sigma_{y'y'} \\ \sigma_{z'z'} \\ \tau_{y'z'} \\ \tau_{x'z'} \\ \tau_{x'y'} \end{Bmatrix} = \begin{bmatrix} l_1^2 & l_2^2 & l_3^2 & 2l_2l_3 & 2l_1l_3 & 2l_1l_2 \\ m_1^2 & m_2^2 & m_3^2 & 2m_2m_3 & 2m_1m_3 & 2m_1m_2 \\ n_1^2 & n_2^2 & n_3^2 & 2n_2n_3 & 2n_1n_3 & 2n_1n_2 \\ m_1n_1 & m_2n_2 & m_3n_3 & m_3n_2 + m_2n_3 & m_3n_1 + m_1n_3 & m_2n_1 + m_1n_2 \\ l_1n_1 & l_2n_2 & l_3n_3 & l_3n_2 + l_2n_3 & l_3n_1 + l_1n_3 & l_2n_1 + l_1n_2 \\ l_1m_1 & l_2m_2 & l_3m_3 & l_3m_2 + l_2m_3 & l_3m_1 + l_1m_3 & l_2m_1 + l_1m_2 \end{bmatrix} \begin{Bmatrix} \sigma_{xx} \\ \sigma_{yy} \\ \sigma_{zz} \\ \tau_{yz} \\ \tau_{xz} \\ \tau_{xy} \end{Bmatrix} \quad (2.1)$$

$$\begin{Bmatrix} \varepsilon_{x'x'} \\ \varepsilon_{y'y'} \\ \varepsilon_{z'z'} \\ \gamma_{y'z'} \\ \gamma_{x'z'} \\ \gamma_{x'y'} \end{Bmatrix} = \begin{bmatrix} l_1^2 & l_2^2 & l_3^2 & l_2l_3 & l_1l_3 & l_1l_2 \\ m_1^2 & m_2^2 & m_3^2 & m_2m_3 & m_1m_3 & m_1m_2 \\ n_1^2 & n_2^2 & n_3^2 & n_2n_3 & n_1n_3 & n_1n_2 \\ 2m_1n_1 & 2m_2n_2 & 2m_3n_3 & m_3n_2 + m_2n_3 & m_3n_1 + m_1n_3 & m_2n_1 + m_1n_2 \\ 2l_1n_1 & 2l_2n_2 & 2l_3n_3 & l_3n_2 + l_2n_3 & l_3n_1 + l_1n_3 & l_2n_1 + l_1n_2 \\ 2l_1m_1 & 2l_2m_2 & 2l_3m_3 & l_3m_2 + l_2m_3 & l_3m_1 + l_1m_3 & l_2m_1 + l_1m_2 \end{bmatrix} \begin{Bmatrix} \varepsilon_{xx} \\ \varepsilon_{yy} \\ \varepsilon_{zz} \\ \gamma_{yz} \\ \gamma_{xz} \\ \gamma_{xy} \end{Bmatrix} \quad (2.2)$$

In equations (2.1) and (2.2), the elements within the transformation matrices are direction cosines for the coordinate systems  $xyz$  and  $x'y'z'$  given by Table 2.2. Depending on the axis about which rotation occurs, direction cosines are set according to Table 2.1.

	$x$	$y$	$z$
$x'$	$l_1 = \cos(\varphi)$	$l_2 = 0$	$l_3 = -\sin(\varphi)$
$y'$	$m_1 = 0$	$m_2 = 1$	$m_3 = 0$
$z'$	$n_1 = \sin(\varphi)$	$n_2 = 0$	$n_3 = \cos(\varphi)$

**Table 2.2** Direction cosines corresponding to taper angle  $\varphi$

The equations (2.1) and (2.2) are expressed in compact form.

$$\{\sigma'\} = [T_{\sigma\varphi}]\{\sigma\} \quad (2.3)$$

$$\{\varepsilon'\} = [T_{\varepsilon\varphi}]\{\varepsilon\} \quad (2.4)$$

The direction cosines in terms of  $\theta_k$  are expressed in a similar manner between the  $x'y'z'$  and  $x''y''z''$  coordinate systems and the corresponding transformation matrices are written.

$$[\sigma''] = [T_{\sigma\theta}][\sigma'] \quad (2.5)$$

$$[\varepsilon''] = [T_{\varepsilon\theta}][\varepsilon'] \quad (2.6)$$

In the local coordinate system  $x''y''z''$ , the stiffness  $[C'']$  and compliance  $[S'']$  matrices of a unidirectional ply considered as a transversely-isotropic material, according to Ref. [2], are expressed. It is noted that  $[C''] = [S'']^{-1}$ .

$$[C''] = \begin{bmatrix} C''_{11} & C''_{12} & C''_{12} & 0 & 0 & 0 \\ C''_{12} & C''_{22} & C''_{23} & 0 & 0 & 0 \\ C''_{12} & C''_{23} & C''_{22} & 0 & 0 & 0 \\ 0 & 0 & 0 & \frac{C''_{22} - C''_{23}}{2} & 0 & 0 \\ 0 & 0 & 0 & 0 & C''_{66} & 0 \\ 0 & 0 & 0 & 0 & 0 & C''_{66} \end{bmatrix} \quad (2.7)$$

$$[S''] = \begin{bmatrix} S''_{11} & S''_{12} & S''_{12} & 0 & 0 & 0 \\ S''_{12} & S''_{22} & S''_{23} & 0 & 0 & 0 \\ S''_{12} & S''_{23} & S''_{22} & 0 & 0 & 0 \\ 0 & 0 & 0 & 2[S''_{22} - S''_{23}] & 0 & 0 \\ 0 & 0 & 0 & 0 & S''_{66} & 0 \\ 0 & 0 & 0 & 0 & 0 & S''_{66} \end{bmatrix} \quad (2.8)$$

Considering equations (2.7) and (2.8), according to Ref. [2], the elements within the transformation matrices are as follows.

$$S''_{11} = 1/E_{x''} \quad (2.9)$$

$$S''_{12} = -(v_{x''y''}/E_{x''}) \quad (2.10)$$

$$S''_{22} = 1/E_{y''} \quad (2.11)$$

$$S''_{23} = -(v_{y''z''}/E_{y''}) \quad (2.12)$$

$$S''_{66} = 1/G_{x''y''} \quad (2.13)$$

Within a coordinate system, the strains and stresses are connected by the stiffness or compliance matrices in the stress-strain equation. For the  $xyz$  and  $x''y''z''$  coordinate systems the stress-strain relations are expressed.

$$\{\sigma\} = [C]\{\varepsilon\} \quad (2.14)$$

$$\{\sigma''\} = [C'']\{\varepsilon''\} \quad (2.15)$$

In local coordinate system  $x''y''z''$  when fibers of the  $k^{\text{th}}$  layer are oriented along the  $x''$  axis, the layer, according to Ref. [2] with fine approximation, is assumed as a transversely-isotropic material with stiffness  $[C'']$  and compliance  $[S'']$  matrices described by equation (2.7) and (2.8), respectively. In the global coordinate system  $xyz$ , the stiffness matrix  $[C]$  of the layer  $k$  with the fibers unparallel to the  $x$  axis is obtained in terms of  $[C'']$  and angles  $\varphi$  and  $\theta_k$ , using the equations (2.3) to (2.6) as well as equations (2.14) and (2.15).

$$[C] = [T_{\sigma\varphi}]^{-1}[T_{\sigma\theta}]^{-1}[C''] [T_{\varepsilon\theta}][T_{\varepsilon\varphi}] \quad (2.16)$$

In equation (2.16), the stiffness matrix  $[C]$  in the global coordinate system is calculated in terms of angles  $\varphi$  and  $\theta_k$  as well as  $[C'']$ , which is the stiffness matrix in local coordinate system  $x''y''z''$  containing the mechanical properties of the transversely-isotropic material (NCT-301 Graphite-Epoxy) ply  $k$ .



Mechanical properties of the unidirectional ply made of NCT-301 Graphite-Epoxy (considered as the transversely-isotropic material) and resin (the isotropic material) obtained experimentally, are given by Ref. [26].

Mechanical Properties of Unidirectional NCT-301 Graphite-Epoxy Ply			
$E_1 = 113.9 \text{ GPa}$	$G_{12} = 3.137 \text{ GPa}$	$\nu_{12} = 0.288$	$\rho_p = 1480 \text{ kg/m}^3$
$E_2 = 7.985 \text{ GPa}$	$G_{23} = 2.852 \text{ GPa}$	$\nu_{21} = 0.018$	
Mechanical Properties of Epoxy Resin			
$E = 3.93 \text{ GPa}$	$G = 1.034 \text{ GPa}$	$\nu = 0.37$	$\rho_r = 1000 \text{ kg/m}^3$

**Table 2.3** Mechanical properties of NCT-301 Graphite-Epoxy ply and resin [26]

The subscripts 1, 2 and 3 in Table 2.3 correspond to  $x''$ ,  $y''$  and  $z''$ , respectively, in local coordinate system  $x''y''z''$ .

## 2.4 CLPT and FSDT

Natural frequencies of the tapered plates are obtained using the Ritz method based on Classical Laminated Plate Theory (CLPT) and First-order Shear Deformation Theory (FSDT). In order to apply the Ritz method and to determine the natural frequencies, the stiffness and mass matrices are obtained from the calculation of displacements, strains and stresses expressed based on CLPT and FSDT.

Displacements based on FSDT are written as follows according to Ref. [2].

$${}_F u(x, y, z, t) = {}_F u_o(x, y, t) + \varphi_x(x, y, t)z \quad (2.17)$$

$${}_F v(x, y, z, t) = {}_F v_o(x, y, t) + \varphi_y(x, y, t)z \quad (2.18)$$

$${}_F w(x, y, z, t) = {}_F w_o(x, y, t) \quad (2.19)$$

where,  ${}_F u$ ,  ${}_F v$  and  ${}_F w$  are displacements in  $x$ ,  $y$  and  $z$  directions, respectively and  ${}_F u_o$ ,  ${}_F v_o$  and  ${}_F w_o$  are displacements of the point of the transverse normal on the midplane ( $z = 0$ ).  $\varphi_x$  and  $\varphi_y$  are rotations of the transverse normal at the midplane and left subscript  $F$  stands for FSDT. Considering the pure bending condition, ( ${}_F u_o = {}_F v_o = 0$ ) from equations (2.17) to (2.19), it is expressed that:

$${}_F u = \varphi_x Z \quad (2.20)$$

$${}_F v = \varphi_y Z \quad (2.21)$$

$${}_F w = {}_F w_o \quad (2.22)$$

Equations (2.20) to (2.22) are for displacements based on FSDT formulation considering the pure bending condition. Strains are directly obtained from equations (2.20) to (2.22) as follows.

$${}_F \varepsilon_x = \frac{\partial {}_F u}{\partial x} = \frac{\partial \varphi_x}{\partial x} Z \quad (2.23)$$

$${}_F \varepsilon_y = \frac{\partial {}_F v}{\partial y} = \frac{\partial \varphi_y}{\partial y} Z \quad (2.24)$$

$${}_F \gamma_{xy} = \frac{\partial ({}_F u)}{\partial y} + \frac{\partial ({}_F v)}{\partial x} = \left( \frac{\partial \varphi_x}{\partial y} + \frac{\partial \varphi_y}{\partial x} \right) Z \quad (2.25)$$

$${}_F \gamma_{yz} = \frac{\partial ({}_F v)}{\partial z} + \frac{\partial ({}_F w)}{\partial y} = \varphi_y + \frac{\partial ({}_F w_o)}{\partial y} \quad (2.26)$$

$${}_F \gamma_{xz} = \frac{\partial ({}_F u)}{\partial z} + \frac{\partial ({}_F w)}{\partial x} = \varphi_x + \frac{\partial ({}_F w_o)}{\partial x} \quad (2.27)$$

Equations (2.23) to (2.27) are for strains based on FSDT formulation considering the pure bending condition. In a similar manner, displacements are written based on CLPT and the strains are derived. Since CLPT neglects the transverse shear strains  $\gamma_{xz} = \gamma_{yz} = 0$ , considering the pure bending condition, strain equations (2.23) to (2.27) and displacement equations (2.20) to (2.22) for CLPT are simplified as follows.

$${}^c u = -\frac{\partial {}^c w_o}{\partial x} z \quad (2.28)$$

$${}^c v = -\frac{\partial {}^c w_o}{\partial y} z \quad (2.29)$$

$${}^c w = {}^c w_o \quad (2.30)$$

$${}^c \varepsilon_x = -\frac{\partial^2 ({}^c w_o)_o}{\partial x^2} z \quad (2.31)$$

$${}^c \varepsilon_y = -\frac{\partial^2 ({}^c w_o)}{\partial y^2} z \quad (2.32)$$

$${}^c \gamma_{xy} = -2 \frac{\partial^2 ({}^c w_o)}{\partial x \partial y} z \quad (2.33)$$

Equations (2.28) - (2.33) are for displacements and strains based on CLPT formulation considering the pure bending condition and left superscript  $C$  stands for CLPT. In order to facilitate the calculations of strain and kinetic energies, equations (2.20) to (2.27) based on FSDT and equations (2.28) to (2.33) based on CLPT, are written in the form of multiplication of matrices using the joint matrix  $\left\{ {}^c_F s \right\}$ . Equations (2.34) to (2.38) represent these matrices in a detailed form.

$$[{}^c Z_u]_{3 \times 12} = \begin{bmatrix} 0 & 0 & 0 & 0 & 0 & 0 & 0 & -z & 0 & 0 & 0 & 0 \\ 0 & 0 & 0 & 0 & 0 & 0 & 0 & 0 & -z & 0 & 0 & 0 \\ 0 & 0 & 0 & 0 & 0 & 0 & 1 & 0 & 0 & 0 & 0 & 0 \end{bmatrix}_{3 \times 12} \quad (2.34)$$

$$[{}^c Z_\varepsilon]_{3 \times 12} = \begin{bmatrix} 0 & 0 & 0 & 0 & 0 & 0 & 0 & 0 & 0 & z & 0 & 0 \\ 0 & 0 & 0 & 0 & 0 & 0 & 0 & 0 & 0 & 0 & z & 0 \\ 0 & 0 & 0 & 0 & 0 & 0 & 0 & 0 & 0 & 0 & 0 & z \end{bmatrix}_{3 \times 12} \quad (2.35)$$

$$[{}_F Z_u]_{3 \times 12} = \begin{bmatrix} z & 0 & 0 & 0 & 0 & 0 & 0 & 0 & 0 & 0 & 0 & 0 \\ 0 & 0 & 0 & z & 0 & 0 & 0 & 0 & 0 & 0 & 0 & 0 \\ 0 & 0 & 0 & 0 & 0 & 0 & 1 & 0 & 0 & 0 & 0 & 0 \end{bmatrix}_{3 \times 12} \quad (2.36)$$

$$[{}^F_Z\varepsilon]_{5 \times 12} = \begin{bmatrix} 0 & z & 0 & 0 & 0 & 0 & 0 & 0 & 0 & 0 & 0 & 0 \\ 0 & 0 & 0 & 0 & 0 & z & 0 & 0 & 0 & 0 & 0 & 0 \\ 0 & 0 & z & 0 & z & 0 & 0 & 0 & 0 & 0 & 0 & 0 \\ 0 & 0 & 0 & 1 & 0 & 0 & 0 & 0 & 1 & 0 & 0 & 0 \\ 1 & 0 & 0 & 0 & 0 & 0 & 0 & 1 & 0 & 0 & 0 & 0 \end{bmatrix}_{5 \times 12} \quad (2.37)$$

$$\left\{ {}^C_S \right\}_{12 \times 1} = \left[ {}^C_F \varphi_x \quad \frac{\partial {}^C_F \varphi_x}{\partial x} \quad \frac{\partial {}^C_F \varphi_x}{\partial y} \quad {}^C_F \varphi_y \quad \frac{\partial {}^C_F \varphi_y}{\partial x} \quad \frac{\partial {}^C_F \varphi_y}{\partial y} \quad {}^C_F w_o \quad \frac{\partial {}^C_F w_o}{\partial x} \quad \frac{\partial {}^C_F w_o}{\partial y} \quad -\frac{\partial^2 {}^C_F w_o}{\partial x^2} \quad -\frac{\partial^2 {}^C_F w_o}{\partial y^2} \quad -2\frac{\partial^2 {}^C_F w_o}{\partial x \partial y} \right]^T \quad (2.38)$$

The left subscript  $F$  and left superscript  $C$  indicate the FSDT-based and CLPT-based formulations. In relations similar to equation (2.38) which is written for FSDT and CLPT at the same time in combined form, the left subscript  $F$  and left superscript  $C$  are simultaneously present for all the corresponding notations meaning that for CLPT-based calculations, only the notation with left superscript  $C$ , and for FSDT-based calculations, only the notation with the left subscript  $F$  is considered. When notations are used specifically for either CLPT or FSDT, only the corresponding letter is used. It is noted that in CLPT-based formulation  ${}^C\varphi_x$  and  ${}^C\varphi_y$  are considered zero for  $\left\{ {}^C_S \right\}$  so that instead of  ${}_F\varphi_x$  and  ${}_F\varphi_y$ , notations  $\varphi_x$  and  $\varphi_y$  are considered in the present thesis. Equations (2.20) to (2.33) are expressed in closed matrix form using equations (2.34) to (2.38).

$$\left\{ {}^C_u \right\}_{3 \times 1} = [{}^C_Zu]_{3 \times 12} \left\{ {}^C_S \right\}_{12 \times 1} \quad (2.39)$$

$$\left\{ {}^C_\varepsilon \right\}_{3 \times 1} = [{}^C_Z\varepsilon]_{3 \times 12} \left\{ {}^C_S \right\}_{12 \times 1} \quad (2.40)$$

$$\left\{ {}_F u \right\}_{3 \times 1} = [{}_F Z u]_{3 \times 12} \left\{ {}_F S \right\}_{12 \times 1} \quad (2.41)$$

$$\left\{ {}_F \varepsilon \right\}_{5 \times 1} = [{}_F Z \varepsilon]_{5 \times 12} \left\{ {}_F S \right\}_{12 \times 1} \quad (2.42)$$

where,  $\left\{ {}^c u \right\}_{3 \times 1} = [{}^c u \quad {}^c v \quad {}^c w_o]^T$ ,  $\left\{ {}^c \varepsilon \right\}_{3 \times 1} = [{}^c \varepsilon_x \quad {}^c \varepsilon_y \quad {}^c \gamma_{xy}]^T$ ,  $\left\{ {}_F u \right\}_{3 \times 1} = [{}_F u \quad {}_F v \quad {}_F w_o]^T$  and  $\left\{ {}_F \varepsilon \right\}_{5 \times 1} = [{}_F \varepsilon_x \quad {}_F \varepsilon_y \quad {}_F \gamma_{xy} \quad {}_F \gamma_{yz} \quad {}_F \gamma_{xz}]^T$ . Equations (2.39) to (2.42) are written in the following form.

$$\left\{ {}^c u \right\} = [{}^c Z_u] \left\{ {}_F s \right\} \quad (2.43)$$

$$\left\{ {}^c \varepsilon \right\} = [{}^c Z_\varepsilon] \left\{ {}_F s \right\} \quad (2.44)$$

The explanation given for  $\left\{ {}^c s \right\}$  in equation (2.38), also corresponds to notations  $[{}^c Z_u]$  and  $[{}^c Z_\varepsilon]$  used in equations (2.43) and (2.44) respectively.  $[{}^c Z_u]$  and  $[{}^c Z_\varepsilon]$  are used in further sections for the computation of strain and kinetic energies.

The elements of stiffness matrix are calculated by substituting engineering constants from Table 2.3 into equation (2.16). Then, using stress-strain relationship the stresses are determined.

$$\begin{Bmatrix} \sigma_x \\ \sigma_y \\ \sigma_z \\ \tau_{yz} \\ \tau_{xz} \\ \tau_{xy} \end{Bmatrix}_k = \begin{bmatrix} C_{11} & C_{12} & C_{13} & C_{14} & C_{15} & C_{16} \\ C_{12} & C_{22} & C_{23} & C_{24} & C_{25} & C_{26} \\ C_{13} & C_{23} & C_{33} & C_{34} & C_{35} & C_{36} \\ C_{14} & C_{24} & C_{34} & C_{44} & C_{45} & C_{46} \\ C_{15} & C_{25} & C_{35} & C_{45} & C_{55} & C_{56} \\ C_{16} & C_{26} & C_{36} & C_{46} & C_{56} & C_{66} \end{bmatrix}_k \begin{Bmatrix} \varepsilon_x \\ \varepsilon_y \\ \varepsilon_z \\ \gamma_{yz} \\ \gamma_{xz} \\ \gamma_{xy} \end{Bmatrix}_k \quad (2.45)$$

In CLPT and FSDT, the out-of-plane normal stress is assumed to be small and negligible compared to other stress components. In addition, CLPT implements further assumptions and neglects the out-of-plane shears. By imposing these assumptions, the reduced stiffness matrix is computed and substituted in stress-strain equation (2.45). Calculation by which the reduced stiffness matrix is derived is available in Ref. [5] as well as in Appendix A.1 in compact form. Reduced stiffness matrix in CLPT-based formulation is expressed as:

$$\begin{Bmatrix} \sigma_x \\ \sigma_y \\ \tau_{xy} \end{Bmatrix} = \begin{bmatrix} Q_{11} & Q_{12} & Q_{16} \\ Q_{12} & Q_{22} & Q_{26} \\ Q_{16} & Q_{26} & Q_{66} \end{bmatrix} \begin{Bmatrix} \varepsilon_x \\ \varepsilon_y \\ \gamma_{xy} \end{Bmatrix} \quad (2.46)$$

Equation (2.46) is written in compact form.

$$\left\{ {}^c \sigma \right\}_{3 \times 1} = [ {}^c Q ]_{3 \times 3} \left\{ {}^c \varepsilon \right\}_{3 \times 1} \quad (2.47)$$

Reduced stiffness matrix in FSDT-based formulation is expressed as:

$$\begin{Bmatrix} \sigma_x \\ \sigma_y \\ \tau_{xy} \\ \tau_{yz} \\ \tau_{xz} \end{Bmatrix}_F = \begin{bmatrix} Q_{11} & Q_{12} & Q_{16} & Q_{14} & Q_{15} \\ Q_{12} & Q_{22} & Q_{26} & Q_{24} & Q_{25} \\ Q_{16} & Q_{26} & Q_{66} & Q_{46} & Q_{56} \\ \frac{5}{6}(Q_{14} & Q_{24} & Q_{46} & Q_{44} & Q_{45}) \\ \frac{5}{6}(Q_{15} & Q_{25} & Q_{56} & Q_{45} & Q_{55}) \end{bmatrix} \begin{Bmatrix} \varepsilon_x \\ \varepsilon_y \\ \gamma_{xy} \\ \gamma_{yz} \\ \gamma_{xz} \end{Bmatrix}_F \quad (2.48)$$

Equation (2.48) is written in compact form.

$$\left\{ {}_F \sigma \right\}_{5 \times 1} = [ {}_F Q ]_{5 \times 5} \left\{ {}_F \varepsilon \right\}_{5 \times 1} \quad (2.49)$$

Equations (2.47) and (2.49) are expressed in the following form.

$$\left\{ {}^c \sigma \right\} = [ {}_F Q ] \left\{ {}^c \varepsilon \right\} \quad (2.50)$$

Since resin is an isotropic material, there is no need for the calculation corresponding to transformation of coordinate systems. The stiffness matrix for resin is identical in  $xyz$ ,  $x'y'z'$  and  $x''y''z''$  coordinate systems and independent of angles  $\varphi$  and  $\theta$ . Therefore, the reduced stiffness matrix based on CLPT and FSDT are obtained from the 6-by-6 material stiffness matrix using the same calculation performed for the plies (Appendix A.1), and the corresponding engineering constants are available in Table 2.3.

Displacements, strains and stresses, represented by equations (2.43), (2.44) and (2.50), respectively, are essential components in energy calculation in the next section. Functions  $w_o$ ,  $\varphi_x$  and  $\varphi_y$  introduced in displacement equations (2.17) to (2.19), are expressed in the form of series, as part of the Rayleigh-Ritz formulation.

For the CLPT-based formulation, the transverse displacement  $w_o$  is written in the form of series as follows.

$${}^c w_o = \sum_{i=1}^I \sum_{j=1}^J A_{ij}^{c w_o} X_i^{c w_o}(x) Y_j^{c w_o}(y) \quad (2.51)$$

For the FSDT-based formulation, the transverse displacement  $w_o$  and functions  $\varphi_x$  and  $\varphi_y$ , the rotations of the transverse normal at the midplane about axes  $x$  and  $y$  respectively, are written in the form of series as follows.

$${}_F w_o = \sum_{i=1}^I \sum_{j=1}^J A_{ij}^{F w_o} X_i^{F w_o} Y_j^{F w_o} \quad (2.52)$$

$$\varphi_x = \sum_{i=1}^I \sum_{j=1}^J A_{ij}^{\varphi_x} X_i^{\varphi_x} Y_j^{\varphi_x} \quad (2.53)$$

$$\varphi_y = \sum_{i=1}^I \sum_{j=1}^J A_{ij}^{\varphi_y} X_i^{\varphi_y} Y_j^{\varphi_y} \quad (2.54)$$

The functions  $X_i$  and  $Y_j$  are admissible functions determined by considering the geometric boundary conditions of the plate. For different boundary conditions considered in the present study, the corresponding admissible functions are presented in a later section.

## 2.5 Strain and kinetic energies

### 2.5.1 Derivations

The stresses and strains are key components for strain energy calculation and the density of the material is the essential factor in kinetic energy computation. Comparing to CLPT, in the calculation of strain energy based on FSDT, two extra terms corresponding to out-of-plane shears are taken into account. Notations  ${}^c U$  and  ${}_F U$  correspond to strain energy based on CLPT and FSDT, respectively, and the same explanation corresponds to kinetic energy  ${}^c T$  and  ${}_F T$ .

$${}^c U = \frac{1}{2} \iiint ({}^c \varepsilon_x {}^c \sigma_x + {}^c \varepsilon_y {}^c \sigma_y + {}^c \gamma_{xy} {}^c \tau_{xy}) dV \quad (2.55)$$

$${}_F U = \frac{1}{2} \iiint ({}_F \varepsilon_x {}_F \sigma_x + {}_F \varepsilon_y {}_F \sigma_y + {}_F \gamma_{xy} {}_F \tau_{xy} + {}_F \gamma_{yz} {}_F \tau_{yz} + {}_F \gamma_{xz} {}_F \tau_{xz}) dV \quad (2.56)$$

Writing equations (2.55) and (2.56) in matrix form:

$${}^c U = \frac{1}{2} \iiint \{ {}^c \sigma \}^T \{ {}^c \varepsilon \} dV \quad (2.57)$$

$${}_F U = \frac{1}{2} \iiint \{ {}_F \sigma \}^T \{ {}_F \varepsilon \} dV \quad (2.58)$$

Equations (2.57) and (2.58) are expressed as follows.

$${}_F^c U = \frac{1}{2} \iiint \{ {}_F^c \sigma \}^T \{ {}_F^c \varepsilon \} dV \quad (2.59)$$

Substituting equation (2.50) in equation (2.59):

$${}_F^c U = \frac{1}{2} \iiint \left( [{}_F^c Q] \{ {}_F^c \varepsilon \} \right)^T \{ {}_F^c \varepsilon \} dV \quad (2.60)$$

The kinetic energy of a laminate  $T = \frac{1}{2} \omega^2 \iiint \rho(u^2 + v^2 + w_o^2) dV$  ( $u$ ,  $v$  and  $w_o$  are displacement functions in  $x$ ,  $y$  and  $z$  directions respectively) is considered according to Ref. [2] and is expressed in matrix form in a similar manner performed for the strain energy for CLPT and FSDT.

$${}_F^c T = \frac{1}{2} \omega^2 \iiint \rho \{ {}_F^c u \}^T \{ {}_F^c u \} dV \quad (2.61)$$

Matrix form is superior in terms of computational efficiency and reduces any possibility of computational errors. For CLPT and FSDT, derivatives of kinetic and strain energies are calculated at the same time in matrix form considering notation  ${}_F^c \hat{U} = \partial {}_F^c U / \partial A_{mn}$  and  ${}_F^c \hat{T} = \partial {}_F^c T / \partial A_{mn}$ ,



where  $A_{mn}$  can be any one of the parameters of the series given by equations (2.51) to (2.54). The same explanation corresponds to matrices  $\left\{^c_F \hat{u}\right\}$ ,  $\left\{^c_F \hat{\varepsilon}\right\}$  and  $\left\{^c_F \hat{s}\right\}$ . Considering equations (2.60) and (2.61):

$$^c_F \hat{U} = \frac{1}{2} \iiint \left( \left[ ^c_F Q \right] \left\{ ^c_F \hat{\varepsilon} \right\} \right)^T \left\{ ^c_F \varepsilon \right\} + \left( \left[ ^c_F Q \right] \left\{ ^c_F \varepsilon \right\} \right)^T \left\{ ^c_F \hat{\varepsilon} \right\} dV \quad (2.62)$$

$$^c_F \hat{T} = \frac{1}{2} \omega^2 \iiint \rho \left( \left\{ ^c_F \hat{u} \right\}^T \left\{ ^c_F u \right\} + \left\{ ^c_F u \right\}^T \left\{ ^c_F \hat{u} \right\} \right) dV \quad (2.63)$$

Equations (2.62) and (2.63) are written as follows.

$$^c_F \hat{U} = \frac{1}{2} \iiint \left\{ ^c_F \hat{\varepsilon} \right\}^T \left[ ^c_F Q \right] \left\{ ^c_F \varepsilon \right\} + \left( \left\{ ^c_F \hat{\varepsilon} \right\}^T \left[ ^c_F Q \right] \left\{ ^c_F \varepsilon \right\} \right)^T dV \quad (2.64)$$

$$^c_F \hat{T} = \frac{1}{2} \omega^2 \iiint \rho \left( \left\{ ^c_F \hat{u} \right\}^T \left\{ ^c_F u \right\} + \left( \left\{ ^c_F \hat{u} \right\}^T \left\{ ^c_F u \right\} \right)^T \right) dV \quad (2.65)$$

The terms  $\left\{ ^c_F \hat{\varepsilon} \right\}^T \left[ ^c_F Q \right] \left\{ ^c_F \varepsilon \right\}$  and  $\left\{ ^c_F \hat{u} \right\}^T \left\{ ^c_F u \right\}$  on the right-hand sides of equations (2.64) and (2.65) are scalars as they follow scalar values of  $^c_F \hat{U}$  and  $^c_F \hat{T}$  on the left-hand sides. In addition, this note is also realized from the size of the matrices. Therefore, considering that terms  $\left\{ ^c_F \hat{\varepsilon} \right\}^T \left[ ^c_F Q \right] \left\{ ^c_F \varepsilon \right\}$  and  $\left\{ ^c_F \hat{u} \right\}^T \left\{ ^c_F u \right\}$  are scalars, they are equal in value to their corresponding transpose.

$$\left\{ ^c_F \hat{\varepsilon} \right\}^T \left[ ^c_F Q \right] \left\{ ^c_F \varepsilon \right\} = \left( \left\{ ^c_F \hat{\varepsilon} \right\}^T \left[ ^c_F Q \right] \left\{ ^c_F \varepsilon \right\} \right)^T \quad (2.66)$$

$$\left\{ ^c_F \hat{u} \right\}^T \left\{ ^c_F u \right\} = \left( \left\{ ^c_F \hat{u} \right\}^T \left\{ ^c_F u \right\} \right)^T \quad (2.67)$$

Equations (2.66) and (2.67) are substituted in equations (2.64) and (2.65), respectively.

$${}^c_F\hat{U} = \iiint \left\{ {}^c_F\hat{\varepsilon} \right\}^T \left[ {}^c_FQ \right] \left\{ {}^c_F\varepsilon \right\} dV \quad (2.68)$$

$${}^c_F\hat{T} = \omega^2 \iiint \rho \left\{ {}^c_F\hat{u} \right\}^T \left\{ {}^c_Fu \right\} dV \quad (2.69)$$

Equations (2.44) and (2.43) are substituted in equations (2.68) and (2.69) , respectively.

$${}^c_F\hat{U} = \iiint \left( \left[ {}^c_FZ_\varepsilon \right] \left\{ {}^c_F\hat{s} \right\} \right)^T \left[ {}^c_FQ \right] \left( \left[ {}^c_FZ_\varepsilon \right] \left\{ {}^c_Fs \right\} \right) dV \quad (2.70)$$

$${}^c_F\hat{T} = \omega^2 \iiint \rho \left( \left[ {}^c_FZ_u \right] \left\{ {}^c_F\hat{s} \right\} \right)^T \left[ {}^c_FZ_u \right] \left\{ {}^c_Fs \right\} dV \quad (2.71)$$

Equations (2.70) and (2.71) are written as follows.

$${}^c_F\hat{U} = \iiint \left\{ {}^c_F\hat{s} \right\}^T \left( \left[ {}^c_FZ_\varepsilon \right]^T \left[ {}^c_FQ \right] \left[ {}^c_FZ_\varepsilon \right] \right) \left\{ {}^c_Fs \right\} dV \quad (2.72)$$

$${}^c_F\hat{T} = \omega^2 \iiint \left\{ {}^c_F\hat{s} \right\}^T \left( \rho \left[ {}^c_FZ_u \right]^T \left[ {}^c_FZ_u \right] \right) \left\{ {}^c_Fs \right\} dV \quad (2.73)$$

Integrating through the laminate thickness  $h(x)$ , matrices containing functions of  $z$  are taken into account within the integral so that matrices  $\left[ {}^c_FZ_\varepsilon \right]$  and  $\left[ {}^c_FZ_u \right]$ ,  $Q_{ij}$  as well as scalar  $\rho$  participate in the integration as the integrands.

$${}^c_F\hat{U} = \iint \left\{ {}^c_F\hat{s} \right\}^T \left( \int_{-\frac{h(x)}{2}}^{\frac{h(x)}{2}} \left[ {}^c_FZ_\varepsilon \right]^T \left[ {}^c_FQ \right] \left[ {}^c_FZ_\varepsilon \right] dz \right) \left\{ {}^c_Fs \right\} dA \quad (2.74)$$

$${}^c_F\hat{T} = \iint \left\{ {}^c_F\hat{s} \right\}^T \left( \omega^2 \int_{-\frac{h(x)}{2}}^{\frac{h(x)}{2}} \rho \left[ {}^c_FZ_u \right]^T \left[ {}^c_FZ_u \right] dz \right) \left\{ {}^c_Fs \right\} dA \quad (2.75)$$

Using notations,  $\left[ {}^c_F\bar{Z}_\varepsilon \right]$  and  $\left[ {}^c_F\bar{Z}_u \right]$ , equations (2.74) and (2.75) are rewritten.

$${}^c_F\hat{U} = \iint \left\{ {}^c_F\hat{s} \right\}^T \left[ {}^c_F\bar{Z}_\varepsilon \right] \left\{ {}^c_Fs \right\} dA \quad (2.76)$$

$${}^c_F\hat{T} = \iint \left\{ {}^c_F\hat{s} \right\}^T \left[ {}^c_F\bar{Z}_u \right] \left\{ {}^c_Fs \right\} dA \quad (2.77)$$

$$\left[ {}^c_F\bar{Z}_\varepsilon \right] = \int_{-\frac{h(x)}{2}}^{\frac{h(x)}{2}} \left[ {}^c_FZ_\varepsilon \right]^T \left[ {}^c_FQ \right] \left[ {}^c_FZ_\varepsilon \right] dz \quad (2.78)$$

$$\left[ {}^c_F\bar{Z}_u \right] = \omega^2 \int_{-\frac{h(x)}{2}}^{\frac{h(x)}{2}} \rho \left[ {}^c_FZ_u \right]^T \left[ {}^c_FZ_u \right] dz \quad (2.79)$$

Considering equations (2.76) to (2.79), the derivations are expressed in the following form.

$${}^c_F\hat{E}_{U,T} = \iint \left\{ {}^c_F\hat{s} \right\}^T \left[ {}^c_F\bar{Z}_{\varepsilon,u} \right] \left\{ {}^c_Fs \right\} dA \quad (2.80)$$

where,  $\left[ {}^c_F\bar{Z}_{\varepsilon,u} \right]$  represents term  $\left[ {}^c_F\bar{Z}_\varepsilon \right]$  or  $\left[ {}^c_F\bar{Z}_u \right]$ , and term  ${}^c_F\hat{E}_{U,T}$  represents  ${}^c_F\hat{U}$  or  ${}^c_F\hat{T}$  when equation (2.80) is considered for derivatives of strain or kinetic energies, respectively. After computation of matrices  $\left[ {}^c_FZ_\varepsilon \right]$  and  $\left[ {}^c_FZ_u \right]$ , derivatives of kinetic and strain energies with respect to parameters  $A_{mn}^{Fw_o}$ ,  $A_{mn}^{\varphi_x}$  and  $A_{mn}^{\varphi_y}$  for FSDT, and  $A_{mn}^{cwo}$  for CLPT, are obtained using equation (2.80).

### 2.5.2 Matrices $\left[ \bar{Z}_\varepsilon \right]$ and $\left[ \bar{Z}_u \right]$

Any nonzero elements of  $\left[ \bar{Z}_\varepsilon \right]$  and  $\left[ \bar{Z}_u \right]$ , are denoted by  $R_{ij}^{(n)}$  and  $R_{ij}^{(n)}$ , respectively, where  $n = 1, 2, 3$ . The matrix  $\left[ \bar{Z}_\varepsilon \right]$  contains the elements of extensional stiffness  $R_{ij}^{(1)}$ , bending-extension coupling  $R_{ij}^{(2)}$  and bending stiffness  $R_{ij}^{(3)}$ .

$${}^c_F R_{ij}^{(n)} = \int_{-\frac{h(x)}{2}}^{\frac{h(x)}{2}} {}^c_F Q_{ij} z^{n-1} dz \quad (2.81)$$

$${}^c_F R^{(n)} = \int_{-\frac{h(x)}{2}}^{\frac{h(x)}{2}} \rho z^{n-1} dz \quad (2.82)$$

Since the taper configurations described within the framework of the present study are symmetric, it is argued that for even values of  $n$ ,  ${}^c_F R^{(n)}_{ij}$  and  ${}^c_F R^{(n)}$  are zero and for odd values:

$${}^c_F R^{(n)}_{ij} = 2 \sum_{k=1}^{k_o/2} \int_{z(l_k)}^{z(u_k)} {}^c_F Q^{[k]}_{ij} z^{n-1} dz = 2 \sum_{k=1}^{k_o/2} {}^c_F Q^{[k]}_{ij} \left( \frac{z^n}{n} \right)_{z(l_k)}^{z(u_k)} \quad (2.83)$$

$${}^c_F R^{(n)} = 2 \sum_{k=1}^{k_o/2} \int_{z(l_k)}^{z(u_k)} \rho^{[k]} z^{n-1} dz = 2 \sum_{k=1}^{k_o/2} \rho^{[k]} \left( \frac{z^n}{n} \right)_{z(l_k)}^{z(u_k)} \quad (2.84)$$

Terms  $z(u_k)$  and  $z(l_k)$  represent the upper and lower surfaces of  $k^{\text{th}}$  layer.  $k_o$  is the number of layers at the left end of the tapered configurations described by Figure 2.1. Completing the mathematical operations, equations (2.83) and (2.84) are written as follows.

$${}^c_F R^{(n)}_{ij} = \frac{2}{n} \sum_{k=1}^{k_o/2} {}^c_F Q^{[k]}_{ij} \left( z^n_{(u_k)} - z^n_{(l_k)} \right) \quad (2.85)$$

$${}^c_F R^{(n)} = \frac{2}{n} \sum_{k=1}^{k_o/2} \rho^{[k]} \left( z^n_{(u_k)} - z^n_{(l_k)} \right) \quad (2.86)$$

## 2.6 Stiffness and mass matrices

By substituting equations (2.85) and (2.86) in equation (2.80), the derivatives of strain and kinetic energies with respect to parameters  $A^{Fw_o}_{mn}$ ,  $A^{\varphi_x}_{mn}$  and  $A^{\varphi_y}_{mn}$  for FSDT, and  $A^{c_{w_o}}_{mn}$  for CLPT, are obtained. The final results are presented here in the open form and the corresponding mathematical operations are available in Appendix A.2.

It is noted that for CLPT-based formulation  ${}^c\hat{U}^{[w_o]} = \partial {}^c U / \partial A_{mn}^{c_{w_o}}$ ,  ${}^c\hat{T}^{[w_o]} = \partial {}^c T / \partial A_{mn}^{c_{w_o}}$  and for FSDT-based formulation  ${}_F\hat{U}^{[w_o]} = \partial {}_F U / \partial A_{mn}^{F_{w_o}}$ ,  ${}_F\hat{U}^{[\varphi_x]} = \partial {}_F U / \partial A_{mn}^{\varphi_x}$ ,  ${}_F\hat{U}^{[\varphi_y]} = \partial {}_F U / \partial A_{mn}^{\varphi_y}$ ,  ${}_F\hat{T}^{[w_o]} = \partial {}_F T / \partial A_{mn}^{F_{w_o}}$ ,  ${}_F\hat{T}^{[\varphi_x]} = \partial {}_F T / \partial A_{mn}^{\varphi_x}$  and  ${}_F\hat{T}^{[\varphi_y]} = \partial {}_F T / \partial A_{mn}^{\varphi_y}$ .

For CLPT-based formulation:

$${}^c\hat{U}^{[w_o]} = \sum_{i=1}^I \sum_{j=1}^J \left( \begin{aligned} & \int_0^L R_{12}^{(3)} X_m^{c_{w_o}} \ddot{X}_i^{c_{w_o}} dx \int_0^L \ddot{Y}_n^{c_{w_o}} Y_j^{c_{w_o}} dy \\ & + \int_0^L R_{11}^{(3)} \ddot{X}_m^{c_{w_o}} \ddot{X}_i^{c_{w_o}} dx \int_0^L Y_n^{c_{w_o}} Y_j^{c_{w_o}} dy \\ & + \int_0^L R_{22}^{(3)} X_m^{c_{w_o}} X_i^{c_{w_o}} dx \int_0^L \ddot{Y}_n^{c_{w_o}} \ddot{Y}_j^{c_{w_o}} dy \\ & + \int_0^L R_{12}^{(3)} \ddot{X}_m^{c_{w_o}} X_i^{c_{w_o}} dx \int_0^L Y_n^{c_{w_o}} \ddot{Y}_j^{c_{w_o}} dy \\ & + 4 \int_0^L R_{66}^{(3)} \dot{X}_m^{c_{w_o}} \dot{X}_i^{c_{w_o}} dx \int_0^L \dot{Y}_n^{c_{w_o}} \dot{Y}_j^{c_{w_o}} dy \end{aligned} \right) A_{ij}^{c_{w_o}} \quad (2.87)$$

$${}^c\hat{T}^{[w_o]} = \omega^2 \sum_{i=1}^I \sum_{j=1}^J \left( \begin{aligned} & \int_{x=0}^{x=L} R^{(3)} \dot{X}_m^{c_{w_o}} \dot{X}_i^{c_{w_o}} dx \int_{y=0}^{y=L} Y_n^{c_{w_o}} Y_j^{c_{w_o}} dy \\ & + \int_{x=0}^{x=L} R^{(3)} X_m^{c_{w_o}} X_i^{c_{w_o}} dx \int_{y=0}^{y=L} \dot{Y}_n^{c_{w_o}} \dot{Y}_j^{c_{w_o}} dy \\ & + \int_{x=0}^{x=L} R^{(1)} X_m^{c_{w_o}} X_i^{c_{w_o}} dx \int_{y=0}^{y=L} Y_n^{c_{w_o}} Y_j^{c_{w_o}} dy \end{aligned} \right) A_{ij}^{c_{w_o}} \quad (2.88)$$

If rotatory inertia is neglected, then equation (2.88) becomes:

$${}^c\hat{T}^{[w_o]} = \omega^2 \sum_{i=1}^I \sum_{j=1}^J \left( \int_{x=0}^{x=L} R^{(1)} X_m^{c_{w_o}} X_i^{c_{w_o}} dx \int_{y=0}^{y=L} Y_n^{c_{w_o}} Y_j^{c_{w_o}} dy \right) A_{ij}^{c_{w_o}} \quad (2.89)$$

For FSDT-based formulation:

$${}_F\hat{U}^{[w_o]} = \frac{5}{6} \sum_{i=1}^I \sum_{j=1}^J \left[ \begin{aligned} & \left( \int_0^L R_{55}^{(1)} \dot{X}_m^{FW_o} \dot{X}_i^{FW_o} dx \int_0^L Y_n^{FW_o} Y_j^{FW_o} dy \right) A_{ij}^{FW_o} \\ & + \left( \int_0^L R_{44}^{(1)} X_m^{FW_o} X_i^{FW_o} dx \int_0^L \dot{Y}_n^{FW_o} \dot{Y}_j^{FW_o} dy \right) A_{ij}^{FW_o} \\ & + \left( \int_0^L R_{55}^{(1)} \dot{X}_m^{FW_o} X_i^{\varphi_x} dx \int_0^L Y_n^{FW_o} Y_j^{\varphi_x} dy \right) A_{ij}^{\varphi_x} \\ & + \left( \int_0^L R_{44}^{(1)} X_m^{FW_o} X_i^{\varphi_y} dx \int_0^L \dot{Y}_n^{FW_o} Y_j^{\varphi_y} dy \right) A_{ij}^{\varphi_y} \end{aligned} \right] \quad (2.90)$$

$${}_F\hat{U}^{[\varphi_x]} = \sum_{i=1}^I \sum_{j=1}^J \left[ \begin{aligned} & \frac{5}{6} \left( \int_0^L R_{55}^{(1)} X_m^{\varphi_x} \dot{X}_i^{FW_o} dx \int_0^L Y_n^{\varphi_x} Y_j^{FW_o} dy \right) A_{ij}^{FW_o} + \\ & \left( \frac{5}{6} \int_0^L R_{55}^{(1)} X_m^{\varphi_x} X_i^{\varphi_x} dx \int_0^L Y_n^{\varphi_x} Y_j^{\varphi_x} dy + \right. \\ & \quad \left. \int_0^L R_{11}^{(3)} \dot{X}_m^{\varphi_x} \dot{X}_i^{\varphi_x} dx \int_0^L Y_n^{\varphi_x} Y_j^{\varphi_x} dy \right. \\ & \quad \left. + \int_0^L R_{66}^{(3)} X_m^{\varphi_x} X_i^{\varphi_x} dx \int_0^L \dot{Y}_n^{\varphi_x} \dot{Y}_j^{\varphi_x} dy \right) A_{ij}^{\varphi_x} \\ & + \left( \int_0^L R_{12}^{(3)} \dot{X}_m^{\varphi_x} X_i^{\varphi_y} dx \int_0^L Y_n^{\varphi_x} \dot{Y}_j^{\varphi_y} dy \right. \\ & \quad \left. + \int_0^L R_{66}^{(3)} X_m^{\varphi_x} \dot{X}_i^{\varphi_y} dx \int_0^L \dot{Y}_n^{\varphi_x} Y_j^{\varphi_y} dy \right) A_{ij}^{\varphi_y} \end{aligned} \right] \quad (2.91)$$

$${}_F\hat{U}^{[\varphi_y]} = \sum_{i=1}^I \sum_{j=1}^J \left[ \begin{aligned} & \frac{5}{6} \left( \int_0^L R_{44}^{(1)} X_m^{\varphi_y} X_i^{FW_o} dx \int_0^L Y_n^{\varphi_y} \dot{Y}_j^{FW_o} dy \right) A_{ij}^{FW_o} \\ & + \left( \int_0^L R_{12}^{(3)} X_m^{\varphi_y} \dot{X}_i^{\varphi_x} dx \int_0^L \dot{Y}_n^{\varphi_y} Y_j^{\varphi_x} dy \right. \\ & \quad \left. + \int_0^L R_{66}^{(3)} \dot{X}_m^{\varphi_y} X_i^{\varphi_x} dx \int_0^L Y_n^{\varphi_y} \dot{Y}_j^{\varphi_x} dy \right) A_{ij}^{\varphi_x} \\ & + \left( \frac{5}{6} \int_0^L R_{44}^{(1)} X_m^{\varphi_y} X_i^{\varphi_y} dx \int_0^L Y_n^{\varphi_y} Y_j^{\varphi_y} dy + \right. \\ & \quad \left. \int_0^L R_{22}^{(3)} X_m^{\varphi_y} X_i^{\varphi_y} dx \int_0^L \dot{Y}_n^{\varphi_y} \dot{Y}_j^{\varphi_y} dy \right. \\ & \quad \left. + \int_0^L R_{66}^{(3)} \dot{X}_m^{\varphi_y} \dot{X}_i^{\varphi_y} dx \int_0^L Y_n^{\varphi_y} Y_j^{\varphi_y} dy \right) A_{ij}^{\varphi_y} \end{aligned} \right] \quad (2.92)$$

$${}_F\hat{T}^{[w_o]} = \omega^2 \sum_{i=1}^I \sum_{j=1}^J \left[ \int_0^L R^{(1)} X_m^{Fw_o} X_i^{Fw_o} dx \int_0^L Y_n^{Fw_o} Y_j^{Fw_o} dy \right] A_{ij}^{Fw_o} dA \quad (2.93)$$

$${}_F\hat{T}^{[\varphi_x]} = \omega^2 \sum_{i=1}^I \sum_{j=1}^J \left[ \int_0^L R^{(3)} X_m^{\varphi_x} X_i^{\varphi_x} dx \int_0^L Y_n^{\varphi_x} Y_j^{\varphi_x} dy \right] A_{ij}^{\varphi_x} dA \quad (2.94)$$

$${}_F\hat{T}^{[\varphi_y]} = \omega^2 \sum_{i=1}^I \sum_{j=1}^J \left[ \int_0^L R^{(3)} X_m^{\varphi_y} X_i^{\varphi_y} dx \int_0^L Y_n^{\varphi_y} Y_j^{\varphi_y} dy \right] A_{ij}^{\varphi_y} dA \quad (2.95)$$

If rotatory inertia is neglected, then  ${}_F\hat{T}^{[\varphi_y]} = {}_F\hat{T}^{[\varphi_x]} = 0$  and equation (2.93) becomes:

$${}_F\hat{T}^{[w_o]} = \omega^2 \sum_{i=1}^I \sum_{j=1}^J \left[ \int_0^L R^{(1)} X_m^{Fw_o} X_i^{Fw_o} dx \int_0^L Y_n^{Fw_o} Y_j^{Fw_o} dy \right] A_{ij}^{Fw_o} dA \quad (2.96)$$

It is noted that the fiber orientation of all the layers within the tapered plates are  $0^\circ$  or  $90^\circ$  meaning that in-plane normals and shears are decoupled. Therefore, in equations (2.90) to (2.92) as well as in equation (2.87), those terms originating from normal-shear coupling within the reduced stiffness matrices, such as  $Q_{16}$  and  $Q_{26}$  in reduced stiffness matrix for CLPT, have been eliminated.

## 2.7 Rayleigh-Ritz formulation

Considering  ${}^c\hat{U}^{[w_o]}$  in equation (2.87) for fixed values of  $m$  and  $n$ , the indexes  $i$  and  $j$  are counted up to the upper bound of the summations  $I$  and  $J$ . Therefore, there are  $I \times J$  number of terms that are written in the form of a row matrix multiplied by a column matrix  $\left\{ {}^c A \right\}$  containing  $I \times J$  number of parameters,  $A_{ij}^{c w_o}$ . By repeating the operation for all possible values of  $m$  and  $n$ , there are produced  $I \times J$  number of row matrices written one beneath the next one forming a matrix with size of  $I \times J$  by  $I \times J$ .

This  $I \times J$  by  $I \times J$  matrix produced from  ${}^c\hat{U}^{[w_o]}$  is called as the stiffness matrix and is denoted by  $[{}^cK]$ . In a similar manner for  ${}^c\hat{T}^{[w_o]}$ , a matrix with the same size is formed and is called as the mass matrix denoted by  $[{}^cM]$ .

For the case of FSDT, instead of one, there exist three parameters, that are  $A_{ij}^{Fw_o}$ ,  $A_{ij}^{\varphi_x}$  and  $A_{ij}^{\varphi_y}$ , for  ${}_F\hat{U}^{[w_o]}$ ,  ${}_F\hat{U}^{[\varphi_x]}$  and  ${}_F\hat{U}^{[\varphi_y]}$  as presented in equations (2.90) to (2.92). Writing the row matrices for all the three as before, they are three times greater in number and are multiplied by the column matrix  $\{{}_FA\}$  with size of  $3I \times J$  by 1 containing elements of  $A_{ij}^{Fw_o}$ ,  $A_{ij}^{\varphi_x}$  and  $A_{ij}^{\varphi_y}$ . Writing for all possible values of  $m$  and  $n$ , for  ${}_F\hat{U}^{[w_o]}$ ,  ${}_F\hat{U}^{[\varphi_x]}$  and  ${}_F\hat{U}^{[\varphi_y]}$  there are produced  $3I \times J$  number of row matrices with size of 1 by  $3I \times J$  written one beneath the next one forming a matrix with size of  $3I \times J$  by  $3I \times J$ . As a result, the number of elements that exist within mass ( $[{}_FM]$ ) and stiffness ( $[{}_FK]$ ) matrices is nine times greater than their equivalents in CLPT-based formulation.

Considering  ${}^c\hat{U}^{[w_o]} = {}^c\hat{T}^{[w_o]}$  in CLPT-based formulation, it is expressed that:

$$[{}^cK]_{IJ \times IJ} \{ {}^cA \}_{IJ \times 1} = \omega^2 [{}^cM]_{IJ \times IJ} \{ {}^cA \}_{IJ \times 1} \quad (2.97)$$

For the FSDT-based formulation:

$${}_F\hat{U}^{[w_o]} = {}_F\hat{T}^{[w_o]} \quad (2.98)$$

$${}_F\hat{U}^{[\varphi_x]} = {}_F\hat{T}^{[\varphi_x]} \quad (2.99)$$

$${}_F\hat{U}^{[\varphi_y]} = {}_F\hat{T}^{[\varphi_y]} \quad (2.100)$$

Writing equations (2.98) to (2.100) in matrix form:

$$[{}_FK]_{3IJ \times 3IJ} \{ {}_FA \}_{3IJ \times 1} = \omega^2 [{}_FM]_{3IJ \times 3IJ} \{ {}_FA \}_{3IJ \times 1} \quad (2.101)$$

Equations (2.97) and (2.101), result in:



$$([\mathbf{{}_F^c K}] - \omega^2 [\mathbf{{}_F^c M}]) \{\mathbf{{}_F^c A}\} = 0 \quad (2.102)$$

Terms  $\{\mathbf{{}_F^c A}\}$  and  $\{\mathbf{{}_F A}\}$  for CLPT-based and FSDT-based formulation, have been written in the combined form of  $\{\mathbf{{}_F^c A}\}$  and the same explanation corresponds to  $[\mathbf{{}_F^c K}]$  and  $[\mathbf{{}_F^c M}]$ . In order to obtain the non-trivial solution:

$$\det([\mathbf{{}_F^c K}] - \omega^2 [\mathbf{{}_F^c M}]) = 0 \quad (2.103)$$

By solving the eigenvalue problem in which  $\omega^2$  and the column matrix  $\{\mathbf{{}_F^c A}\}$  are eigenvalues and eigenvectors, respectively, the natural frequencies and mode shapes are determined. The square root of the smallest eigenvalue is the fundamental frequency and the mode shapes are obtained by substituting the eigenvectors in transverse displacement equations (2.51) and (2.52).

In the case of FSDT, when rotatory inertia from which term  $R^{(3)}$  emerges in equation (2.88), is neglected, equations (2.98) to (2.100) become:

$${}_F \hat{U}^{[w_o]} = {}_F \hat{T}^{[w_o]} \quad (2.104)$$

$${}_F \hat{U}^{[\varphi_x]} = 0 \quad (2.105)$$

$${}_F \hat{U}^{[\varphi_y]} = 0 \quad (2.106)$$

In this case, mass matrix is no longer invertible. Considering equations (2.90) to (2.92) in matrix form as well as equations (2.104) to (2.106), it is written that:

$${}_F \hat{U}^{[w_o]} = [\varphi_x^{Fw_o}]_{IJ \times IJ} \{A^{\varphi_x}\} + [\varphi_y^{Fw_o}]_{IJ \times IJ} \{A^{\varphi_y}\} + [w_o^{Fw_o}]_{IJ \times IJ} \{A^{Fw_o}\} \quad (2.107)$$

$${}_F \hat{U}^{[\varphi_x]} = [\varphi_x^{\varphi_x}]_{IJ \times IJ} \{A^{\varphi_x}\} + [\varphi_y^{\varphi_x}]_{IJ \times IJ} \{A^{\varphi_y}\} + [w_o^{\varphi_x}]_{IJ \times IJ} \{A^{Fw_o}\} \quad (2.108)$$

$${}_F \hat{U}^{[\varphi_y]} = [\varphi_x^{\varphi_y}]_{IJ \times IJ} \{A^{\varphi_x}\} + [\varphi_y^{\varphi_y}]_{IJ \times IJ} \{A^{\varphi_y}\} + [w_o^{\varphi_y}]_{IJ \times IJ} \{A^{Fw_o}\} \quad (2.109)$$

From equations (2.108) and (2.109), the column matrices  $\{A^{\varphi_x}\}$  and  $\{A^{\varphi_y}\}$  are obtained in terms of  $\{A^{Fw_o}\}$  and by substituting them in equation (2.107), the following relation is obtained (Appendix A.3).

$$\left[ {}_F\hat{U}^{[w_o]} \right] = \left[ {}_F\bar{K} \right]_{IJ \times IJ} \{A^{Fw_o}\}_{IJ \times 1} \quad (2.110)$$

where,

$$\left[ {}_F\bar{K} \right] = \left[ w_o^{Fw_o} \right] - \left[ \varphi_x^{Fw_o} \right] \left[ \varphi_x^{\varphi_x} \right]^{-1} \left[ w_o^{\varphi_x} \right] + \left( \left[ \varphi_y^{Fw_o} \right] - \left[ \varphi_x^{Fw_o} \right] \left[ \varphi_x^{\varphi_x} \right]^{-1} \left[ \varphi_y^{\varphi_x} \right] \right) \left[ Str \right] \quad (2.111)$$

$$\left[ Str \right] = \left[ \left[ \varphi_y^{\varphi_y} \right] - \left[ \varphi_x^{\varphi_y} \right] \left[ \varphi_x^{\varphi_x} \right]^{-1} \left[ \varphi_y^{\varphi_x} \right] \right]^{-1} \left[ \left[ \varphi_x^{\varphi_y} \right] \left[ \varphi_x^{\varphi_x} \right]^{-1} \left[ w_o^{\varphi_x} \right] - \left[ w_o^{\varphi_y} \right] \right] \quad (2.112)$$

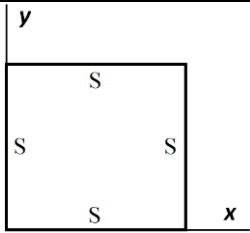
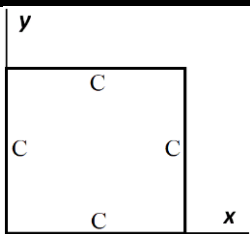
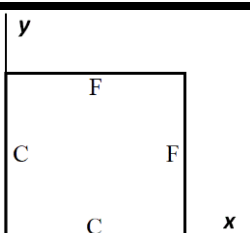
Then, the eigenvalue problem can be established and by solving it the solution is obtained.

## 2.8 Boundary conditions

The natural frequencies are obtained for the tapered composite plates for different boundary conditions. For CLPT and FSDT, in equations (2.51) to (2.54), admissible functions  $X_i(x)$  and  $Y_j(y)$  of the series are selected in a manner that satisfies the geometric boundary conditions. In this section, the following geometric boundary conditions and the corresponding functions considered for the study are introduced for Classical Laminated Plate Theory (CLPT) and First-order Shear Deformation Theory (FSDT). It is noted that CCFF boundary condition is only considered for CLPT.

1. All edges simply supported (SSSS)
2. All edges clamped (CCCC)
3. Clamped at two adjacent edges with other two free (CCFF). The clamped edges correspond to  $x = 0$  and  $y = 0$  lines and free edges correspond to  $x = L$  and  $y = L$  lines. It is noted that the  $x = 0$  and  $x = L$  lines correspond to the thick and thin sides of the tapered laminates, respectively.

The SSSS, CCCC and CCFF boundary conditions are given in Table 2.4 and the corresponding admissible functions are given in Tables 2.5 - 2.7 using Refs. [2], [5], [27] and [28].

1.	<b>All edges simply supported (SSSS)</b>		
	$\begin{cases} x = 0 \\ x = L \end{cases} \rightarrow w_o = 0 \text{ and } M_x = 0$	$\begin{cases} y = 0 \\ y = L \end{cases} \rightarrow w_o = 0 \text{ and } M_y = 0$	
2.	<b>All edges clamped (CCCC)</b>		
	$\begin{cases} x = 0 \\ x = L \end{cases} \rightarrow w_o = 0 \text{ and } \frac{\partial w_o}{\partial x} = 0$	$\begin{cases} y = 0 \\ y = L \end{cases} \rightarrow w_o = 0 \text{ and } \frac{\partial w_o}{\partial y} = 0$	
3.	<b>Clamped at two adjacent edges with other two free (CCFF)</b>		
	$x = L \rightarrow \frac{d^2 w_o}{dx^2} = 0 \text{ and } \frac{d^3 w_o}{dx^3} = 0$	$y = L \rightarrow \frac{d^2 w_o}{dy^2} = 0 \text{ and } \frac{d^3 w_o}{dy^3} = 0$	

**Table 2.4** Boundary conditions for the plates

SSSS	CLPT	$X_i^{c_{w_o}} = \sin\left(i\pi \frac{x}{L}\right) \quad , \quad Y_j^{c_{w_o}} = \sin\left(j\pi \frac{y}{L}\right)$
	FSDT	$X_i^{F_{w_o}} = \sin\left(i\pi \frac{x}{L}\right) \quad , \quad Y_j^{F_{w_o}} = \sin\left(j\pi \frac{y}{L}\right)$ $X_i^{\varphi_x} = \cos\left(i\pi \frac{x}{L}\right) \quad , \quad Y_j^{\varphi_x} = \sin\left(j\pi \frac{y}{L}\right)$ $X_i^{\varphi_y} = \sin\left(i\pi \frac{x}{L}\right) \quad , \quad Y_j^{\varphi_y} = \cos\left(j\pi \frac{y}{L}\right)$

**Table 2.5** Appropriate series for SSSS

CCCC	CLPT	$X_i^{c_{w_o}} = \cos\left(\lambda_i \frac{x}{L}\right) - \cosh\left(\lambda_i \frac{x}{L}\right) - \gamma_i \left[\sin\left(\lambda_i \frac{x}{L}\right) - \sinh\left(\lambda_i \frac{x}{L}\right)\right]$ $Y_j^{c_{w_o}} = \cos\left(\lambda_j \frac{y}{L}\right) - \cosh\left(\lambda_j \frac{y}{L}\right) - \gamma_j \left[\sin\left(\lambda_j \frac{y}{L}\right) - \sinh\left(\lambda_j \frac{y}{L}\right)\right]$			
	FSDT	$X_i^{F_{w_o}} = \cos\left(\lambda_i \frac{x}{L}\right) - \cosh\left(\lambda_i \frac{x}{L}\right) - \gamma_i \left[\sin\left(\lambda_i \frac{x}{L}\right) - \sinh\left(\lambda_i \frac{x}{L}\right)\right]$ $Y_j^{F_{w_o}} = \cos\left(\lambda_j \frac{y}{L}\right) - \cosh\left(\lambda_j \frac{y}{L}\right) - \gamma_j \left[\sin\left(\lambda_j \frac{y}{L}\right) - \sinh\left(\lambda_j \frac{y}{L}\right)\right]$			
		$X_i^{\varphi_x} = \sin\left(i\pi \frac{x}{L}\right) \quad , \quad Y_j^{\varphi_x} = \sin\left(j\pi \frac{y}{L}\right)$			
		$X_i^{\varphi_y} = \sin\left(i\pi \frac{x}{L}\right) \quad , \quad Y_j^{\varphi_y} = \sin\left(j\pi \frac{y}{L}\right)$			
	$i$	$i = 1$	$i = 2$	$i = 3$	$i = 4$
	$\lambda_i$	4.730 040 744 863	7.853 204 624 096	10.995 607 838 002	14.137 165 491 258
	$\gamma_i$	0.982 502 214 576	1.000 777 311 907	0.999 966 450 125	1.000 001 449 898
	$i$	$i = 5$	$i = 6$	$i = 7$	$i = 8$
	$\lambda_i$	17.278 759 657 400	20.420 352 245 626	23.561 944 902 040	26.703 537 555 508
	$\gamma_i$	0.999 999 937 344	1.000 000 002 708	0.999 999 999 883	1.000 000 000 005

**Table 2.6** Appropriate series for CCCC

CCFF	CLPT	$X_i^{c_{w_o}} = \cos\left(\lambda_i \frac{x}{L}\right) - \cosh\left(\lambda_i \frac{x}{L}\right) - \gamma_i \left[\sin\left(\lambda_i \frac{x}{L}\right) - \sinh\left(\lambda_i \frac{x}{L}\right)\right]$ $Y_j^{c_{w_o}} = \cos\left(\lambda_j \frac{y}{L}\right) - \cosh\left(\lambda_j \frac{y}{L}\right) - \gamma_j \left[\sin\left(\lambda_j \frac{y}{L}\right) - \sinh\left(\lambda_j \frac{y}{L}\right)\right]$			
	$i$	$i = 1$	$i = 2$	$i = 3$	$i = 4$
	$\lambda_i$	1.875 104 068 712	4.694 0911 329 742	7.854 757 438 238	10.995 540 734 875
	$\gamma_i$	0.734 095 513 759	1.018 467 318 759	0.999 224 496 517	1.000 033 553 252
	$i$	$i = 5$	$i = 6$	$i = 7$	$i = 8$
	$\lambda_i$	14.137 168 391 046	17.278 759 532 088	20.420 352 251 041	23.561 944 901 806
	$\gamma_i$	0.999 998 550 109	1.000 000 0626 556	0.999 999 997 292	1.000 000 000 117

**Table 2.7** Appropriate series for CCFF

Imposing the boundary conditions of CCCC and CCFF given in Table 2.4 on the corresponding admissible functions given in Table 2.6 for CCCC and Table 2.7 for CCFF, results in equations (2.113) and (2.114) for CCCC and equations (2.115) and (2.116) for CCFF. By solving equations (2.113) to (2.116),  $\lambda_i$  and  $\gamma_i$  are determined and have been given in Ref. [2], up to  $i = 4$ . In Table 2.6 for CCCC and Table 2.7 for CCFF,  $\lambda_i$  and  $\gamma_i$  have been given up to  $i = 8$ . Since  $\lambda_i$  and  $\gamma_i$  are passed into hyperbolic functions, in order to obtain sufficiently accurate results, several decimal places are considered and given in Table 2.6 and Table 2.7. In the present study, for equations (2.51) to (2.54),  $I$  and  $J$  are increased to 13 in order to obtain sufficient number of natural frequencies required in the next chapter. Therefore,  $\lambda_i$  and  $\gamma_i$  are obtained up to  $i = 13$  by solving equations (2.113) and (2.114) for CCCC and equations (2.115) and (2.116) for CCFF.

For the CCCC boundary condition:

$$\cos(\lambda_i) \cosh(\lambda_i) = 1 \quad (2.113)$$

$$\gamma_i = \frac{\cos(\lambda_i) - \cosh(\lambda_i)}{\sin(\lambda_i) - \sinh(\lambda_i)} \quad (2.114)$$

For CCFF boundary condition:

$$\cos(\lambda_i) \cosh(\lambda_i) = -1 \quad (2.115)$$

$$\gamma_i = \frac{\cos(\lambda_i) + \cosh(\lambda_i)}{\sin(\lambda_i) + \sinh(\lambda_i)} \quad (2.116)$$

Considering the hyperbolic functions in CCCC and CCFF, high accuracy of  $\lambda_i$  and  $\gamma_i$  are required depending on the integer values  $I$  and  $J$  considered in equations (2.50) and (2.51). The higher integer values of  $I$  and  $J$  require more accuracy in values obtained for  $\lambda_i$  and  $\gamma_i$ .

## 2.9 Software limitation

In this study, the calculations are performed in MATLAB<sup>®</sup>. To the knowledge and experience of the present author, the software is designed with high capability in numerical computations according to predetermined aims. However, the software is not capable in mathematical and symbolic calculations as it is in numerical calculations. Therefore, computationally complex integrals, combination of hyperbolic, polynomial (coming from bending stiffness elements) and trigonometric functions which are present as the integrands in equations (2.87) to (2.96), cannot be passed into the software. Therefore, in order to cope up with this problem, one may use a software such as MAPLE<sup>®</sup> for symbolic computations besides. Nevertheless, the solution of the integrals when solved is extensive and is still difficult to apply.

In the present thesis, this symbolic calculation problem is solved by converting the integrands including hyperbolic, polynomial and trigonometric functions into respective fully-polynomial functions using Taylor series. Fully-polynomial functions are simple for the software (MATLAB<sup>®</sup>) to process. By this approach, no other software is needed while the result is obtained without complications in a few seconds (i.e. for  $I = J = 7$ ). It is noted that the order of the Taylor series is increased to 200 or 250 when the fluctuation of the original function is severe (for smaller laminate lengths) and the order of 160 or even in some cases 110, is sufficient for less fluctuating functions.

## 2.10 Validation

Experimental measurement is a reliable way of validation. However, the related test facilities and financial support are required. In addition, considering the symmetric configuration of the tapered laminates in the present thesis, the production of the symmetric tapered plates is complicated and expensive. Therefore, for demonstration, the formulation developed in the present chapter is applied to a uniform laminated composite plate and the obtained numerical result for fundamental frequency of the uniform plate is compared with that of the exact solution. In addition, since various software packages are commonly used in numerous literature for validation purposes, the obtained results using the Ritz method for the tapered configurations are compared with that of the FEM obtained using ANSYS®. Furthermore, the layer reduction test is carried out.

### 2.10.1 Uniform composite plate

By solving the eigenvalue problem given by equation (2.103) for taper configurations considering admissible functions selected based on boundary conditions, free vibration analysis for the tapered plates is completed. For demonstration, the developed formulation has been applied to a uniform laminate using data given in Ref. [29] and the numerical results were in agreement with that of the article.

In addition, the exact solution available for natural frequencies of the uniform laminates with all simply supported edges, is used for comparison in the example below.

**Example:** Obtain the fundamental frequency of a square plate with side length of 0.35 m and configuration of  $(0/90)_{3s}$  made of unidirectional NCT-301 Graphite-Epoxy material (mechanical properties were given in Table 2.3) with ply thickness of  $125 \times 10^{-6}$  m, simply supported at all edges.

**Solution:** For a uniform laminate, the condition of pure bending simplifies the equilibrium equations leading to the following equation of motion derived from Ref. [2].

$$\left[ R_{11}^{(3)} \frac{\partial^4({}^c w_o)}{\partial x^4} + 2(R_{12}^{(3)} + 2R_{66}^{(3)}) \frac{\partial^4({}^c w_o)}{\partial x^2 \partial y^2} + R_{22}^{(3)} \frac{\partial^4({}^c w_o)}{\partial y^4} \right] - f(x, y, t) \quad (2.117)$$

$$= -R^{(1)} c\ddot{w}_o + R^{(3)} \left( \frac{\partial^2(c\ddot{w}_o)}{\partial x^2} + \frac{\partial^2(c\ddot{w}_o)}{\partial y^2} \right)$$

Term  $f(x, y, t)$  is the transverse loading applied onto the laminate which is set to zero for the free vibration analysis.

$$\begin{aligned} R_{11}^{(3)} \frac{\partial^4(cw_o)}{\partial x^4} + 2(R_{12}^{(3)} + 2R_{66}^{(3)}) \frac{\partial^4(cw_o)}{\partial x^2 \partial y^2} + R_{22}^{(3)} \frac{\partial^4(cw_o)}{\partial y^4} \\ = -R^{(1)} c\ddot{w}_o + R^{(3)} \left( \frac{\partial^2(c\ddot{w}_o)}{\partial x^2} + \frac{\partial^2(c\ddot{w}_o)}{\partial y^2} \right) \end{aligned} \quad (2.118)$$

Equation (2.118) has been solved in Refs. [2] and [9] and the solution for natural frequencies for a uniform square plate that is simply supported at all edges is:

$$\omega_{ij} = \frac{\pi^2}{L^2} \sqrt{\frac{1}{R^{(1)}} \left( R_{11}^{(3)} i^4 + 2(R_{12}^{(3)} + 2R_{66}^{(3)}) i^2 j^2 + R_{22}^{(3)} j^4 \right)} \quad (2.119)$$

In order to obtain the fundamental frequency, the values  $i$  and  $j$  are set to 1.

$$\omega_{11} = \frac{\pi^2}{L^2} \sqrt{\frac{1}{R^{(1)}} \left( R_{11}^{(3)} + 2(R_{12}^{(3)} + 2R_{66}^{(3)}) + R_{22}^{(3)} \right)} \quad (2.120)$$

Considering equation (2.120), the value obtained for the fundamental frequency is 339 *rad/s* which is the same as the one calculated in the present work using the Ritz method.

### 2.10.2 Solution using Finite Element Method (FEM)

Numerical results from calculations worked out by using the Ritz method in the present chapter, are compared with that of the FEM obtained using ANSYS® for the tapered laminated composite square plates [30]. Details about the finite element solution are available in Ref. [30] and are reproduced in Appendix B. The finite element solution has been obtained using the four-node element SHELL 181 in ANSYS® and converged meshes of 2808 and 195 elements have been obtained for the plates of side length 0.8594 m and 0.17188 m, respectively.



Fundamental Frequency ( <i>rad/s</i> )					
Configuration	Boundary Condition	$\varphi = 0.1^\circ$ $L = 0.8594\text{ m}$		$\varphi = 0.5^\circ$ $L = 0.17188\text{ m}$	
		Ritz Method (CLPT)	Finite Element Method [30]	Ritz Method (CLPT)	Finite Element Method [30]
<b>A</b>	SSSS	111	111	2784	2656
	CCCC	235	233	5866	5694
	CCFF	50	49	1259	1216
<b>B</b>	SSSS	108	108	2700	2699
	CCCC	229	230	5728	5710
	CCFF	52	52	1304	1245
<b>D</b>	SSSS	105	104	2627	2633
	CCCC	221	216	5527	5594
	CCFF	49	51	1235	1240

**Table 2.8** Comparison between Finite Element Method and Ritz Method Solutions

Considering Table 2.8, it can be seen that the values for the fundamental frequencies of the tapered configurations for the given lengths and boundary conditions, obtained using FEM and Ritz method, are in good agreement.

### 2.10.3 Layer reduction test

In this sub-section, in order to compare the fundamental frequencies of the uniform and tapered plates with SSSS boundary condition, a computational investigation called herein as the “layer reduction test” is implemented.

Three identical uniform laminated plates are considered with configuration of  $(0/90)_{9s}$  made of unidirectional NCT-301 Graphite-Epoxy material (mechanical properties were given in Table 2.3) with ply thickness and side length of  $125 \times 10^{-6}$  m and 0.08593 m, respectively (Figure 2.4). The two laminates on the left and right sides with same length as that of the middle laminate, have been displayed only in part due to insufficient horizontal space.

During the 12-stepped “layer reduction test” shown by Figures 2.4 - 2.16, two plies, one from the top half and the other from the bottom half of the laminate in the middle, are dropped and replaced with resin such that the thickness of the left side stays the same while that of the right end is reduced and a small taper angle is revealed at the first step so that the plate is considered as the tapered laminate (Figure 2.5). As can be seen, in each new step of the test for the middle laminate (tapered laminate), the thickness of the left end stays the same while that of the right end is decreased and considering the fixed length of the laminate (0.08593 m), the taper angle increases such that at the last step of the test (for the middle laminate shown by Figure 2.16) the taper angle is equal to  $1^\circ$ . Note that during the “layer reduction test” the lengths for all the laminates are fixed and equal to 0.08593 m as described before.

At each step during the 12-stepped “layer reduction test”, one ply from the top half and the other from the bottom half of the right-side laminate is removed and no dropped plies are replaced with the resin. Therefore, the laminate stays uniform during the test while the thickness is decreased at each step so that it is called the thin laminate. (The laminates on the right side are shown by Figures 2.4 - 2.16)

The laminate on the left side with the configuration and properties described at the beginning of the sub-section, remains intact throughout the test and the thickness stays the same so that it is called the thick laminate. (The laminates on the left side are shown by Figures 2.4 - 2.16)

At the end of the 12-stepped “layer reduction test”, the middle plate corresponds to configuration A while the configuration of the thick laminate stays the same as  $(0/90)_{9s}$ , and the thin laminate becomes  $(0/90)_{3s}$ .

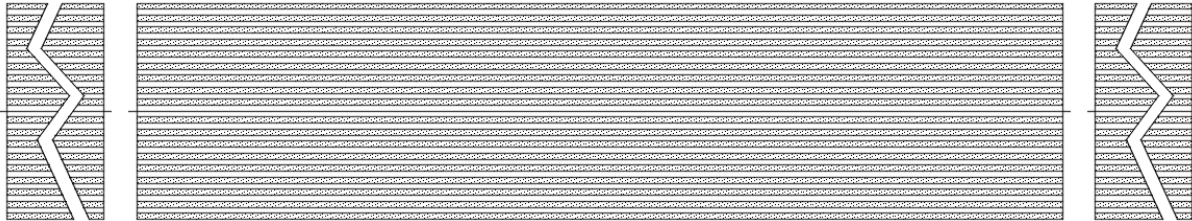


*Figure 2.4 Identical laminates considered for layer reduction test (no ply drop-off)*



*Figure 2.5 Step 1: 2 plies dropped-off*

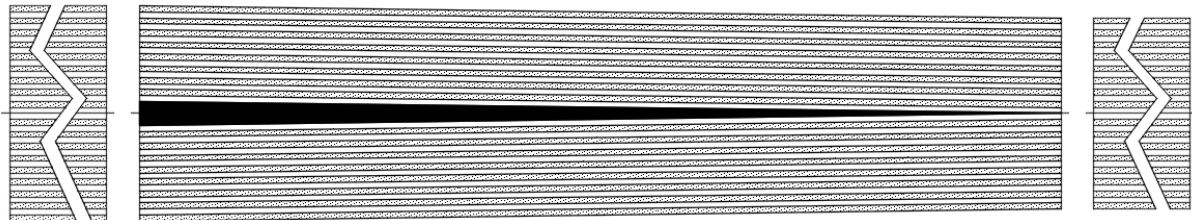


*Figure 2.6 Step 2: 4 plies dropped-off*

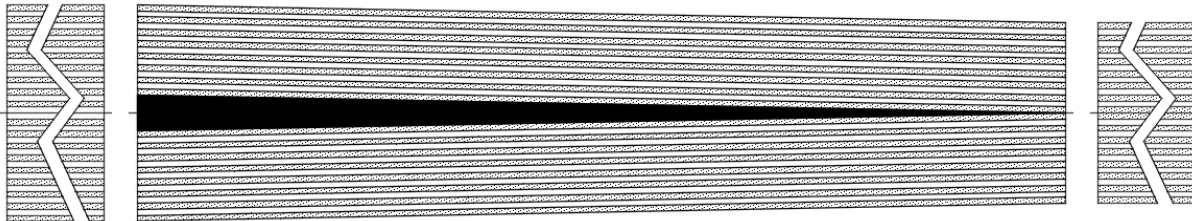


*Figure 2.7 Step 3: 6 plies dropped-off*

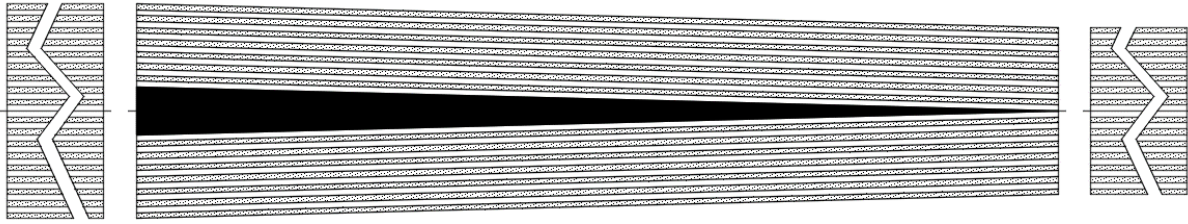


*Figure 2.8 Step 4: 8 plies dropped-off*

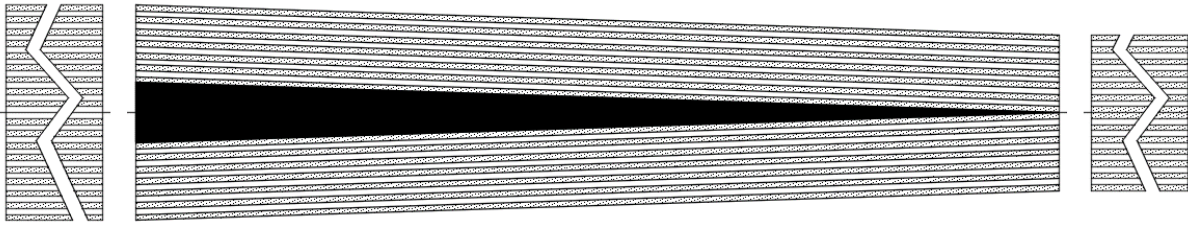


*Figure 2.9 Step 5: 10 plies dropped-off*

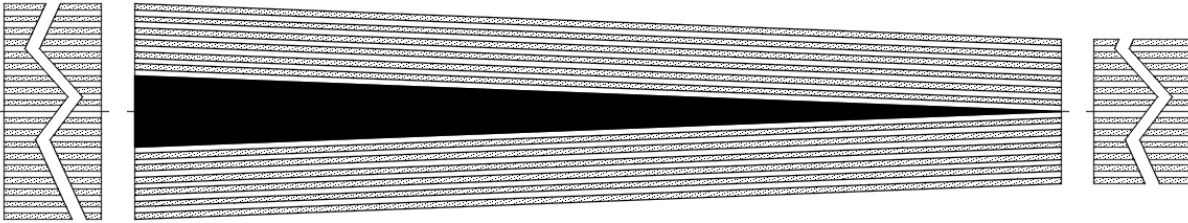


*Figure 2.10 Step 6: 12 plies dropped-off*

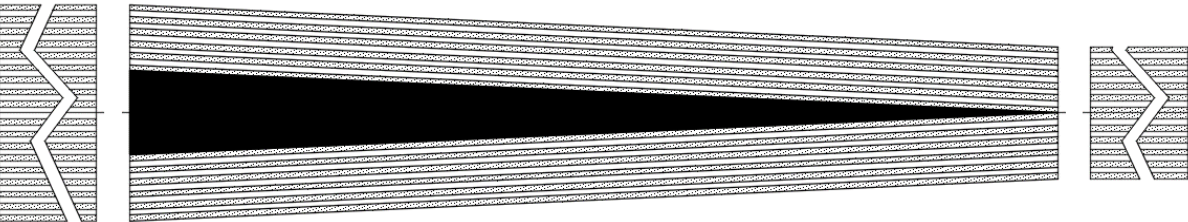


*Figure 2.11 Step 7: 14 plies dropped-off*

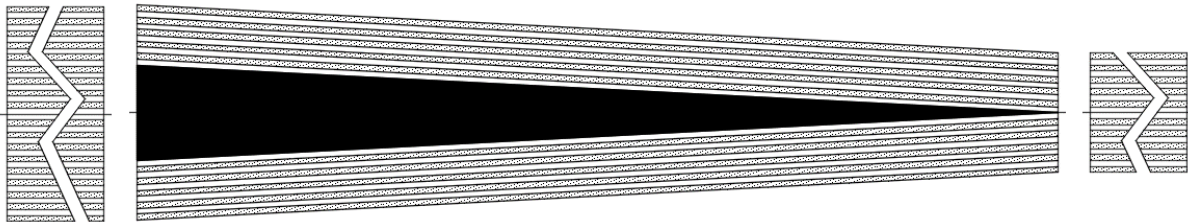


*Figure 2.12 Step 8: 16 plies dropped-off*



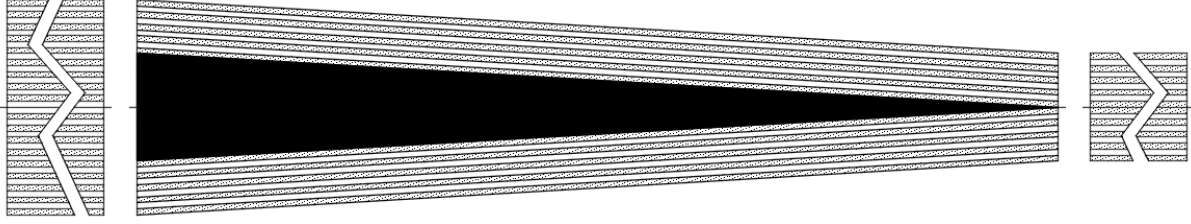


*Figure 2.13 Step 9: 18 plies dropped-off*

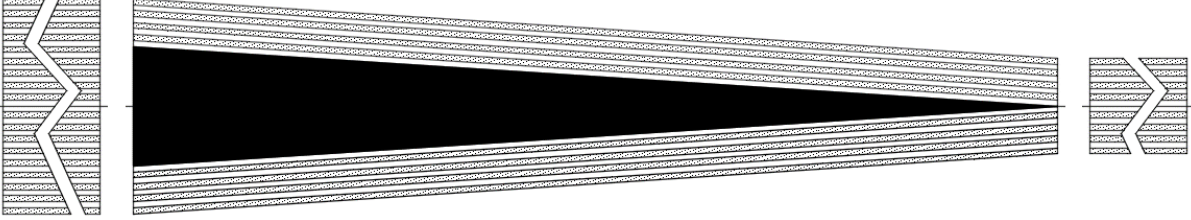


*Figure 2.14 Step 10: 20 plies dropped-off*

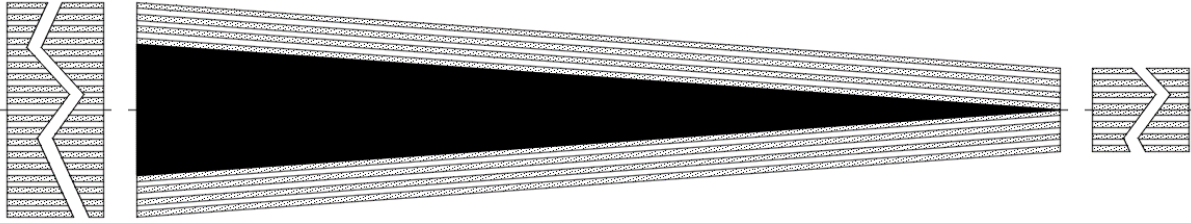


*Figure 2.15 Step 11: 22 plies dropped-off*

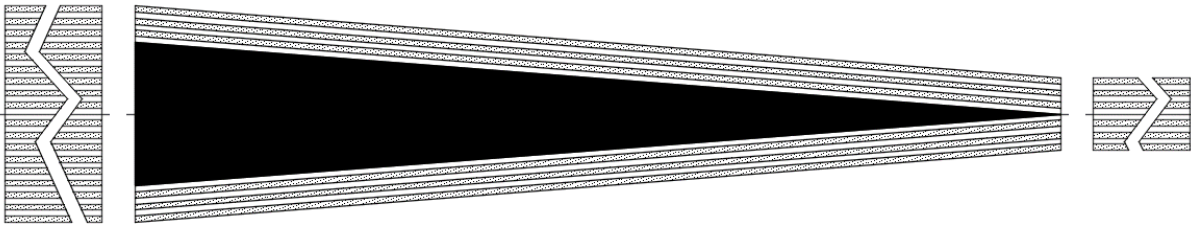


*Figure 2.16 Step 12: 24 plies dropped-off*

The numerical results obtained for the fundamental frequencies of the thick, tapered and thin laminates at each step of the test are calculated using the developed formulation. By solving the eigenvalue problem given by equation (2.103), the fundamental frequencies are obtained and displayed in Table 2.9.

<p style="text-align: center;"><b>Fundamental Frequency (<math>rad/s</math>) of the plate</b></p> <p style="text-align: center;"><b>B.C: SSSS      <math>L = 0.08593</math> m</b></p>						
Number of Reduced Layers	CLPT			FSDT		
	Thick	Tapered	Thin	Thick	Tapered	Thin
0	16850	16850	16850	16218	16218	16218
2	16850	16456	15914	16218	15857	15365
4	16850	16056	14978	16218	15490	14505
6	16850	15648	14042	16218	15115	13637
8	16850	15233	13105	16218	14730	12761
10	16850	14802	12169	16218	14330	11879
12	16850	14362	11233	16218	13920	10991
14	16850	13893	10296	16218	13482	10096
16	16850	13418	9360	16218	13036	9196
18	16850	12891	8424	16218	12539	8291
20	16850	12366	7488	16218	12043	7381
22	16850	11744	6551	16218	11453	6468
24	16850	11145	5615	16218	10880	5550

*Table 2.9 Fundamental frequency values for the laminates from layer reduction test*

In Table 2.9, for the CLPT, the fundamental frequencies for the thick and thin laminates are calculated using the exact solution and that of the tapered laminate are calculated using the Ritz method. When no plies are reduced from the plates, the obtained fundamental frequencies for the left (thick), middle and right (thin) plates obtained based on different approaches, are equal.

It is grasped from Table 2.9 that by increasing the number of removed plies from the tapered laminate, the fundamental frequency of the plate is decreased. This explanation corresponds to the thin laminate as well, however, this decline in fundamental frequency value for the thin plate is remarkable in comparison with that of the tapered plate. The results for the thick

laminate stay the same as it remains intact throughout the 12-stepped test. During the 12-stepped test, the fundamental frequency of the tapered laminate is numerically lower than that of the thick laminate and higher than that of the thin laminate.

Comparing the numerical values that have been obtained based on CLPT and FSDT, the FSDT-based results are lower than that of CLPT at any single step of the test. In order to obtain the difference between the FSDT-based and CLPT-based fundamental frequencies for each laminate at each step given by Table 2.9, the fundamental frequencies of the laminates based on FSDT, are deducted from that of CLPT and the results are shown in Table 2.10.

<b>Fundamental Frequency Difference in <math>rad/s</math></b> <b>B.C: SSSS      <math>L = 0.08593</math> m</b>			
<b>Number of Reduced Layers</b>	<b>Thick</b>	<b>Tapered</b>	<b>Thin</b>
<b>0</b>	632	632	632
<b>2</b>	632	599	549
<b>4</b>	632	566	473
<b>6</b>	632	533	405
<b>8</b>	632	503	344
<b>10</b>	632	472	290
<b>12</b>	632	442	242
<b>14</b>	632	411	200
<b>16</b>	632	382	164
<b>18</b>	632	352	133
<b>20</b>	632	323	107
<b>22</b>	632	291	83
<b>24</b>	632	265	65

**Table 2.10** Difference between the fundamental frequencies obtained based on CLPT and FSDT

Considering the fixed length of the laminates throughout the layer reduction test, by removing the plies from the tapered and thin laminates at each step of the test, the length-to-thickness ratio gradually increases such that the numerical difference between CLPT-based and FSDT-based fundamental frequencies are decreased. For the thin laminate, this decline is considerable compared to that of the tapered laminate.

Figure 2.17 has been illustrated using data from Table 2.9 showing the trend by which the fundamental frequencies for the plates change when the plies are gradually dropped-off.

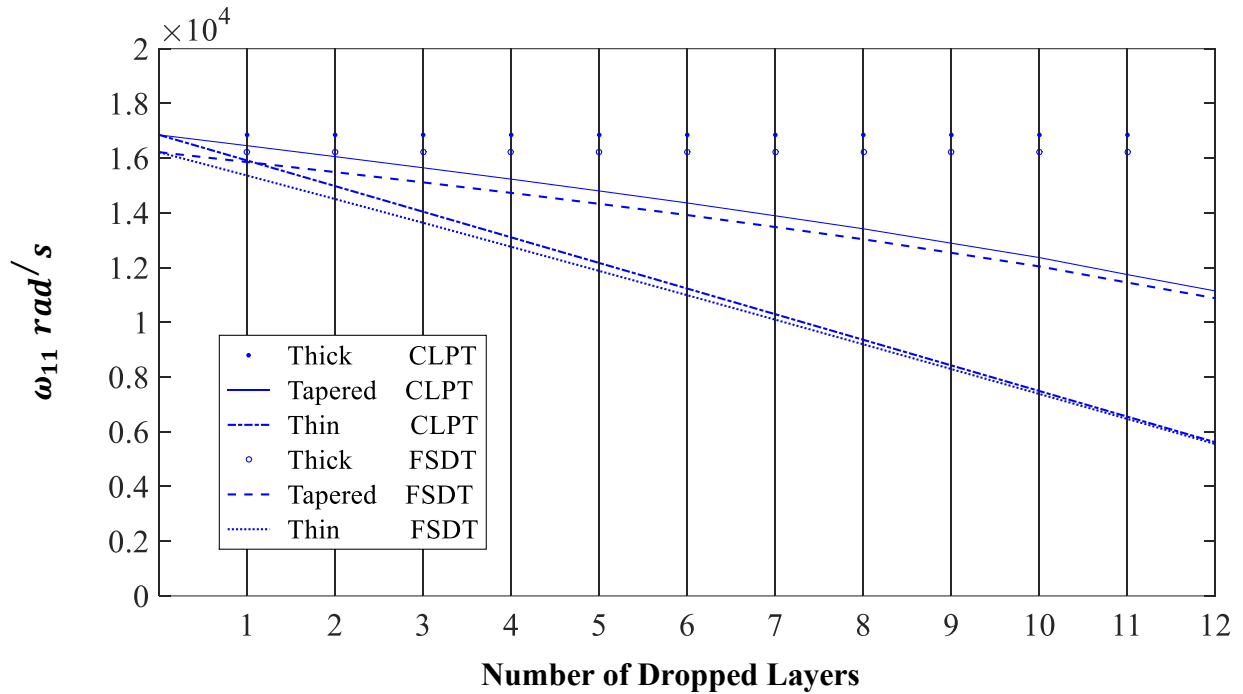


**Figure 2.17** The variation of fundamental frequencies of the thick, thin and tapered laminates with increase of dropped layers (CLPT and FSDT)

The graph shows that the decrease for the thin plate is faster compared to the tapered laminate regardless of the theory. The line that corresponds to the FSDT is well below the CLPT line showing that the fundamental frequencies obtained based on FSDT formulation, are lower than that of CLPT. This decrease in numerical difference between CLPT-based and FSDT-based results for the tapered and thin laminates is also observed in Figure 2.17. The vertical distance between the CLPT and FSDT lines corresponding to the tapered laminate, is gradually decreased



by removing the plies. This explanation also corresponds to the thin laminate as the results obtained from the two theories almost coincide at the last step of the test.

## **2.11 Number of terms of the shape function and the accuracy of the calculation**

The shape function is expressed in the form of series in equation (2.51) using admissible functions and the summations count the integer values of  $i$  and  $j$  up to the upper bounds of  $I$  and  $J$ . Increasing the values of  $I$  and  $J$ , increases the size of mass and stiffness matrices, and the natural frequencies obtained by solving equation (2.103) are more accurate. In this section, the influence of the values for  $I$  and  $J$  on the accuracy with which the natural frequencies are computed, is investigated. In addition, some notifications are given in order to avoid any probable calculation error caused by inappropriate selection of  $I$  and  $J$ .

Configuration B with length of 0.1719 m corresponding to taper angle of  $0.5^\circ$  is considered. The natural frequencies of the plate are calculated considering  $I = J = 5$  in equation (2.51) and the computation is repeated for different values for  $I$  and  $J$  ( $I = J = 7, 9, 11, 13$ ). Then, the natural frequencies obtained, each time based on specific values for  $I$  and  $J$ , are sorted in ascending order and are plotted in Figure 2.18, Figure 2.19 and Figure 2.20 for SSSS, CCCC and CCFF boundary conditions, respectively.

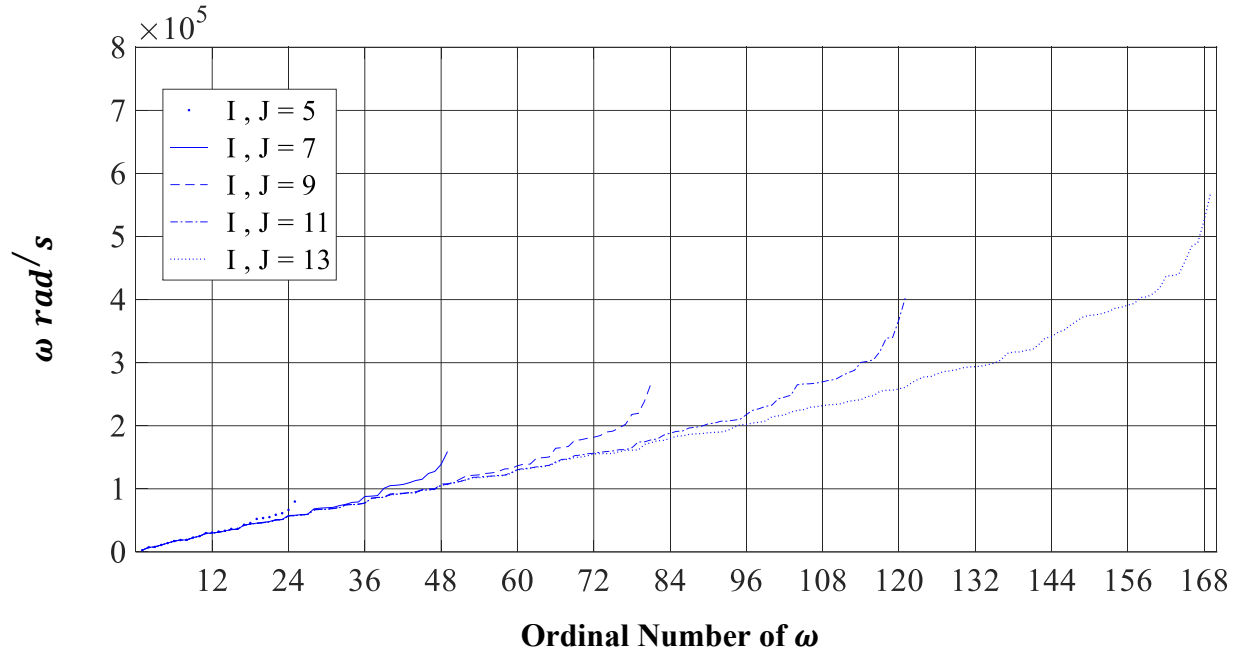


**Figure 2.18** Influence of  $I$  and  $J$  values on natural frequency calculation (configuration B, SSSS)

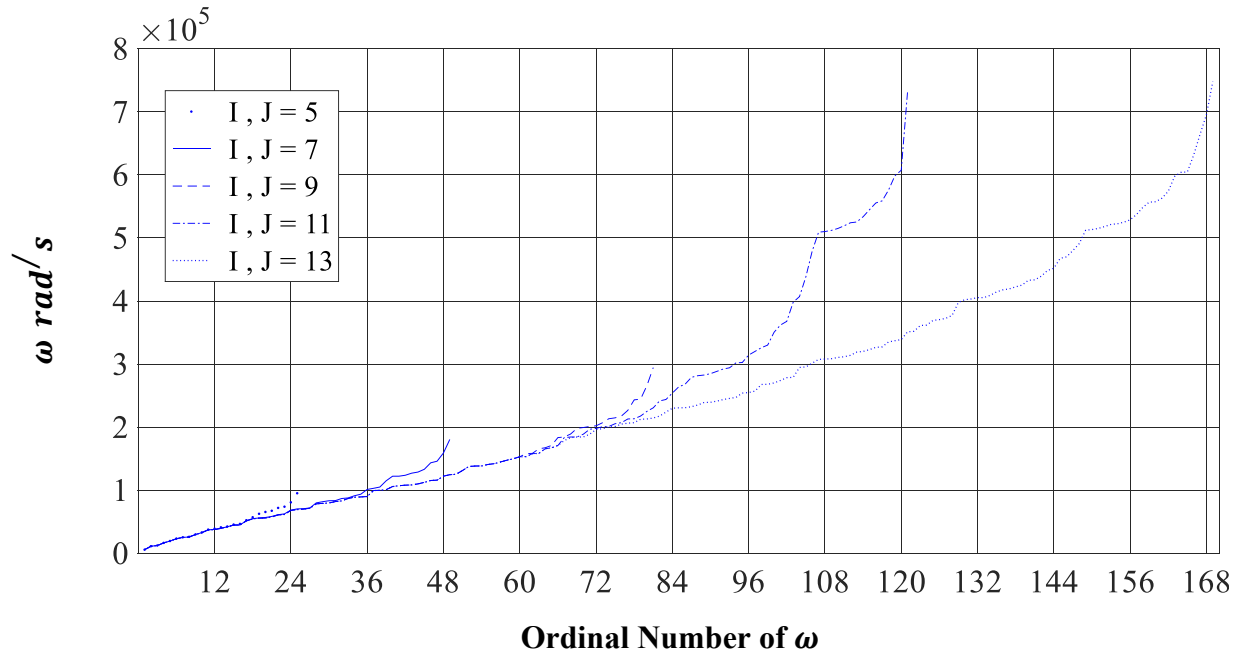


**Figure 2.19** Influence of  $I$  and  $J$  values on natural frequency calculation (configuration B, CCCC)

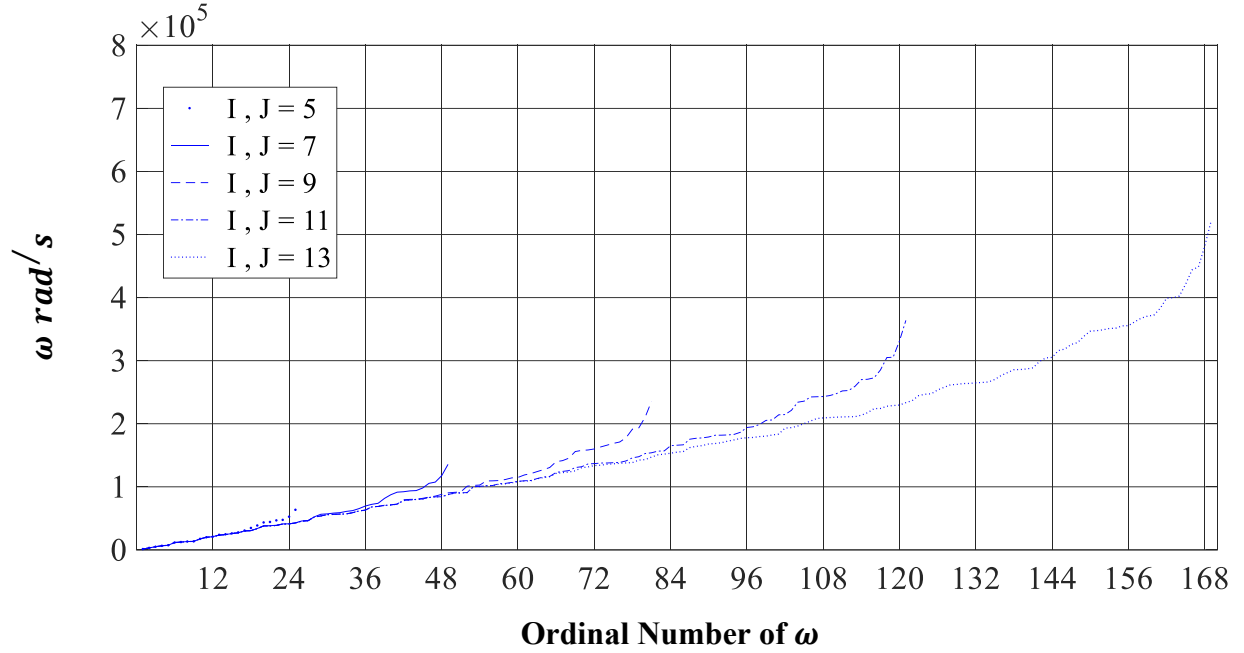


**Figure 2.20** Influence of  $I$  and  $J$  values on natural frequency calculation (configuration B, CCFF)

Consider the curves corresponding to  $I = J = 7$  and  $I = J = 9$  for SSSS plate as the first and second curves. According to the second curve, the first 75% of the obtained natural frequencies reported by the first curve are almost accurate while for the rest, the accuracy gradually decreases and the curves diverge so that the last 15% of the frequencies obtained based on  $I = J = 7$  are not reliable. The curves corresponding to the higher values for  $I$  and  $J$  ( $I = J = 11, 13$ ) confirm the starting point of the error. Therefore, it can be concluded that the first 75% of the natural frequencies obtained based on  $I = J = 7$  are reliable.

In a similar manner as explained for  $I = J = 7$ , this explanation corresponds to  $I = J = 9$  and  $I = J = 11$ . Therefore, it can be concluded that the last 15% of the frequencies obtained based on a fixed  $I$  and  $J$ , (at least up to 11) are not reliable.

The starting point of the error for CCFF plate is almost the same as that of SSSS and is equal to 75% while that of the CCCC plate is 65%. In order to avoid any miscalculation caused by this inaccuracy, two suggestions are offered.

**Suggestion 1:** In order to obtain accurate values of natural frequencies, the upper bound values for  $I$  and  $J$  are selected higher than what is required such that the frequencies within the accurate range are sufficiently numerous. Then, by excluding the inaccurate frequencies, the rest of the values are accurate and are sufficient in number as the upper bound values of  $I$  and  $J$  are high. Besides, for eigenvectors, values corresponding to reserved frequencies are retained and the rest are excluded. Furthermore, for each set of eigenvectors, values corresponding to the last terms of the shape function are omitted such that the matrix of the eigenvectors remains square. By this approach, eigenvalues and eigenvectors derived from Ritz method are filtered and reliable values are put into further use in forced vibration analysis.

**Suggestion 2:** For the forced vibration analysis, using high order of  $I$  and  $J$  ensures that accurate frequencies play the important role in the deflection function while inaccurate ones correspond to sufficiently weak terms. Therefore, by testing different values for  $I$  and  $J$  until when the numerical result converges, the solution is made reliable. By this approach, the complications caused by the previous suggestion is avoided.

In the present study, considering suggestion 2, the calculations have been performed based on  $I = J = 13$  and the derived mass and stiffness matrices as well as eigen values and eigenvectors are used in the next chapter for the forced vibration analysis.

It can be observed from Figures 2.18 - 2.20 that the natural frequency values calculated by the Ritz method for the tapered configurations, are over estimated and by increasing the number of terms considered for the out of plane displacement function in equation (2.51), this error is reduced.

## **2.12 Numerical results and discussion**

After demonstration, the developed formulation based on CLPT and FSDT are applied to study tapered plates of various lengths, with four taper configurations, and with three different boundary conditions. The obtained results for each case, including eigenvalues and eigenvectors determined by solving the eigenvalue problem, as well as mass and stiffness matrices, are reserved for further use in the next chapter. The fundamental frequency for each case is given in Tables 2.11 - 2.13.

Length (cm); Angle (deg)	Length Mean Thickness	Configuration A				Configuration B			
		SSSS		CCCC		SSSS		CCCC	
		CLPT	FSDT	CLPT	FSDT	CLPT	FSDT	CLPT	FSDT
85.94; 0.1°	286.5	111.4	110.3	234.7	231.7	108.0	107.0	229.2	226.9
34.38; 0.25°	114.60	696	688	1467	1452	675	668	1432	1418
17.19; 0.5°	57.3	2784	2751	5866	5746	2700	2670	5728	5623
11.46; 0.75°	38.2	6264	6160	13198	12749	6075	5983	12888	12498
8.59; 1°	28.6	11138	10879	23469	22278	10802	10576	22917	21895
6.87; 1.25°	22.9	17409	16902	36682	35614	16884	16392	35821	34778
5.73; 1.5°	19.1	25045	24003	52770	46830	24289	23391	51532	46332

*Table 2.11 Fundamental frequency (rad/s) values of tapered composite plates for different lengths and taper angles for configurations A and B*

Length (cm); Angle (deg)	Length Mean Thickness	Configuration C				Configuration D			
		SSSS		CCCC		SSSS		CCCC	
		CLPT	FSDT	CLPT	FSDT	CLPT	FSDT	CLPT	FSDT
85.94; 0.1°	286.5	110.7	109.7	236.2	233.9	105.1	104	221.2	218.4
34.38; 0.25°	114.6	692	685	1476	1461	657	651	1382	1370
17.19; 0.5°	57.3	2766	2736	5902	5792	2627	2597	5527	5427
11.46; 0.75°	38.2	6224	6130	13280	12862	5909	5820	12434	12071
8.59; 1°	28.6	11066	10831	23614	22508	10507	10292	22111	21179
6.87; 1.25°	22.9	17297	16808	36909	34335	16423	15964	34560	32175
5.73; 1.5°	19.1	24883	23933	53095	47489	23628	22786	49721	44970

*Table 2.12 Fundamental frequency (rad/s) values of tapered composite plates for different lengths and taper angles for configurations C and D*

In the case of FSDT, the admissible functions corresponding to CCFF plate have not been found among the references. Therefore, the results for CCFF plate are obtained solely based on CLPT and displayed in Table 2.13.

<b>CCFF; Based on CLPT</b>					
<b>Length (cm); Angle (deg)</b>	<b>Length Mean Thickness</b>	<b>Configuration A</b>	<b>Configuration B</b>	<b>Configuration C</b>	<b>Configuration D</b>
<b>85.94; 0.1°</b>	<b>286.5</b>	50.4	52.2	54.7	49.4
<b>34.38; 0.25°</b>	<b>114.60</b>	315	326	341.61	308
<b>17.19; 0.5°</b>	<b>57.3</b>	1259	1304	1366	1235
<b>11.46; 0.75°</b>	<b>38.2</b>	2833	2934	3073	2779
<b>8.59; 1°</b>	<b>28.6</b>	5038	5216	5465	4942
<b>6.87; 1.25°</b>	<b>22.9</b>	7873	8151	8540	7723
<b>5.73; 1.5°</b>	<b>19.1</b>	11328	11729	12287	11114

*Table 2.13 Fundamental frequency (rad/s) values of tapered composite plates for different lengths and taper angles*

According to Tables 2.11 - 2.13, the fundamental frequencies for the CCCC and CCFF plates are the highest and the lowest respectively. It is observed from the tables that regardless of the boundary condition, by increasing the taper angle which results in smaller length, the fundamental frequency of the plate increases.

In order to visualize the data given in Tables 2.11 - 2.13, the following graphs are depicted by Figures 2.21 - 2.24.  ${}^c\omega_{11}$  and  ${}_F\omega_{11}$  are the fundamental frequencies obtained based on CLPT and FSDT formulations, respectively. Figures 2.21 and 2.22 illustrate the change of frequency ratio  ${}_F\omega_{11} / {}^c\omega_{11}$  with increase of length over mean thickness ratio. Figure 2.23 and Figure 2.24 illustrate the change of fundamental frequency with increase of length over mean thickness ratio for different boundary conditions for CLPT and FSDT.

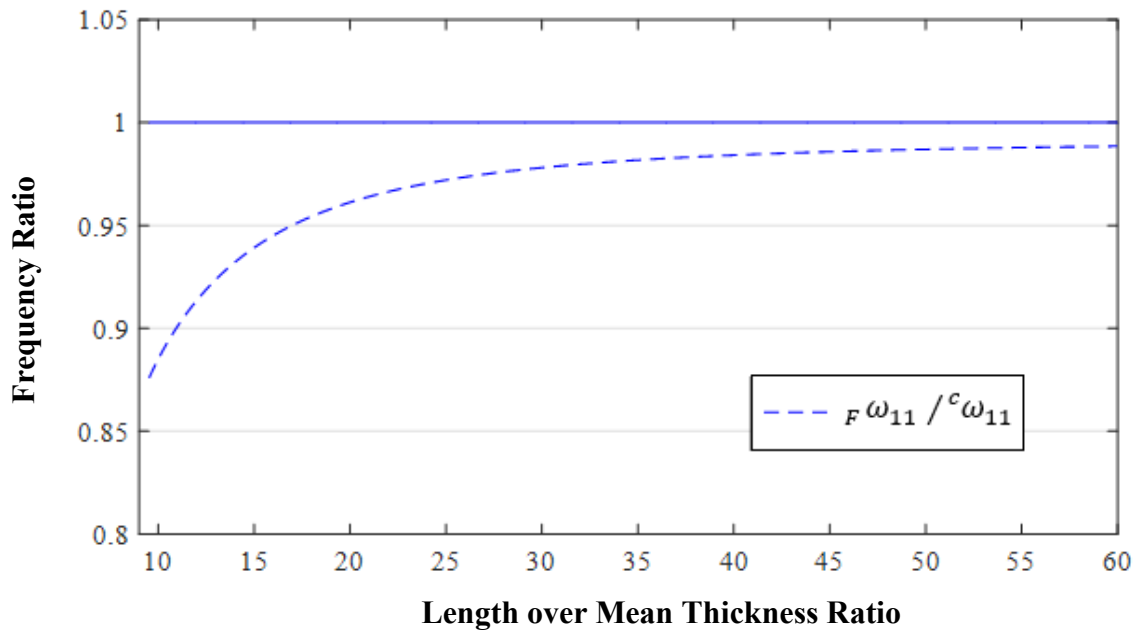


**Figure 2.21** Frequency ratio  ${}_F\omega_{11} / {}^c\omega_{11}$  for different lengths of the taper configuration A



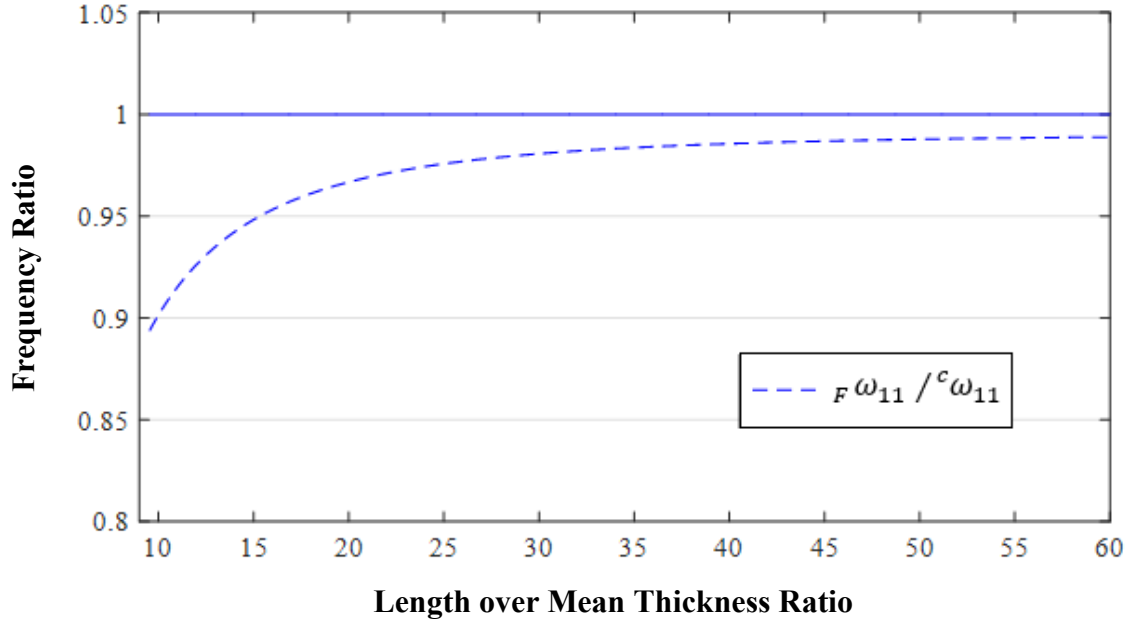


**Figure 2.22** Frequency ratio  $F \omega_{11} / {}^c \omega_{11}$  for different lengths of the taper configuration D

For different lengths of the tapered laminates with configurations described by Figure 2.1, the mean thickness is constant as the thickness of the left and right ends of the plate stays the same. Therefore, increase in the length to mean thickness ratio means that the laminate's length increases. It is grasped from Figures 2.21 and 2.22 that by increase in the laminate length, the difference between the CLPT-based and FSDT-based fundamental frequencies decreases such that the FSDT to CLPT frequency ratio tends to 1.

Figures 2.23 and 2.24 illustrate the fundamental frequency values for different lengths of the tapered laminates.

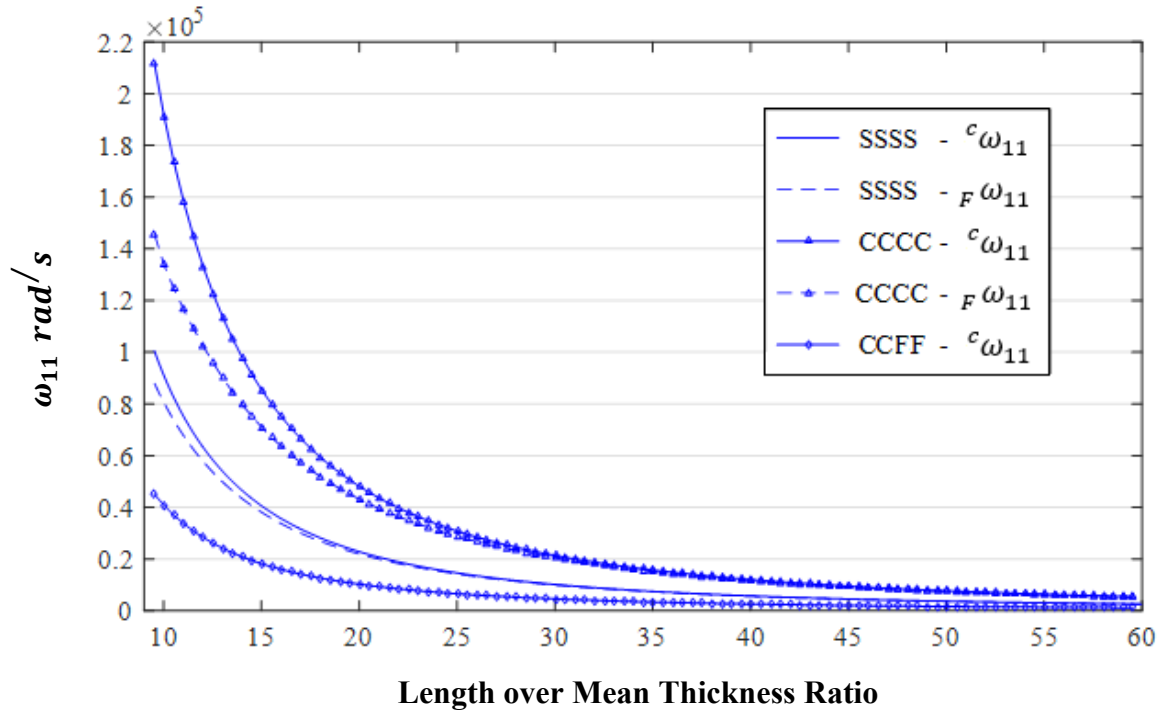


**Figure 2.23** CLPT-based and FSDT-based fundamental frequencies for different boundary conditions and lengths (configuration A)

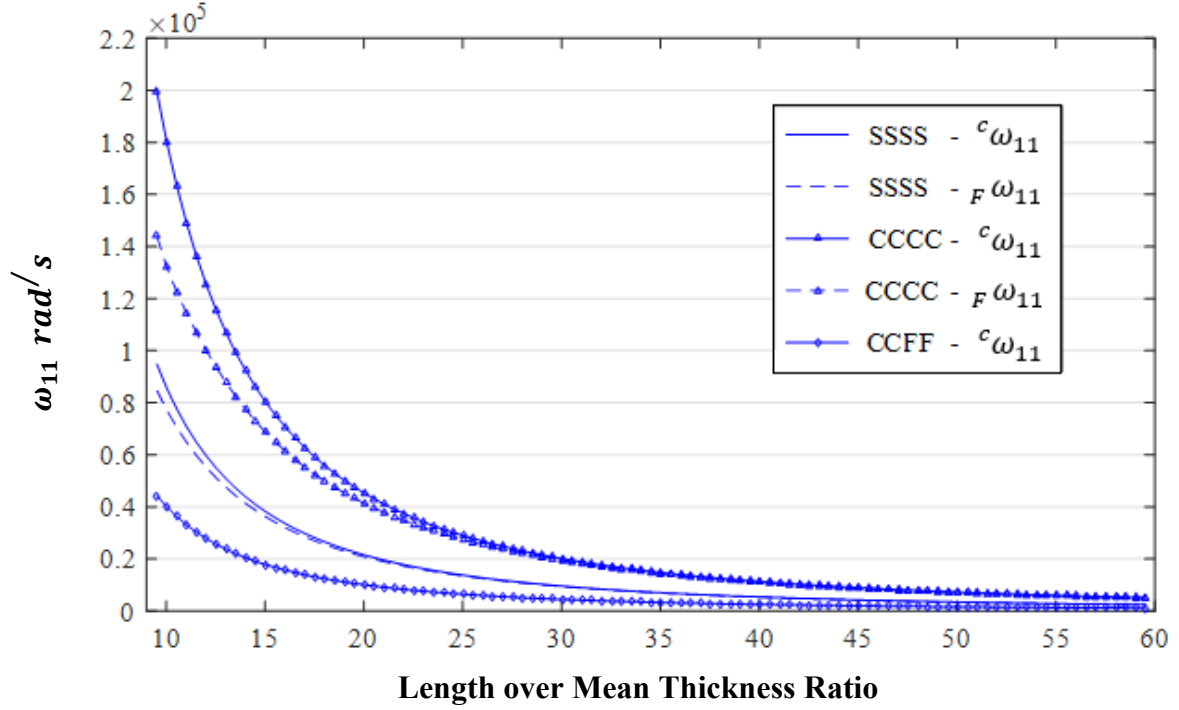


**Figure 2.24** CLPT-based and FSDT-based fundamental frequencies for different boundary conditions and lengths (configuration D)

From Figure 2.24 and Figure 2.23 it can be observed that by increase in laminate length, the fundamental frequency decreases and the difference between the CLPT-based and FSDT-based results decreases. Since the trends for all taper configurations are the same, the results corresponding to configurations A and D which display a greater difference, have been illustrated. The numerical results for the CCFF plates are the lowest and that of the CCCC plates are the highest.

By increase in the length over mean thickness ratio the fundamental frequency decreases such that when this ratio starting from 19.1 approaches 57.3, the fundamental frequency is reduced to 11%. This explanation is true for all the boundary conditions; however, this reduction in fundamental frequency for CCFF and SSSS plates, with slight difference, are the highest and the lowest, respectively.

The difference in the taper configurations subjected to the study is mainly in the internal regions while the external layers are similar. The following example shows the important role of the external plies in determining the fundamental frequency value of a plate.

**Example:** Consider the two uniform square laminated plates shown in Figure 2.25, with the mechanical and geometrical properties described as below.

Two uniform laminated square plates with all simply supported edges are considered with the configuration of  $(0/90)_{9s}$  made of unidirectional plies of NCT-301 Graphite-Epoxy material (Table 2.3) with ply thickness and length of  $125 \times 10^{-6}$  m and 0.35 m, respectively.

In the second laminate, 24 plies in the middle of the plate are replaced by resin with the same thickness as depicted in Figure 2.25. Obtain and compare the fundamental frequencies.

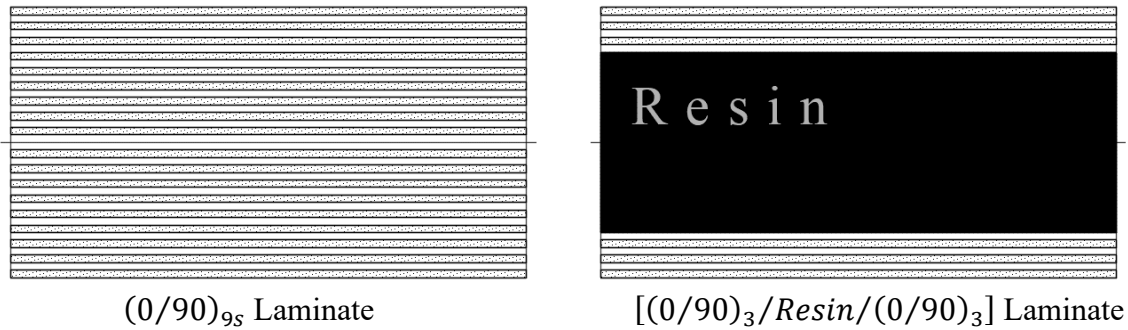


**Figure 2.25** Two uniform laminates of same thickness and with difference in internal structure

**Solution:** The natural frequencies of a uniform laminated composite plate with all simply supported edges are determined using the exact solution given by equation (2.119). In order to obtain the fundamental frequency, the condition is  $i, j = 1$  resulting in equation (2.120).

Fundamental frequencies obtained for the first and the second plates are equal to 1016 *rad/s* and 989 *rad/s*, respectively. Therefore, in spite of using three times more plies in the structure of the first laminate, there is merely a slight difference between the two fundamental frequencies. This example shows that the stiffness of a ply that is close to the midplane is significantly less responsible for increasing the fundamental frequency in comparison with an external ply.

Consider the order of 3 for the variable  $z$ , the distance from the midplane, in the bending stiffness elements  $R_{ij}^{(3)}$  in equation (2.85) when  $n = 3$ . It shows that the external plies are mostly responsible for increasing the bending stiffness elements of the laminate as their distance  $z$  is greater than that of the internal plies. On the other hand, the density of the plies is greater than that

of the resin regardless of the region they are used in. Therefore, the internal plies close to the midplane do not significantly contribute in increasing the fundamental frequency of the plates compared to external plies while they still increase the mass of the plate as much as the external plies.

## 2.13 Conclusion

In this chapter, the stiffness and mass matrices based on CLPT and FSDT, for the tapered laminated plates have been obtained. The eigenvalue problems for the plates under three different boundary conditions and with various lengths have been solved. The natural frequencies and mode shapes of the plate have been obtained and the so-called layer reduction test has been carried out. The numerical results have been given in tables and graphs. Considering the obtained results, the following conclusions are made:

1. Regardless of the taper configuration, the fundamental vibration frequency for CCCC plate is the highest and that of the CCFF plate is the lowest such that for configuration A with the highest difference rate, fundamental frequency of the CCCC plate is 465% of that of the CCFF plate and for configuration D with the lowest difference rate, fundamental frequency of the CCCC plate is 448% of the CCFF plate when the side length of the plate is 0.8594 m.

2. Regardless of the boundary condition and taper configuration, decrease in the length over mean thickness ratio results in higher fundamental frequency such that when this ratio is reduced from 57.3 to 19.1, the fundamental frequency (in general, from 2700  $rad/s$  for SSSS plates, 5750  $rad/s$  for CCCC plates and 1300  $rad/s$  for CCFF plates) increases roughly by 800% for all the plates. However, this increase for CCFF and SSSS plates, with slight difference, are the highest and lowest, respectively.

3. Layer reduction test shows that for a fixed-length laminate, increasing the taper angle by removing the plies results in a decrease in the fundamental frequency. At beginning of the test with no ply drop-off, the fundamental frequency obtained for the tapered laminate based on the Ritz method is equal to that of the thick and thin laminates obtained based on the exact solution method. The fundamental frequency for the tapered laminate is lower than that of the thick plate and higher

than that of the thin plate at each single step of the test. The obtained results for the thick, tapered and thin laminates based on FSDT are slightly lower than that of the CLPT-based results at each single step of the test and this slight difference is reduced with increase of dropped-off plies as the length over mean thickness ratio increases.

4. Since transverse shear stresses are considered in FSDT, numerical results obtained for the natural frequencies based on this theory are more accurate. For the square tapered plates with smaller side length, the difference between the fundamental frequencies obtained based on CLPT and FSDT are greater. In general, for a fixed side length, this difference for CCCC plate is larger compared with SSSS plates. However, the difference is not sufficiently great to justify the expense of computational effort imposed by FSDT, especially in modal analysis. Therefore, CLPT is selected for further analysis including forced vibration study in further chapters.

5. In composite plates, the plies close to the midplane do not significantly contribute to increasing the natural frequencies even though their inertia (mass) contribution is the same as that of other plies.

6. For the SSSS boundary condition, configuration A with sufficient outer plies and resin as a lighter inner material vibrates with the highest frequency among all the tapered configurations and configuration C comes the second. By using plies in inner layers of configuration C, it becomes heavier in comparison with configuration A while such plies do not contribute significantly in increasing the stiffness, therefore, configuration A with considerably fewer plies, still exhibits high fundamental frequency. However, in CCCC and CCFF boundary conditions, fundamental frequency of the configuration C, is the highest among all the tapered configurations.

7. Considering configuration C with the resin used at the core along the midplane and configurations B and D, all possessing the same mass distribution, configuration C vibrates with the highest natural frequency since the resin as the weaker material is used at the core along the midplane and the plies contribute in the best way among the configurations B, C and D. For configurations B and D, resin is used in the regions farther from the midplane which prevents the plies from using their stiffness potential to the full capacity. In configuration D, resin is used in the region close to the external layers such that it vibrates with the lowest natural frequency among all the configurations.

## **Chapter 3 :**

### **Forced vibration analysis of tapered composite plates**

#### **3.1 Introduction**

In chapter 2, free vibration analysis was carried out and the mass and stiffness matrices were obtained based on CLPT and FSDT. Then, using these matrices, the Ritz method was applied forming an eigenvalue problem leading to the determination of natural frequencies and the parameters corresponding to the mode shapes.

In the present chapter, the assumed modes method is used to study the forced vibrations of tapered composite plates. According to Ref. [31], the solution of the problem is assumed in the form of series composed of linear combination of admissible functions of the spatial coordinates satisfying essential (geometric) boundary conditions, multiplied by time-dependent generalized coordinates. Strain and kinetic energies as well as virtual work of conservative and nonconservative forces are expressed in terms of the assumed modes solution. The CLPT is used. The mass and stiffness matrices derived in chapter 2 based on CLPT, are reused here in chapter 3 in the assumed modes method. The Lagrange's equations are used to establish the equations of motion of the equivalent  $n$ -degrees-of-freedom discrete system of the continuous system. Parameters of the mode shapes and the natural frequencies, as the eigenvectors and square roots of corresponding eigenvalues respectively, are the essential requirements for the forced vibration analysis of tapered laminated composite plates using assumed modes method. Afterward, with the mathematical operations performed on the Multi Degree of Freedom (MDOF) discrete system, the solution is obtained. The deflection function composed of spatial and time-dependent functions describes the dynamic behavior of the laminate.

#### **3.2 Forced vibration response based on CLPT**

In forced vibration analysis, the transverse deflection function is expressed in the form of series according to Ref. [32].

$$w_o^F = \sum_{i=1}^I \sum_{j=1}^J A_{ij}^F(t) X_i(x) Y_j(y) \quad (3.1)$$

where,  $w_o^F$  is the transverse displacement function in forced vibration analysis and  $A_{ij}^F$  is the parameter corresponding to the admissible functions  $X_i$  and  $Y_j$  determined by geometric boundary conditions discussed in chapter 2. The right superscript  $F$  in the terms  $w_o^F$  and  $A_{ij}^F$  stands for forced vibration response. The derivative of transverse displacement function  $w_o^F$  with respect to time is obtained as follows.

$$\dot{w}_o^F = \sum_{i=1}^I \sum_{j=1}^J \dot{A}_{ij}^F X_i Y_j \quad (3.2)$$

The overdot notation indicates the derivative with respect to time, for example:  $\dot{w}_o^F = dw_o^F/dt$ . The admissible spatial functions  $X_i$  and  $Y_j$  corresponding to the geometric boundary conditions explained in chapter 2 are substituted in equation (3.1).

### 3.2.1 Undamped forced vibration

Stiffness and mass matrices obtained from strain and kinetic energies in chapter 2, are used in the assumed modes method in the present chapter. Following Ref. [31], in addition to strain and kinetic energies, virtual work of external forces is taken into consideration in forced vibration analysis.

$$\delta W = \iint f(x, y, t) \delta w_o^F dA \quad (3.3)$$

where,  $W$  is the work done by the external force  $f(x, y, t)$  and  $\delta$  denotes virtual quantities. Substituting equation (3.1) in (3.3):

$$\delta W = \sum_{i=1}^I \sum_{j=1}^J \iint f(x, y, t) X_i(x) Y_j(y) dA (\delta A_{ij}^F) \quad (3.4)$$



Writing the above expression in the form below:

$$\delta W = \sum_{i=1}^I \sum_{j=1}^J F_{ij} (\delta A_{ij}^F) \quad (3.5)$$

$$F_{ij} = \iint f(x, y, t) X_i(x) Y_j(y) dA \quad (3.6)$$

Lagrange's equations are expressed according to Ref. [31]:

$$\frac{d}{dt} \left( \frac{\partial (^c T)}{\partial \dot{A}_{ij}^F} \right) + \frac{\partial (^c U)}{\partial A_{ij}^F} = F_{ij} \quad (3.7)$$

where,  $i = 1, 2, 3, \dots, I$  and  $j = 1, 2, 3, \dots, J$ . Considering all possible integer values of  $i$  and  $j$  in equation (3.7), the mass  $[^c M]$  and stiffness  $[^c K]$  matrices and force matrix  $\{F\}$  are obtained from equation (3.7).

$$[^c M]_{IJ \times IJ} \{\ddot{A}^F\}_{IJ \times 1} + [^c K]_{IJ \times IJ} \{A^F\}_{IJ \times 1} = \{F\}_{IJ \times 1} \quad (3.8)$$

Equation (3.8) represents the matrix equation of motion of the equivalent n-degrees-of-freedom discrete system of the continuous system. According to Ref. [33], the general solution is in the form of:

$$\{A^F\} = \sum_{i=1}^I \sum_{j=1}^J \{A^{\omega_{ij}}\} q_{ij}(t) \quad (3.9)$$

where,  $\{A^{\omega_{ij}}\}$  contains the eigenvector corresponding to the  $ij^{\text{th}}$  natural frequency  $\omega_{ij}$  that has been normalized with respect to mass matrix  $[^c M]$ . In the n-degrees-of-freedom discrete system of the continuous system,  $q_{ij}(t)$  is known as the time-dependent generalized coordinate.

The derivatives of  $\{A^F\}$  with respect to time are calculated and expressed in matrix form after the summations have been taken care of.

$$\{A^F\} = [A^\omega]_{IJ \times IJ} \{q\}_{IJ \times 1} \quad (3.10)$$

$$\{\dot{A}^F\} = [A^\omega]_{IJ \times IJ} \{\dot{q}\}_{IJ \times 1} \quad (3.11)$$

$$\{\ddot{A}^F\} = [A^\omega]_{IJ \times IJ} \{\ddot{q}\}_{IJ \times 1} \quad (3.12)$$

Square matrix  $[A^\omega]$  contains all column matrices  $\{A^{\omega_{ij}}\}$ , and column matrix  $\{q\}$  contains elements  $q_{ij}$ , and column matrices  $\{\dot{q}\}$  and  $\{\ddot{q}\}$  are derivatives of  $\{q\}$  with respect to time. Substituting equations (3.10) and (3.12) in equation (3.8):

$$[{}^c M][A^\omega]\{\ddot{q}\} + [{}^c K][A^\omega]\{q\} = \{F\} \quad (3.13)$$

Multiplying both sides by  $[A^\omega]^T$ :

$$[A^\omega]^T [{}^c M][A^\omega]\{\ddot{q}\} + [A^\omega]^T [{}^c K][A^\omega]\{q\} = [A^\omega]^T \{F\} \quad (3.14)$$

Since  $[A^\omega]$  is normalized matrix with respect to mass matrix, the terms  $[A^\omega]^T [{}^c M][A^\omega]$  and  $[A^\omega]^T [{}^c K][A^\omega]$  are equal to  $[I]$  and  $[\omega^2]$ , respectively.  $[I]$  is the identity matrix. Matrix  $[\omega^2]$  is the diagonal matrix containing the natural frequencies obtained by solving the eigenvalue problem in chapter 2. Using notation  $\{\bar{F}\} = [A^\omega]^T \{F\}$ , equation (3.14) is rewritten as follows.

$$\{\ddot{q}\} + [\omega^2]\{q\} = \{\bar{F}\} \quad (3.15)$$

Considering that  $[\omega^2]$  is a diagonal matrix, equation (3.15) is decoupled as follows.

$$\ddot{q}_{ij} + \omega_{ij}^2 q_{ij} = \bar{F}_{ij} \quad (3.16)$$

where,  $\bar{F}_{ij}$  is the  $ij^{\text{th}}$  element of the column matrix  $\{\bar{F}\}$  and  $i = 1, 2, \dots, I$  and  $j = 1, 2, \dots, J$ . The solution of equation (3.16) is given by Ref. [33] as follows.

$$q_{ij}(t) = q_{ij}(0) \cos(\omega_{ij}t) + \frac{1}{\omega_{ij}} \left[ \dot{q}_{ij}(0) \sin(\omega_{ij}t) + \int_0^t \bar{F}_{ij}(\tau) \sin(\omega_{ij}(t - \tau)) d\tau \right] \quad (3.17)$$

By setting the initial displacement and velocity to zero, terms  $q_{ij}(0)$  and  $\dot{q}_{ij}(0)$  for any integer values of  $i$  and  $j$  are zero (Appendix A.4) and equation (3.17) becomes:

$$q_{ij}(t) = \frac{1}{\omega_{ij}} \int_0^t \bar{F}_{ij}(\tau) \sin(\omega_{ij}(t - \tau)) d\tau \quad (3.18)$$

where,  $i = 1, 2, 3, \dots, I$  and  $j = 1, 2, 3, \dots, J$ . By substituting (3.18) in (3.9),  $\{A^F\}$  is obtained. Then, in order to determine the transverse displacement function  $w_o^F$  for the forced vibration analysis with no damping, elements of  $\{A^F\}$  are substituted in equation (3.1).

### 3.2.2 Forced vibration with viscous damping

In this sub-section, the viscous damping effect is taken into consideration and corresponding transverse displacement function is obtained. In a similar manner to that of the previous sub-section, the investigation is conducted using Refs. [31] and [33]. Considering viscous damping, Lagrange's equation is expressed as follows.

$$\frac{d}{dt} \left( \frac{\partial(^c T)}{\partial \dot{A}_{ij}^F} \right) + \frac{\partial U_d}{\partial \dot{A}_{ij}^F} + \frac{\partial(^c U)}{\partial A_{ij}^F} = F_{ij} \quad (3.19)$$

where,  $i = 1, 2, 3, \dots, I$  and  $j = 1, 2, 3, \dots, J$ . Dissipation of energy is represented by  $U_d$  and considering all integer values of  $i$  and  $j$  in equation (3.19), the mass  $[^c M]$ , stiffness  $[^c K]$  and damping  $[U_d]$  matrices are substituted in equation (3.19) according to Ref. [32].

$$[^c M]_{IJ \times IJ} \{\ddot{A}^F\}_{IJ \times 1} + [U_d]_{IJ \times IJ} \{\dot{A}^F\}_{IJ \times 1} + [^c K]_{IJ \times IJ} \{A^F\}_{IJ \times 1} = \{F\}_{IJ \times 1} \quad (3.20)$$

For simplicity, it is assumed that the Rayleigh damping is capable of describing the damping effect of the tapered laminates. By this assumption,  $[U_d]_{IJ \times IJ}$  can be written into a linear combination of mass and stiffness matrices as below.

$$[U_d]_{IJ \times IJ} = \alpha [{}^c M]_{IJ \times IJ} + \beta [{}^c K]_{IJ \times IJ} \quad (3.21)$$

where,  $\alpha$  and  $\beta$  are material parameters. Values of  $\alpha$  and  $\beta$  for the material considered in the present work are given in Refs. [3] and [34]. The general solution is given by equation (3.9) which is expressed by equation (3.10) in matrix form. Substituting equations (3.10), (3.11), (3.12) and (3.21) in (3.20):

$$[{}^c M][A^\omega]\{\ddot{q}\} + (\alpha [{}^c M] + \beta [{}^c K])[A^\omega]\{\dot{q}\} + [{}^c K][A^\omega]\{q\} = \{F\} \quad (3.22)$$

Multiplying both sides by  $[A^\omega]^T$ :

$$\begin{aligned} [A^\omega]^T [{}^c M][A^\omega]\{\ddot{q}\} + (\alpha [A^\omega]^T [{}^c M][A^\omega] + \beta [A^\omega]^T [{}^c K][A^\omega])\{\dot{q}\} + [A^\omega]^T [{}^c K][A^\omega]\{q\} \\ = [A^\omega]^T \{F\} \end{aligned} \quad (3.23)$$

Since  $[A^\omega]$  is normalized matrix with respect to mass matrix, according to Ref. [31], terms  $[A^\omega]^T [{}^c M][A^\omega]$  and  $[A^\omega]^T [{}^c K][A^\omega]$  are equal to  $[I]$  and  $[\omega^2]$ , respectively. Matrix  $[I]$  is the identity matrix and  $[\omega^2]$  is the diagonal matrix containing the natural frequencies obtained by solving the eigenvalue problem in chapter 2. Using notation  $[A^\omega]^T \{F\} = \{\bar{F}\}$ , equation (3.23) is rewritten.

$$\{\ddot{q}\} + (\alpha [I] + \beta [\omega^2])\{\dot{q}\} + [\omega^2]\{q\} = \{\bar{F}\} \quad (3.24)$$

Considering that  $[\omega^2]$  is a diagonal matrix, equation (3.24) is decoupled as follows.

$$\ddot{q}_{ij} + (\alpha + \beta \omega_{ij}^2)\dot{q}_{ij} + \omega_{ij}^2 q_{ij} = \bar{F}_{ij} \quad (3.25)$$

According to Ref. [33], the following equation is written:

$$\alpha + \beta \omega_{ij}^2 = 2\zeta_{ij}\omega_{ij} \quad (3.26)$$

where,  $\zeta_{ij}$  is the damping ratio. Substituting equation (3.26) in (3.25):

$$\ddot{q}_{ij} + 2\zeta_{ij}\omega_{ij}\dot{q}_{ij} + \omega_{ij}^2 q_{ij} = \bar{F}_{ij} \quad (3.27)$$

The solution of the equation (3.27) is given by Ref. [33].

$$q_{ij}(t) = e^{-\zeta_{ij}\omega_{ij}t} \left[ \cos(\omega_{dij}t) + \frac{\zeta_{ij}\omega_{ij}}{\omega_{dij}} \sin(\omega_{dij}t) \right] q_{ij}(0) + \frac{1}{\omega_{dij}} \left[ e^{-\zeta_{ij}\omega_{ij}t} \sin(\omega_{dij}t) \dot{q}_{ij}(0) + \int_0^t \bar{F}_{ij}(\tau) e^{-\zeta_{ij}\omega_{ij}(t-\tau)} \sin(\omega_{dij}(t-\tau)) d\tau \right] \quad (3.28)$$

where,  $\omega_{dij} = \omega_{ij}\sqrt{1 - \zeta_{ij}^2}$  and  $i = 1, 2, 3, \dots, I$  and  $j = 1, 2, 3, \dots, J$ .

Considering zero initial displacement and velocity,  $q_{ij}(0)$  and  $\dot{q}_{ij}(0)$  are zero (Appendix A.4) and equation (3.28) is simplified.

$$q_{ij}(t) = \frac{1}{\omega_{dij}} \int_0^t \bar{F}_{ij}(\tau) e^{-\zeta_{ij}\omega_{ij}(t-\tau)} \sin(\omega_{dij}(t-\tau)) d\tau \quad (3.29)$$

where,  $i = 1, 2, 3, \dots, I$  and  $j = 1, 2, 3, \dots, J$ . By substituting equation (3.29) in (3.9),  $\{A^F\}$  is obtained. Then, in order to determine the transverse displacement function for the forced vibration analysis with damping effect, elements of  $\{A^F\}$  are substituted in equation (3.1).

### 3.3 Loading types

In the forced vibration analysis of the tapered laminates, the response of the plates due to external force is studied. In this section, 4 different types of line loads as the external forces are described. The corresponding expressions of the excitations have been given in Table 3.1.

	Loading ( $N/m^2$ ) Types			
	Type 1	Type 2	Type 3	Type 4
Spatial Function	$\delta\left(x-\frac{L}{2}\right)$	$\delta\left(y-\frac{L}{2}\right)$	$\delta\left(x-\frac{L}{2}\right)\sin\left(\pi\frac{x}{L}\right)$	$\delta\left(y-\frac{L}{2}\right)\sin\left(\pi\frac{y}{L}\right)$
Time Function	$(-500)\cos(\Omega t)$			
$\Omega=0.3\omega_{11}$				

**Table 3.1** Four types of loading

where,  $\delta$  is the Dirac delta function and  $\omega_{11}$  and  $\Omega$  are the fundamental frequency of the plate and excitation frequency, respectively. Figures 3.1 - 3.4 provide a visual perception of the spatial variation in coordinate system  $xyz$ , of the excitation types given in Table 3.1.

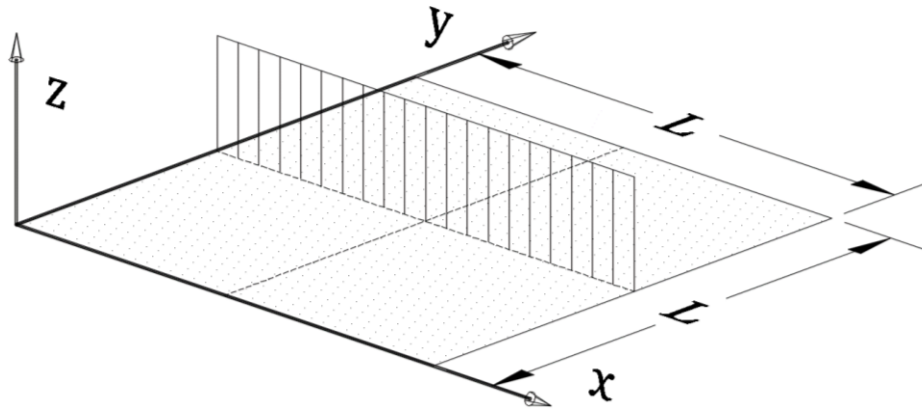


**Figure 3.1** Line load type 1

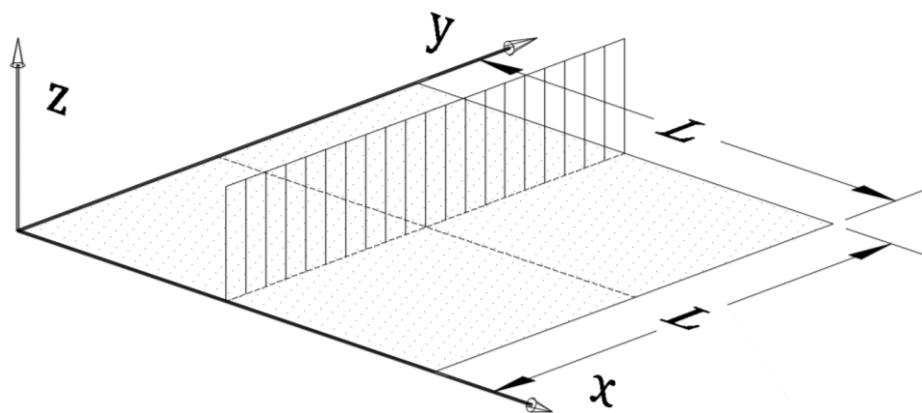


*Figure 3.2 Line load type 2*

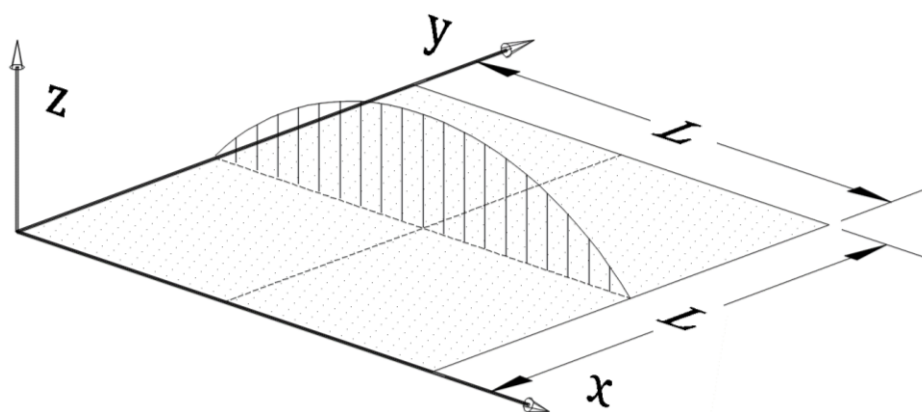


*Figure 3.3 Line load type 3*

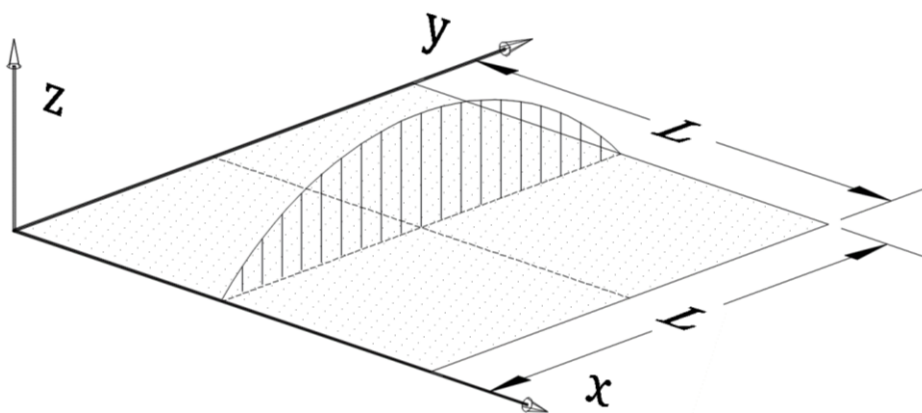


*Figure 3.4 Line load type 4*

The loading types 1 and 3 have been applied at the middle of the laminate along the taper direction  $x$ . The difference between loading types 1 and 3 is that the magnitude of the loading type 1 is constant along the laminate's length while the magnitude of loading type 3 shows a sinusoidal variation along  $x$ .

The loading types 2 and 4 have been applied at the middle of the laminate perpendicular to the taper direction  $x$ . The difference between loading types 2 and 4 is that the magnitude of the loading type 2 is constant along the laminate's width while the magnitude of loading type 4 shows a sinusoidal variation along  $y$ .

The excitations described in present section, are applied to the tapered laminates and the responses are analyzed. In the present paper, the deflection of the transverse normal at the center of the laminate is investigated.

Consider the vibration of a uniform SSSS or CCCC square plate due to a uniformly distributed loading with sinusoidal time function. The peak deflection of the plate occurs exactly at the point located at the center of the plate. For a SSSS or CCCC plate with taper configuration, the peak deflection does not necessarily occur at the plate center (see Ref. [23]). In addition, for CCFF plate, the peak deflection of the laminate occurs at the point located at the intersection of the two free edges. However, in the present work, the time-maximum value (amplitude) of the deflection of the point located at the center of the tapered laminate is studied regardless of the peak deflection of the plate.

### **3.4 Validation**

#### **3.4.1 Isotropic plate**

In this section, for demonstration purposes, forced vibration investigations conducted in available literature using different approaches are considered. The assumed modes method solution is applied to the data given in the literature and the obtained results are compared. For a case of an isotropic plate subjected to harmonic loading, results obtained by Galerkin method and exact solution [31] are compared with that of the assumed modes method solution developed in the present study, in Table 3.2.



Using data from Ref. [35], for an isotropic square plate with all simply supported edges subjected to a harmonic excitation  $f(x, y, t) = f_o \cos(\Omega t)$ , the numerical results are displayed in Table 3.2 for the deflection of the point located at the center of the laminate. Note that for the exact solution, the numerical result is obtained using Ref. [31] that also corresponds to the exact solution given by Ref. [35]. Then the results obtained using the Galerkin method [35] and the formulation developed in the present study, are compared. Since the results given by Ref. [35], are in dimensionless form, an arbitrary plate and loading amplitude ( $f_o$ ) can be used.

$w(a/2, b/2) \times D/(f_o a^4)$ (dimensionless)			
Loading Frequency	Exact Solution [31]	Solution Using Galerkin Method [35]	Present Assumed Modes Method Solution
$\Omega = 0.3\omega_{11}$	0.0006984	0.00072	0.0006983
$\Omega = 0.5\omega_{11}$	0.0008537	0.00088	0.000829
$\Omega = 0.8\omega_{11}$	0.001813	0.00184	0.00177

**Table 3.2** Comparison between assumed modes method, Galerkin method and Exact solutions

In Table 3.2,  $w$  denotes the maximum deflection of the plate,  $a$  and  $b$  are length and width of the plate respectively (which are equal for the square plate), and  $D = Eh^3/12(1 - \nu^2)$  is the flexural rigidity of the plate.  $E, \nu$  and  $h$  are Young's Modulus, Poisson's Ratio and plate's thickness, respectively. Table 3.2 shows that the numerical results determined by using the assumed modes method are in good agreement with that of the other methods.

### 3.4.2 Composite plate

The exact solution for the deflection function for the uniform-thickness composite plate subjected to transverse harmonic loading is given in Ref. [9] provided that the boundary conditions are simply supported on all edges. In order to validate the formulation developed in the present chapter, a problem is solved based on assumed modes method and the result is compared with the numerical output obtained by using the exact solution [9].

A square laminated plate  $(0/90)_s$  with side length  $L$  of 0.1719 m made of unidirectional plies of NCT-301 Graphite-Epoxy material (mechanical properties were given in Table 2.3) with ply thickness of  $125 \times 10^{-6}$  m is at rest in equilibrium position. All edges are simply supported. The maximum transverse deflection of the plate at the center, when it is subjected to the given distributed loading, in  $N/m^2$ .

$$f(x, y, t) = -10 \cos(0.3\omega_{11}t) \sin \frac{\pi x}{L} \sin \frac{\pi y}{L} \quad (3.30)$$

where,  $\omega_{11}$  is the fundamental frequency of the plate.

**Solution [9]:** Considering notations  $(\alpha_i = i\pi/L)$  and  $(\beta_j = j\pi/L)$  given in Ref. [9], the transverse loading and deflection,  $f$  and  $w_o^F$ , are written in the form of series.

$$f(x, y, t) = \sum_{i=1}^{\infty} \sum_{j=1}^{\infty} P_{ij}(t) \sin(\alpha_i x) \sin(\beta_j y) \quad (3.31)$$

$$P_{ij}(t) = \frac{4}{L^2} \int_0^L \int_0^L f(x, y, t) \sin(\alpha_i x) \sin(\beta_j y) dx dy \quad (3.32)$$

The transverse deflection function is expressed in the following form:

$$w_o^F(x, y, t) = \sum_{i=1}^{\infty} \sum_{j=1}^{\infty} A_{ij}^F(t) \sin(\alpha_i x) \sin(\beta_j y) \quad (3.33)$$

Equations (3.31) and (3.33) are substituted in equation of motion (2.118).

$$\begin{aligned} \sum_{i=1}^{\infty} \sum_{j=1}^{\infty} A_{ij}^F \left[ R_{11}^{(3)} \alpha_i^4 + 2(R_{12}^{(3)} + 2R_{66}^{(3)}) \alpha_i^2 \beta_j^2 + R_{22}^{(3)} \beta_j^4 \right] \sin(\alpha_i x) \sin(\beta_j y) \\ - \sum_{i=1}^{\infty} \sum_{j=1}^{\infty} P_{ij} \sin(\alpha_i x) \sin(\beta_j y) = \end{aligned} \quad (3.34)$$

$$-R^{(1)} \sum_{i=1}^{\infty} \sum_{j=1}^{\infty} \ddot{A}_{ij}^F \sin(\alpha_i x) \sin(\beta_j y) - R^{(3)} \sum_{i=1}^{\infty} \sum_{j=1}^{\infty} (\alpha_i^2 \ddot{A}_{ij}^F + \beta_j^2 \ddot{A}_{ij}^F) \sin(\alpha_i x) \sin(\beta_j y)$$

Equation (3.34) is written in the following form:

$$\sum_{i=1}^{\infty} \sum_{j=1}^{\infty} \left( \left[ R_{11}^{(3)} \alpha_i^4 + 2(R_{12}^{(3)} + 2R_{66}^{(3)}) \alpha_i^2 \beta_j^2 + R_{22}^{(3)} \beta_j^4 \right] A_{ij}^F + [R^{(1)} + (\alpha_i^2 + \beta_j^2) R^{(3)}] \ddot{A}_{ij}^F - P_{ij} \right) \times \sin(\alpha_i x) \sin(\beta_j y) = 0 \quad (3.35)$$

Taking advantage of the orthogonality property in equation (3.35), for  $i, j = 1, 2, 3, \dots, \infty$ , it is expressed that:

$$P_{ij} - \left[ R_{11}^{(3)} \alpha_i^4 + 2(R_{12}^{(3)} + 2R_{66}^{(3)}) \alpha_i^2 \beta_j^2 + R_{22}^{(3)} \beta_j^4 \right] A_{ij}^F = (R^{(1)} + (\alpha_i^2 + \beta_j^2) R^{(3)}) \ddot{A}_{ij}^F \quad (3.36)$$

According to Ref. [9], some denotations are defined as follows.

$$K_{ij} = R_{11}^{(3)} \alpha_i^4 + 2(R_{12}^{(3)} + 2R_{66}^{(3)}) \alpha_i^2 \beta_j^2 + R_{22}^{(3)} \beta_j^4 \quad (3.37)$$

$$M_{ij} = R^{(1)} + R^{(3)} (\alpha_i^2 + \beta_j^2) \quad (3.38)$$

$$\bar{P}_{ij} = (P_{ij} / M_{ij}) \quad (3.39)$$

Substituting equations (3.37) and (3.38) in (3.36):

$$M_{ij} \ddot{A}_{ij}^F + K_{ij} A_{ij}^F = P_{ij} \quad (3.40)$$

Substituting equation (3.39) in (3.40):

$$\ddot{A}_{ij}^F + \left( \frac{K_{ij}}{M_{ij}} \right) A_{ij}^F = \bar{P}_{ij} \quad (3.41)$$

Considering equation (3.30), the distributed sinusoidal loading given in the problem, and equation (3.31), the series by which the loading has been expressed, for  $i = j = 1$ ,

$\bar{P}_{11} = -10 \cos(0.3\omega_{11}t)/M_{11}$  and for any integer values of  $i$  and  $j$ ,  $i, j \neq 1$ ,  $\bar{P}_{ij} = 0$ . Therefore, equation (3.41) is written in the following form.

$$\ddot{A}_{11}^F + \left(\frac{K_{11}}{M_{11}}\right)A_{11}^F = \frac{-10 \cos(0.3\omega_{11}t)}{M_{11}} \quad (3.42)$$

$$\ddot{A}_{ij}^F + \left(\frac{K_{ij}}{M_{ij}}\right)A_{ij}^F = 0 \quad i, j \neq 1 \quad (3.43)$$

The solution for the differential equation (3.41) is given by Ref. [9].

$$A_{ij}^F(t) = e_{ij} \cos(\mu_{ij}t) + e'_{ij} \sin(\mu_{ij}t) + A_{ij}^p(t) \quad (3.44)$$

$$\mu_{ij} = \sqrt{\frac{K_{ij}}{M_{ij}}} \quad (3.45)$$

where,  $e_{ij}$  and  $e'_{ij}$  are constants to be determined using the initial conditions,  $A_{ij}^p(t)$  is the particular solution. Considering equations (3.42), (3.43) and (3.44):

$$A_{11}^F(t) = e_{11} \cos(\mu_{11}t) + e'_{11} \sin(\mu_{11}t) - \frac{10 \cos(0.3\omega_{11}t)}{K_{11} - (0.3\omega_{11})^2 M_{11}} \quad (3.46)$$

$$A_{ij}^F(t) = e_{ij} \cos(\mu_{ij}t) + e'_{ij} \sin(\mu_{ij}t) \quad i, j \neq 1 \quad (3.47)$$

Considering zero initial displacement in equation (3.33), for any integer values of  $i$  and  $j$ ,  $A_{ij}^F(0) = 0$ . Therefore, in equation (3.47), when  $i, j \neq 1$ ,  $e_{ij} = 0$  and  $e_{11} = 10/K_{11} - (0.3\omega_{11})^2 M_{11}$ . Initial zero velocity results in  $e'_{ij} = 0$ , for any integer values of  $i$  and  $j$ . Therefore, equations (3.46) and (3.47) become:

$$A_{11}^F(t) = 10 \frac{\cos(\mu_{11}t) - \cos(0.3\omega_{11}t)}{K_{11} - (0.3\omega_{11})^2 M_{11}} \quad (3.48)$$

$$A_{ij}^F(t) = 0 \quad i, j \neq 1 \quad (3.49)$$

Equations (3.48) and (3.49) are substituted in equation (3.33), and the solution is derived.

$$w_o^F(x, y, t) = 10 \frac{\cos(\mu_{11}t) - \cos(0.3\omega_{11}t)}{K_{11} - (0.3\omega_{11})^2 M_{11}} \sin(\alpha_1 x) \sin(\beta_1 y) \quad (3.50)$$

In order to obtain the deflection function for the point located at the center of the laminate,  $x = L/2$  and  $y = L/2$  are substituted into equation (3.50).

$$w_o^F\left(\frac{L}{2}, \frac{L}{2}, t\right) = 10 \frac{\cos(\mu_{11}t) - \cos(0.3\omega_{11}t)}{K_{11} - (0.3\omega_{11})^2 M_{11}} \quad (3.51)$$

where,  $\mu_{11}$  is determined using equation (3.45).

This exact solution given by equation (3.51) and the results obtained by using the formulation developed in the present chapter, are plotted. Figure 3.5 illustrates the transverse deflection at the center over time by the two approaches. It is observed from Figure 3.5 that the results calculated by the two approaches correspond very well such that the curves corresponding to the two methods, coincide. The maximum deflection is equal to  $0.136 \times 10^{-3}$  m.

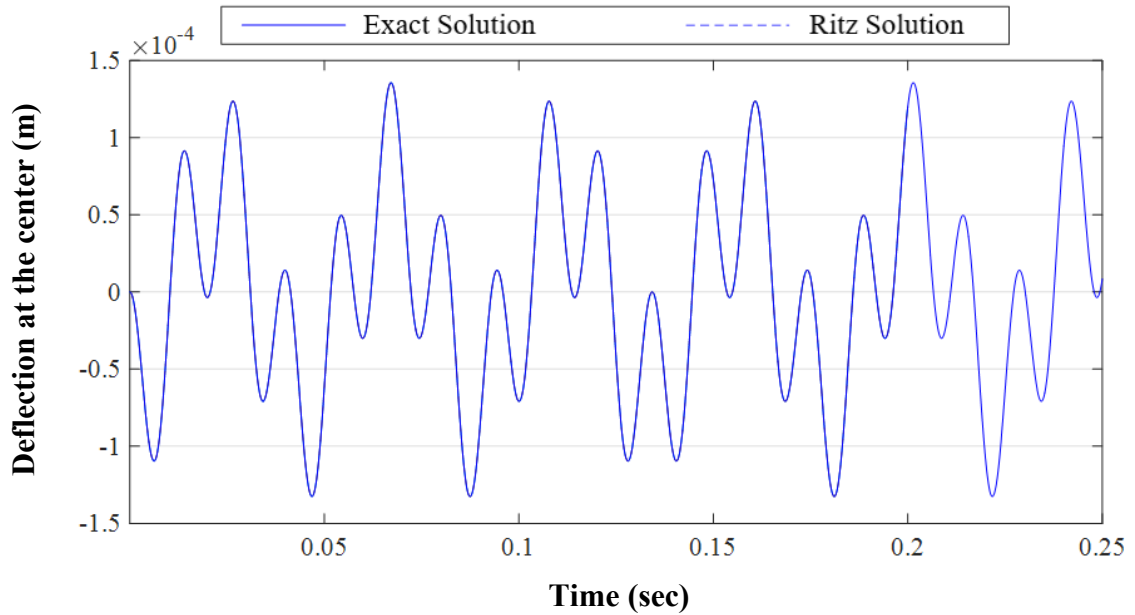


**Figure 3.5** Deflection at the center of the laminate over time due to transverse sinusoidal excitation

### 3.4.3 Layer reduction test

In this sub-section, in order to compare the transverse deflection of the uniform and tapered plates with SSSS boundary conditions due to predetermined excitation, a 12-stepped “layer reduction test” is implemented. The arrangement of the laminates (thick, thin and tapered plates) in different steps of the test, the layer removal and resin replacement process, are the same as that of the “layer reduction test” carried out and explained in chapter 2 and depicted by Figures 2.4 - 2.16. In the “layer reduction test” conducted in chapter 2, the subjects of the study are the fundamental frequencies of the thick, thin and tapered plates. However, in the “layer reduction test” in the present sub-section, the deflections at the center of the laminates described in the following, due to predetermined excitation are studied.

Three identical uniform-thickness laminated plates are considered with configuration of  $(0/90)_{95}$ , length of  $L_1 = 0.1719$  m, and width of  $L_2 = \frac{6}{5}L_1$  made of unidirectional NCT-301 Graphite-Epoxy material (mechanical properties were given in Table 2.3) with ply thickness of  $125 \times 10^{-6}$  m (Figure 2.4 shows the three identical uniform-thickness plates). The laminates on the left, middle and right sides are called thick, tapered and thin laminates according to the explanations given in the “layer reduction test” in chapter 2.

For each laminate at each step of the test, corresponding stiffness  $[{}^c K]$  and mass  $[{}^c M]$  matrices are obtained and substituted in equation (2.102) and by solving it, the natural frequencies and the corresponding mode shapes are determined. Then, the eigenvalues and eigenvectors as well as the stiffness and mass matrices are used in the forced vibration formulation developed in the present chapter to determine the deflection at the center of the laminate. Undamped vibration response is considered.

The amplitude of distributed loading ( $N/m^2$ ) applied to the laminates is kept the same throughout the test and is described by the following equation.

$$f = -1000 \cos (0.3\omega_{11}t) \quad (3.52)$$

where,  $\omega_{11}$  is the fundamental frequency of the plate.

For the tapered and thin laminates, at each step, the deflection at the center of the laminates over time are calculated and depicted by Figures 3.7 - 3.18. At the beginning of the test when no plies are removed (Figure 2.4), the deflections over time for the thick, thin and tapered laminates are equal as their configurations are the same and the corresponding curves coincide (Figure 3.6). Since the thick laminate remains the same throughout the test, the variation of the deflection over time for the laminate does not change throughout the test and it is the same as that of the thin and tapered laminates depicted by Figure 3.6. Therefore, in order to prevent any congestion in Figures 3.9 - 3.18, the deflection of the thick laminate over time is not traced.

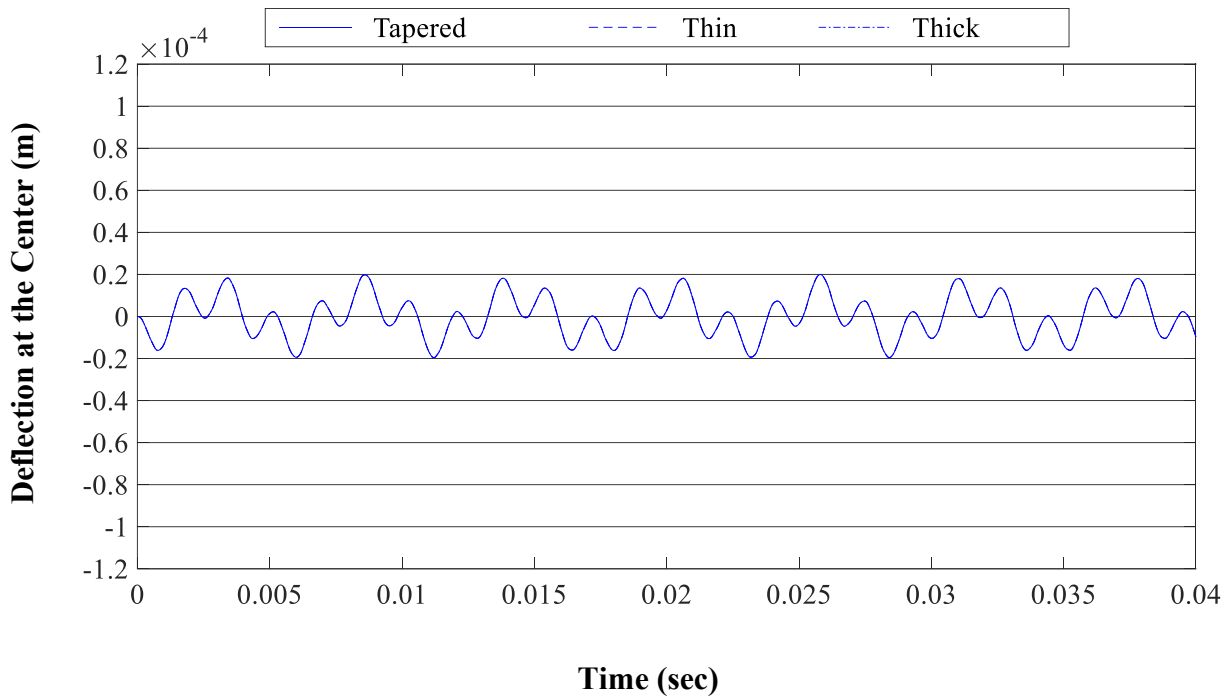


**Figure 3.6** Layer reduction test in forced vibration analysis (no ply drop-off)

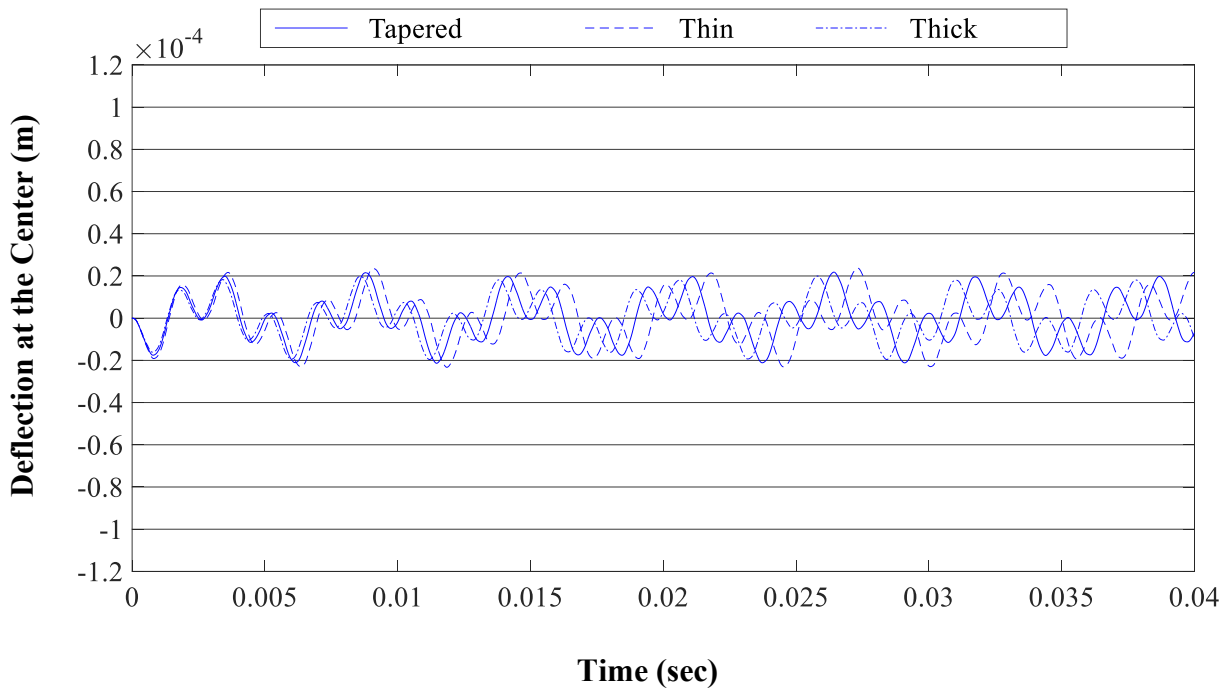


**Figure 3.7** Layer reduction test in forced vibration analysis (step 1: 2 plies dropped-off)

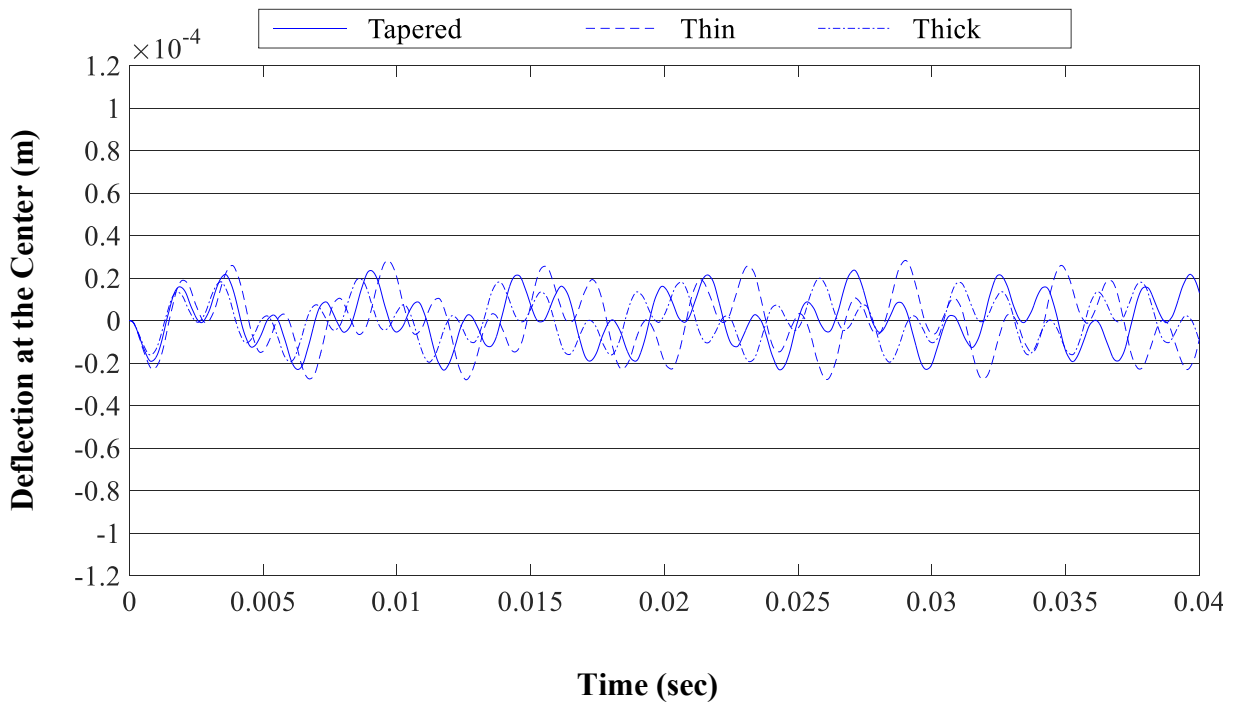


**Figure 3.8** Layer reduction test in forced vibration analysis (step 2: 4 plies dropped-off)



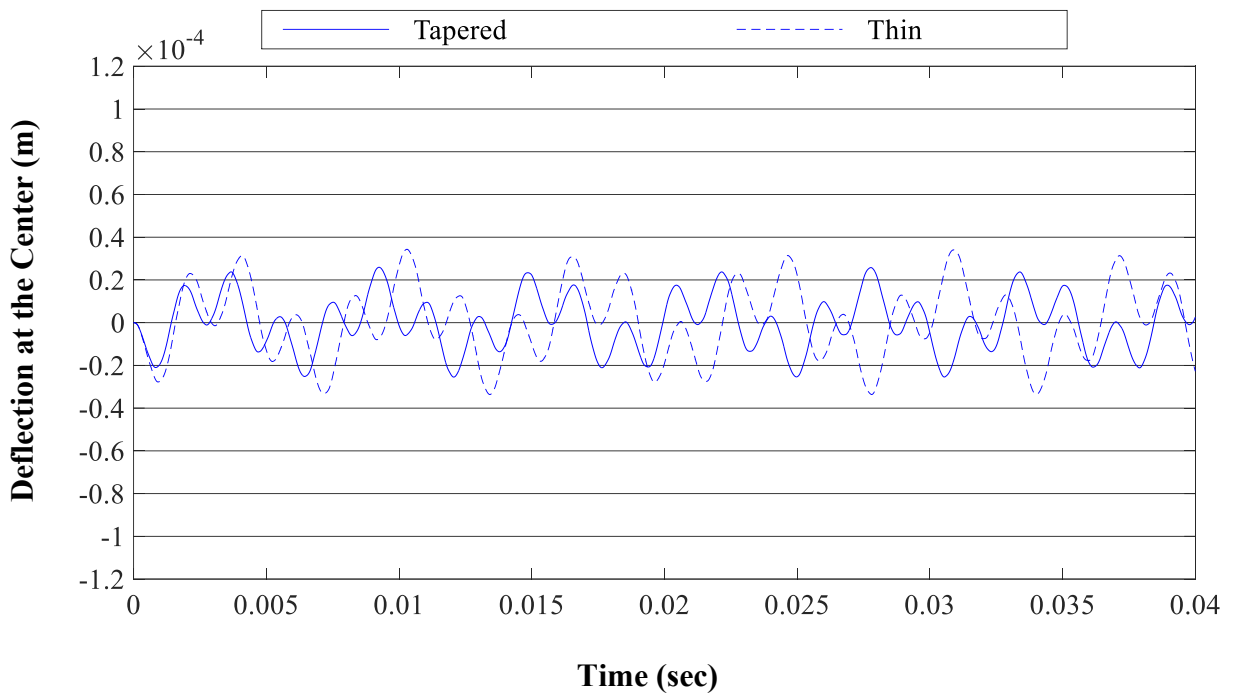


**Figure 3.9** Layer reduction test in forced vibration analysis (step 3: 6 plies dropped-off)

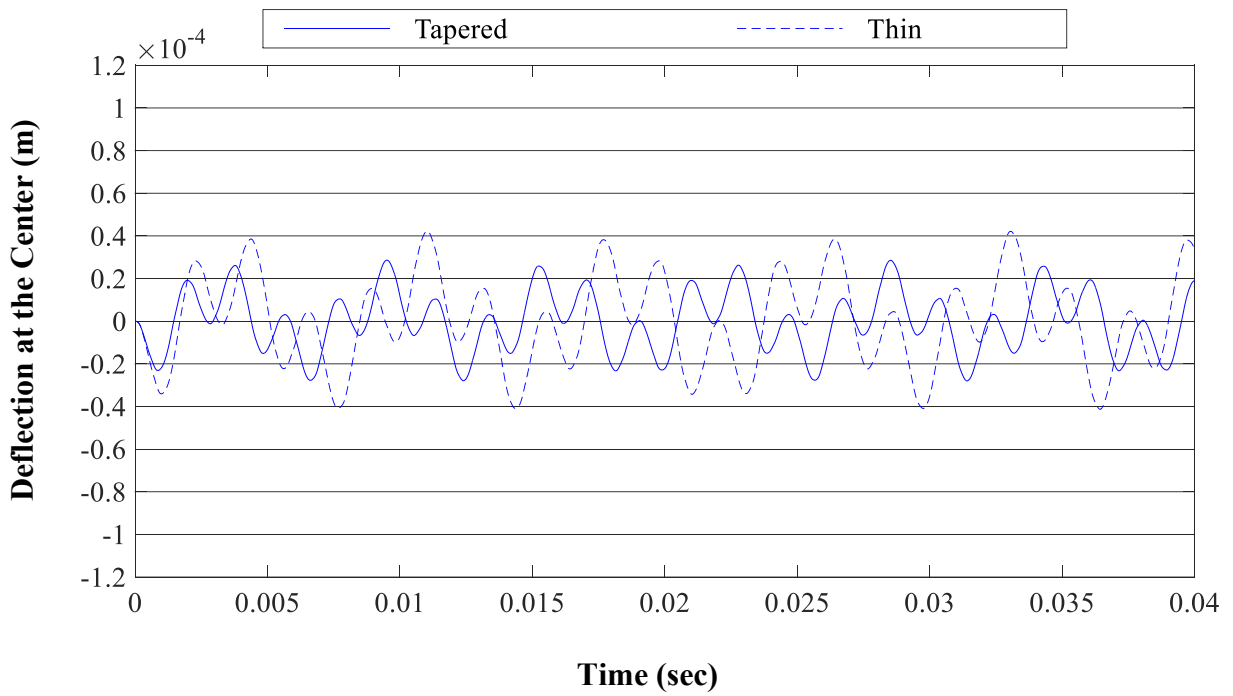


**Figure 3.10** Layer reduction test in forced vibration analysis (step 4: 8 plies dropped-off)

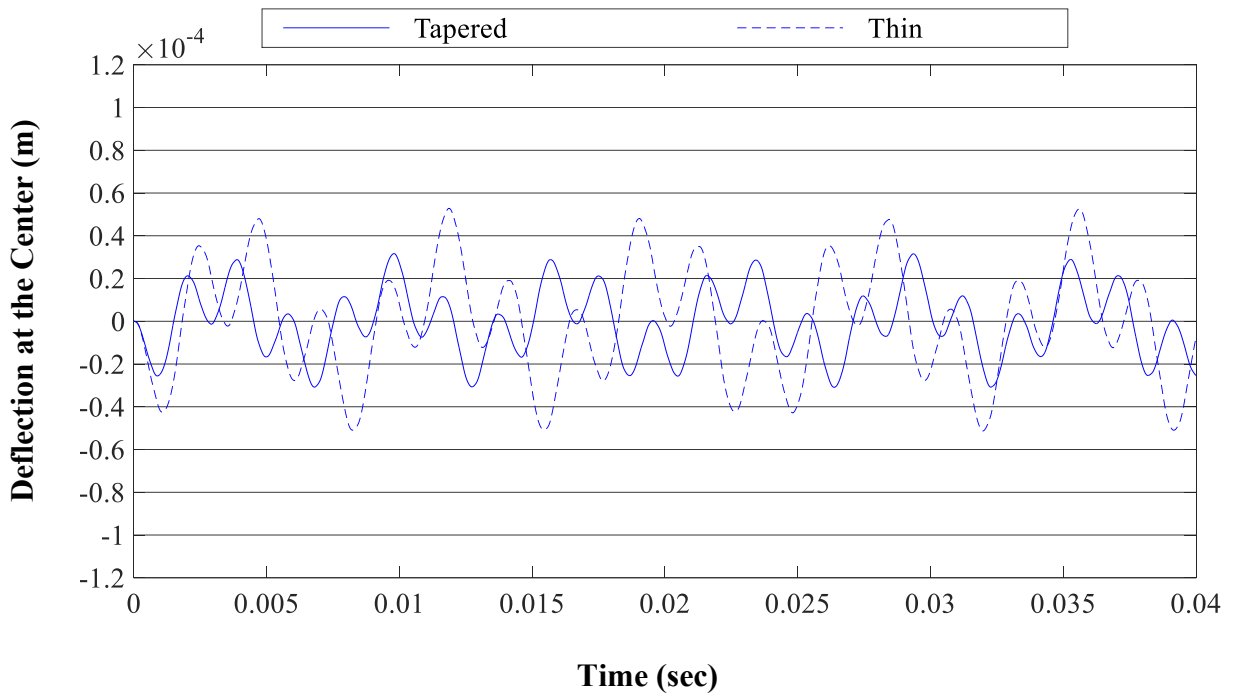


**Figure 3.11** Layer reduction test in forced vibration analysis (step 5: 10 plies dropped-off)

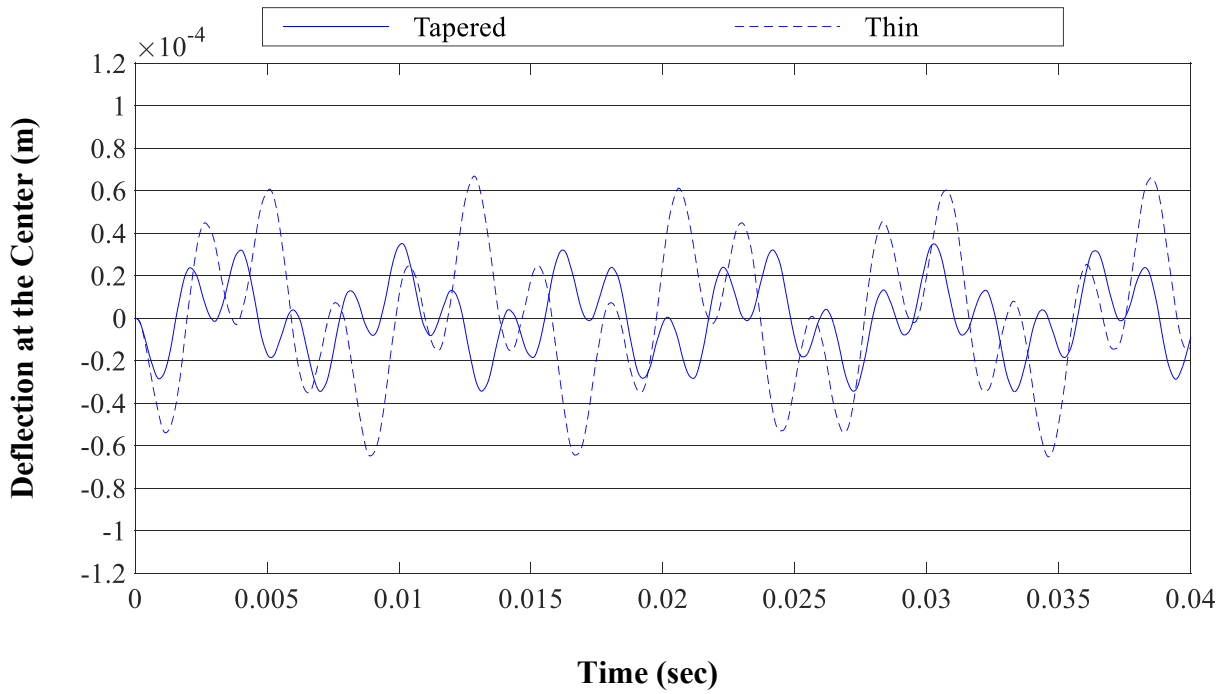


**Figure 3.12** Layer reduction test in forced vibration analysis (step 6: 12 plies dropped-off)

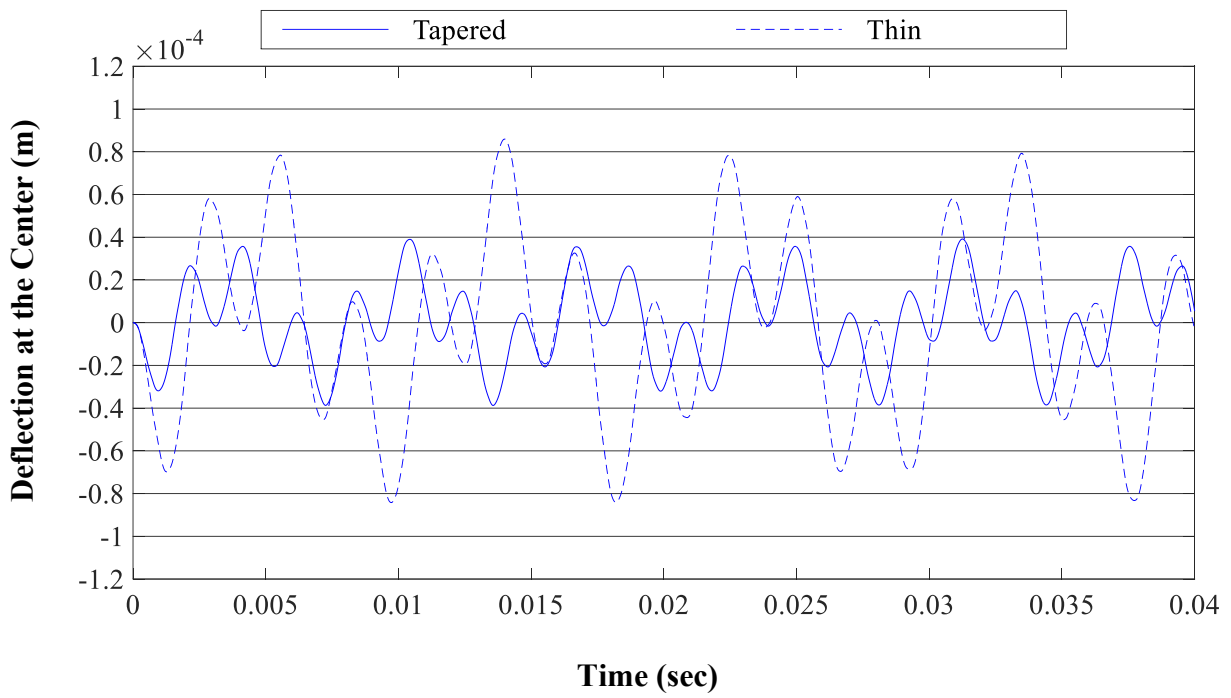


**Figure 3.13** Layer reduction test in forced vibration analysis (step 7: 14 plies dropped-off)

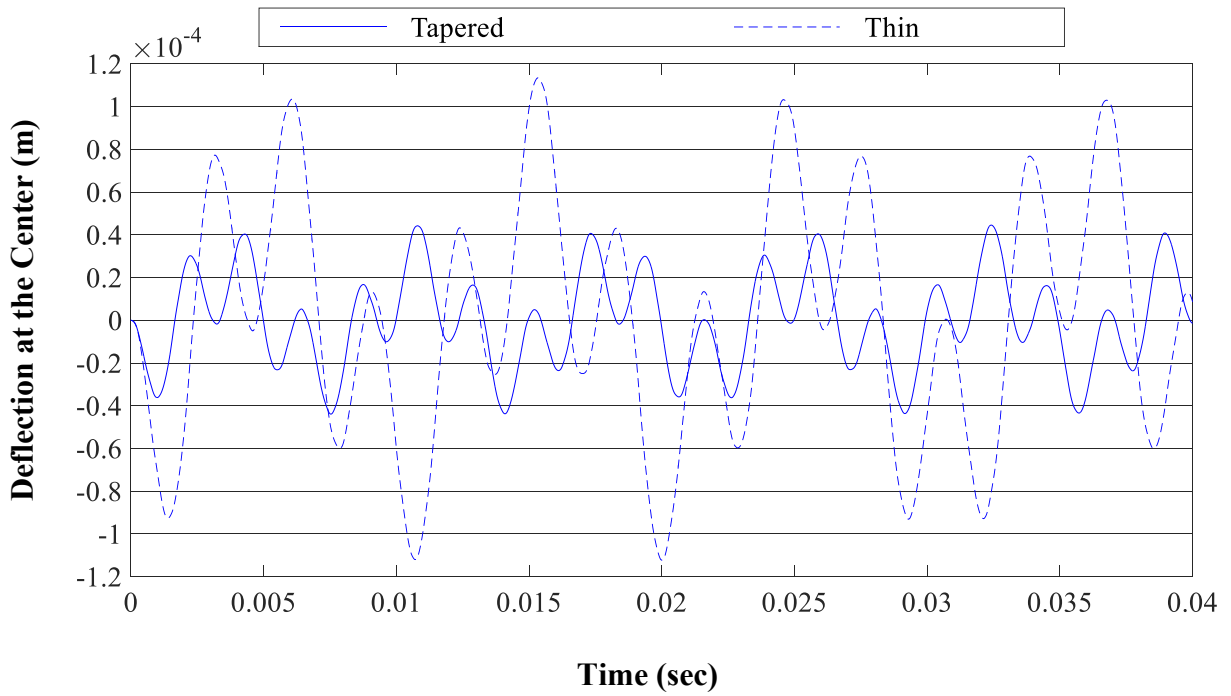


**Figure 3.14** Layer reduction test in forced vibration analysis (step 8: 16 plies dropped-off)

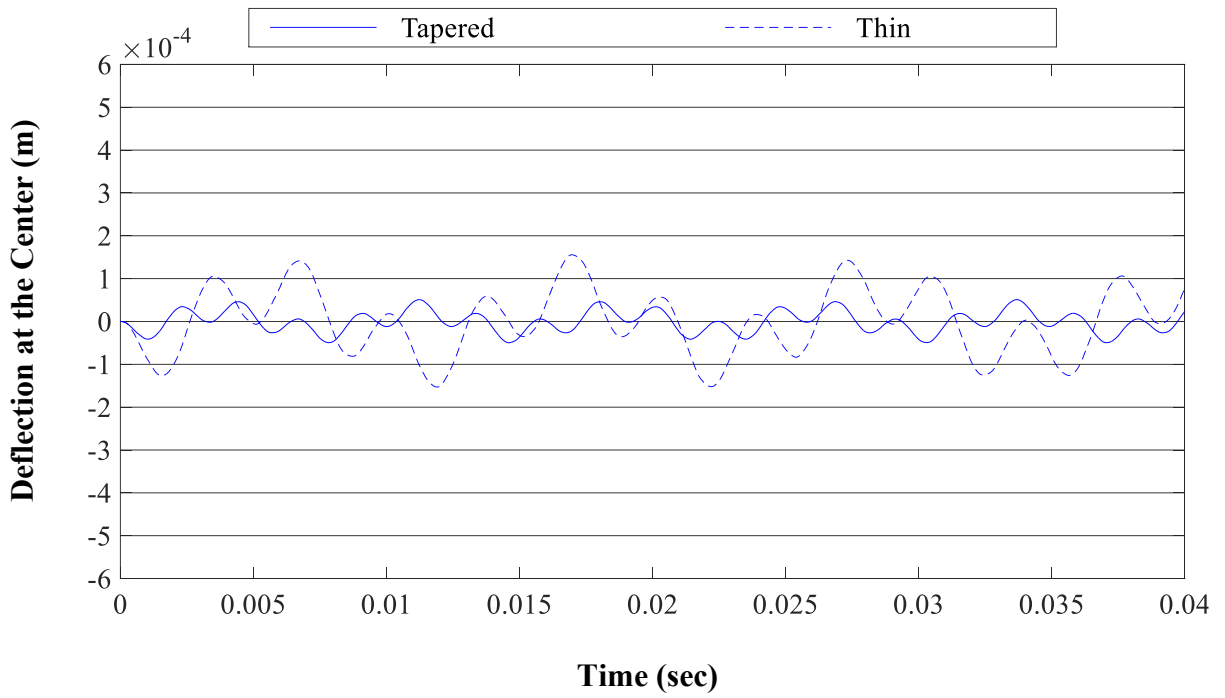


**Figure 3.15** Layer reduction test in forced vibration analysis (step 9: 18 plies dropped-off)

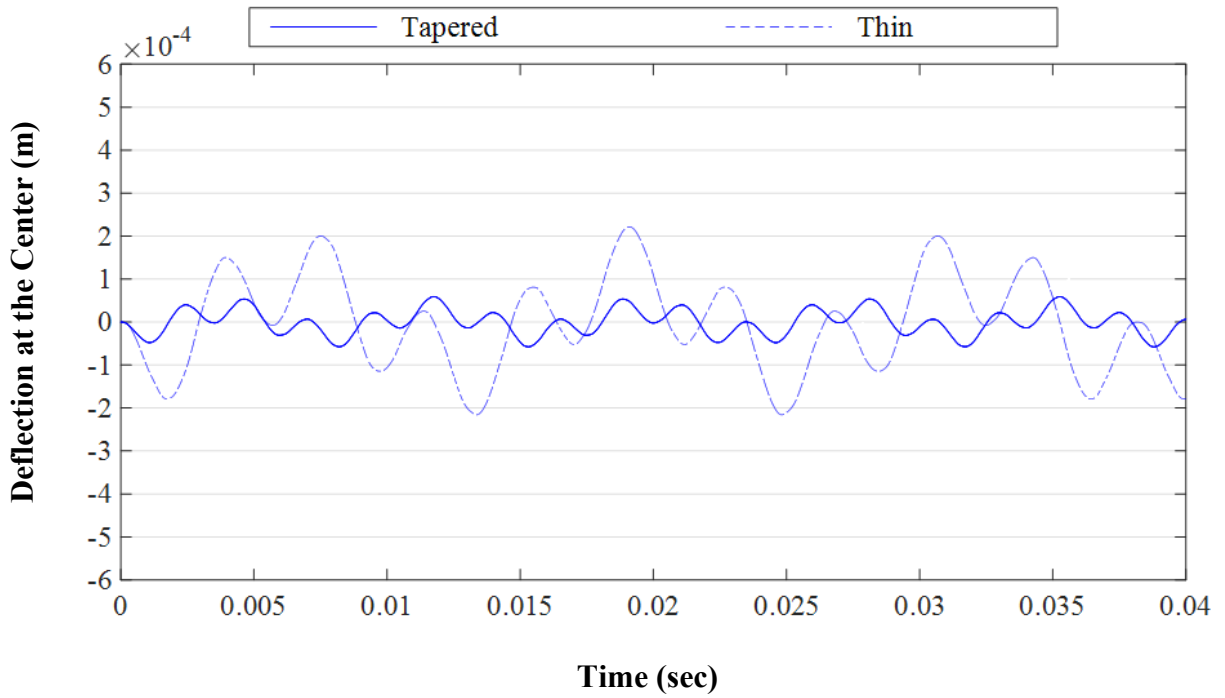


**Figure 3.16** Layer reduction test in forced vibration analysis (step 10: 20 plies dropped-off)

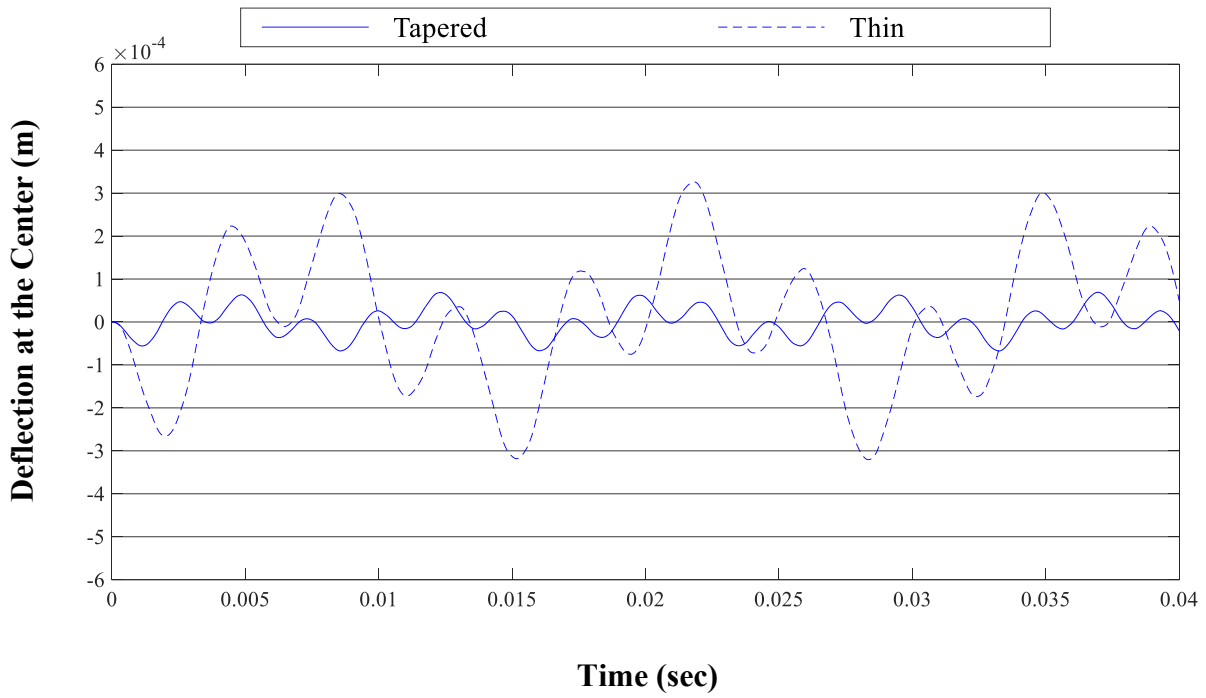


**Figure 3.17** Layer reduction test in forced vibration analysis (step 11: 22 plies dropped-off)

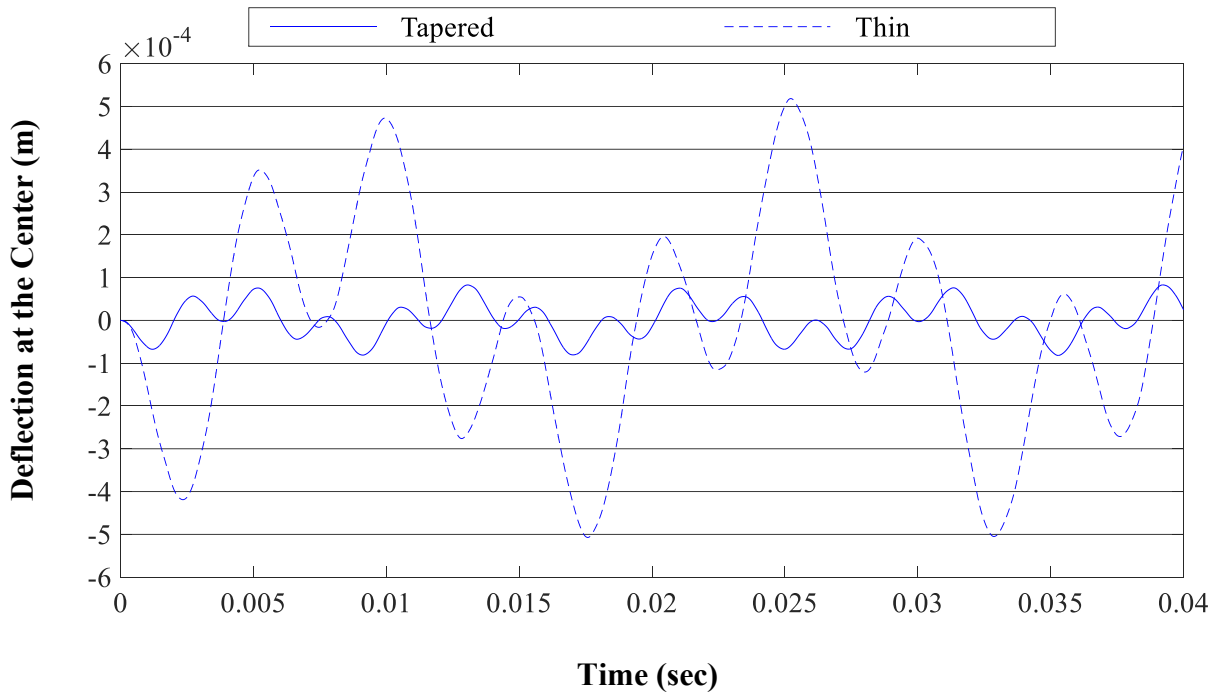


**Figure 3.18** Layer reduction test in forced vibration analysis (step 12: 24 plies dropped-off)

Considering Figures 3.6 - 3.18, for the thin and tapered laminates, the deflection at the center of the laminates due to the excitation, is increased as the layers are removed from the plates at each step. However, this increase for the thin laminate is greater at each step of the test such that in Figure 3.6 the two curves corresponding to the deflections of the two laminates coincide, and through Figure 3.18, the difference between the two curves gradually increases.

Considering the small deflection of the thick plate which is the same as that of the thin and tapered laminates in Figure 3.6 when no plies are removed, it can be said that the deflection amplitude of the tapered laminate is lower than that of the thin plate and higher than that of the thick plate at each step of the test.

### 3.5 Maximum deflection and excitation frequency

In this section, the variation of the response of the laminates due to the change of excitation frequency is studied. The square plates with taper configurations described in section 2.2 (configurations A, B, C and D) are considered with side length of 0.1719 m (taper angle  $\varphi = 0.5^\circ$ ) and different boundary conditions (SSSS, CCCC and CCFF). The mechanical properties were given in Table 2.3. A loading described by equation (3.53) below and with excitation frequency of  $\Omega$  ( $0 < \Omega < 1.1\omega_{11}$ ) is applied to the tapered laminates. The fundamental frequency  $\omega_{11}$  for each configuration with corresponding boundary conditions was given in Tables 2.11 - 2.13. The maximum deflection of the transverse normal (located at the center of the plate) due to the excitation and the corresponding excitation frequency are recorded. The same process is repeated for different values of excitation frequency  $\Omega$  and using the obtained data the following graphs are illustrated by Figures 3.19 - 3.30 showing the maximum deflection at the center of the laminate with respect to change of excitation frequency.

The study is repeated in the same way considering the damping effect and the results are shown by Figures 3.19 - 3.30. The results can be compared with that of the case with no damping. The values of  $\alpha$  and  $\beta$  have been given in Refs. [3] and [34] as  $\alpha = 2.14$  and  $\beta = 2.76 \times 10^{-5}$ .

$$f = -500 \cos(\Omega t) \delta \left( x - \frac{0.1719}{2} \right) \quad (N/m^2), \quad (0 < \Omega < 1.1\omega_{11}) \quad (3.53)$$

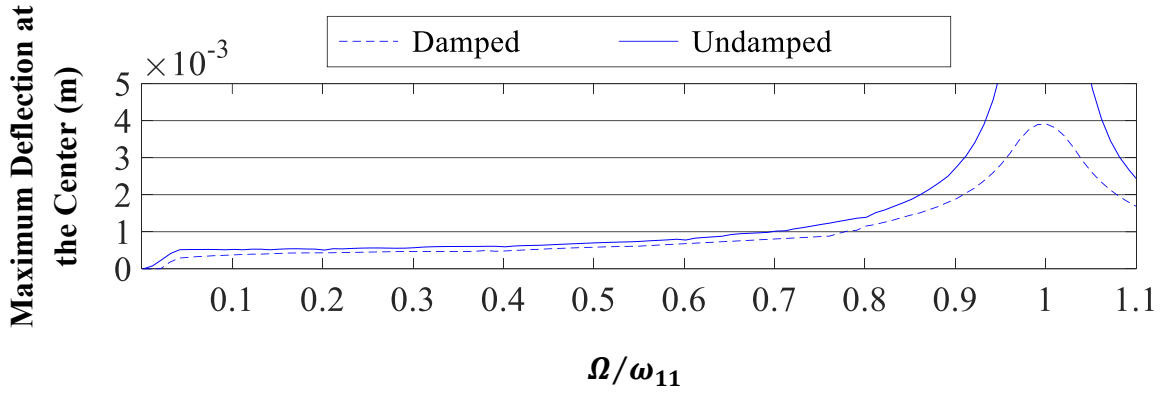


**Figure 3.19** Effect of excitation frequency on maximum deflection (configuration A, SSSS)

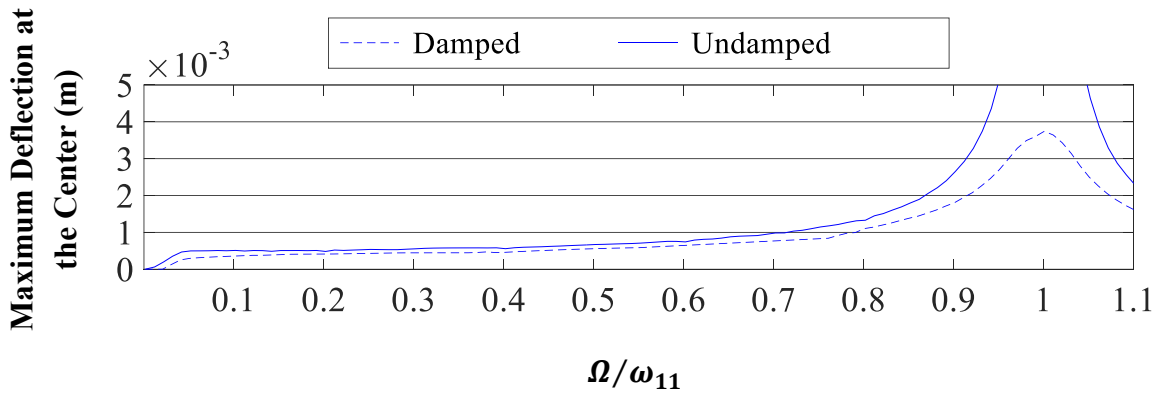


**Figure 3.20** Effect of excitation frequency on maximum deflection (configuration B, SSSS)

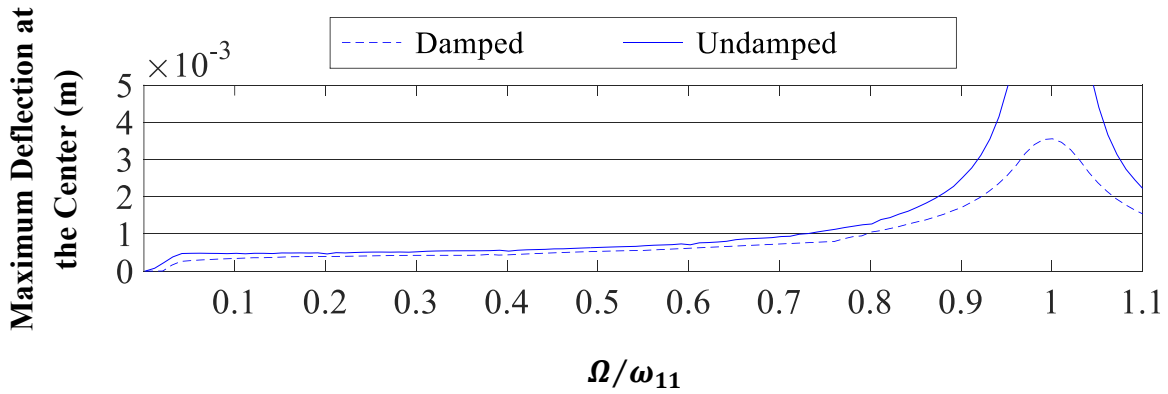


**Figure 3.21** Effect of excitation frequency on maximum deflection (configuration C, SSSS)

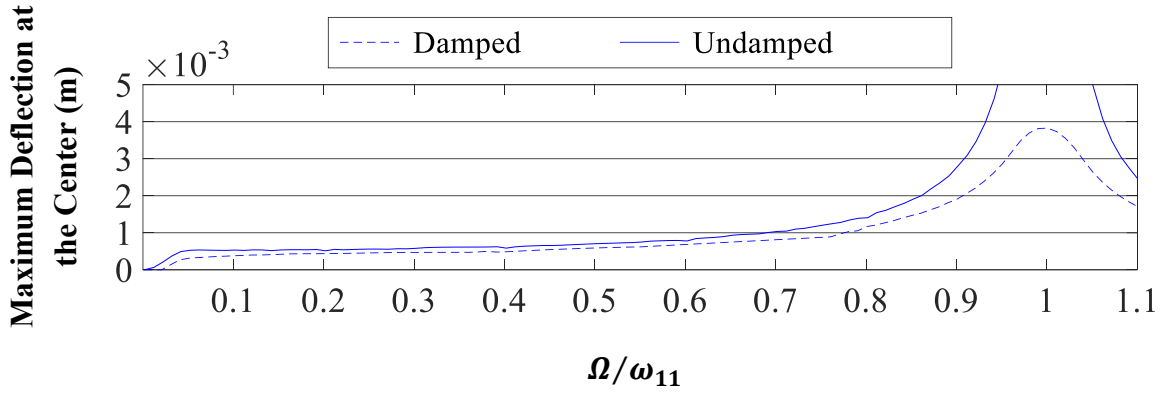


**Figure 3.22** Effect of excitation frequency on maximum deflection (configuration D, SSSS)

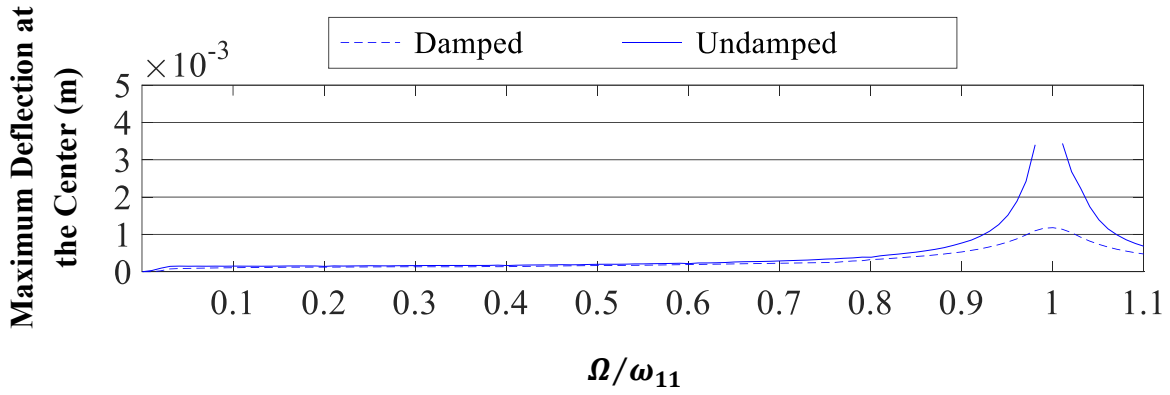


**Figure 3.23** Effect of excitation frequency on maximum deflection (configuration A, CCCC)

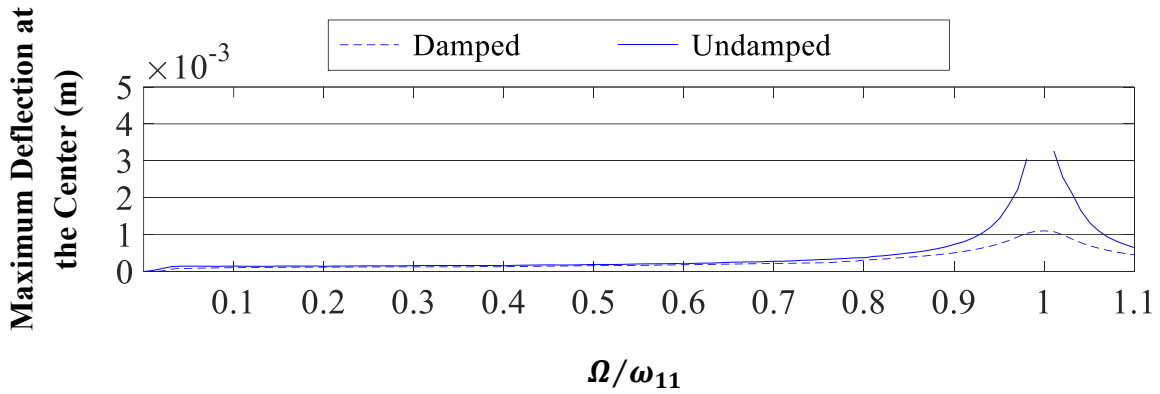


**Figure 3.24** Effect of excitation frequency on maximum deflection (configuration B, CCCC)



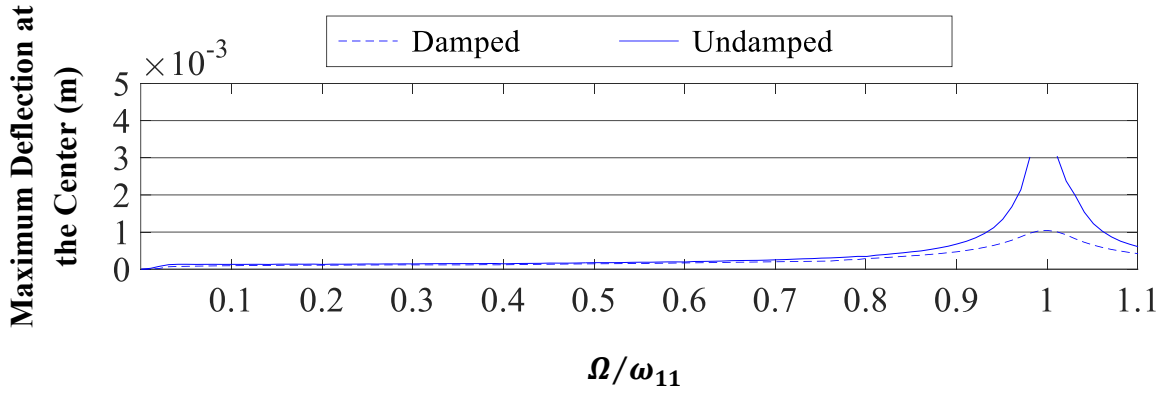


**Figure 3.25** Effect of excitation frequency on maximum deflection (configuration C, CCCC)

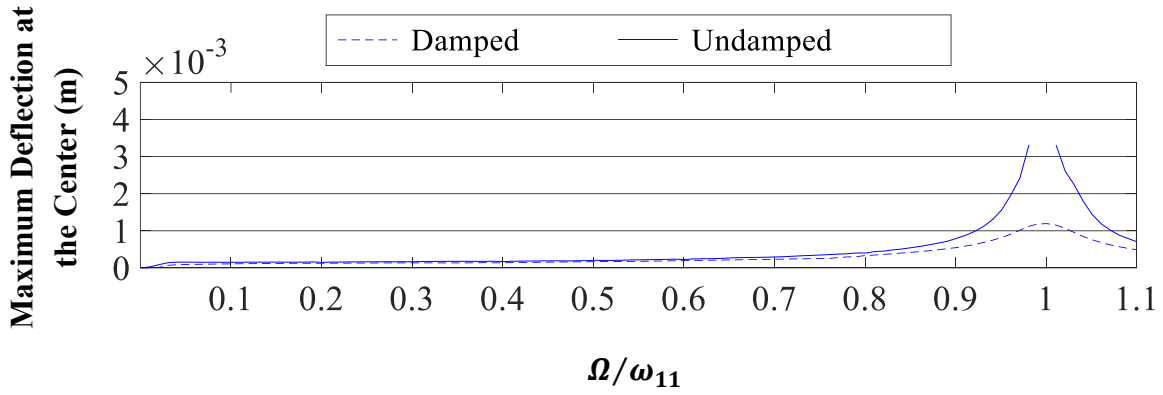


**Figure 3.26** Effect of excitation frequency on maximum deflection (configuration D, CCCC)

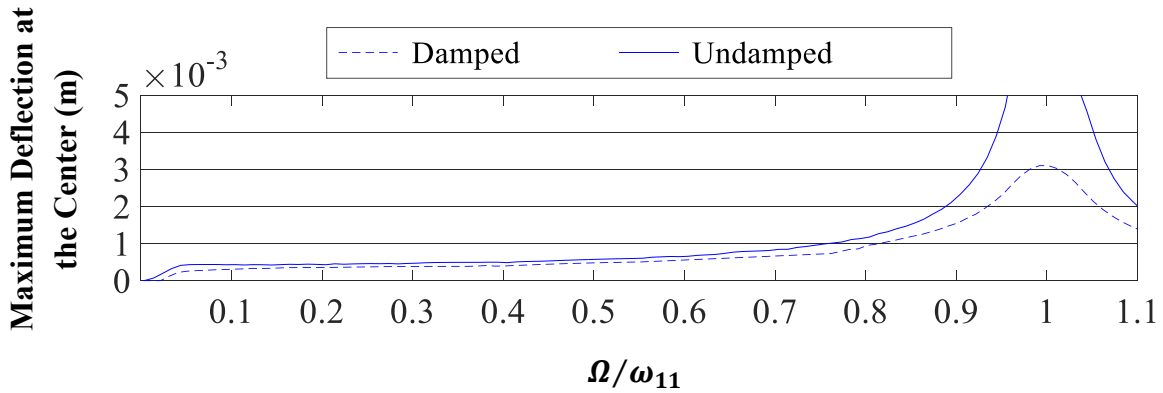


**Figure 3.27** Effect of excitation frequency on maximum deflection (configuration A, CCFF)

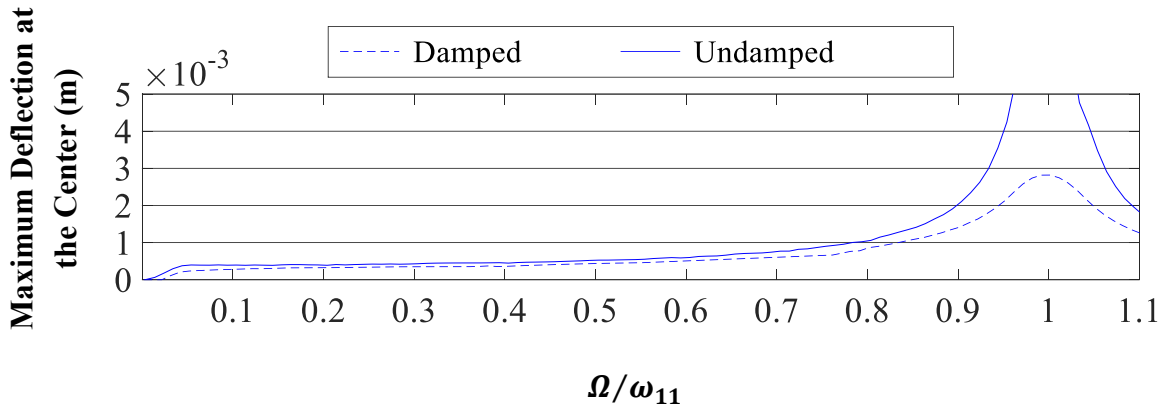


**Figure 3.28** Effect of excitation frequency on maximum deflection (configuration B, CCFF)

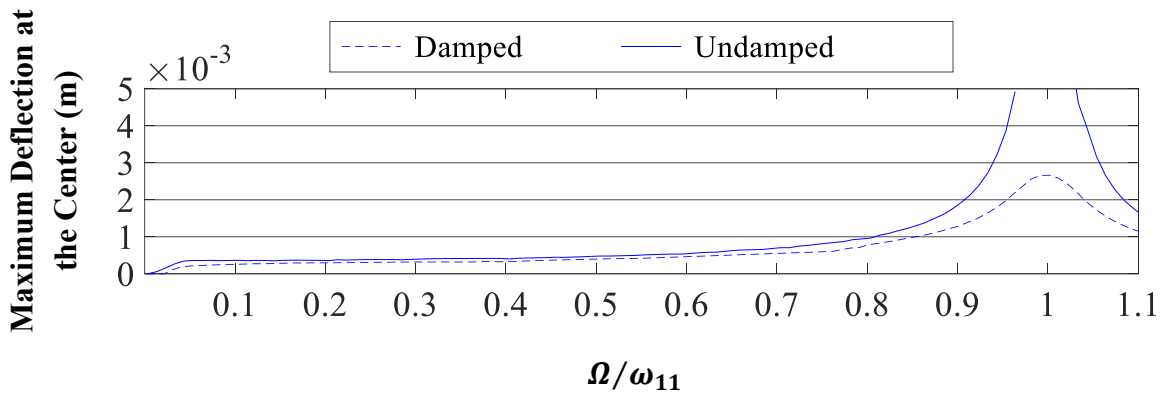


**Figure 3.29** Effect of excitation frequency on maximum deflection (configuration C, CCFF)

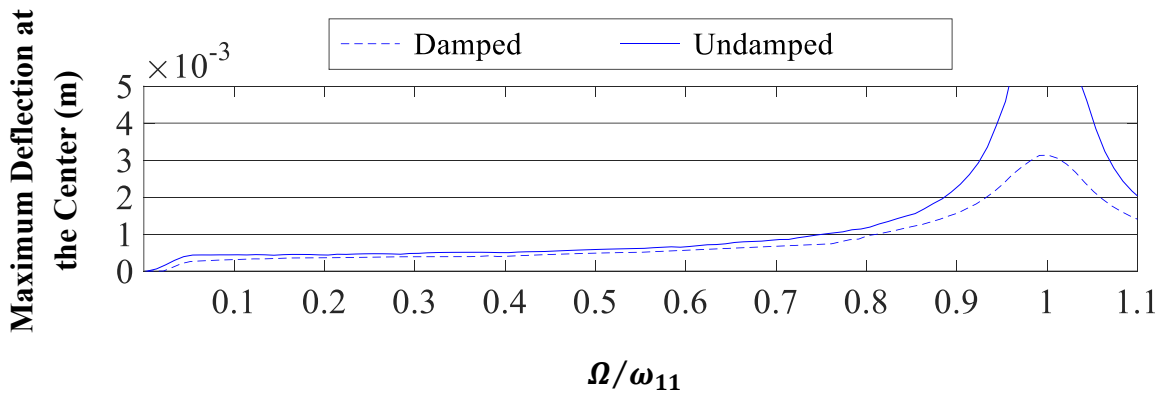


**Figure 3.30** Effect of excitation frequency on maximum deflection (configuration D, CCFF)

It is grasped from Figures 3.19 - 3.30 that for all the boundary conditions and taper configurations, as expected, the deflection at the center point of the tapered laminates increases remarkably when the excitation frequency approaches the fundamental frequency of the laminate. When the excitation frequency coincides with the fundamental frequency, for the undamped case, the deflection tends to a very high value and for the corresponding case with damping, the maximum deflection is noticeably large. When the excitation frequency value exceeds the fundamental frequency, the maximum deflection decreases for the damped and undamped cases.

It is observed from Figures 3.19 - 3.30 that regardless of the configuration, the maximum deflection of the tapered laminate at the point located at the center of the laminate for the CCCC plate is the lowest and that of the SSSS plate is the highest. For CCFF plate, it should be noted that the peak deflection of the plate occurs at the corner point located at the intersection of the two free edges. Therefore, the maximum deflection at the center for the CCFF plate is not the peak deflection. For SSSS and CCCC tapered plates, the location of the peak deflection is not necessarily at the center of the tapered laminates, however, since the taper angle is small, this location is expected to be close to the center of the laminate.

### 3.6 Numerical results

In the present section, different loading types given in Table 3.1 are applied to the tapered laminates with different configurations (Figure 2.1) described in section 2.2 (mechanical properties were given in Table 2.3) considering various lengths and three boundary conditions (SSSS, CCCC and CCFF) with no damping. Then, the responses are calculated using the forced vibration formulation developed in the present chapter and the maximum deflections at the point located at the center of the tapered laminate due to the excitations, are recorded and written in Tables 3.3 - 3.5. The excitation frequency  $\Omega = 0.3\omega_{11}$  and the fundamental frequency  $\omega_{11}$  were given in Tables 2.11 - 2.13 for each case.

In addition, for the tapered configurations with different boundary conditions and with length of 0.1719 m, loading types given in Table 3.1 are applied to the tapered laminates and the deflections at the centers of the plates over time are calculated using the developed formulation

and are illustrated by Figures 3.31 - 3.78 for damped and undamped cases. Then, the results displayed in Tables 3.3 - 3.5 and illustrated by Figures 3.31 - 3.78 are discussed.

<b>Maximum Deflection at the Center of the Laminate (mm)</b>									
<b>Configuration</b>	<b>Boundary Condition</b>	$\varphi = 0.1^\circ$ , $L = 0.8594\text{ m}$ $\frac{\text{Length}}{\text{Mean Thickness Ratio}} = 286.5$				$\varphi = 0.5^\circ$ , $L = 0.1719\text{ m}$ $\frac{\text{Length}}{\text{Mean Thickness Ratio}} = 57.3$			
		Loading Type 1	Loading Type 2	Loading Type 3	Loading Type 4	Loading Type 1	Loading Type 2	Loading Type 3	Loading Type 4
<b>A</b>	SSSS	3.906	3.811	3.070	3.008	0.569	0.555	0.447	0.438
	CCCC	1.119	1.0234	0.9339	0.872	0.163	0.149	0.136	0.127
	CCFF	3.297	2.802	2.115	1.895	0.480	0.408	0.308	0.276
<b>B</b>	SSSS	3.802	3.584	2.966	2.835	0.554	0.522	0.432	0.413
	CCCC	1.077	0.967	0.899	0.830	0.157	0.141	0.131	0.121
	CCFF	3.226	2.457	2.018	1.708	0.470	0.358	0.294	0.249
<b>C</b>	SSSS	3.571	3.378	2.781	2.677	0.520	0.492	0.405	0.390
	CCCC	0.976	0.913	0.817	0.776	0.142	0.133	0.119	0.113
	CCFF	2.754	2.074	1.716	1.435	0.401	0.302	0.250	0.209
<b>D</b>	SSSS	3.969	3.819	3.093	3.012	0.580	0.558	0.452	0.440
	CCCC	1.136	1.061	0.9443	0.903	0.166	0.155	0.138	0.132
	CCFF	3.336	2.689	2.190	1.895	0.488	0.393	0.320	0.277

*Table 3.3 Maximum deflection (mm) at the center for all taper configurations and BCs*

Maximum Deflection at the Center of the Laminate (mm)									
Configuration	Boundary Condition	$\varphi = 0.75^\circ$ , $L = 0.1146\text{ m}$ $\frac{\text{Length}}{\text{Mean Thickness Ratio}} = 38.2$				$\varphi = 1^\circ$ , $L = 0.0859\text{ m}$ $\frac{\text{Length}}{\text{Mean Thickness Ratio}} = 28.6$			
		Loading Type 1	Loading Type 2	Loading Type 3	Loading Type 4	Loading Type 1	Loading Type 2	Loading Type 3	Loading Type 4
<b>A</b>	SSSS	0.170	0.165	0.133	0.130	0.116	0.112	0.0906	0.089
	CCCC	0.049	0.046	0.040	0.039	0.033	0.031	0.027	0.027
	CCFF	0.142	0.120	0.091	0.082	0.097	0.082	0.062	0.056
<b>B</b>	SSSS	0.163	0.156	0.128	0.123	0.111	0.106	0.087	0.084
	CCCC	0.047	0.043	0.039	0.036	0.032	0.029	0.027	0.025
	CCFF	0.138	0.105	0.087	0.074	0.094	0.072	0.059	0.050
<b>C</b>	SSSS	0.154	0.147	0.120	0.116	0.105	0.100	0.082	0.079
	CCCC	0.043	0.039	0.036	0.034	0.0293	0.0266	0.0245	0.023
	CCFF	0.126	0.096	0.082	0.069	0.086	0.065	0.056	0.047
<b>D</b>	SSSS	0.173	0.167	0.135	0.132	0.118	0.114	0.092	0.090
	CCCC	0.051	0.046	0.042	0.039	0.035	0.031	0.029	0.027
	CCFF	0.152	0.122	0.098	0.086	0.104	0.083	0.067	0.059

*Table 3.4 Maximum deflection (mm) at the center for all taper configurations and BCs*

Maximum Deflection at the Center of the Laminate (mm)									
Configuration	Boundary Condition	$\varphi = 1.25^\circ$ , $L = 0.0687\text{ m}$ $\frac{\text{Length}}{\text{Mean Thickness Ratio}} = 22.9$				$\varphi = 1.5^\circ$ , $L = 0.0573\text{ m}$ $\frac{\text{Length}}{\text{Mean Thickness Ratio}} = 19.1$			
		Loading Type 1	Loading Type 2	Loading Type 3	Loading Type 4	Loading Type 1	Loading Type 2	Loading Type 3	Loading Type 4
<b>A</b>	SSSS	0.096	0.093	0.075	0.073	0.072	0.070	0.056	0.055
	CCCC	0.028	0.026	0.023	0.022	0.0208	0.0195	0.0169	0.017
	CCFF	0.080	0.068	0.051	0.046	0.060	0.051	0.039	0.035
<b>B</b>	SSSS	0.092	0.0881	0.072	0.070	0.069	0.066	0.054	0.052
	CCCC	0.027	0.0242	0.022	0.020	0.020	0.018	0.017	0.015
	CCFF	0.078	0.0593	0.049	0.042	0.058	0.045	0.037	0.031
<b>C</b>	SSSS	0.087	0.0830	0.068	0.066	0.065	0.062	0.051	0.049
	CCCC	0.024	0.0220	0.020	0.019	0.018	0.017	0.015	0.014
	CCFF	0.071	0.0542	0.046	0.039	0.053	0.041	0.035	0.029
<b>D</b>	SSSS	0.098	0.0943	0.076	0.075	0.073	0.071	0.057	0.056
	CCCC	0.029	0.0260	0.024	0.022	0.022	0.0195	0.018	0.017
	CCFF	0.086	0.0689	0.055	0.049	0.064	0.0517	0.042	0.036

*Table 3.5 Maximum deflection (mm) at the center for all taper configurations and BCs*

It is grasped from Tables 3.3 - 3.5 that regardless of the boundary conditions, taper configurations and loading types, with increase in the length over mean thickness ratio, the deflection at the center of the laminate increases such that when this ratio from 19.1 approaches 57.3, the deflection at the center is increased roughly by 690%. However, this increase in transverse deflection for SSSS and CCFF plates, with slight difference, are the highest and the lowest, respectively.

Considering loading types 1 and 3, the deflection of the plates corresponding to the loading type 1 is higher than that of the loading type 3. The same explanation corresponds to loading types 2 and 4, respectively.

The deflections for the CCCC plates are the lowest and that of the SSSS plates are the highest. It is noted that the peak deflections of the CCFF plates occur at the corner of the plates at the intersection of the free edges while that of the CCCC and SSSS plates are expected to be close to the center where the magnitudes of the deflections have been recorded.

Considering the different taper configurations, the deflection corresponding to taper configuration C, is the lowest and that of configuration D (with fewer external plies), with slight difference compared to configuration A, is the highest.

The deflection at the center over time for the square laminates with side length of 0.1719 m ( $\varphi = 0.5^\circ$ ) for different taper configurations and with three boundary conditions (SSSS, CCCC and CCFF) due to the excitation types given in Table 3.1, are determined next. The excitation frequency  $\Omega = 0.3\omega_{11}$  and the fundamental frequency  $\omega_{11}$  for each configuration and boundary condition were given in Tables 2.11 - 2.13.

For all boundary conditions (SSSS, CCCC and CCFF) and taper configurations with length of 0.1719 m corresponding to taper angle of  $0.5^\circ$ , the deflection at the center over time due to excitation types given in Table 3.1, are illustrated by Figures 3.31 - 3.78. The dashed and solid curves correspond to the deflection of the plate with and without damping, respectively.

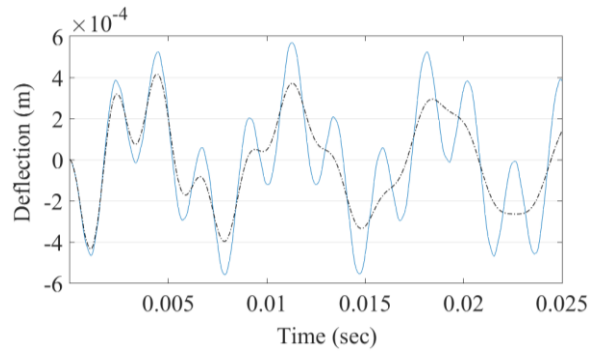


**Figure 3.31** Configuration A, SSSS, loading type 1

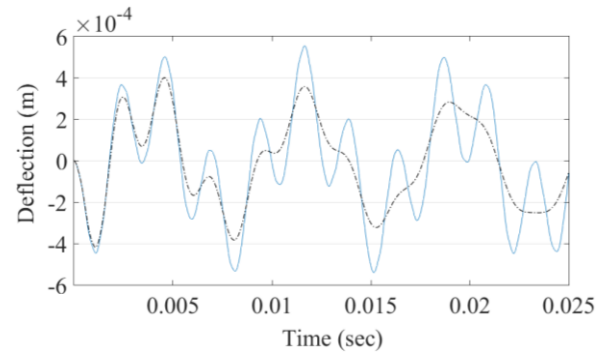


**Figure 3.32** Configuration B, SSSS, loading type 1

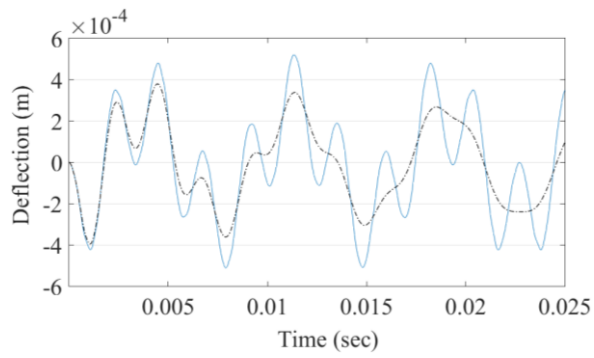


**Figure 3.33** Configuration C, SSSS, loading type 1

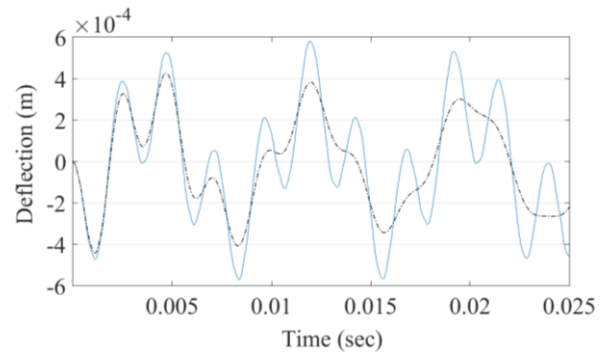


**Figure 3.34** Configuration D, SSSS, loading type 1

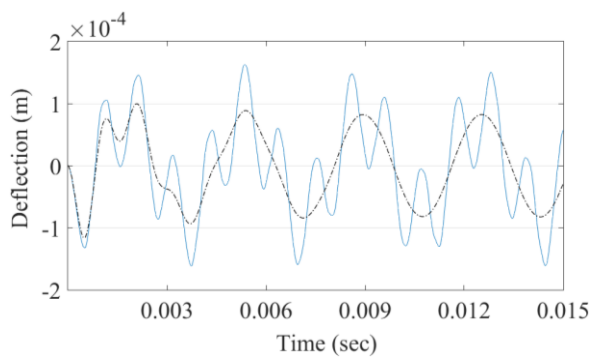


**Figure 3.35** Configuration A, CCCC, loading type 1

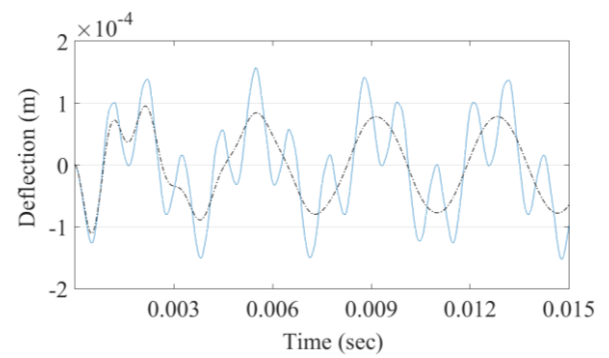


**Figure 3.36** Configuration B, CCCC, loading type 1



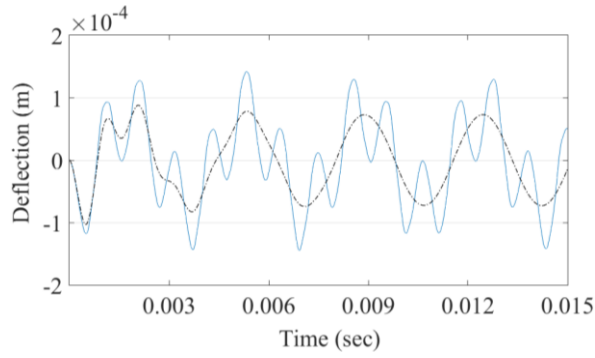


**Figure 3.37** Configuration C, CCCC, loading type 1

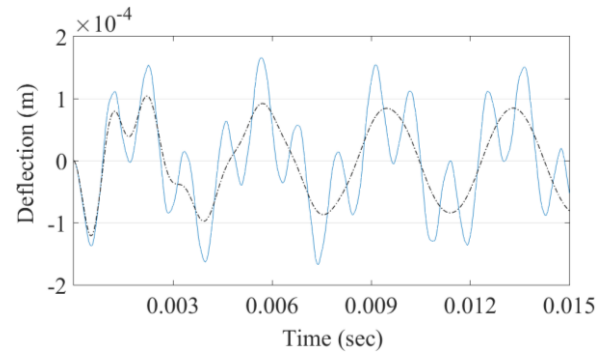


**Figure 3.38** Configuration D, CCCC, loading type 1

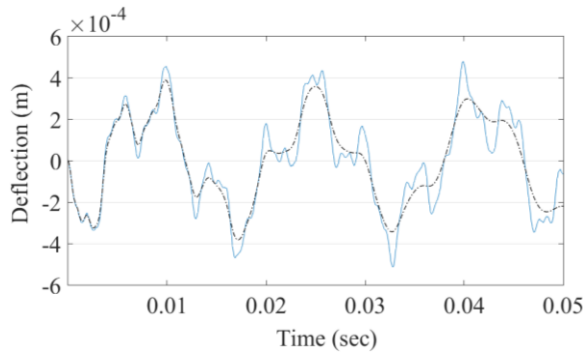


**Figure 3.39** Configuration A, CCFF, loading type 1

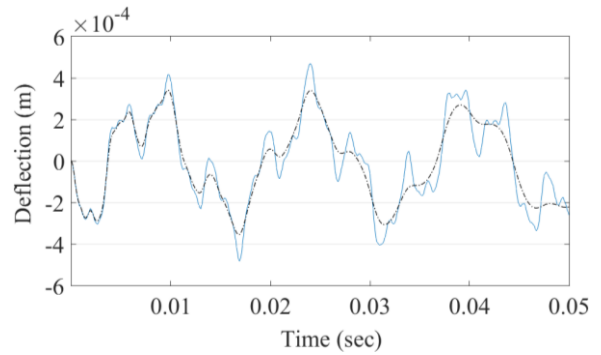


**Figure 3.40** Configuration B, CCFF, loading type 1

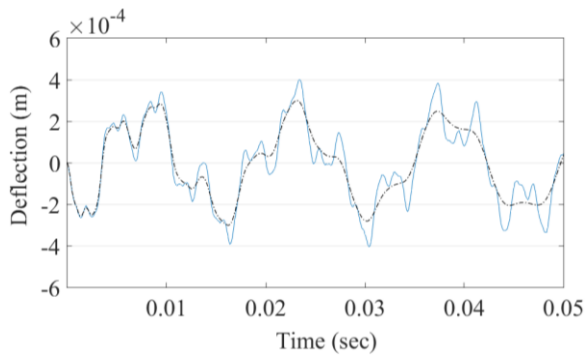


**Figure 3.41** Configuration C, CCFF, loading type 1

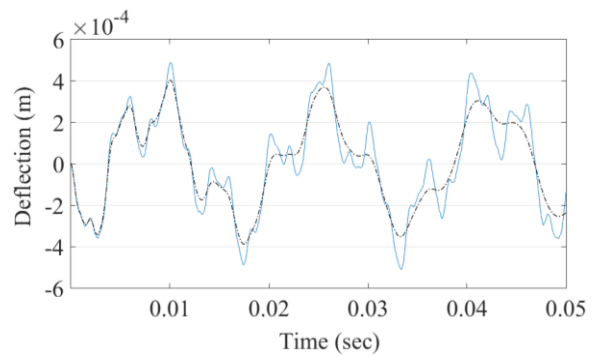


**Figure 3.42** Configuration D, CCFF, loading type 1

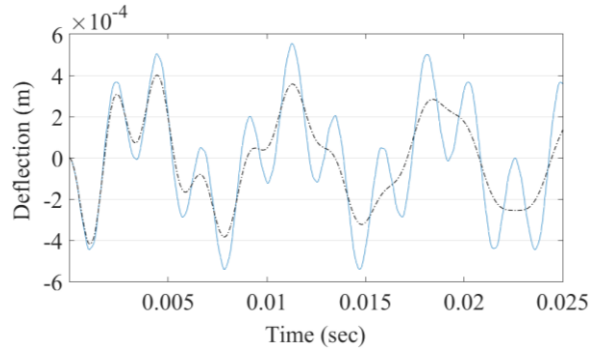


**Figure 3.43** Configuration A, SSSS, loading type 2

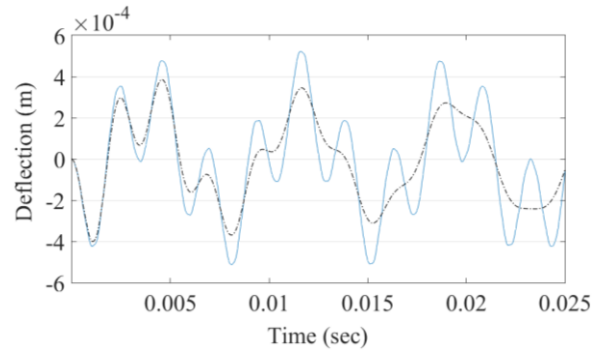


**Figure 3.44** Configuration B, SSSS, loading type 2

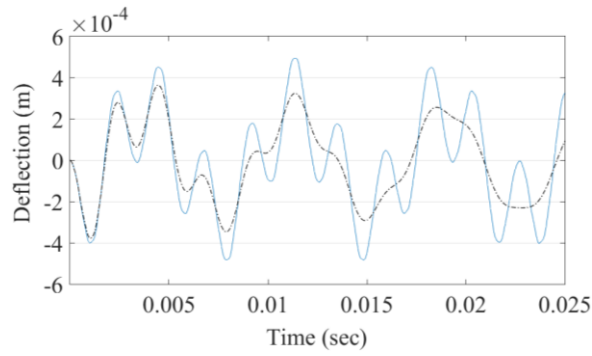


**Figure 3.45** Configuration C, SSSS, loading type 2

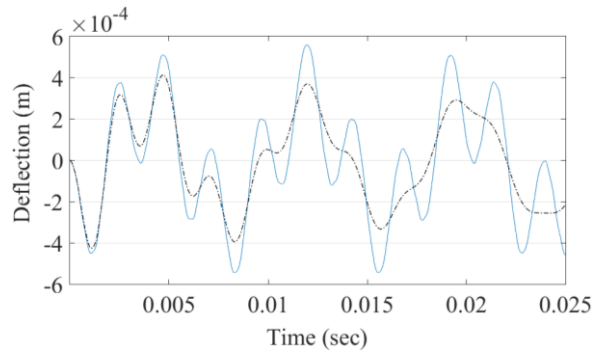


**Figure 3.46** Configuration D, SSSS, loading type 2

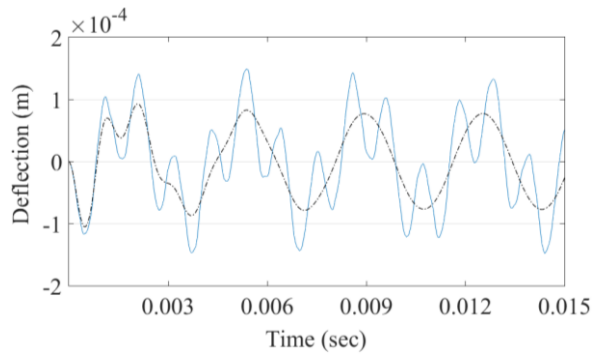


**Figure 3.47** Configuration A, CCCC, loading type 2

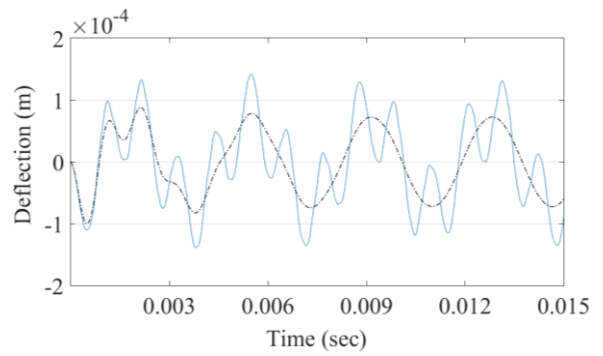


**Figure 3.48** Configuration B, CCCC, loading type 2

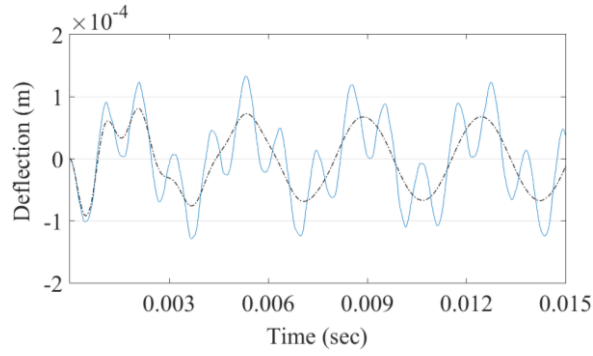


**Figure 3.49** Configuration C, CCCC, loading type 2

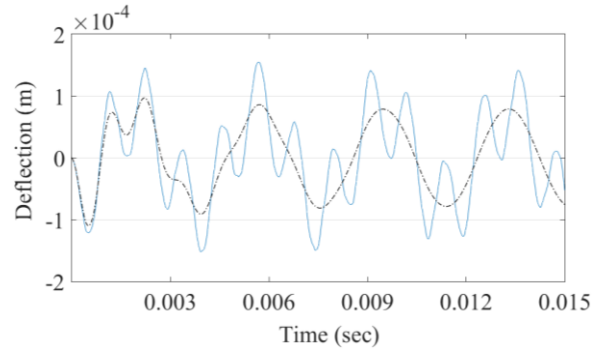


**Figure 3.50** Configuration D, CCCC, loading type 2

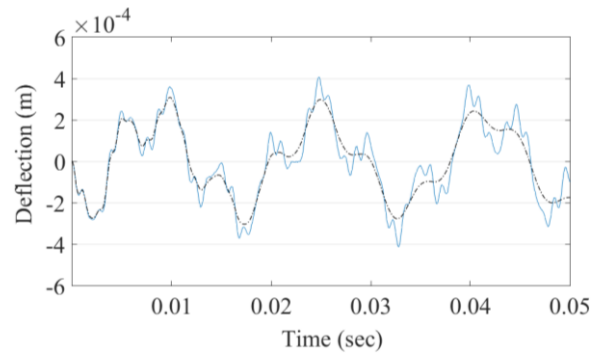


**Figure 3.51** Configuration A, CCFF, loading type 2

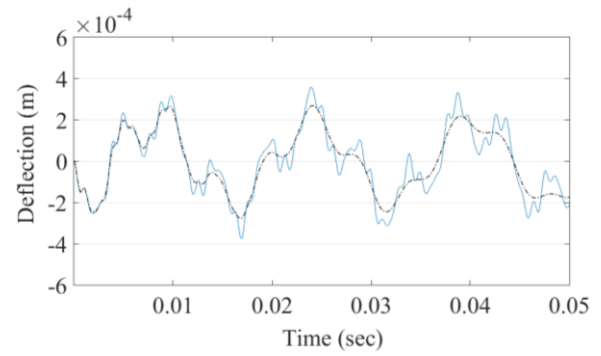


**Figure 3.52** Configuration B, CCFF, loading type 2

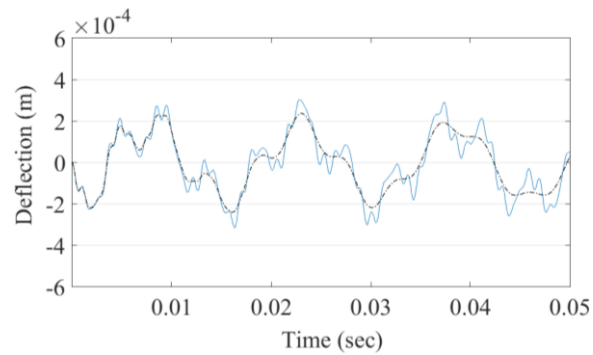


**Figure 3.53** Configuration C, CCFF, loading type 2

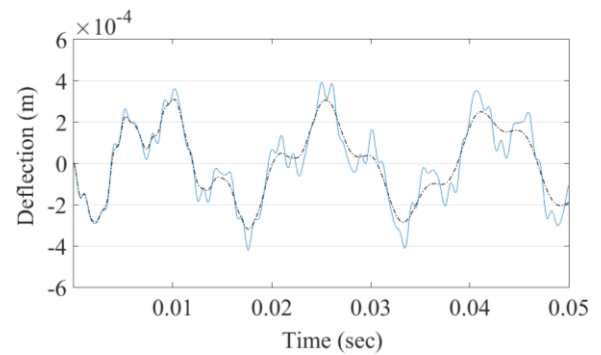


**Figure 3.54** Configuration D, CCFF, loading type 2

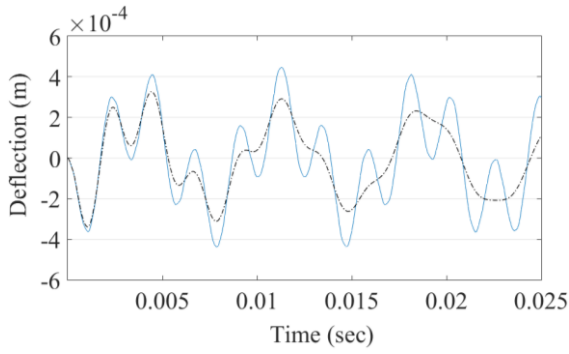


**Figure 3.55** Configuration A, SSSS, loading type 3

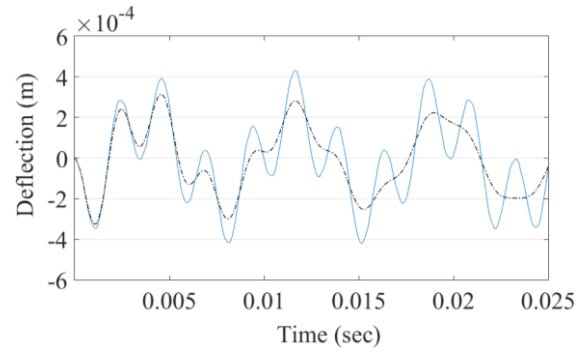


**Figure 3.56** Configuration B, SSSS, loading type 3

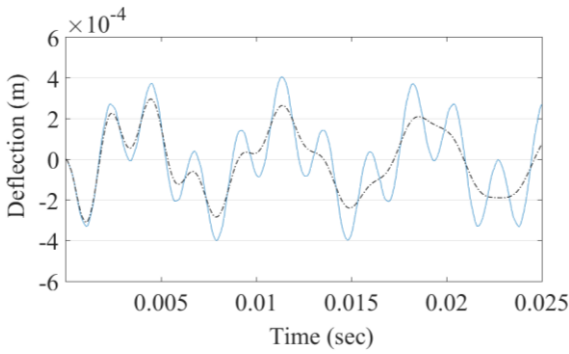


**Figure 3.57** Configuration C, SSSS, loading type 3

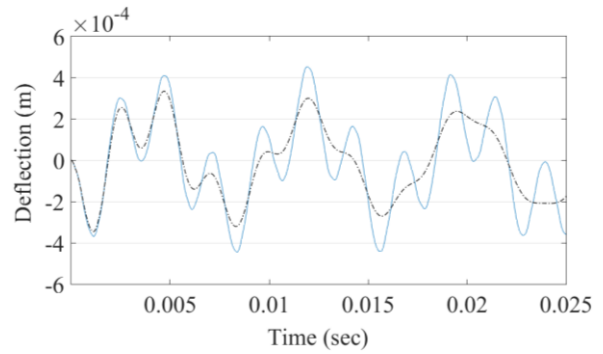


**Figure 3.58** Configuration D, SSSS, loading type 3

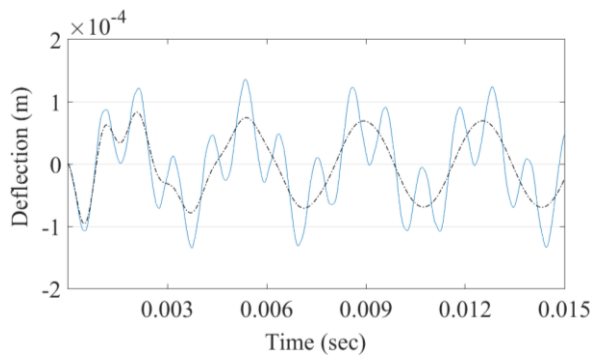


**Figure 3.59** Configuration A, CCCC, loading type 3

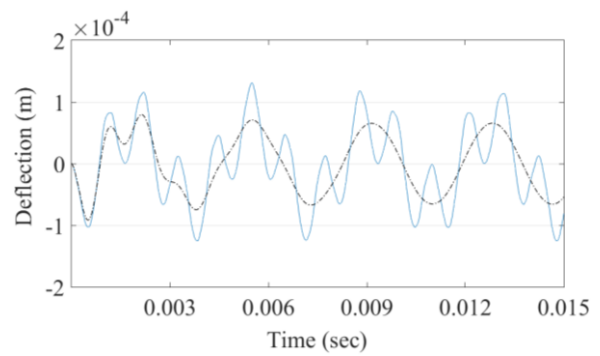


**Figure 3.60** Configuration B, CCCC, loading type 3

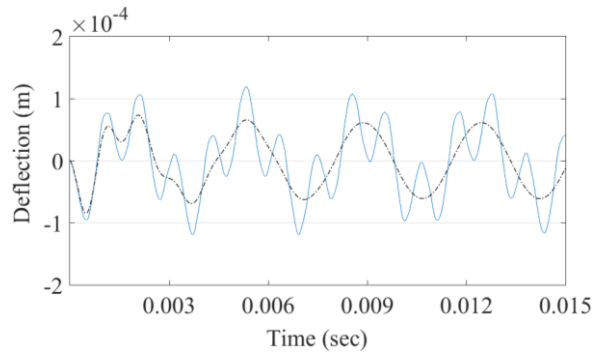


**Figure 3.61** Configuration C, CCCC, loading type 3

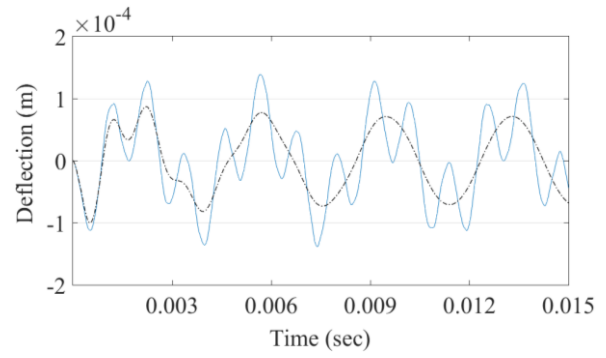


**Figure 3.62** Configuration D, CCCC, loading type 3

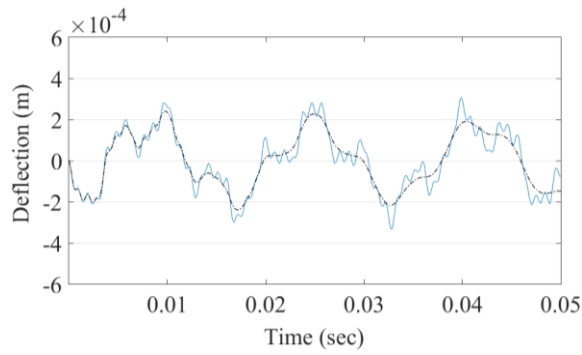


**Figure 3.63** Configuration A, CCFF, loading type 3

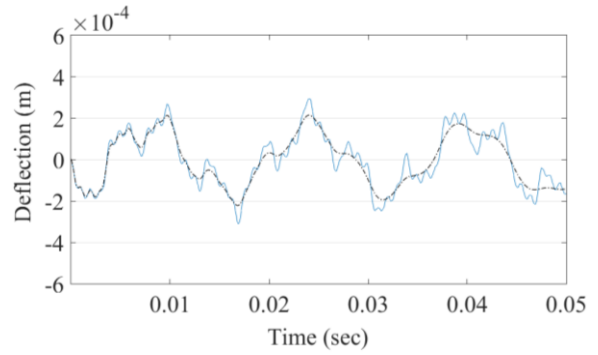


**Figure 3.64** Configuration B, CCFF, loading type 3

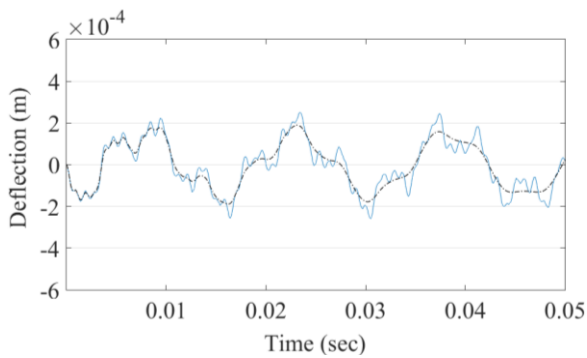


**Figure 3.65** Configuration C, CCFF, loading type 3

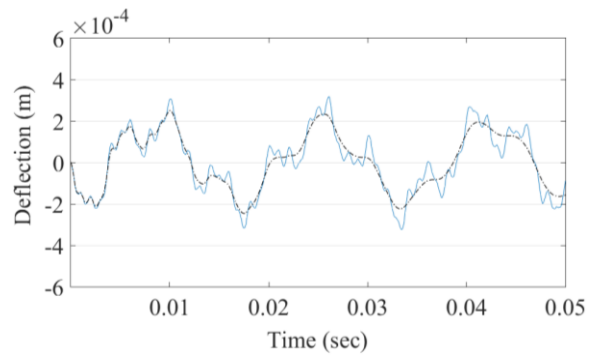


**Figure 3.66** Configuration D, CCFF, loading type 3

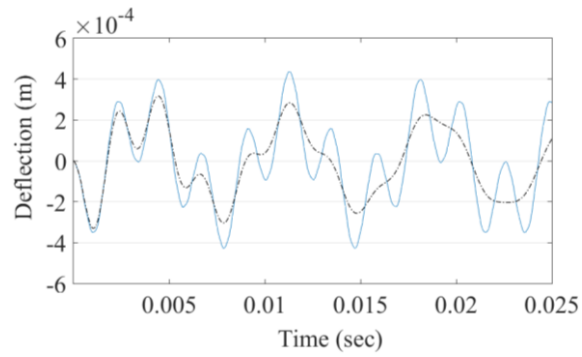


**Figure 3.67** Configuration A, SSSS, loading type 4

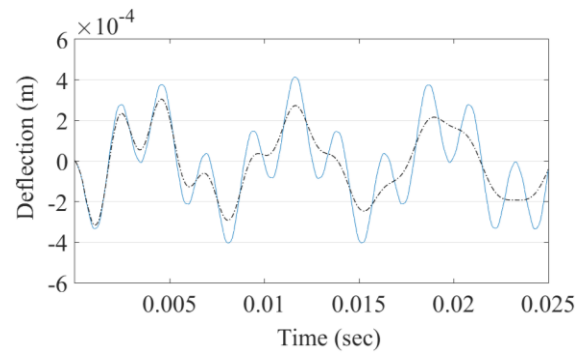


**Figure 3.68** Configuration B, SSSS, loading type 4

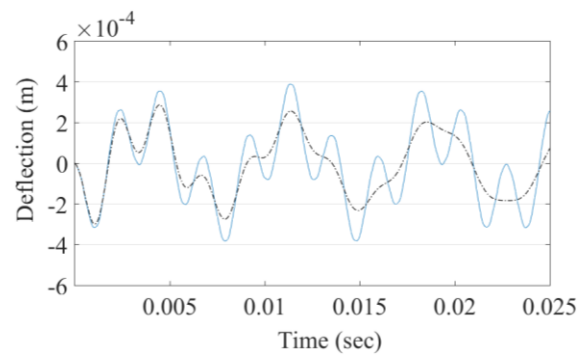


**Figure 3.69** Configuration C, SSSS, loading type 4

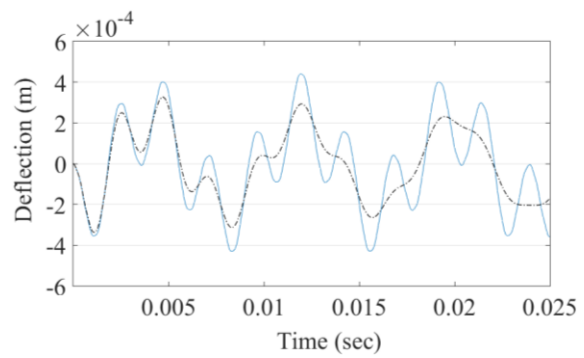


**Figure 3.70** Configuration D, SSSS, loading type 4

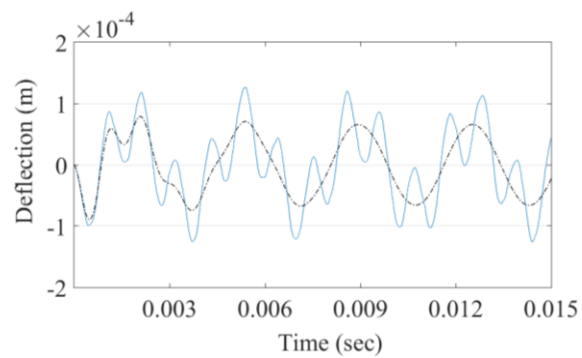


**Figure 3.71** Configuration A, CCCC, loading type 4

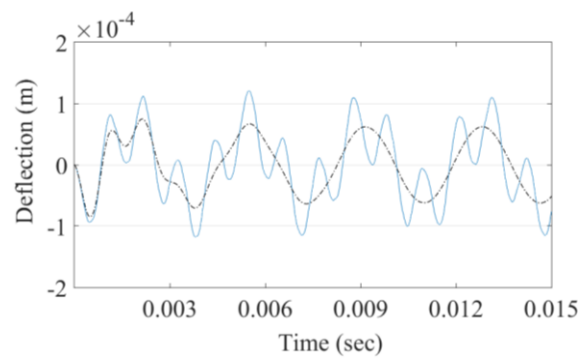


**Figure 3.72** Configuration B, CCCC, loading type 4

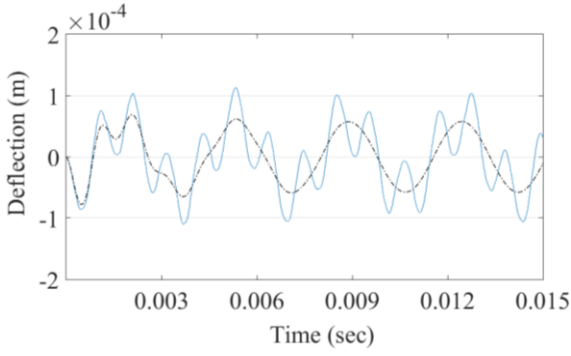


**Figure 3.73** Configuration C, CCCC, loading type 4

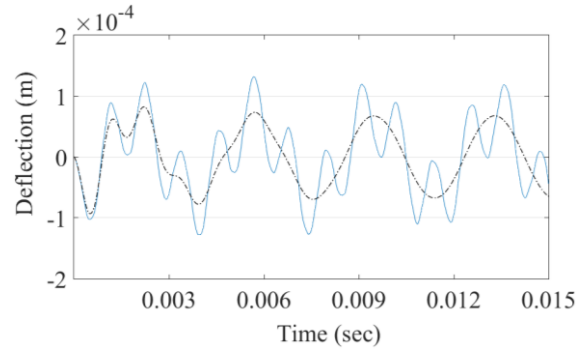


**Figure 3.74** Configuration D, CCCC, loading type 4

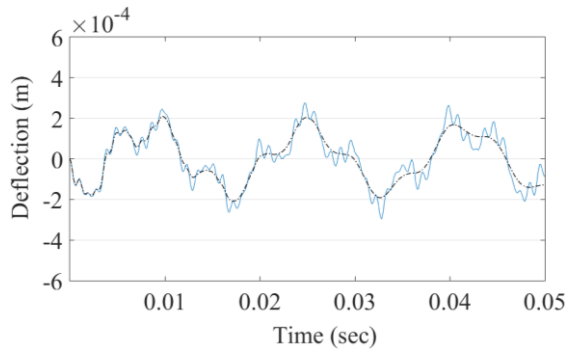


**Figure 3.75** Configuration A, CCFF, loading type 4

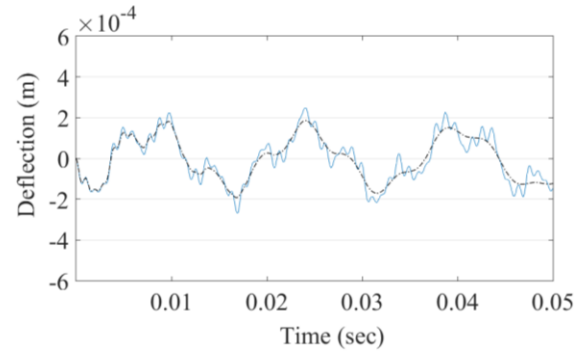


**Figure 3.76** Configuration B, CCFF, loading type 4

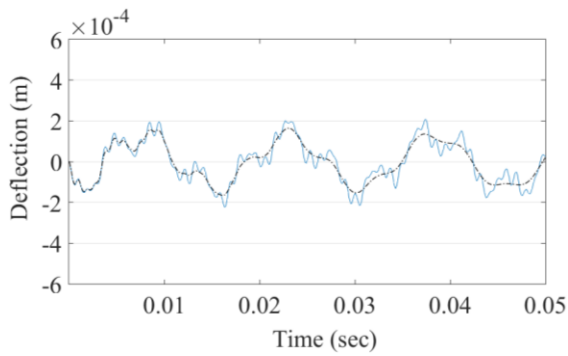


**Figure 3.77** Configuration C, CCFF, loading type 4

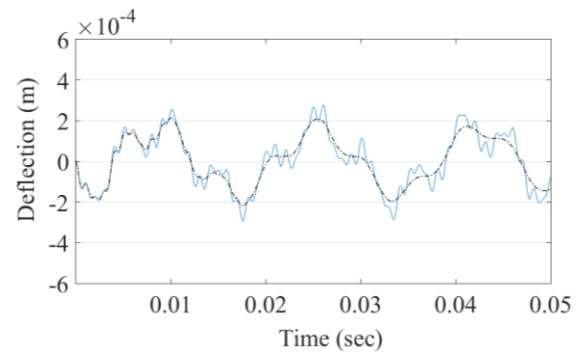


**Figure 3.78** Configuration D, CCFF, loading type 4

It is grasped from Figures 3.31 - 3.78 that for each boundary condition, the amplitude of the deflection of the taper configuration C is the least. This can be expected from the stiff structure and large mass of the configuration. Among the four taper configurations, A and D show higher deflection. Considering the low mass of A and lack of external plies in D, these configurations vibrate with higher amplitude when excitations are applied.

It is observed from Figures 3.31 - 3.78 that the effect of the boundary condition on the deflection amplitude is more important than the laminate's taper configuration. The deflections of the CCCC plates are the least regardless of the taper configuration. Therefore, due to the stiff structure and large mass, deflection of the configuration C clamped at all edges is much less than that of A with weaker and lighter structure. Regardless of the loading type, the deflection for configuration C with all clamped edges is the least among different configurations and boundary conditions.

Although the deflection for CCCC plate is the least in comparison with SSSS and CCFF plates, considering the time span, it vibrates severely compared to the SSSS and CCFF plates.

The amplitude of vibration considering viscous damping effect is smaller than that of the case with no damping, for all boundary conditions and taper configurations.

### **3.7 Conclusion**

In the present chapter, the formulation for the forced vibration with and without damping has been developed for tapered composite plates excited by arbitrary excitations; Then, demonstration is performed and the formulation has been examined by the layer reduction test. Afterward, four different line loads were defined and applied to the taper configurations with different lengths, taper angles and boundary conditions. The results were presented in the tables and displayed by the graphs. According to the study conducted in the present chapter, it is concluded that:

1. The deflection due to loading type 1 (line loading along the taper) is greater in comparison with that due to the loading type 2.



2. The deflection due to loading type 3 (line loading along the taper) is greater in comparison with that due to the loading type 4.

3. Since loading types 3 and 4 die away when approaching the laminate's ends, the deflections due to these loading types are less compared to that due to the loading types 1 and 2, respectively.

4. The boundary conditions in which the plates vibrate with higher natural frequencies in free CLPT vibration analysis, show lower deflections in forced vibration investigation. The CCCC plates show the highest resistance to excitations so that the laminates with this boundary condition deflect the least.

5. Deflection of the CCFF plates, due to clamped edges, is lower at the center than that of SSSS plates. However, the maximum deflection of the CCFF plates takes place at the intersection of the free edges.

6. Since configurations B, C and D are the same in terms of inertia (mass) and are heavier than configuration A, configuration C that is the stiffest among all, shows the least deflection and then configuration B comes the second and configurations A and D are almost the same in terms of transverse deflection. Configuration B is heavier than configuration A and, to some extent, is stiffer which results in lower deflection.

7. For all boundary conditions, taper configurations and loading types, with increase in the length over mean thickness ratio, the deflection at the center of the laminate increases such that when this ratio from 19.1 approaches 57.3, the deflection at the center is increased roughly by 690%. However, the increase in transverse deflections for SSSS and CCFF plates are the highest and the lowest, respectively.

## **Chapter 4 :**

### **Tapered composite plates with hybrid configuration**

#### **4.1 Introduction**

In chapter 2, free vibration analysis of the tapered composite plates was carried out and using the mass and stiffness matrices obtained based on CLPT, the Ritz method was applied and the natural frequencies and the corresponding mode shapes were determined. In chapter 3, the forced vibration analysis of the tapered composite plates was carried out using the assumed modes method and considering the mass and stiffness matrices as well as the natural frequencies and the corresponding mode shapes obtained in chapter 2.

In the present chapter, the tapered composite plates with hybrid configuration composed of thick-uniform, tapered and thin-uniform parts are considered and the formulations developed in chapters 2 and 3 are used to study the free and forced vibrations of the hybrid plates. The mass and stiffness matrices are obtained based on CLPT and the natural frequencies and the corresponding mode shapes are determined using the Ritz method. The fundamental frequencies of the hybrid configurations are displayed in the corresponding tables and depicted by the graphs. Then, the steady state response of the hybrid plates due to harmonic transverse excitation are computed for different taper configurations and boundary conditions and the obtained results are analyzed and discussed.

## 4.2 Hybrid configurations

In this section, four tapered composite plates with hybrid configurations are described for the analysis. Figure 4.1 provides a visual perception of configurations  $A^h$ ,  $B^h$ ,  $C^h$  and  $D^h$ .

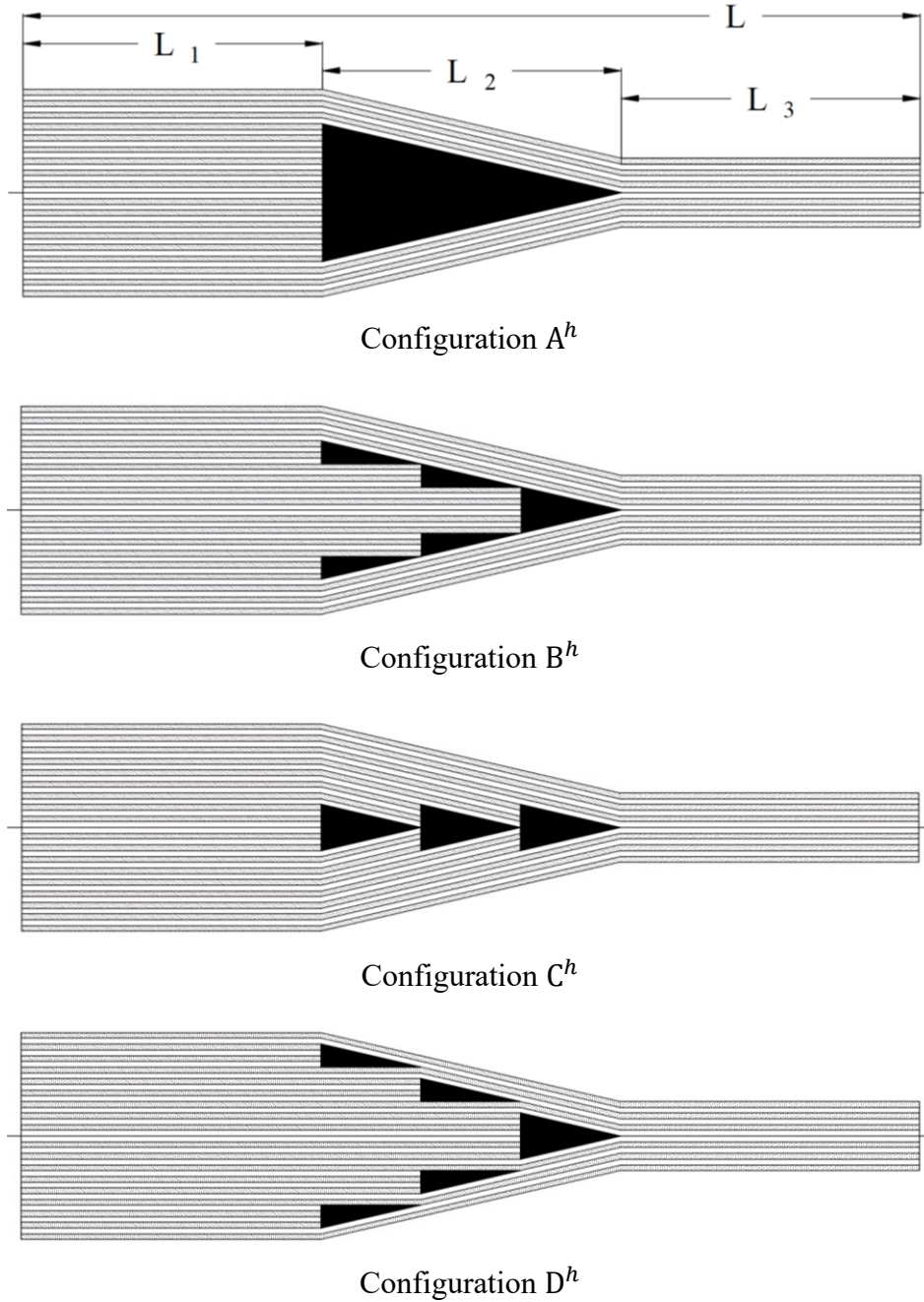


**Figure 4.1** Hybrid (uniform-tapered-uniform) Configurations

The tapered laminated square hybrid plates are considered with  $L = 0.18$  m composed of thick-uniform, tapered and thin-uniform parts and laminate configuration of  $(0/90)_{9s}$  and  $(0/90)_{3s}$  for the thick-uniform and thin-uniform parts. The configuration of the tapered part is  $(0/90)_{9s}$  and  $(0/90)_{3s}$  at the left and right ends, respectively. The lengths of the thick-uniform, tapered and thin-uniform parts are notated by  $L_1$ ,  $L_2$  and  $L_3$ , respectively (Figure 4.1). The laminate is made of resin and unidirectional NCT-301 Graphite-Epoxy material (mechanical properties were given in Table 2.3) with ply thickness of  $125 \times 10^{-6}$  m.

Figure 4.1 shows that the resin has been used only in the structure of the tapered parts of the hybrid laminates. Considering the fixed thickness of the left and right ends of the tapered parts which are the same as that of the thick-uniform and thin-uniform parts, respectively, the length and taper angle of the tapered part,  $L_2$  and  $\varphi$ , are such that with decrease in taper angle  $\varphi$ ,  $L_2$  is increased. Since the total length of the hybrid plates,  $L$ , is fixed and is equal to 0.18 m as described before, for a fixed  $L_1$ , with increase in  $L_2$ , the length of the thin-uniform part,  $L_3$ , is decreased such that the total length,  $L$ , is kept the same.

It is noted that in the analysis carried out in the present chapter, the length of the thick-uniform part for all the hybrid configurations, is fixed.

### 4.3 Free vibration analysis of the hybrid plates

In the present section, the free vibration analysis of the hybrid plates is carried out using the formulation developed in chapter 2. The stiffness and mass matrices are obtained based on CLPT for the hybrid plates and are used in the Ritz method in order to determine the natural frequencies and the mode shapes.

The free vibration analysis of the hybrid plates is carried out considering different taper angles, taper configurations and boundary conditions. The taper angles corresponding to different lengths of the tapered part, have been displayed in Table 4.1.

$L$ (cm)	0.18	0.18	0.18	0.18	0.18	0.18	0.18	0.18	0.18
$L_1$ (cm)	3	3	3	3	3	3	3	3	3
$L_2$ (cm)	15	13.5	12	10.5	9	7.5	6	4.5	3
$L_3$ (cm)	0	1.5	3	4.5	6	7.5	9	10.5	12
$\varphi$ (deg)	0.57°	0.64°	0.72°	0.82°	0.95°	1.15°	1.43°	1.91°	2.86°

**Table 4.1** Lengths (cm) of laminate parts corresponding to different taper angles

The fundamental frequencies for hybrid plates with taper angles given in Table 4.1 are obtained for different taper configurations and boundary conditions and are displayed in Table 4.2.

Fundamental Frequency (rad/s)										
Boundary Conditions	Configuration	$\varphi$ (deg)								
		0.57°	0.64°	0.72°	0.82°	0.95°	1.15°	1.43°	1.91°	2.86°
SSSS	$A^h$	3196	2871	2564	2303	2112	1937	1854	1788	1725
	$B^h$	3099	2784	2486	2233	2048	1878	1798	1734	1679
	$C^h$	3175	2852	2547	2288	2098	1924	1842	1776	1721
	$D^h$	3017	2710	2420	2174	1993	1828	1750	1688	1639
CCCC	$A^h$	6753	6067	5418	4866	4463	4093	3917	3778	3664
	$B^h$	6594	5924	5290	4752	4357	3996	3825	3689	3578
	$C^h$	6795	6104	5451	4896	4490	4118	3941	3801	3686
	$D^h$	6362	5715	5104	4584	4204	3855	3690	3559	3452
CCFF	$A^h$	1494	1342	1199	1077	987	906	867	836	810
	$B^h$	1443	1296	1157	1040	953	874	837	807	782
	$C^h$	1564	1405	1255	1127	1034	948	907	875	848
	$D^h$	1417	1272	1136	1021	936	858	822	792	768

**Table 4.2** Fundamental frequency (rad/s) of the hybrid plates

It can be grasped from Table 4.2 that regardless of the taper angle, for CCCC and CCFF boundary conditions, the obtained fundamental frequencies for configuration  $C^h$  are the highest among all the configurations. However, for SSSS plates, the fundamental frequencies corresponding to configuration  $A^h$  is the highest and configuration  $C^h$ , with slight difference comes second.

According to Table 4.2, the fundamental frequencies of the CCCC and CCFF plates are the highest and lowest respectively.

For all boundary conditions and taper angles of the hybrid laminates, the fundamental frequency corresponding to configuration  $D^h$  is the lowest among all the hybrid configurations.

Using the data given in Table 4.2, the change in fundamental frequency with increase in the taper angle  $\varphi$ , is depicted by Figures 4.2 - 4.5 for all the hybrid configurations and boundary conditions.

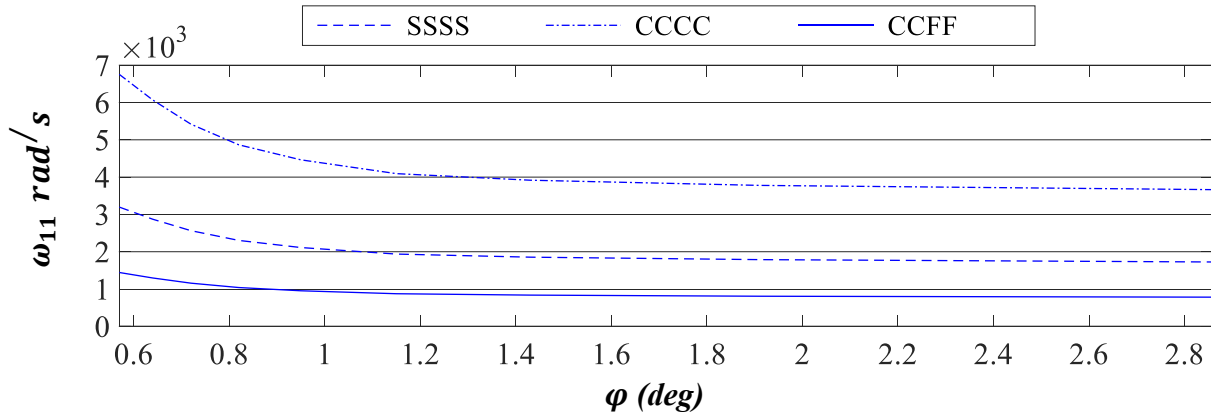


**Figure 4.2** Fundamental frequency (rad/s) variation with increase in taper angle  $\varphi$  (configuration  $A^h$ )

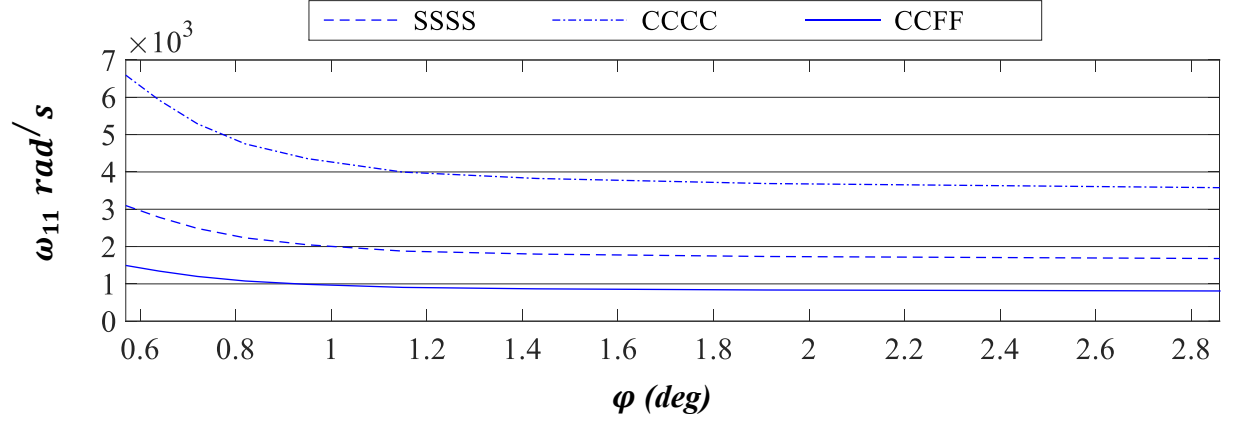


**Figure 4.3** Fundamental frequency (rad/s) variation with increase in taper angle  $\phi$  (configuration  $B^h$ )

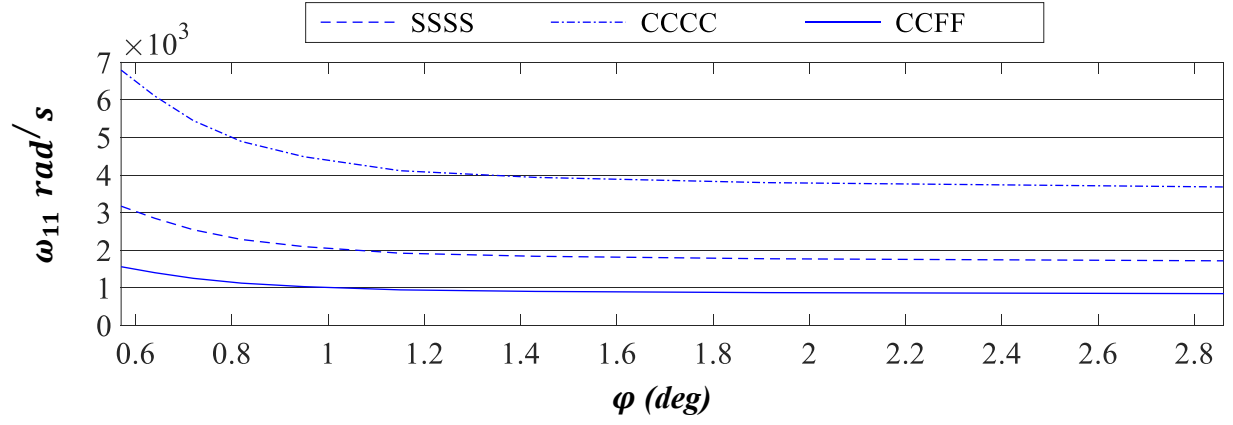


**Figure 4.4** Fundamental frequency (rad/s) variation with increase in taper angle  $\phi$  (configuration  $C^h$ )

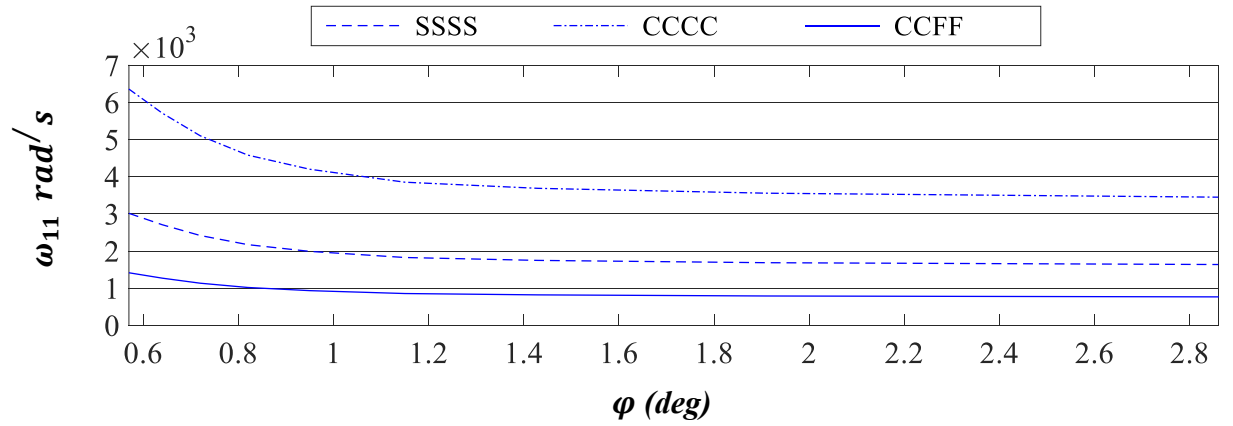


**Figure 4.5** Fundamental frequency (rad/s) variation with increase in taper angle  $\phi$  (configuration  $D^h$ )

It is observed from Figures 4.2 - 4.5 that for all the boundary conditions and hybrid configurations, with increase in taper angle (increase in the length of the thin-uniform part) the fundamental frequency of the laminate decreases such that when the taper angle approaches  $2.86^\circ$  from  $0.57^\circ$ , the fundamental frequencies are reduced roughly to 55% and this reduction for the CCCC plates is numerically greater than that of the SSSS and CCFF plates.

In addition, it is grasped from Figures 4.2 - 4.5 that regardless of the laminate configuration, the obtained fundamental frequencies for CCCC and CCFF plates are the highest and lowest, respectively.

#### 4.4 Forced vibration analysis of the hybrid plates

In this section, considering the mass and stiffness matrices as well as the natural frequencies and the corresponding mode shapes obtained in the free vibration analysis of the hybrid plates in the previous section, the response of the laminates due to transverse excitation is calculated using the formulation developed in chapter 3.

The loading described by equation (4.1) in below, is applied to all the hybrid configurations with different boundary conditions and taper angles displayed in Table 4.2. Then, the maximum transverse deflection corresponding to the center of the laminates due to the excitation, is calculated and the results are displayed in Table 4.3.

$$f = -500 \cos(0.3\omega_{11}t) \delta\left(x - \frac{L}{2}\right) \quad (4.1)$$



Maximum Deflection at the Center (mm)										
Boundary Conditions	Configuration	$\varphi$ (deg)								
		0.57°	0.64°	0.72°	0.82°	0.95°	1.15°	1.43°	1.91°	2.86°
SSSS	A <sup>h</sup>	0.441	0.492	0.551	0.613	0.664	0.713	0.752	0.790	0.819
	B <sup>h</sup>	0.434	0.484	0.542	0.603	0.652	0.701	0.739	0.776	0.802
	C <sup>h</sup>	0.413	0.460	0.515	0.572	0.619	0.666	0.702	0.738	0.762
	D <sup>h</sup>	0.449	0.500	0.560	0.623	0.674	0.722	0.783	0.803	0.826
CCCC	A <sup>h</sup>	0.126	0.140	0.157	0.175	0.190	0.204	0.216	0.225	0.232
	B <sup>h</sup>	0.124	0.138	0.154	0.172	0.187	0.200	0.211	0.221	0.228
	C <sup>h</sup>	0.118	0.132	0.147	0.163	0.178	0.191	0.201	0.211	0.218
	D <sup>h</sup>	0.128	0.143	0.160	0.178	0.193	0.208	0.219	0.229	0.237
CCFF	A <sup>h</sup>	0.323	0.360	0.403	0.449	0.486	0.522	0.550	0.578	0.599
	B <sup>h</sup>	0.303	0.338	0.378	0.421	0.455	0.489	0.516	0.542	0.559
	C <sup>h</sup>	0.295	0.328	0.368	0.409	0.442	0.476	0.502	0.527	0.544
	D <sup>h</sup>	0.337	0.375	0.4200	0.467	0.506	0.542	0.587	0.602	0.6200

**Table 4.3** Maximum deflection (mm) at the center of the laminates due to transverse excitation

Table 4.3 shows that, regardless of the boundary conditions and taper angle, the deflection corresponding to configuration C<sup>h</sup> is the lowest and that of configuration B<sup>h</sup> comes the second and deflection for configuration D<sup>h</sup> is the highest.

It is noted that considering the hybrid configuration of the plates, the peak deflection of the plates do not occur necessarily at the center of the laminates.

In order to illustrate the change in maximum deflection at the center of the hybrid laminates with respect to taper angle  $\varphi$ , following graphs are depicted by Figures 4.6 - 4.9 using data from Table 4.3.

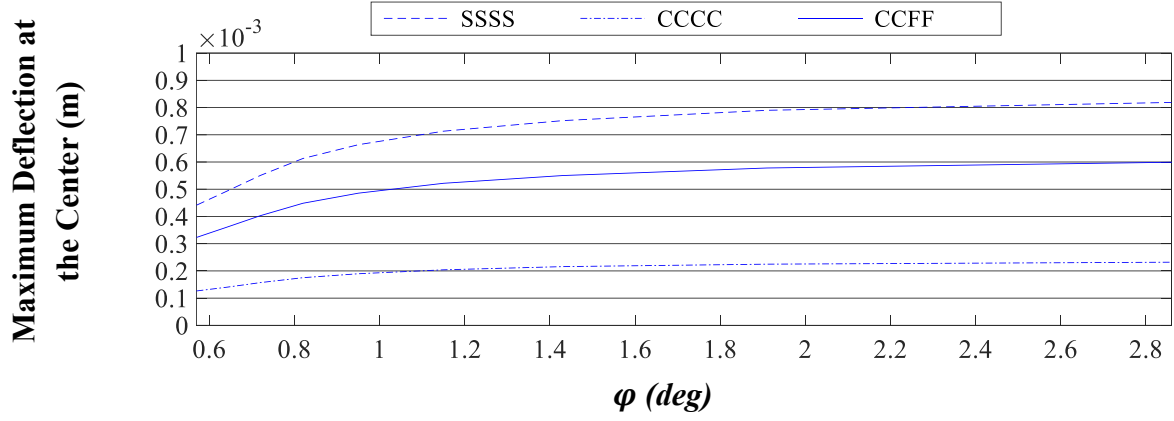


**Figure 4.6** Maximum deflection at the center for different taper angles (configuration  $A^h$ )

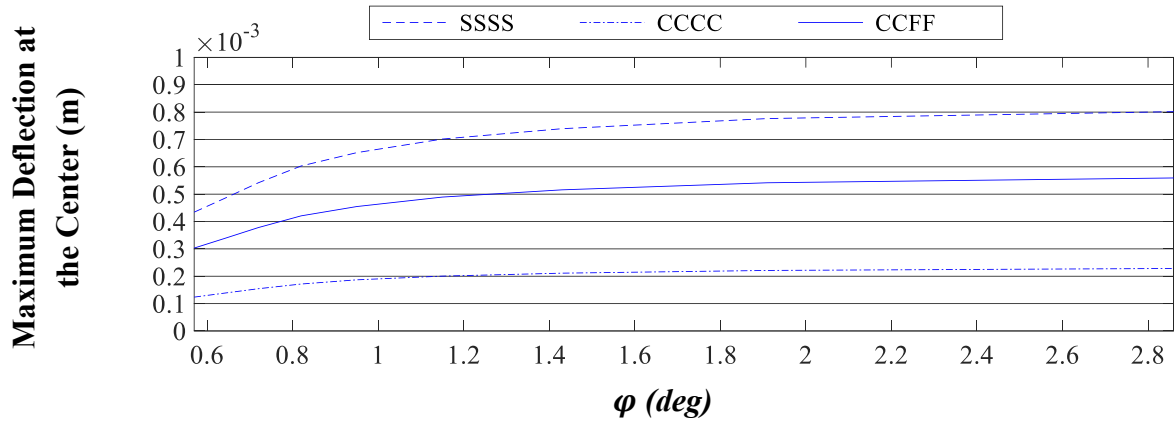


**Figure 4.7** Maximum deflection at the center for different taper angles (configuration  $B^h$ )

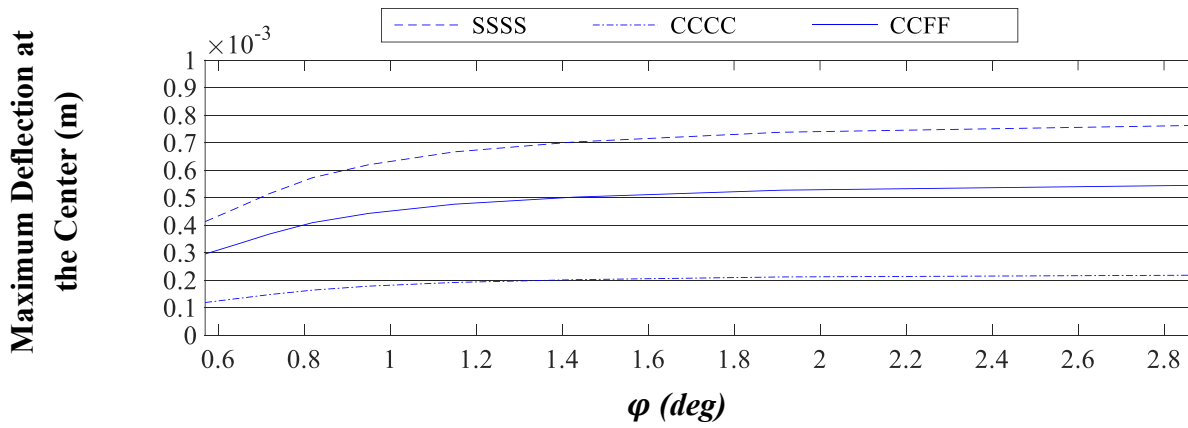


**Figure 4.8** Maximum deflection at the center for different taper angles (configuration  $C^h$ )

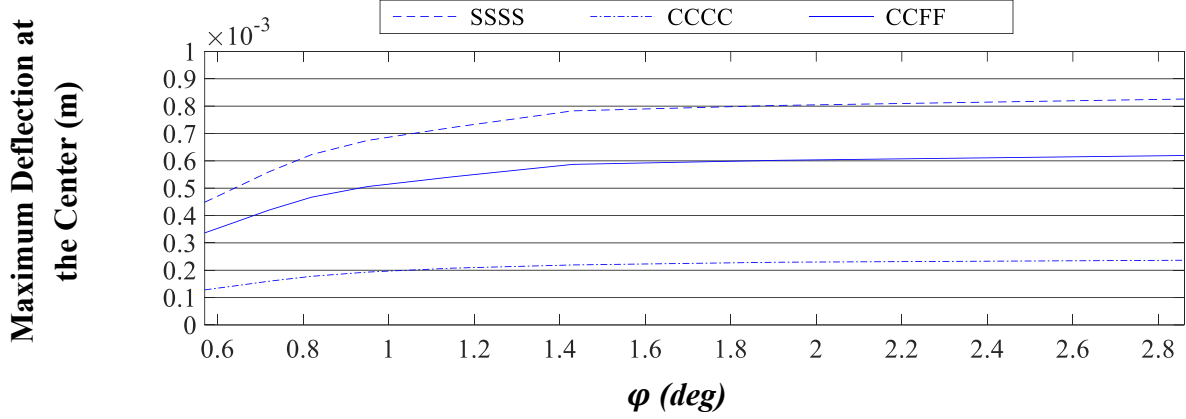


**Figure 4.9** Maximum deflection at the center for different taper angles (configuration  $D^h$ )

It is grasped from Figures 4.6 - 4.9 that, with increase in taper angle, the maximum deflection at the center of the laminate increases such that when the taper angle approaches  $2.86^\circ$  from  $0.57^\circ$ , the maximum deflection at the center of the laminate is increased roughly to 185% for all hybrid configurations and boundary conditions.

In addition, it is grasped from Figures 4.6 - 4.9 that regardless of the laminate configuration, the transverse deflection at the center for SSSS and CCCC plates are the highest and lowest, respectively. It is noted that for CCFF plates, the peak deflection of the laminates is expected to occur at the corner of the plate, at the intersection of the free edges.

## 4.5 Conclusion

In chapter 4, four different hybrid laminate configurations were described and the free vibration analysis of the laminates was conducted based on CLPT and using the Ritz method. The effect of change in taper angle on the variation of the fundamental frequencies was investigated for different boundary conditions. Then, the forced vibration analysis of the hybrid plates was carried out using the assumed modes method and the effect of change in taper angle on the variation of the maximum deflection of the center point of the laminates, was investigated considering different boundary conditions. From the study performed in the present chapter, it can be concluded that:

1. Regardless of the boundary conditions and hybrid configurations, with increase in taper angle the fundamental frequencies of the laminates decrease such that when the taper angle approaches  $2.86^\circ$  from  $0.57^\circ$ , the fundamental frequencies are reduced roughly to 55%.
2. Regardless of the hybrid configurations and boundary conditions, with increase in taper angle, the maximum deflection at the center of the laminates increase such that when the taper angle approaches  $2.86^\circ$  from  $0.57^\circ$ , the maximum deflection is increased roughly to 185%.
3. Because of fewer external plies in configuration  $D^h$ , it vibrates with the lowest fundamental frequency among all the configurations for all boundary conditions. Configuration  $C^h$ , with stiff structure, shows the highest fundamental frequency for CCCC and CCFF boundary conditions and configuration  $A^h$  vibrates with the highest fundamental frequency among the SSSS plates.
4. For all boundary conditions and taper angles, the deflections corresponding to configurations  $C^h$  and  $D^h$  are the lowest and the highest, respectively, and that of configuration  $B^h$  is the second lowest.

## **Chapter 5 :**

### **Conclusion**

#### **5.1 Contribution**

In the present thesis, free vibration analyses of the tapered and hybrid laminated composite plates have been conducted based on the Classical Laminated Plate Theory (CLPT) as well as First-order Shear Deformation Theory (FSDT) using Ritz method for four taper configurations and three boundary conditions. In the analysis, the stiffness matrix and the mass matrix were derived for CLPT as well as FSDT and the calculations leading to mass and stiffness matrices are performed in matrix form facilitating the derivation of the matrices and reducing the possibility of computational error. This compact matrix-form formulation describes the mass and stiffness matrices for CLPT and FSDT in a unified manner.

An investigation has been carried out regarding the increase of the calculation accuracy of the natural frequencies that are used in the derivation of the solution for the forced vibration response. Then, further suggestions have been given in order to minimize the frequency calculation errors and to avoid any extra computational effort.

In order to obtain the numerical results efficiently, an approach has been given to cope up with the computational problems caused by the presence of the integrands that are combinations of hyperbolic, polynomial and trigonometric functions. In this approach, by taking advantage of the Taylor series, one can obtain the numerical results using MATLAB<sup>®</sup> in a very short time.

Forced vibrations of the tapered and hybrid laminated composite plates have been investigated based on CLPT using assumed modes method for all the taper configurations and boundary conditions. The maximum deflection of the plates at the center have been given in the tables for different cases and the deflection response at the plate center over time have been depicted using the solution derived in the analysis and the software MATLAB<sup>®</sup>.

## 5.2 Conclusion

The study conducted on tapered laminated composite plates, begins with the free vibration analysis based on CLPT and FSDT using the Ritz method and continues with the forced vibration investigation using the assumed modes method and the derivations from the free vibration analysis, and ends with the free and forced vibration analyses of the hybrid laminates. In the following, the principal conclusions of the present study are given.

1. In order to obtain the fundamental frequencies of the tapered plates with good accuracy, considering the first 4 terms of the series expansion of the Ritz shape function is sufficient. However, in order to determine the solution for the forced vibration that requires numerous natural frequencies, higher number of terms should be taken into account. In the present thesis, 13 terms have been considered for all the cases in the calculations corresponding to the free and forced vibration analyses using the Taylor series and the approach explained in section 2.9.

2. For all taper configurations, the fundamental frequencies for CCCC plates are the highest and that of the CCFF plates are the lowest.

3. In composite plates, the plies close to the midplane absorb less energy than the external plies and they do not significantly take part in increasing the natural frequencies while their inertial (mass) contribution is the same as that of the other plies. The order of 3 for variable  $z$  (the distance from the midplane) in the bending stiffness coefficients  $R_{ij}^3$ , clarifies the importance of this fact.

4. Among the tapered laminated composite plates considered, the configuration C is the stiffest configuration. The resin considered as the weaker material is positioned at the core while the plies are used in farther layers from the midplane, thus, taking advantage of their high stiffness property to the full capacity. Therefore, it is observed from the numerical results that this configuration vibrates with highest fundamental frequency among all the configurations for CCCC and CCFF boundary conditions. Furthermore, it shows the lowest deflection when subjected to excitation in forced vibration investigation compared to the rest of the configurations for all the boundary conditions.

5. It is grasped from the results that the configuration A containing considerably fewer plies compared to other configurations, vibrates with frequencies that are close to that of the other configurations in free vibration analysis. This behavior comes from the use of the plies at the most external layers and resin which is the weaker material, in internal layers, such that the configuration is lighter and is still able to compensate for the absence of notable numbers of stiff plies within the structure.

6. The structure of configuration C with the resin used at the core, is stiffer than that of the configuration B and D with the resin used at farther layers from the midplane. In addition, configuration D has fewer external plies. Therefore, the fundamental frequency of C is the highest and that of the D is the lowest among configurations B, C and D for all boundary conditions.

7. The “Layer reduction test” in free vibration analysis shows that the fundamental frequency of the tapered plate is between the fundamental frequencies of the thick-uniform and thin-uniform plates with the laminate configurations identical to that of the left and right ends of the tapered plate.

8. From the “Layer reduction test” in free vibration analysis, it is observed that by removing the plies from the tapered and uniform-thin laminates, the fundamental frequencies corresponding to the plates, decrease. However, this reduction in fundamental frequency value is faster in the uniform-thin laminate.

9. The “Layer reduction test” in forced vibration analysis shows that the deflection at the center of the tapered plate is higher than that of the thick-uniform laminate and lower than that of the thin-uniform laminate.

10. From the “Layer reduction test” in forced vibration analysis, it is observed that by removing the plies from the tapered and uniform-thin laminates, the deflection at the center of laminates increase. However, this increase in transverse deflection magnitude is faster in the uniform-thin laminate.

11. The magnitude of the deflection at the center corresponding to the line loads, for all the configurations, are slightly higher when the line loads are distributed along the length (along the

taper) in  $x$  direction compared to the case with the line loads distributed along the width in  $y$  direction.

12. For all boundary conditions and taper configurations, the magnitudes of the deflection at the center of the laminates, due to the distributed sinusoidal loadings that dies away when approaching the laminate's ends, are lower compared to that due to the line loads with constant magnitude throughout the laminate length.

13. In the forced vibration analysis, a laminate with higher fundamental frequency compared to another laminate, does not necessarily deflect less when subjected to the same excitation. The Configuration C is denser and stiffer than configuration A and fundamental frequency of A is slightly higher than that of C for SSSS boundary condition. However, in forced vibration analysis, for all boundary conditions including SSSS, configuration C compared to A, deflects less when subjected to the same excitation. The mass and stiffness of configuration C provide higher resistance to excitation. The fundamental frequency of a heavy and stiff laminate can be comparable to that of a light and weak laminate. However, due to stiffness and inertial effect, the magnitude of the deflection for the heavy and stiff laminate can be less than that of the light and weak laminate when subjected to the same excitation.

14. With increase in taper angle of the tapered part in hybrid laminate, the fundamental frequency of the plates decreases.

15. With increase in taper angle of the tapered part in hybrid laminate, the magnitude of the deflection at the center of the laminate due to transverse excitation increases.

### **5.3 Recommendations for future works**

Considering the content of the study and the contributions made in the present thesis, the following suggestions are proposed for the future works.

1. Free and forced vibration analysis of tapered laminated composite plates presented in this thesis can be extended for thick laminates based on Higher-order Shear Deformation Theory (HSDT).



2. Damped and undamped free vibration analysis can be conducted on equilateral and trapezoidal tapered laminated composite plates.
3. Damped and undamped forced vibration analysis can be conducted on equilateral and trapezoidal tapered laminated composite plates.
4. Random vibration analysis can be performed on tapered laminated composite plates.

## References

- [1] S. Seraj, “Free Vibration and Dynamic Instability Analyses of Doubly-Tapered Rotating Laminated Composite Beams”, MSc Thesis, Concordia University, 2016.
- [2] J. M. Berthelot, *Composite Materials - Mechanical Behavior and Structural Analysis*, Springer - Verlag Berlin Heidelberg New York, 1999.
- [3] P. Salajegheh, "Vibrations of Thickness-and-width Tapered Laminated Composite Beams with Rigid and Elastic Supports," MSc Thesis, Concordia University, 2013.
- [4] K. He, S.V. Hoa and R. Ganesan, “The Study of Tapered Laminated Composite Structures: A Review”, *Composites Science and Technology*, Vol. 60, pp. 2643 – 2657, 2000.
- [5] S. M. Akhlaque-E-Rasul, “Buckling Analysis of Tapered Composite Plates Using Ritz Method Based on Classical and Higher-order Theories”, MSc Thesis, Concordia University, 2005.
- [6] R. Ganesan and D.Y. Liu, “Progressive Failure and Post-Buckling Response of Tapered Composite Plates Under Uni-Axial Compression”, *Composite Structures*, Vol. 82, No 2, pp. 159 – 176, 2008.
- [7] P. Venni and C. Mariani, “Free Vibration of Uncertain Composite Plates via Stochastic Rayleigh-Ritz Approach”, *Computers and Structures*, Vol. 64, No. 1 – 4, pp. 407 – 423, 1997.
- [8] A. Zabihollah, “Vibration and Buckling Analysis of Tapered Composite Beams Using Conventional and Advanced Finite Element Formulations”, MSc Thesis, Concordia University, 2003.
- [9] J.N. Reddy, *Mechanics of Laminated Composite Plates and Shells - Theory and Analysis*, CRC Press, 2003.
- [10] R. M. Jones, *Mechanics of Composite Materials*, 2<sup>nd</sup> Edition, Taylor and Francis, 1999.

- [11] J. M. Whitney, “The Effect of Boundary Conditions on the Response of Laminated Composite”, *Journal of Composite Materials*, Vol. 4, No. 2, pp. 360 – 378, 1970.
- [12] B. Baharlou and A. W. Leissa, “Vibration and Buckling of Generally Laminated Composite Plates with Arbitrary Edge Conditions”, *International Journal of Mechanical Sciences*, Vol. 29, No. 8, pp. 545 – 555, 1987.
- [13] H. Matsunaga, “Vibration and Stability of Cross-ply Laminated Composite Plates According to a Global Higher-Order Plate Theory”, *Composite Structures*, Vol. 48, No. 4, pp. 231 – 244, 2000.
- [14] C. P. Wu and W. Y. Chen, “Vibration and Stability of Laminated Plates Based on a Local High Order Plate Theory”, *Journal of Sound and Vibration*, Vol. 177, No. 4, pp. 503 – 520, 1994.
- [15] S. Mohamed Nabi and N. Ganesan, "A Generalized Element for the Free Vibration Analysis of Composite Beams" *Computers and Structures*, Vol. 51, No. 5. pp. 607 – 610, 1994.
- [16] C. W. Bert and M. Malik, “Free Vibration Analysis of Tapered Rectangular Plates by Differential Quadrature Method: A Semi-Analytical Approach”, *Journal of Sound and Vibration*, Vol. 190, No. 1, pp. 41 – 63, 1996.
- [17] P. Malekzadeh, “Nonlinear Free Vibration of Tapered Mindlin Plates with Edges Elastically Restrained Against Rotation Using DQM”, *Thin-Walled Structures*, Vol. 46, No. 1, pp 11 – 26, 2008.
- [18] H. Zhang, D. Shi and Q. Wang, “An Improved Fourier Series Solution for Free Vibration Analysis of the Moderately Thick Laminated Composite Rectangular Plate with Non-Uniform Boundary Conditions”, *International Journal of Mechanical Sciences*, Vol. 121, pp. 1 – 20, 2017.
- [19] A. Houmat, “Three-Dimensional Free Vibration Analysis of Variable Stiffness Laminated Composite Rectangular Plates”, *Composite Structures*, Vol. 194, pp. 398 – 412, 2018.

- [20] A. Ananda Babu, P. Edwin Sudhagar, R. Vasudevan and P. Jeyaraj, “Vibration Analysis of a Tapered Laminated Thick Composite Plate with Ply Drop-Offs”, *Archive of Applied Mechanics*, Vol. 85, No. 7, pp. 969 – 990, 2015.
- [21] H. Eftakher, “Free and Forced Vibrations of Tapered Composite Beams Including the Effects of Axial Force and Damping”, MASc Thesis, Concordia University, 2008.
- [22] A. Kumar Gupta, M. Saini, S. Singh and R. Kumar, “Forced Vibrations of Non-Homogeneous Rectangular Plate of Linearly Varying Thickness”, *Journal of Vibration and Control*, Vol. 20, No. 6, pp. 876 – 884, 2014.
- [23] A. Ananda Babu, P. Edwin Sudhagar and R. Vasudevan, “Dynamic Characterization of Thickness Tapered Laminated Composite Plates”, *Journal of Vibration and Control*, Vol. 22, No. 16, pp. 3555 - 3575, 2016.
- [24] M. Darabi and R. Ganesan, “Non-Linear Vibration and Dynamic Instability of Internally-Thickness-Tapered Composite Plates Under Parametric Excitation”, *Composite Structures*, Vol. 176, pp. 82 – 104, 2016.
- [25] S. Seraj and R. Ganesan, “Dynamic Instability of Rotating Doubly-Tapered Laminated Composite Beams Under Periodic Rotational Speeds”, *Composite Structures*, Vol. 200, pp. 711 – 728, 2018.
- [26] P. Salajegheh and R. Ganesan, “Free Vibrations of Variable-thickness Variable-width Laminated Composite Beams with Elastic Supports”, *American Society of Composites*, 28th Technical Conference, 2013.
- [27] H. R. H. Kabir, “On the Frequency Response of Moderately Thick Simply Supported Rectangular Plates with Arbitrarily Lamination”, *International Journal of Solids and Structures*, Vol. 36, No. 15, pp. 2285 – 2301, 1999.
- [28] C.W. Bert and B.L. Mayberry, “Free Vibration of Unsymmetrically Laminated Anisotropic Plates with Clamped Edges”, *Journal of Composite Materials*, Vol. 3, No. 2, pp. 282 – 293, 1969.

- [29] A. K. NOOR, “Free Vibrations of Multilayered Composite Plates”, *AIAA Journal*, Vol. 11, No. 7, pp. 1038 – 1039, 1973.
- [30] B. Arab, R. Ganesan and M. Malaki, “Fundamental Frequency of Composite Plate with Staircase Internal-Thickness-Taper”, *26<sup>th</sup> International Congress on Sound and Vibration*, 2019. (The paper has been accepted and will be published in July 2019)
- [31] S. S. Rao, *Vibration of Continuous Systems*, John Wiley & Sons, 2007.
- [32] D. S. Cho, B. H. Kim, J. H. Kim, N. Vladimir and T. M. Choi, “Forced Vibration Analysis of Arbitrarily Constrained Rectangular Plates and Stiffened Panels Using the Assumed Mode Method”, *Thin-Walled Structures*, Vol. 90, pp. 182 – 190, 2015.
- [33] S. S. Rao, *Mechanical Vibrations*, 5<sup>th</sup> Edition, Pearson Education, 2004.
- [34] M. A. Fazili, “Vibration Analysis of Thickness-and Width-Tapered Laminated Composite Beams using Hierarchical Finite Element Method”, MSc Thesis, Concordia University, 2013.
- [35] P. A. A. Laura and R. Duran, “A Note on Forced Vibration of a Clamped Rectangular Plate”, *Journal of Sound and Vibration*, Vol.42, No.1, pp.129 – 135, 1975.
- [36] R. Ganesan, *Stress Analysis in Mechanical Design*, Lecture Notes, Mechanical, Industrial and Aerospace Engineering Department, Concordia University, 2018.
- [37] A. C. Ugural and S. K. Fenster, *Advanced Mechanical of Materials and Applied Elasticity*, 5<sup>th</sup> Edition, Pearson Education, 2012.
- [38] M. T. DiNardo and A. P. Lagace, “Buckling and Post-buckling of Laminated Composite Plates with Ply Drop-offs” *AIAA Journal*, Vol. 27, No. 10, pp. 1392 – 1398, 1989.
- [39] J. M. Whitney, *Structural Analysis of Laminated Anisotropic Plates*, Taylor and Francis Group, 1987.
- [40] A. K. Kaw, *Mechanics of Composite Materials*, Taylor and Francis, 2006.

- [41] J. R. Vinson and R. L. Sierakowski, *The Behavior of Structures Composed of Composite Materials*, 2<sup>nd</sup> Edition, Kluwer Academic Publishers, 2002.
- [42] J. M. Whitney, “The Effect of Transverse Shear Deformation on the Bending of Laminated Plates” *The Journal of Composite Materials*, Vol. 3, No. 3, pp. 534 – 547, 1969.
- [43] J. N. Reddy And A. Khdeir, “Buckling and Vibration of Laminated Composite Plates Using Various Plate Theories”, *AIAA Journal*, Vol. 27, No. 12, pp. 1808 – 1817, 1989.
- [44] J. N. Reddy and D. H. Robbins, “Theories and Computational Models for Composite Laminates”, *Applied Mechanics Reviews*, Vol. 47, No. 6, pp. 147 – 169, 1994.
- [45] A. Tessler, E. Saether and T. Tsui, “Vibration of Thick Laminated Composite Plates”, *Journal of sound and vibration*, Vol. 179, No. 3, pp.475 – 498, 1995.
- [46] M. Huang, X.Q. Ma, T. Sakiyama, H. Matuda, C. Morita, “Free vibration analysis of orthotropic rectangular plates with variable thickness and general boundary conditions”, *Journal of Sound and Vibration*, Vol. 288, No. 4 - 5, pp. 931 - 955, 2005.

## Appendix A

### A.1 Reduced stiffness matrices based on CLPT and FSDT

The stress-strain relationship, considering negligible out of plane normal stress, is written for the  $k^{\text{th}}$  layer as follows using equation (2.45).

$$\begin{Bmatrix} \sigma_x = \sigma_1 \\ \sigma_y = \sigma_2 \\ \sigma_z = \sigma_3 = 0 \\ \tau_{yz} = \sigma_4 \\ \tau_{xz} = \sigma_5 \\ \tau_{xy} = \sigma_6 \end{Bmatrix}_k = \begin{bmatrix} C_{11} & C_{12} & C_{13} & C_{14} & C_{15} & C_{16} \\ C_{12} & C_{22} & C_{23} & C_{24} & C_{25} & C_{26} \\ C_{13} & C_{23} & C_{33} & C_{34} & C_{35} & C_{36} \\ C_{14} & C_{24} & C_{34} & C_{44} & C_{45} & C_{46} \\ C_{15} & C_{25} & C_{35} & C_{45} & C_{55} & C_{56} \\ C_{16} & C_{26} & C_{36} & C_{46} & C_{56} & C_{66} \end{bmatrix}_k \begin{Bmatrix} \varepsilon_x = \varepsilon_1 \\ \varepsilon_y = \varepsilon_2 \\ \varepsilon_z = \varepsilon_3 \\ \gamma_{yz} = \varepsilon_4 \\ \gamma_{xz} = \varepsilon_5 \\ \gamma_{xy} = \varepsilon_6 \end{Bmatrix}_k \quad (1)$$

Similar to Ref. [5], calculation is performed here in order to derive the reduced stiffness matrices based on CLPT and FSDT. Considering  $\sigma_3 = 0$  in equation (1), it is expressed that:

$$\sum_{j=1}^6 C_{3j} \varepsilon_j = 0 \quad (2)$$

Using equation (2), the following expression is written.

$$\varepsilon_3 = - \sum_{\substack{j=1 \\ j \neq 3}}^6 \left( \frac{C_{3j}}{C_{33}} \right) \varepsilon_j \quad (3)$$

In addition, using equation (1), it is written that:

$$\sigma_i = \left[ \sum_{\substack{j=1 \\ j \neq 3}}^6 C_{ij} \varepsilon_j \right] + C_{i3} \varepsilon_3 \quad (i \neq 3) \quad (4)$$

Equation (3) is substituted in equation (4).

$$\sigma_i = \left[ \sum_{\substack{j=1 \\ j \neq 3}}^6 C_{ij} \varepsilon_j \right] + C_{i3} \left[ - \sum_{\substack{j=1 \\ j \neq 3}}^6 \left( \frac{C_{3j}}{C_{33}} \right) \varepsilon_j \right] \quad (i \neq 3) \quad (5)$$

Equation (5) is written in the following from.

$$\sigma_i = \sum_{\substack{j=1 \\ j \neq 3}}^6 \left( C_{ij} - i3 \frac{C_{3j}}{C_{33}} \right) \varepsilon_j \quad (i \neq 3) \quad (6)$$

Considering notation  $Q_{ij} = \left( C_{ij} - C_{i3} \frac{C_{3j}}{C_{33}} \right)$ , equation (6) is rewritten as follows:

$$\sigma_i = \sum_{\substack{j=1 \\ j \neq 3}}^6 Q_{ij} \varepsilon_j \quad (i \neq 3) \quad (7)$$

Writing equation (7) in matrix form:

$$\begin{Bmatrix} \sigma_1 \\ \sigma_2 \\ \sigma_4 \\ \sigma_5 \\ \sigma_6 \end{Bmatrix}_k = \begin{bmatrix} Q_{11} & Q_{12} & Q_{14} & Q_{15} & Q_{16} \\ Q_{21} & Q_{22} & Q_{24} & Q_{25} & Q_{26} \\ Q_{41} & Q_{42} & Q_{44} & Q_{45} & Q_{46} \\ Q_{51} & Q_{52} & Q_{54} & Q_{55} & Q_{56} \\ Q_{61} & Q_{62} & Q_{64} & Q_{65} & Q_{66} \end{bmatrix}_k \begin{Bmatrix} \varepsilon_1 \\ \varepsilon_2 \\ \varepsilon_4 \\ \varepsilon_5 \\ \varepsilon_6 \end{Bmatrix}_k \quad (8)$$

Considering the relation  $C_{ij} = C_{ji}$  which results in  $Q_{ij} = Q_{ji}$ , equation (8) is expressed as follows.

$$\begin{bmatrix} \sigma_1 \\ \sigma_2 \\ \sigma_4 \\ \sigma_5 \\ \sigma_6 \end{bmatrix} = \begin{bmatrix} Q_{11} & Q_{12} & Q_{14} & Q_{15} & Q_{16} \\ Q_{12} & Q_{22} & Q_{24} & Q_{25} & Q_{26} \\ Q_{14} & Q_{24} & Q_{44} & Q_{45} & Q_{46} \\ Q_{15} & Q_{25} & Q_{45} & Q_{55} & Q_{56} \\ Q_{16} & Q_{26} & Q_{46} & Q_{56} & Q_{66} \end{bmatrix} \begin{bmatrix} \varepsilon_1 \\ \varepsilon_2 \\ \varepsilon_4 \\ \varepsilon_5 \\ \varepsilon_6 \end{bmatrix} \quad (9)$$

Rearranging the stresses and considering shear correction factor using Refs. [2] and [5], the reduced stiffness matrix for FSDT becomes:

$$\begin{bmatrix} \sigma_x = \sigma_1 \\ \sigma_y = \sigma_2 \\ \tau_{xy} = \sigma_6 \\ \tau_{yz} = \sigma_4 \\ \tau_{xz} = \sigma_5 \end{bmatrix} = \begin{bmatrix} Q_{11} & Q_{12} & Q_{16} & Q_{14} & Q_{15} \\ Q_{12} & Q_{22} & Q_{26} & Q_{24} & Q_{25} \\ Q_{16} & Q_{26} & Q_{66} & Q_{46} & Q_{56} \\ 5 \left( Q_{14} & Q_{24} & Q_{46} & Q_{44} & Q_{45} \right) \\ 6 \left( Q_{15} & Q_{25} & Q_{56} & Q_{45} & Q_{55} \right) \end{bmatrix} \begin{bmatrix} \varepsilon_x = \varepsilon_1 \\ \varepsilon_y = \varepsilon_2 \\ \gamma_{xy} = \varepsilon_6 \\ \gamma_{yz} = \varepsilon_4 \\ \gamma_{xz} = \varepsilon_5 \end{bmatrix} \quad (10)$$

Considering  $\varepsilon_4 = \varepsilon_5 = 0$  for CLPT in equation (6), it is expressed that:



$$\sigma_i = \sum_{\substack{j=1 \\ j \neq 3,4,5}}^6 \left( C_{ij} - C_{i3} \frac{C_{3j}}{C_{33}} \right) \varepsilon_j \quad (i \neq 3, 4, 5) \quad (11)$$

Considering the relation  $Q_{ij} = Q_{ji}$  in equation (11), the reduced stiffness matrix for CLPT is derived.

$$\begin{bmatrix} \sigma_x = \sigma_1 \\ \sigma_y = \sigma_2 \\ \tau_{xy} = \sigma_6 \end{bmatrix} = \begin{bmatrix} Q_{11} & Q_{12} & Q_{16} \\ Q_{12} & Q_{22} & Q_{26} \\ Q_{16} & Q_{26} & Q_{66} \end{bmatrix} \begin{bmatrix} \varepsilon_x = \varepsilon_1 \\ \varepsilon_y = \varepsilon_2 \\ \gamma_{xy} = \varepsilon_6 \end{bmatrix} \quad (12)$$

## A.2 Derivatives of kinetic and strain energies

In order to derive the derivatives of strain and kintic energies based on CLPT, equation (2.85) is substituted in equation (2.80), and equation (2.86) is substituted in equation (2.80).

$${}^c\hat{U}^{[w_o]} = \iint \left[ \begin{aligned} & \left[ R_{12}^3 X_m^{c_{w_o}} \ddot{Y}_n^{c_{w_o}} + R_{11}^3 \ddot{X}_m^{c_{w_o}} Y_n^{c_{w_o}} \right] \frac{\partial^2(c_{w_o})}{\partial x^2} + \\ & \left[ R_{22}^3 X_m^{c_{w_o}} \ddot{Y}_n^{c_{w_o}} + R_{12}^3 \ddot{X}_m^{c_{w_o}} Y_n^{c_{w_o}} \right] \frac{\partial^2(c_{w_o})}{\partial y^2} \\ & + 4R_{66}^3 \dot{X}_m^{c_{w_o}} \dot{Y}_n^{c_{w_o}} \frac{\partial^2(c_{w_o})}{\partial x \partial y} \end{aligned} \right] dA \quad (13)$$

$${}^c\hat{T}^{[w_o]} = \omega^2 \iint \left[ \begin{aligned} & R^3 \dot{X}_m^{c_{w_o}} Y_n^{c_{w_o}} \frac{\partial(c_{w_o})}{\partial x} + R^3 X_m^{c_{w_o}} \dot{Y}_n^{c_{w_o}} \frac{\partial(c_{w_o})}{\partial y} \\ & + R^1 X_m^{c_{w_o}} Y_n^{c_{w_o}} (c_{w_o}) \end{aligned} \right] dA \quad (14)$$

Substituting equation (2.51) in equations (13) and (14), it is written that:

$${}^c\hat{U}^{[w_o]} = \sum_{i=1}^I \sum_{j=1}^J \iint \left( \begin{aligned} & \left[ X_m^{c_{w_o}} \ddot{Y}_n^{c_{w_o}} R_{12}^3 + R_{11}^3 \ddot{X}_m^{c_{w_o}} Y_n^{c_{w_o}} \right] \ddot{X}_i^{c_{w_o}} Y_j^{c_{w_o}} + \\ & \left[ R_{22}^3 X_m^{c_{w_o}} \ddot{Y}_n^{c_{w_o}} + R_{12}^3 \ddot{X}_m^{c_{w_o}} Y_n^{c_{w_o}} \right] X_i^{c_{w_o}} \ddot{Y}_j^{c_{w_o}} + \\ & 4R_{66}^3 \dot{X}_m^{c_{w_o}} \dot{Y}_n^{c_{w_o}} \dot{X}_i^{c_{w_o}} \dot{Y}_j^{c_{w_o}} \end{aligned} \right) A_{ij}^{c_{w_o}} dA \quad (15)$$

$${}^c\hat{T}^{[w_o]} = \omega^2 \sum_{i=1}^I \sum_{j=1}^J \iint \left[ \begin{array}{l} R^3 \dot{X}_m^{c_{w_o}} Y_n^{c_{w_o}} \dot{X}_i^{c_{w_o}} Y_j^{c_{w_o}} + \\ R^3 X_m^{c_{w_o}} \dot{Y}_n^{c_{w_o}} X_i^{c_{w_o}} \dot{Y}_j^{c_{w_o}} \\ + R^1 X_m^{c_{w_o}} Y_n^{c_{w_o}} X_i^{c_{w_o}} Y_j^{c_{w_o}} \end{array} \right] A_{ij}^{c_{w_o}} dA \quad (16)$$

Equations (15) and (16) result in the following expressions:

$${}^c\hat{U}^{[w_o]} = \sum_{i=1}^I \sum_{j=1}^J \left( \begin{array}{l} \int_0^L R_{12}^3 X_m^{c_{w_o}} \dot{X}_i^{c_{w_o}} dx \int_0^L \dot{Y}_n^{c_{w_o}} Y_j^{c_{w_o}} dy \\ + \int_0^L R_{11}^3 \dot{X}_m^{c_{w_o}} \dot{X}_i^{c_{w_o}} dx \int_0^L Y_n^{c_{w_o}} Y_j^{c_{w_o}} dy \\ + \int_0^L R_{22}^3 X_m^{c_{w_o}} X_i^{c_{w_o}} dx \int_0^L \ddot{Y}_n^{c_{w_o}} \ddot{Y}_j^{c_{w_o}} dy \\ + \int_0^L R_{12}^3 \dot{X}_m^{c_{w_o}} X_i^{c_{w_o}} dx \int_0^L Y_n^{c_{w_o}} \dot{Y}_j^{c_{w_o}} dy \\ + 4 \int_0^L R_{66}^3 \dot{X}_m^{c_{w_o}} \dot{X}_i^{c_{w_o}} dx \int_0^L \dot{Y}_n^{c_{w_o}} \dot{Y}_j^{c_{w_o}} dy \end{array} \right) A_{ij}^{c_{w_o}} \quad (17)$$

$${}^c\hat{T}^{[w_o]} = \omega^2 \sum_{i=1}^I \sum_{j=1}^J \left( \begin{array}{l} \int_{x=0}^{x=L} R^3 \dot{X}_m^{c_{w_o}} \dot{X}_i^{c_{w_o}} dx \int_{y=0}^{y=L} Y_n^{c_{w_o}} Y_j^{c_{w_o}} dy \\ + \int_{x=0}^{x=L} R^3 X_m^{c_{w_o}} X_i^{c_{w_o}} dx \int_{y=0}^{y=L} \dot{Y}_n^{c_{w_o}} \dot{Y}_j^{c_{w_o}} dy \\ + \int_{x=0}^{x=L} R^1 X_m^{c_{w_o}} X_i^{c_{w_o}} dx \int_{y=0}^{y=L} Y_n^{c_{w_o}} Y_j^{c_{w_o}} dy \end{array} \right) A_{ij}^{c_{w_o}} \quad (18)$$

For FSDT, by substituting equation (2.85) in (2.80) for derivative of strain energy and by substituting equation (2.86) in (2.80) for derivative of kinetic energy, it is expressed that:

$${}_F\hat{U}^{[w_o]} = \iint \left[ \begin{array}{l} \frac{5}{6} R_{55}^1 \dot{X}_m^{Fw_o} Y_n^{Fw_o} \frac{\partial(Fw_o)}{\partial x} + \frac{5}{6} R_{44}^1 X_m^{Fw_o} \dot{Y}_n^{Fw_o} \frac{\partial(Fw_o)}{\partial y} \\ + \frac{5}{6} R_{55}^1 \dot{X}_m^{Fw_o} Y_n^{Fw_o} \varphi_x + \frac{5}{6} R_{44}^1 X_m^{Fw_o} \dot{Y}_n^{Fw_o} \varphi_y \end{array} \right] dA \quad (19)$$

$${}_F\hat{U}^{[\varphi_x]} = \iint \left[ \begin{array}{l} \frac{5}{6} R_{55}^1 X_m^{\varphi_x} Y_n^{\varphi_x} \frac{\partial(Fw_o)}{\partial x} + \frac{5}{6} R_{55}^1 X_m^{\varphi_x} Y_n^{\varphi_x} \varphi_x + R_{11}^3 \dot{X}_m^{\varphi_x} Y_n^{\varphi_x} \frac{\partial \varphi_x}{\partial x} \\ + R_{66}^3 X_m^{\varphi_x} \dot{Y}_n^{\varphi_x} \frac{\partial \varphi_x}{\partial y} + R_{66}^3 X_m^{\varphi_x} \dot{Y}_n^{\varphi_x} \frac{\partial \varphi_y}{\partial x} + R_{12}^3 \dot{X}_m^{\varphi_x} Y_n^{\varphi_x} \frac{\partial \varphi_y}{\partial y} \end{array} \right] dA \quad (20)$$

$${}_F\hat{U}^{[\varphi_y]} = \iint \left[ \frac{5}{6} R_{44}^1 X_m^{\varphi_y} Y_n^{\varphi_y} \frac{\partial({}_F w_o)}{\partial y} + R_{12}^3 X_m^{\varphi_y} \dot{Y}_n^{\varphi_y} \frac{\partial \varphi_x}{\partial x} + R_{66}^3 \dot{X}_m^{\varphi_y} Y_n^{\varphi_y} \frac{\partial \varphi_x}{\partial y} \right. \\ \left. + \frac{5}{6} R_{44}^1 X_m^{\varphi_y} Y_n^{\varphi_y} \varphi_y + R_{22}^3 X_m^{\varphi_y} \dot{Y}_n^{\varphi_y} \frac{\partial \varphi_y}{\partial y} + R_{66}^3 \dot{X}_m^{\varphi_y} Y_n^{\varphi_y} \frac{\partial \varphi_y}{\partial x} \right] dA \quad (21)$$

$${}_F\hat{T}^{[w_o]} = \omega^2 \iint [R^1 X_m^{Fw_o} Y_n^{Fw_o} ({}_F w_o)] dA \quad (22)$$

$${}_F\hat{T}^{[\varphi_x]} = \omega^2 \iint [R^3 X_m^{\varphi_x} Y_n^{\varphi_x} \varphi_x] dA \quad (23)$$

$${}_F\hat{T}^{[\varphi_y]} = \omega^2 \iint [R^3 X_m^{\varphi_y} Y_n^{\varphi_y} \varphi_y] dA \quad (24)$$

By substituting equations (2.52), (2.53) and (2.54) in equations (19) to (24), it is expressed that:

$${}_F\hat{U}^{[w_o]} = \sum_{i=1}^I \sum_{j=1}^J \iint \left[ \left( \frac{5}{6} R_{55}^1 \dot{X}_m^{Fw_o} Y_n^{Fw_o} \dot{X}_i^{Fw_o} Y_j^{Fw_o} \right) A_{ij}^{Fw_o} \right. \\ \left. + \left( \frac{5}{6} R_{44}^1 X_m^{w_o} \dot{Y}_n^{w_o} X_i^{w_o} \dot{Y}_j^{w_o} \right) A_{ij}^{Fw_o} \right. \\ \left. + \left( \frac{5}{6} R_{55}^1 \dot{X}_m^{w_o} Y_n^{w_o} X_i^{\varphi_x} Y_j^{\varphi_x} \right) A_{ij}^{\varphi_x} \right. \\ \left. + \left( \frac{5}{6} R_{44}^1 X_m^{w_o} \dot{Y}_n^{w_o} X_i^{\varphi_y} Y_j^{\varphi_y} \right) A_{ij}^{\varphi_y} \right] dA \quad (25)$$

$${}_F\hat{U}^{[\varphi_x]} = \sum_{i=1}^I \sum_{j=1}^J \iint \left[ \left( \frac{5}{6} R_{55}^1 X_m^{\varphi_x} Y_n^{\varphi_x} \dot{X}_i^{Fw_o} Y_j^{Fw_o} \right) A_{ij}^{Fw_o} \right. \\ \left. + \left( \frac{5}{6} R_{55}^1 X_m^{\varphi_x} Y_n^{\varphi_x} X_i^{\varphi_x} Y_j^{\varphi_x} \right) A_{ij}^{\varphi_x} \right. \\ \left. + R_{11}^3 \dot{X}_m^{\varphi_x} Y_n^{\varphi_x} \dot{X}_i^{\varphi_x} Y_j^{\varphi_x} \right. \\ \left. + R_{66}^3 X_m^{\varphi_x} \dot{Y}_n^{\varphi_x} X_i^{\varphi_x} \dot{Y}_j^{\varphi_x} \right) A_{ij}^{\varphi_x} \\ \left. + \left( R_{66}^3 X_m^{\varphi_x} \dot{Y}_n^{\varphi_x} \dot{X}_i^{\varphi_y} Y_j^{\varphi_y} \right) A_{ij}^{\varphi_y} \right. \\ \left. + R_{12}^3 \dot{X}_m^{\varphi_x} Y_n^{\varphi_x} X_i^{\varphi_y} \dot{Y}_j^{\varphi_y} \right) A_{ij}^{\varphi_y} \right] dA \quad (26)$$

$${}_F\hat{U}^{[\varphi_y]} = \sum_{i=1}^I \sum_{j=1}^J \iint \left[ \begin{aligned} &\left( \frac{5}{6} R_{44}^1 X_m^{\varphi_y} Y_n^{\varphi_y} X_i^{FW_o} \dot{Y}_j^{FW_o} \right) A_{ij}^{FW_o} \\ &+ \left( R_{12}^3 X_m^{\varphi_y} \dot{Y}_n^{\varphi_y} \dot{X}_i^{\varphi_x} Y_j^{\varphi_x} \right) A_{ij}^{\varphi_x} \\ &+ \left( \frac{5}{6} R_{44}^1 X_m^{\varphi_y} Y_n^{\varphi_y} X_i^{\varphi_y} Y_j^{\varphi_y} \right) \\ &+ \left( R_{22}^3 X_m^{\varphi_y} \dot{Y}_n^{\varphi_y} X_i^{\varphi_y} \dot{Y}_j^{\varphi_y} \right) A_{ij}^{\varphi_y} \\ &+ \left( R_{66}^3 \dot{X}_m^{\varphi_y} Y_n^{\varphi_y} \dot{X}_i^{\varphi_y} Y_j^{\varphi_y} \right) \end{aligned} \right] dA \quad (27)$$

$${}_F\hat{T}^{[w_o]} = \omega^2 \sum_{i=1}^I \sum_{j=1}^J \iint \left[ R^1 X_m^{FW_o} Y_n^{FW_o} X_i^{FW_o} Y_j^{FW_o} \right] A_{ij}^{FW_o} dA \quad (28)$$

$${}_F\hat{T}^{[\varphi_x]} = \omega^2 \sum_{i=1}^I \sum_{j=1}^J \iint \left[ R^3 X_m^{\varphi_x} Y_n^{\varphi_x} X_i^{\varphi_x} Y_j^{\varphi_x} \right] A_{ij}^{\varphi_x} dA \quad (29)$$

$${}_F\hat{T}^{[\varphi_y]} = \omega^2 \sum_{i=1}^I \sum_{j=1}^J \iint \left[ R^3 X_m^{\varphi_y} Y_n^{\varphi_y} X_i^{\varphi_y} Y_j^{\varphi_y} \right] A_{ij}^{\varphi_y} dA \quad (30)$$

By rearranging the equations (25) to (30) and performing some mathematical operations, the following expressions are derived for derivatives of strain and kinetic energy based on FSDT.

$${}_F\hat{U}^{[w_o]} = \frac{5}{6} \sum_{i=1}^I \sum_{j=1}^J \left[ \begin{aligned} &\left( \int_0^L R_{55}^1 \dot{X}_m^{FW_o} \dot{X}_i^{FW_o} dx \int_0^L Y_n^{FW_o} Y_j^{FW_o} dy + \int_0^L R_{44}^1 X_m^{FW_o} X_i^{FW_o} dx \int_0^L \dot{Y}_n^{FW_o} \dot{Y}_j^{FW_o} dy \right) A_{ij}^{FW_o} \\ &+ \left( \int_0^L R_{55}^1 \dot{X}_m^{FW_o} X_i^{\varphi_x} dx \int_0^L Y_n^{FW_o} Y_j^{\varphi_x} dy \right) A_{ij}^{\varphi_x} \\ &+ \left( \int_0^L R_{44}^1 X_m^{FW_o} X_i^{\varphi_y} dx \int_0^L \dot{Y}_n^{FW_o} Y_j^{\varphi_y} dy \right) A_{ij}^{\varphi_y} \end{aligned} \right] \quad (31)$$

$$\begin{aligned}
{}_F\hat{U}^{[\varphi_x]} &= \sum_{i=1}^I \sum_{j=1}^J \\
&\left[ \begin{aligned} &\frac{5}{6} \left( \int_0^L R_{55}^1 X_m^{\varphi_x} \dot{X}_i^{FW_o} dx \int_0^L Y_n^{\varphi_x} Y_j^{FW_o} dy \right) A_{ij}^{FW_o} + \\ &\left( \frac{5}{6} \int_0^L R_{55}^1 X_m^{\varphi_x} X_i^{\varphi_x} dx \int_0^L Y_n^{\varphi_x} Y_j^{\varphi_x} dy + \int_0^L R_{11}^3 \dot{X}_m^{\varphi_x} \dot{X}_i^{\varphi_x} dx \int_0^L Y_n^{\varphi_x} Y_j^{\varphi_x} dy \right. \\ &\quad \left. + \int_0^L R_{66}^3 X_m^{\varphi_x} X_i^{\varphi_x} dx \int_0^L \dot{Y}_n^{\varphi_x} \dot{Y}_j^{\varphi_x} dy \right) A_{ij}^{\varphi_x} \\ &+ \left( \int_0^L R_{12}^3 \dot{X}_m^{\varphi_x} X_i^{\varphi_y} dx \int_0^L Y_n^{\varphi_x} \dot{Y}_j^{\varphi_y} dy + \int_0^L R_{66}^3 X_m^{\varphi_x} \dot{X}_i^{\varphi_y} dx \int_0^L \dot{Y}_n^{\varphi_x} Y_j^{\varphi_y} dy \right) A_{ij}^{\varphi_y} \end{aligned} \right] \quad (32)
\end{aligned}$$

$$\begin{aligned}
{}_F\hat{U}^{[\varphi_y]} &= \sum_{i=1}^I \sum_{j=1}^J \\
&\left[ \begin{aligned} &\frac{5}{6} \left( \int_0^L R_{44}^1 X_m^{\varphi_y} X_i^{FW_o} dx \int_0^L Y_n^{\varphi_y} \dot{Y}_j^{FW_o} dy \right) A_{ij}^{FW_o} + \\ &\left( \int_0^L R_{12}^3 X_m^{\varphi_y} \dot{X}_i^{\varphi_x} dx \int_0^L \dot{Y}_n^{\varphi_y} Y_j^{\varphi_x} dy + \int_0^L R_{66}^3 \dot{X}_m^{\varphi_y} X_i^{\varphi_x} dx \int_0^L Y_n^{\varphi_y} \dot{Y}_j^{\varphi_x} dy \right) A_{ij}^{\varphi_x} + \\ &\left( \frac{5}{6} \int_0^L R_{44}^1 X_m^{\varphi_y} X_i^{\varphi_y} dx \int_0^L Y_n^{\varphi_y} Y_j^{\varphi_y} dy + \int_0^L R_{22}^3 X_m^{\varphi_y} X_i^{\varphi_y} dx \int_0^L \dot{Y}_n^{\varphi_y} \dot{Y}_j^{\varphi_y} dy \right. \\ &\quad \left. + \int_0^L R_{66}^3 \dot{X}_m^{\varphi_y} \dot{X}_i^{\varphi_y} dx \int_0^L Y_n^{\varphi_y} Y_j^{\varphi_y} dy \right) A_{ij}^{\varphi_y} \end{aligned} \right] \quad (33)
\end{aligned}$$

$${}_F\hat{T}^{[w_o]} = \omega^2 \sum_{i=1}^I \sum_{j=1}^J \left[ \int_0^L R^1 X_m^{FW_o} X_i^{FW_o} dx \int_0^L Y_n^{FW_o} Y_j^{FW_o} dy \right] A_{ij}^{FW_o} dA \quad (34)$$

$${}_F\hat{T}^{[\varphi_x]} = \omega^2 \sum_{i=1}^I \sum_{j=1}^J \left[ \int_0^L R^3 X_m^{\varphi_x} X_i^{\varphi_x} dx \int_0^L Y_n^{\varphi_x} Y_j^{\varphi_x} dy \right] A_{ij}^{\varphi_x} dA \quad (35)$$

$${}_F\hat{T}^{[\varphi_y]} = \omega^2 \sum_{i=1}^I \sum_{j=1}^J \left[ \int_0^L R^3 X_m^{\varphi_y} X_i^{\varphi_y} dx \int_0^L Y_n^{\varphi_y} Y_j^{\varphi_y} dy \right] A_{ij}^{\varphi_y} dA \quad (36)$$

### A.3 Rearrangement of stiffness and mass matrices

Equations (2.107) to (2.109) are rewritten.

$${}_F\hat{U}^{[w_o]} = [\varphi_x^{Fw_o}]_{IJ \times IJ} \{A^{\varphi_x}\}_{IJ \times 1} + [\varphi_y^{Fw_o}]_{IJ \times IJ} \{A^{\varphi_y}\}_{IJ \times 1} + [w_o^{Fw_o}]_{IJ \times IJ} \{A^{Fw_o}\}_{IJ \times 1} \quad (37)$$

$${}_F\hat{U}^{[\varphi_x]} = [\varphi_x^{\varphi_x}]_{IJ \times IJ} \{A^{\varphi_x}\}_{IJ \times 1} + [\varphi_y^{\varphi_x}]_{IJ \times IJ} \{A^{\varphi_y}\}_{IJ \times 1} + [w_o^{\varphi_x}]_{IJ \times IJ} \{A^{Fw_o}\}_{IJ \times 1} \quad (38)$$

$${}_F\hat{U}^{[\varphi_y]} = [\varphi_x^{\varphi_y}]_{IJ \times IJ} \{A^{\varphi_x}\}_{IJ \times 1} + [\varphi_y^{\varphi_y}]_{IJ \times IJ} \{A^{\varphi_y}\}_{IJ \times 1} + [w_o^{\varphi_y}]_{IJ \times IJ} \{A^{Fw_o}\}_{IJ \times 1} \quad (39)$$

Equations (2.104) to (2.106)  $\left( {}_F\hat{U}^{[w_o]} = {}_F\hat{T}^{[w_o]}, {}_F\hat{U}^{[\varphi_x]} = 0, {}_F\hat{U}^{[\varphi_y]} = 0 \right)$  are considered and used in equations (38) and (39).

$$\{A^{\varphi_x}\} = -[\varphi_x^{\varphi_x}]^{-1}([\varphi_y^{\varphi_x}][A^{\varphi_y}] + [w_o^{\varphi_x}]\{A^{Fw_o}\}) \quad (40)$$

$$[\varphi_y^{\varphi_y}]\{A^{\varphi_y}\} + [w_o^{\varphi_y}]\{A^{Fw_o}\} = [\varphi_x^{\varphi_y}][\varphi_x^{\varphi_x}]^{-1}([\varphi_y^{\varphi_x}]\{A^{\varphi_y}\} + [w_o^{\varphi_x}]\{A^{Fw_o}\}) \quad (41)$$

Equation (41) is rearranged as follows.

$$\{A^{\varphi_y}\} = ([\varphi_y^{\varphi_y}] - [\varphi_x^{\varphi_y}][\varphi_x^{\varphi_x}]^{-1}[\varphi_y^{\varphi_x}])^{-1}([\varphi_x^{\varphi_y}][\varphi_x^{\varphi_x}]^{-1}[w_o^{\varphi_x}] - [w_o^{\varphi_y}])\{A^{Fw_o}\} \quad (42)$$

Considering equation (42), the notation  $[Str]$  is used in the equation.

$$\{A^{\varphi_y}\} = [Str]\{A^{Fw_o}\} \quad (43)$$

Equation (43) is substituted in equation (40).

$$\{A^{\varphi_x}\} = -[\varphi_x^{\varphi_x}]^{-1}([\varphi_y^{\varphi_x}][Str] + [w_o^{\varphi_x}])\{A^{Fw_o}\} \quad (44)$$

Substituting equations (44) and (43) in equation (37) results in the following expression.

$$[{}_F\hat{U}^{[w_o]}] = ([\varphi_y^{w_o}][Str] + [w_o^{Fw_o}] - [\varphi_x^{w_o}][\varphi_x^{\varphi_x}]^{-1}([\varphi_y^{\varphi_x}][Str] + [w_o^{\varphi_x}]))\{A^{Fw_o}\} \quad (45)$$

Equation (45) is rewritten considering notation  $[{}_F\bar{K}]$ .

$$[_F \hat{U}^{[w_o]}] = [_F \bar{K}]_{IJ \times IJ} \{A^F\}_{IJ \times 1} \quad (46)$$

$$[_F \bar{K}] = \left[ [\varphi_y^{w_o}] - [\varphi_x^{w_o}][\varphi_x^{\varphi_x}]^{-1}[\varphi_y^{\varphi_x}] \right] [Str] - [\varphi_x^{w_o}][\varphi_x^{\varphi_x}]^{-1}[w_o^{\varphi_x}] + [w_o^{Fw_o}] \quad (47)$$

$$[Str] = \left( [\varphi_y^{\varphi_y}] - [\varphi_x^{\varphi_y}][\varphi_x^{\varphi_x}]^{-1}[\varphi_y^{\varphi_x}] \right)^{-1} ([\varphi_x^{\varphi_y}][\varphi_x^{\varphi_x}]^{-1}[w_o^{\varphi_x}] - [w_o^{\varphi_y}]) \quad (48)$$

#### A.4 Forced vibration formulation for zero initial displacement and velocity

Equations (3.1), (3.2), (3.10) and (3.11) are rewritten here for convenience.

$$w_o^F = \sum_{i=1}^I \sum_{j=1}^J A_{ij}^F(t) X_i(x) Y_j(y) \quad (49)$$

$$\dot{w}_o^F = \sum_{i=1}^I \sum_{j=1}^J \dot{A}_{ij}^F(t) X_i(x) Y_j(y) \quad (50)$$

$$\{A^F\} = [A^\omega]_{IJ \times IJ} \{q\}_{IJ \times 1} \quad (51)$$

$$\{\dot{A}^F\} = [A^\omega]_{IJ \times IJ} \{\dot{q}\}_{IJ \times 1} \quad (52)$$

Since the plate is in static state at equilibrium position at  $t = 0$ , the transverse displacement and velocity,  $w_o^F$  and  $\dot{w}_o^F$ , are zero meaning that  $\{A^F\}$  and  $\{\dot{A}^F\}$  are zero. Therefore, equations (51) and (52) become:

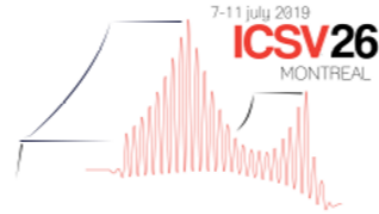
$$\{0\} = [A^\omega]_{IJ \times IJ} \{q\}_{IJ \times 1} \quad (53)$$

$$\{0\} = [A^\omega]_{IJ \times IJ} \{\dot{q}\}_{IJ \times 1} \quad (54)$$

From equations (53) and (54) it is concluded that  $\{q\} = \{\dot{q}\} = 0$  and by substituting them in equation (3.28), equation (3.29) is obtained.

## Appendix B

26<sup>th</sup> INTERNATIONAL CONGRESS ON SOUND AND VIBRATION  
7-11 July 2019, Montreal



# FUNDAMENTAL FREQUENCY OF COMPOSITE PLATE WITH STAIRCASE INTERNAL-THICKNESS-TAPER

Babak Arab, Rajamohan Ganesan and Milad Malaki

*Department of Mechanical, Industrial and Aerospace Engineering, Concordia University,  
Montreal, Quebec, Canada*

*Email: b.arab862016@gmail.com*

Considering the outstanding engineering properties, such as high strength/stiffness to weight ratios and the capability to be stiff at one location and flexible at another location as desired, internally-thickness-tapered composite plates are used in aerospace, mechanical and green power generation structures. Due to its distinct characteristics, such plates require comprehensive research to understand their dynamic response. In the present paper, the free vibration response of composite plates with staircase internal-thickness-taper configuration is considered considering clamped-free boundary condition. Since closed-form exact solution cannot be obtained for the resulting complex partial differential equation with variable coefficients in space and time coordinates, the Ritz method in conjunction with the Classical Laminated Plate Theory (CLPT) is used to obtain the system mass and stiffness matrices for out-of-plane bending vibration. In this approach, the stress and strain distributions in the laminated plate are determined in terms of mid-plane displacements and rotations corresponding to CLPT and as functions of taper angle and fiber orientation angle, and using these the kinetic and strain energies of the plate are calculated. Following the variational approach of the Rayleigh-Ritz method, the eigenvalue problem for the free vibration response is obtained, and the natural frequencies and mode shapes of the plate are determined by solving this eigenvalue problem. Numerical and symbolic computations have been performed using the software MATLAB. The influences of taper angle under thickness constraint and length constraint on the natural frequencies of the laminated composite plate are investigated for different stacking sequences of the laminate. Important design aspects are systematically brought out.

Keywords: Rayleigh-Ritz method, free vibration, composite plates

---

## 1. INTRODUCTION

Due to outstanding mechanical properties, composite materials are widely used in industry for years and they come in various shapes and structures depending on the requirements. As an instance, the tapered composite plates are popular in the aerospace industry and are used in manufacturing the structures such as rotor blades of helicopters and aircraft wings. Thickness reduction in tapered composites can be implemented by the termination of plies at different locations providing the tapered plate with customized stiffness property which is an absent capability in uniform laminates. The initial application of tapered laminated composites dates back to mid-1980s when commercial and military sectors demanded, elastically customizable components with higher weight to stiffness ratio [1].



In the course of the recent decades, few researchers have conducted analysis of such tapered structures. Recently, Seraj and Ganesan [2] investigated the dynamic instability of rotating doubly-tapered laminated composite beams under periodic rotational speeds. Liu and Ganesan [3] studied tapered composite plates for their dynamic instability. Ananda Babu *et al* [4] performed the dynamic characterization of thickness-tapered laminated composite plates using finite element analysis. Free vibration analysis of variable-stiffness laminated composite plates using Ritz method has not so far been conducted in existing literature and it is addressed in the present paper.

## 2. STRESS AND STRAIN TRANSFORMATIONS

The local coordinate system  $x''y''z''$  is considered for the  $k^{\text{th}}$  layer with the  $x''$  axis directed along the fiber orientation and  $z''$  perpendicular to the surface of the layer as shown in Fig. 1. By the angle  $\alpha$ , global coordinate system  $xyz$  is rotated counter-clockwise about the  $y$ -axis to establish the  $x'y'z'$  coordinate system and in turn,  $x'y'z'$  is rotated by angle  $\beta$ , counter-clockwise, to correspond to the local coordinate system  $x''y''z''$ .

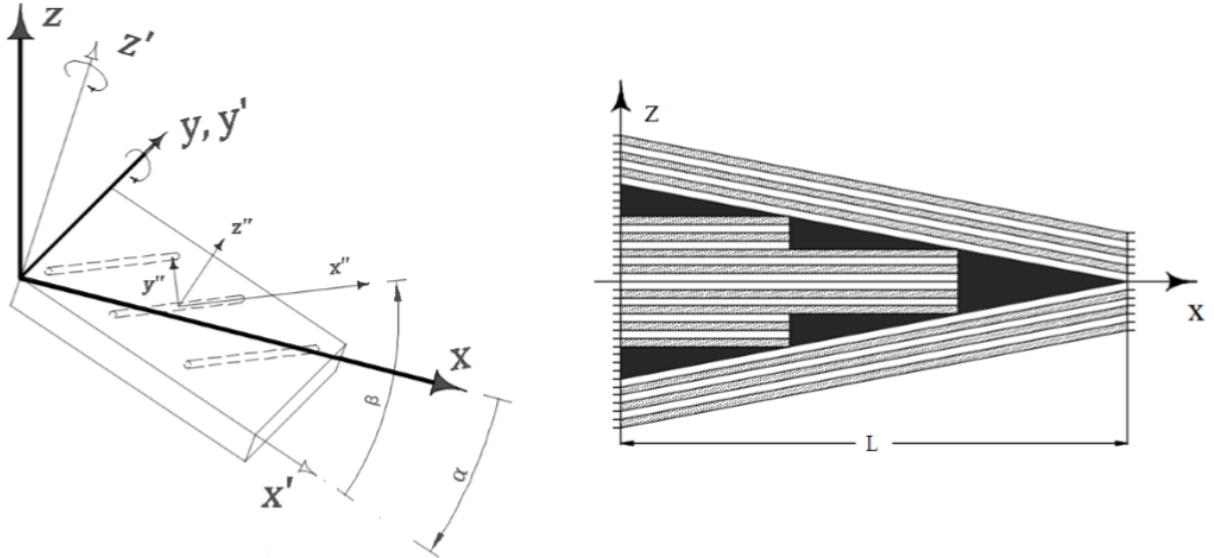


Figure 1: Ply orientation in the tapered laminated plate (left) and staircase taper configuration (right)

The stress-strain relationship in the global coordinate system is written for the  $k^{\text{th}}$  layer.

$$[\sigma]_{6 \times 1}^{[k]} = [C]_{6 \times 6}^{[k]} [\varepsilon]_{6 \times 1} \quad (1)$$

Where  $[C]_{6 \times 6}^{[k]}$ ,  $[C']_{6 \times 6}^{[k]}$  and  $[C'']_{6 \times 6}^{[k]}$  are stiffness matrices in  $xyz$ ,  $x'y'z'$ , and  $x''y''z''$  coordinate systems respectively. The relation between stress and strain matrices, in  $x'y'z'$  and  $xyz$  coordinate systems, according to [6] is expressed:

$$[\sigma'] = [T_{\sigma\alpha}] [\sigma] \quad (2)$$

$$[\varepsilon'] = [T_{\varepsilon\alpha}] [\varepsilon] \quad (3)$$

Considering Eqs. (1), (2) and (3) for the coordinate systems depicted by Fig. 1, the relation between the stiffness matrices in local and global coordinate systems  $x''y''z''$  and  $xyz$  for the  $k^{\text{th}}$  layer is as follows.

$$[C]^{[k]} = [T_{\sigma\alpha}]^{-1} [T_{\sigma\beta}]^{-1} [C'']^{[k]} [T_{\varepsilon\beta}] [T_{\varepsilon\alpha}] \quad (4)$$

### 3. FORMULATION BASED ON CLPT

In order to apply the Ritz method and to determine the fundamental frequency, stiffness and mass matrices are obtained from the calculation of displacements, strains and stresses expressed based on Classical Laminated Plate Theory (CLPT). Considering the pure bending condition (displacement on midplane is zero in  $x$  and  $y$  directions), displacements and strains are as follows.

$$u = -(\partial w_o / \partial x)z \quad (5)$$

$$v = -(\partial w_o / \partial y)z \quad (6)$$

$$w = w_o \quad (7)$$

$$\varepsilon_x = -(\partial^2 w_o / \partial x^2)z \quad (8)$$

$$\varepsilon_y = -(\partial^2 w_o / \partial y^2)z \quad (9)$$

$$\gamma_{xy} = -2(\partial^2 w_o / \partial x \partial y)z \quad (10)$$

Where  $u$ ,  $v$  and  $w$  are displacements in  $x$ ,  $y$  and  $z$  directions, respectively. In order to facilitate further calculation of strain and kinetic energies, Eqs. (5) to (10) are written in form of multiplication of matrices using the joint matrix  $[s]$ . Equations (11) to (13) represents these matrices in a detailed form.

$$[Z_u]_{3 \times 6} = \begin{bmatrix} 0 & z & 0 & 0 & 0 & 0 \\ 0 & 0 & z & 0 & 0 & 0 \\ 1 & 0 & 0 & 0 & 0 & 0 \end{bmatrix} \quad (11)$$

$$[Z_\varepsilon]_{3 \times 6} = \begin{bmatrix} 0 & 0 & 0 & z & 0 & 0 \\ 0 & 0 & 0 & 0 & z & 0 \\ 0 & 0 & 0 & 0 & 0 & z \end{bmatrix} \quad (12)$$

$$[s]_{6 \times 1} = \left[ w_o \quad -\frac{\partial w_o}{\partial x} \quad -\frac{\partial w_o}{\partial y} \quad -\frac{\partial^2 w_o}{\partial x^2} \quad -\frac{\partial^2 w_o}{\partial y^2} \quad -2\frac{\partial^2 w_o}{\partial x \partial y} \right]^t \quad (13)$$

Equations (5) to (10) are expressed in matrix using Eqs. (11) to (13).

$$[u]_{3 \times 1} = [Z_u]_{3 \times 6} [s]_{6 \times 1} \quad (14)$$

$$[\varepsilon]_{3 \times 1} = [Z_\varepsilon]_{3 \times 6} [s]_{6 \times 1} \quad (15)$$

Where  $[u]$  and  $[\varepsilon]$  are column matrices containing displacements and strains elements, respectively. The stresses are determined using the stress-strain relationship. The elements of the stiffness matrix are obtained using Eq. (4) and engineering constants of the material which have been given by Table 2.

Considering the CLPT assumptions, the reduced stiffness matrix in the stress-strain relationship is expressed.

$$\begin{bmatrix} \sigma_x \\ \sigma_y \\ \tau_{xy} \end{bmatrix} = \begin{bmatrix} Q_{11} & Q_{12} & Q_{16} \\ Q_{12} & Q_{22} & Q_{26} \\ Q_{16} & Q_{26} & Q_{66} \end{bmatrix} \begin{bmatrix} \varepsilon_x \\ \varepsilon_y \\ \gamma_{xy} \end{bmatrix} \quad (16)$$

Equation (16) is express in compact form as follows.

$$[\sigma]_{3 \times 1} = [Q]_{3 \times 3} [\varepsilon]_{3 \times 1} \quad (17)$$

The resin is considered as an isotropic material and the corresponding stiffness matrix is independent of angles  $\alpha$  and  $\beta$ . The reduced stiffness matrix based on CLPT can be obtained considering the CLPT assumptions.

Displacements, strains, and stresses presented by Eqs. (14), (15) and (17) are essential in energy calculation in the next section. Function  $w_o$  introduced by Eq. (7), is expressed in the form of series.

$$w_o = \sum_{i=1}^I \sum_{j=1}^J A_{ij} X_i(x) Y_j(y) \quad (18)$$

Terms  $X_i$  and  $Y_j$  are admissible functions dependent on the boundary conditions. The stresses and strains are key components for strain energy  $U$  calculation, and the density of the material is the essential factor in kinetic energy  $T$  computation. The strain and kinetic energies are expressed according to [6] and written in matrix form as follows.

$$U = \frac{1}{2} \iiint [\sigma]^t [\varepsilon] dV \quad (19)$$

$$T = \frac{1}{2} \omega^2 \iiint \rho [u]^t [u] dV \quad (20)$$

Matrix form is superior in terms of computational efficiency. Hence, kinetic and strain energies are calculated at the same time in this form. In order to apply the Ritz method, the derivatives of the strain and kinetic energies with respect to parameters  $A_{mn}$  are denoted by  $\bar{U} = \partial U / \partial A_{mn}$  and  $\hat{T} = \partial T / \partial A_{mn}$  and calculated using Eqs. (19) and (20).

$$\bar{U} = \frac{1}{2} \iiint ([Q] [\hat{\varepsilon}])^t [\varepsilon] + ([Q] [\varepsilon])^t [\hat{\varepsilon}] dV \quad (21)$$

$$\hat{T} = \frac{1}{2} \omega^2 \iiint \rho ([\hat{u}]^t [u] + [u]^t [\hat{u}]) dV \quad (22)$$

Equations (21) and (22) are written in the following form.

$$\bar{U} = \frac{1}{2} \iiint [\hat{\varepsilon}]^t [Q] [\varepsilon] + ([\hat{\varepsilon}]^t [Q] [\varepsilon])^t dV \quad (23)$$

$$\hat{T} = \frac{1}{2} \omega^2 \iiint \rho ([\hat{u}]^t [u] + ([\hat{u}]^t [u])^t) dV \quad (24)$$

The terms  $[\hat{\varepsilon}]^t [Q] [\varepsilon]$  and  $[\hat{u}]^t [u]$  on the right-hand side of the Eqs. (23) and (24) should be scalars as they follow scalar values of  $\bar{U}$  and  $\hat{T}$  on the left-hand side. In addition, this can also be realized from the size of the matrices on the right-hand side. Therefore, considering scalars  $[\hat{\varepsilon}]^t [Q] [\varepsilon]$  and  $[\hat{u}]^t [u]$ :

$$[\hat{\varepsilon}]^t [Q] [\varepsilon] = ([\hat{\varepsilon}]^t [Q] [\varepsilon])^t \quad (25)$$

$$[\hat{u}]^t [u] = ([\hat{u}]^t [u])^t \quad (26)$$

Equations. (25) and (26) are substituted in Eqs. (23) and (24).

$$\bar{U} = \iiint [\hat{\varepsilon}]^t [Q] [\varepsilon] dV \quad (27)$$

$$\hat{T} = \omega^2 \iiint \rho [\hat{u}]^t [u] dV \quad (28)$$

Substituting Eqs. (15) and (14), in Eqs. (27) and (28), respectively, one can get:

$$\bar{U} = \iiint [\hat{s}]^t [Z_\varepsilon]^t [Q] [Z_\varepsilon] [s] dV \quad (29)$$

$$\hat{T} = \omega^2 \iiint \rho [\hat{s}]^t [Z_u]^t [Z_u] [s] dV \quad (30)$$

Equations (29) and (30) are written in the following form.

$$\bar{U} = \iint [\hat{s}]^t \left( \int_{-\frac{h}{2}}^{\frac{h}{2}} [Z_\varepsilon]^t [Q] [Z_\varepsilon] dz \right) [s] dA \quad (31)$$

$$\hat{T} = \iint [\hat{s}]^t \left( \omega^2 \int_{-\frac{h}{2}}^{\frac{h}{2}} \rho [Z_u]^t [Z_u] dz \right) [s] dA \quad (32)$$

Integration through the laminate thickness, matrices containing functions of  $z$  are taken into account within the integral so that matrices  $[Z_\varepsilon]$ ,  $[Z_u]$  and  $Q_{ij}$  as well as scalar  $\rho$  participate in the integration.

$$\hat{U} = \iint [\hat{s}]^t [\bar{Z}_\varepsilon] [s] dA \quad (33)$$

$$\hat{T} = \iint [\hat{s}]^t [\bar{Z}_u] [s] dA \quad (34)$$

$$[\bar{Z}_\varepsilon] = \int_{-\frac{h}{2}}^{\frac{h}{2}} [Z_\varepsilon]^t [Q] [Z_\varepsilon] dz \quad (35)$$

$$[\bar{Z}_u] = \omega^2 \int_{-\frac{h}{2}}^{\frac{h}{2}} \rho [Z_u]^t [Z_u] dz \quad (36)$$

Equations (33) and (34) are written in the following form.

$$\hat{E}_{U,T} = \iint [\hat{s}]^t [\bar{Z}_{\varepsilon,u}] [s] dA \quad (37)$$

Equation (37) has been written in combined form such that depending on the calculation performed for derivatives of strain or kinetic energies ( $\hat{U}$  or  $\hat{T}$ ), matrices  $[\bar{Z}_\varepsilon]$  or  $[\bar{Z}_u]$  is considered. After computation of matrices  $[\bar{Z}_\varepsilon]$  and  $[\bar{Z}_u]$ , derivatives of kinetic and strain energies with respect to parameters  $A_{mn}$  are obtained using Eq. (37). Any nonzero elements of  $[\bar{Z}_\varepsilon]$  and  $[\bar{Z}_u]$ , are denoted by  $R_{ij}^{(n)}$  and  $R^{(n)}$ , respectively. The matrix  $[\bar{Z}_\varepsilon]$  contain the elements of the extensional stiffness matrix  $R_{ij}^{(1)}$ , bending-extension coupling matrix  $R_{ij}^{(2)}$  and bending stiffness matrix  $R_{ij}^{(3)}$ .

The final results for system coefficients are computed by replacing Eq. (18) in Eq. (37) and are presented here in the open form. Since the configurations of tapered laminates are made of (0/90) ply layup, elements  $Q_{16}$  and  $Q_{26}$  from reduced stiffness matrix are zero meaning that in-plane normal and shear are decoupled. The expressions for stiffness and mass coefficients are given within the brackets in the following two expressions for strain and kinetic energies.

$$\hat{U} = \sum_{i=1}^I \sum_{j=1}^J \left( \int_0^L R_{12}^{(3)} X_m \ddot{X}_i dx \int_0^L \ddot{Y}_n Y_j dy + \int_0^L R_{11}^{(3)} \ddot{X}_m \ddot{X}_i dx \int_0^L Y_n Y_j dy \right. \\ \left. + \int_0^L R_{22}^{(3)} X_m X_i dx \int_0^L \ddot{Y}_n \ddot{Y}_j dy + \int_0^L R_{12}^{(3)} \ddot{X}_m X_i dx \int_0^L Y_n \ddot{Y}_j dy \right. \\ \left. + 4 \int_0^L R_{66}^{(3)} \dot{X}_m \dot{X}_i dx \int_0^L \dot{Y}_n \dot{Y}_j dy \right) A_{ij} \quad (38)$$

$$\hat{T} = \omega^2 \sum_{i=1}^I \sum_{j=1}^J \left( \int_{x=0}^{x=L} R^{(3)} \dot{X}_m \dot{X}_i dx \int_{y=0}^{y=L} Y_n Y_j dy + \int_{x=0}^{x=L} R^{(3)} X_m X_i dx \int_{y=0}^{y=L} \dot{Y}_n \dot{Y}_j dy \right) \\ + \int_{x=0}^{x=L} R^{(1)} X_m X_i dx \int_{y=0}^{y=L} Y_n Y_j dy \quad A_{ij} \quad (39)$$

#### 4. FREE VIBRATION ANALYSIS

Considering  $\hat{U}$ , in Eq. (38), for the fixed values of  $m$  and  $n$ , the indices  $i$  and  $j$  are counted up to the upper bound of the summations  $I$  and  $J$ . Therefore, there are  $I \times J$  number of terms that are written in the form of a row matrix multiplied by a column matrix  $[A]$  containing  $I \times J$  number of parameters,  $A_{ij}$ . By repeating the operation for all possible values for  $m$  and  $n$ , there are produced  $I \times J$  number of row matrices written one beneath the next one forming a matrix with the size of  $I \times J$  by  $I \times J$ .

This  $I \times J$  by  $I \times J$  matrix produced from  $\hat{U}$  is called stiffness matrix and denoted by  $[K]$ . In a similar manner for  $\hat{T}$ , a matrix with the same size is formed and called mass matrix denoted by  $[M]$ . considering  $\hat{U} = \hat{T}$ :

$$[K]_{IJ \times IJ} [A]_{IJ \times 1} = \omega^2 [M]_{IJ \times IJ} [A]_{IJ \times 1} \quad (40)$$

In order to obtain a non-trivial solution from eigenvalue problem given by Eq. (40):

$$\det([K] - \omega^2 [M]) = 0 \quad (41)$$

By solving the eigenvalue problem in which  $\omega^2$  and the column matrix  $[A]$  are eigenvalues and eigenvectors, respectively, natural frequencies and mode shapes are determined. The square root of the smallest eigenvalue is the fundamental frequency.

The fundamental frequency is obtained for the described taper laminate (Fig. 1) for different boundary conditions. Considering Eq. (18), admissible functions  $X_i(x)$  and  $Y_j(y)$  corresponding to the boundary conditions SSSS, CCCC and CCFF are in the Table 1. The clamped edges for the CCFF boundary condition correspond to  $x = 0$  and  $y = 0$  lines and free edges to  $x = L$  and  $y = L$  lines.

Table 1: Admissible functions corresponding to the boundary conditions [6, 7]

SSSS	$X_i = \sin\left(i\pi \frac{x}{L}\right) \quad , \quad Y_j = \sin\left(j\pi \frac{y}{L}\right) \quad i, j = 1, 2, 3, \dots$				
CCCC	$X_m = \cos\left(\lambda_i \frac{x}{L}\right) - \cosh\left(\lambda_i \frac{x}{L}\right) - \gamma_i \left[\sin\left(\lambda_i \frac{x}{L}\right) - \sinh\left(\lambda_i \frac{x}{L}\right)\right]$				
	$Y_n = \cos\left(\lambda_j \frac{y}{L}\right) - \cosh\left(\lambda_j \frac{y}{L}\right) - \gamma_j \left[\sin\left(\lambda_j \frac{y}{L}\right) - \sinh\left(\lambda_j \frac{y}{L}\right)\right]$				
	$i, j$	$i, j = 1$	$i, j = 2$	$i, j = 3$	$i, j = 4$
	$\lambda_i$	4.730,040,08	7.853,204,6	10.995,607,8	10.995,540,7
CCFF	$\gamma_i$	0.982,502,2	1.000,777,3	0.999,966,4	1.000,033,553,2
	$X_m = \cos\left(\lambda_i \frac{x}{L}\right) - \cosh\left(\lambda_i \frac{x}{L}\right) - \gamma_i \left[\sin\left(\lambda_i \frac{x}{L}\right) - \sinh\left(\lambda_i \frac{x}{L}\right)\right]$				
	$Y_n = \cos\left(\lambda_j \frac{y}{L}\right) - \cosh\left(\lambda_j \frac{y}{L}\right) - \gamma_j \left[\sin\left(\lambda_j \frac{y}{L}\right) - \sinh\left(\lambda_j \frac{y}{L}\right)\right]$				
	$i, j$	$i, j = 1$	$i, j = 2$	$i, j = 3$	$i, j = 4$
	$\lambda_i$	1.875,104,069	4.694,091,133	7.854,757,438	10.995,540,735
	$\gamma_i$	0.734,095,514	1.018,467,319	0.999,224,497	1.000,033,553

#### 5. NUMERICAL RESULTS

Two tapered laminated square plates with configuration of  $(0/90)_{9s}$  and  $(0/90)_{3s}$  at the left and right ends, respectively, made of resin and unidirectional plies of NCT-301 Graphite-Epoxy material

with ply thickness of  $125 \times 10^{-6}$  m are considered (Fig. 1). The lengths of the laminates are dependent on the taper angle and are 85.944 cm and 17.188 cm for  $0.1^\circ$  and  $0.5^\circ$  taper angles, respectively.

The composite layer is considered as a transversely-isotropic material and the corresponding stiffness matrix is denoted by  $[C'']$ . The mechanical properties of NCT-301 Graphite-Epoxy material are given in Table 2.

Table 2: Mechanical Properties of NCT-301 Graphite-Epoxy [5] Ply and epoxy resin

Mechanical Properties of Unidirectional NCT-301 Graphite – Epoxy		Resin
$E_1 = 113.9 \text{ GPa}$	$E_2 = 7.985 \text{ GPa}$	$E = 3.93 \text{ GPa}$
$G_{12} = 3.137 \text{ GPa}$	$G_{23} = 2.852 \text{ GPa}$	$G = 1.034 \text{ GPa}$
$\nu_{12} = 0.288$	$\nu_{21} = 0.018$	$\nu = 0.37$
$\rho_{ply} = 1480 \text{ kg/m}^3$		$\rho_{resin} = 1000 \text{ kg/m}^3$

Solving the eigenvalue problem given by Eq. (41), the first natural frequencies obtained for the square plates with the staircase taper configuration with different boundary conditions are given in Table 3. Numerical solutions using the finite element software ANSYS® were also obtained and compared with the present Ritz solutions. The finite element solution has been obtained using the four-node element SHELL 181 in ANSYS® and converged meshes of 2808 and 195 elements have been obtained for the plates of side length 85.944 cm and 17.188 cm, respectively. The finite element model developed in ANSYS® is shown in Fig. 2. First mode shape of the plate of side length 85.944 cm is shown in Fig. 2(b) for different boundary conditions.

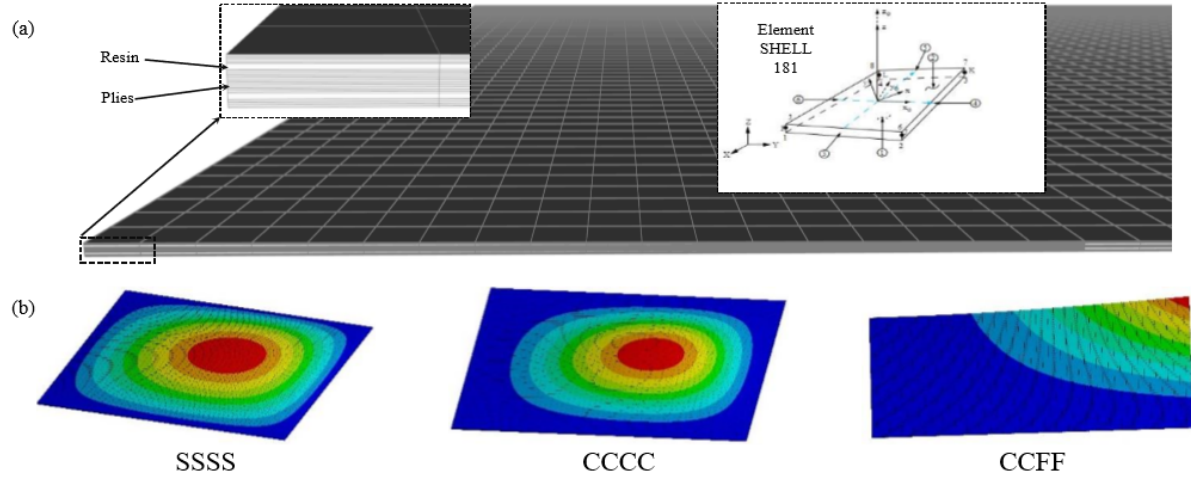


Figure 2: Finite element model of the tapered laminate: (a) Converged mesh and (b) First mode shapes

Table 3: Fundamental frequencies of plates ( $rad/s$ ) for different boundary conditions

BC	Length/Mean Thickness = 286.5		Length/Mean Thickness = 57.3	
	Length (cm)/Angle (deg) = 85.944/0.1°		Length (cm)/Angle (deg) = 17.188/0.5°	
	Ritz Method	Finite Element Method	Ritz Method	Finite Element Method
SSSS	108.0	108.5	2700	2699
CCCC	229.2	230.0	5728	5710
CCFF	52.2	52.3	1304	1245

## 6. CONCLUSION

Tapered composite plate with staircase taper configuration has been considered. The displacements, strains, and stresses based on CLPT are expressed, and then, the mass and stiffness matrices were developed based on the Ritz method for the tapered plates with different boundary conditions. From the analysis of the results, it is concluded that:

- The fundamental vibration frequency for the CCCC plate is the highest and that of the CCFF plate is the lowest, having a ratio of 4.39. The frequencies of CCCC and SSSS plates have a ratio of 2.12.
- The plies close to the midplane do not significantly contribute to increasing the fundamental frequency even though their inertial (mass) contribution is the same as that of other plies.
- The resin which is the weaker material is used in the regions close to the midplane, and the composite plies are used in farther layers. Therefore, composite plies contribute with higher capacity in increasing the stiffness of the plate and the resin does not take part notably in tailoring the stiffness yet used instead of plies to avoid any significant increase in the plate's weight. Hence, in order to maximize the fundamental frequency, the materials with higher stiffness property should be used for the external layers of the plate, and weaker materials should be used for inner layers close to the midplane.

## ACKNOWLEDGEMENT

The authors thank NSERC and Concordia University for their support to the present work.

## REFERENCES

- 1 He, K., Hoa, S.V. and Ganesan, R. The study of tapered laminated composite structures: a review, *Composites Science and Technology*, **60**, 2643-2657, (2000).
- 2 Seraj, S. and Ganesan, R. Dynamic instability of rotating doubly-tapered laminated composite beams under periodic rotational speeds, *Composite Structures*, **200**, 717-728, (2018).
- 3 Liu, W., *Dynamic Instability Analysis of Tapered Composite Plates Using Ritz and Finite Element Methods*, Master of Science Thesis, Graduate Program in mechanical engineering, Concordia University, (2005).
- 4 Ananda Babu, A., Edwin Sudhagar, P. and Vasudevan, R. Dynamic Characterization of Thickness Tapered Laminated Composite Plates, *Journal of Vibration and Control*, **22** (16), 3555-3575, (2016).
- 5 Salajegheh, P. and Ganesan, R. Free Vibrations of variable-thickness variable-width laminated composite beams with elastic supports, *American Society of Composites*, 28th Technical Conference, (2013).
- 6 Berthelot, J. M., *Composite Materials - Mechanical Behavior and Structural Analysis*, Springer - Verlag Berlin Heidelberg, New York, (1999).
- 7 Akhlaque-E-Rasul, S. M., *Buckling Analysis of Tapered Composite Plates Using Ritz Method Based on Classical and Higher-order Theories*, Master of Science Thesis, Graduate Program in mechanical engineering, Concordia University, (2005).